SEISMIC ANALYSIS OF LINKED GEOLOGICAL PROCESSES IN THE TRANSITIONAL DOMAIN OF GRAVITY DETACHMENT SYSTEMS: DEEPWATER WESTERN NIGER DELTA

LEDUC, AMELIE

SEISMIC ANALYSIS OF LINKED GEOLOGICAL PROCESSES IN THE TRANSITIONAL DOMAIN OF GRAVITY DETACHMENT SYSTEMS: DEEPWATER WESTERN

NIGER DELTA

AMÉLIE MARIE LEDUC

A thesis submitted in partial fulfillment of the requirements for the degree of Doctor of Philosophy at Durham University

Department of Earth Sciences

2013

Amélie Marie LEDUC

SEISMIC ANALYSIS OF LINKED GEOLOGICAL PROCESSES IN THE TRANSITIONAL DOMAIN OF GRAVITY DETACHMENT SYSTEMS: DEEPWATER WESTERN NIGER DELTA

ABSTRACT

Two and three-dimensional seismic data are used to investigate some stratigraphic relationships between sedimentation, deformation and fluid flow at the lateral margin of a gravity detachment system. Three themes were studied.

In the Niger Delta, a right-lateral strike-slip fault with a displacement of around 7 km occurs across 75 km. It is interpreted as the lateral strike-slip domain, linked to the updip extensional domain and the downdip compression zone of a gravity detachment system. Structural and kinematic evidence, such as present-day propagating strike-slip faults, for possible future lateral expansions of the lateral strike-slip domain, is described. We expect to observe similar domains at the margins of other preserved gravitational collapse sliding over a detachment whose efficiency in causing downdip slip may vary laterally.

Using 3D data from both Mauritania and Nigeria, the interactions between tear faults and deepwater channels are studied. Structural observations combined with channel analysis are performed in four case studies, illustrating that tear faults influence channel development throughout their evolution. Some examples across tear fault zones are presented, and it is expected to find such interactions elsewhere in the world.

A simple model of development of vertical fluid flow pipes is established using two examples that are 400 - 600 m wide and ~ 2000 - 2500 m high. Both examples are located at the crest of rollover anticlines and rooted in buried channel-complexes tilted during fold growth. At the crest of the structures and within the connected permeable reservoir intervals of the channel complexes, lateral pressure transfer caused the pore pressure to reach critical levels, leading to hydraulic fracturing of the overburden. Although hydrocarbons may migrate upwards through the consequent chimney systems, the pipes are not necessarily indicators of hydrocarbon charge of the channel complexes.

CONTENTS

LIST OF FIGURES

LIST OF TABLES

DECLARATION

No part of this thesis has previously been submitted for a degree at this or any other university. The work described in this thesis is entirely that of the author, except where reference is made to previously published or unpublished work.

ACKNOWLEDGEMENTS

I wish to thank, first and foremost my PhD supervisors, Richard Davies, Alexander Densmore and Jonny Imber for offering me this PhD opportunity at Durham. I am deeply grateful to my PhD supervisors for setting up the project with Eni and for their encouragement and their guidance, as well as for their valuable advice and support they have given me in the writing of this thesis.

Eni is thanked for making this research possible in fully funding the project and giving permission to use 3D data, as well as for their hospitality in San Donato Milanese. I would like to thank Marco Orsi and Franco Fonnesu for their tutorship in Eni. Richard Swarbrick is thanked for his help and teaching about pore pressure. PGS, CGG Veritas, Tullow and Petronas gave permissions for the release of some of the seismic data images respectively from the Niger Delta and offshore Mauritania on which this research is based. Landmark Graphics Corporation provided the seismic interpretation software as part of the LGC University Grant Scheme. Dave Stevenson and Gary Wilkinson are thanked for their contribution and help with the IT systems used for this work and the office staff in the Department of Earth Sciences at Durham University for their essential support. I would also like to thank David Iacopini, Stephen Laubach, Finn Surlyk, Graham Yielding, and the anonymous reviewers of my papers and editors for their useful remarks.

I am grateful to Philippe Ruelland at Total E&P UK for offering me an internship in Aberdeen during the PhD. I thank the research staff and students at Durham University for the more than three years and a half spent with them; I enjoyed a lot the discussions about science, the experience shared with them, especially during student field trips, and their presence for both fun times and when painful events happened.

Finally I owe a big thank-you to my friends, especially Steve, Juan Carlos, James, Kirstie, Sarah, Aurore, Babeth, Thibault, Stéphane, Caroline, l'AGEOL and people and friends from Lille 1 for their permanent support over the years and over great distances. And I cannot find words to express my deepest gratitude to my grandmother, my mum, Caroll and Séverin who have always encouraged and supported me in everything I have done – mille mercis!

CHAPTER 1: INTRODUCTION

1.1 Rationale

A lot of research focuses on the evolution of gravity detachment systems (e.g. Butler and Turner, 2010; Morley *et al.*, 2011). In deepwater continental margins settings, gravity detachment systems occur at a variety of scales (Butler and Turner, 2010). They can be mass-transport complexes from ~ 10^{-2} km² to more than 10^{2} km² of extent (e.g. Martisen and Bakken, 1990; Frey-Martinez *et al.*, 2005; Cobbold *et al.*, 2010) and up to the scale of continental margin collapses (e.g. Cobbold and Szatmari, 1991; Morley and Guerin, 1996; Rowan *et al.*, 2004). They are fairly ubiquitous and occur on passive continental margins (e.g. Gulf of Mexico: Peel *et al.*, 1995; Niger Delta: Cohen and McClay, 1996; Nile Delta: Gaullier *et al.*, 2000; Amazon Fan: Cobbold *et al.*, 2004; Orange Basin: De Vera *et al.*, 2009) and tectonically active regions (e.g. Champion Delta: Van Rensbergen and Morley, 2003; Barbados: Deville *et al.*, 2003; offshore Iran: Grando and McClay, 2007). In these regions, a number of processes occur and interact. They include sedimentation and loading (e.g. Anderson *et al.*, 2000; Gaullier and Vendeville, 2005), detachment weakening (e.g. how deformation styles take place and faulting develops when detachment levels are thick or thin: Stewart, 1996; overpressure: Swarbrick and Osborne, 1998; Cobbold *et al.*, 2004), fluid flow and structural deformation (e.g. Butler and Turner, 2010). In this thesis, the investigation will focus on some of the fundamental links between these processes as general characteristics of gravity detachment systems.

Over the past three decades, hydrocarbon exploration in deepwater margins initiated a dramatic increase in seismic data acquisition, in particular 3D seismic data (Davies *et al.*, 2004). Seismic interpretation is nowadays a popular method used to understand geological processes

occurring on continental margins, including deepwater sedimentation and its interaction with bathymetry created by deformational processes (e.g. Davies *et al.*, 2004). Recent works in gravity detachment systems focused on the characterization of the structural growth of folds and the influence of this on mass-transport complexes or channel evolution (e.g. Heiniö and Davies, 2006 and 2007; Morley, 2009). Morphological changes in channel systems due to interaction with salt and shale diapirs (e.g. Hooper *et al.*, 2002; Catterall *et al.*, 2010; Mayall *et al.*, 2010). Clark and Cartwright (2009 and 2011) proposed a method to assess and quantify these changes in contractional and strike-slip settings. In addition, other publications have also focused on these interactions in extensional settings (e.g. Broucke *et al.*, 2004; Pochat *et al.*, 2009). Gravitational collapse events have also been linked to climate-induced sea-level changes (e.g. Förster *et al.*, 2010; Jermannaud *et al.*, 2010; Rouby *et al.*, 2011).

In summary, a number of studies now relate some processes interacting between each other in gravity detachment systems. But the lateral margins of these systems have not been a focus of research. In this study, using relative seismic geometries and relative timing, the lateral margins of a gravity detachment system are analysed in order to understand deformation, sedimentation and pore pressure and what the likely interactions are between these processes are.

1.2 Terminology

1.2.1 Gravity Detachment Systems

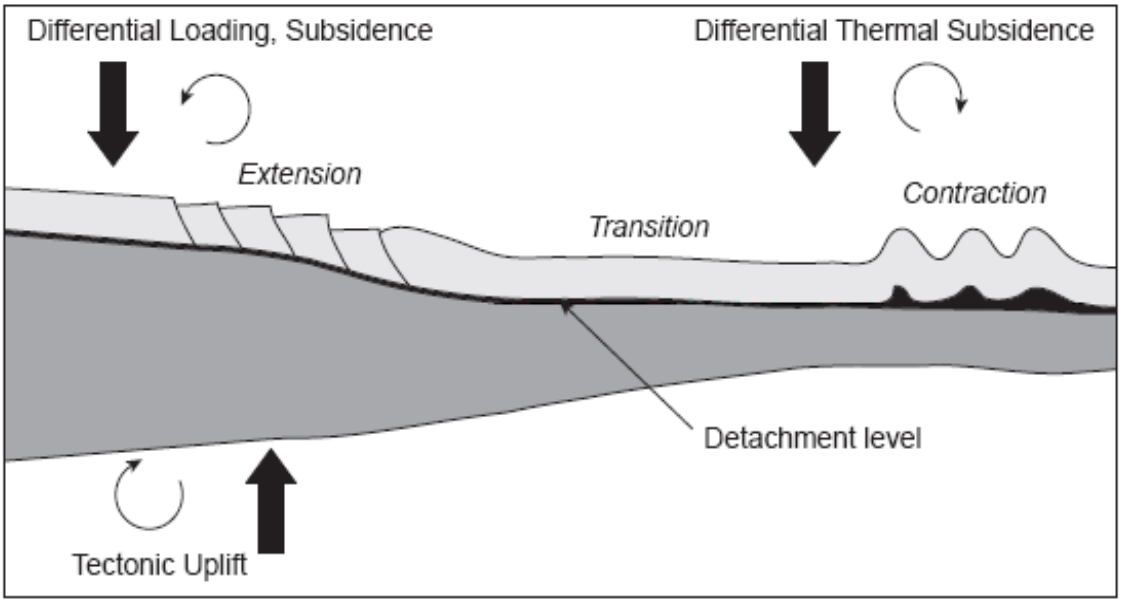

Figure 1.1 - Gravitational tectonics (after Rowan *et al.* (2004), not to scale).

Research on submarine gravitational collapse has developed along with exploration of oceans since the early 20th century. Gravitational collapses are composed of an upslope head region, a transitional zone and a downslope toe zone (e.g. Martisen, 1989; Fig.1.1). The upslope region is where occurs extensional deformation, which is characterized by the presence of regional listric faults (Crans *et al.*, 1980) which sole out on a basal detachment level. Planar or listric antithetic extensional faulting also occur, and collapse of the footwall can also be observed, accompanied with a landward migration of the rollover (e.g. Imber *et al.*, 2003). These complex structural patterns can be related to smaller-scale deformation occurring at detachment levels (Maloney *et al.*, 2011). Gravity-driven movement is accommodated by shear strain along a thin basal interface, known as the detachment level (Fig. 1.1; Maltman, 1994). At passive margins, gravitational collapse can occur as a response to differential loading and subsidence, tectonic uplift and differential thermal subsidence (Fig. 1.1; Rowan *et al.*, 2004).

Growth faulting is common and represents both a lateral translation and subsidence of

the down-faulted sedimentary unit. They also are major fluid pathways (e.g. Galloway, 1986). Syn-sedimentary, gravity-driven growth faults can develop much faster than tectonic faults (e.g. Childs *et al.*, 2003). Fault growth generates substantial depocentres and control sedimentary deposits thicknesses and facies with thick sand accumulations in fault hanging walls. There are a number of examples of this in the Niger Delta (e.g. Rouby and Cobbold, 1996; Pochat *et al.*, 2009).

The transition zone generally shows little evidence of the slide itself (Maltman, 1994). Some contractional deformation (detachment folding or shears) exists but overall little evidence for slide movement is found, and when they are defined, lateral margins display strike-slip deformation. This is important evidence as it can present complex deformation (transpressional to transtensional), which may result from an accommodation process of variations in the geometry of the basal slip plane (variations in dip or friction coefficient of the slip plane for example). Kinematic indicators such as local lateral collapse, lateral ramps and *en echelon* sigmoids can be found (Bull *et al.*, 2009). The fact that such lateral margins can be identified shows that a gravity detachment system hosts distinct structural domains between the head or toe regions of the system. In these specific domains, key information on the evolution of the slide system, such as kinematic indicators, or accommodation structures can be found. In the toe region, contractional folding and imbricate thrusting can be found (Maltman, 1994). They are assumed to be commonly found in gravity detachment systems and their presence is generally related to the location of underlying basement buttresses and changes in detachment dip or weakness (Rowan, 2009).

The contractional domain has largely been studied and a variety of structural styles can be found, including detachment folds (e.g. Gonzales-Mieres and Suppe, 2006), imbricate thrusts, and backthrusts (Maltman, 1994). Duplexes and imbricate fault geometries are observed at both

continental margin and smaller-scale mass-transport complexes, and distributed strain as well as volume loss can be observed (e.g. Martinsen and Bakken, 1990; Rowan *et al.*, 2004; Frey-Martinez *et al.*, 2005; Butler and Turner, 2010). At passive margins, regional overpressure migrates basinward in respect to sediment progradation, resulting in a forward-propagating contractional sequence (Rowan *et al.*, 2004).

At passive margins, deformation occurs as a result of a combination of gravity spreading process and gravity gliding (Fig. 1.2; Rowan *et al*., 2004) Loading, for instance induced by high sedimentation rates, can trigger gravity spreading (e.g. Pedersen, 1987). Gravity spreading can occur above weak detachments and triggers proximal extension (e.g. Galloway, 1986). As the load is spreading, a lateral stress component, oriented towards the direction of propagation of propagation, takes place (e.g. Galloway, 1986). As a result, in the case of gravity spreading, contractional deformation is oriented basinward (Pedersen, 1987; Maltman, 1994). Episodes of high sedimentation rate can also reactivate pre-existing structures (e.g. Gaullier and Vendeville, 2005). Gravity spreading also results in curved or irregular margins; examples of this process can be found in the Nile Delta, the Gulf of Mexico and the Amazon Fan (Cobbold and Szatmari, 1991). Gravity gliding represents the rigid downslope translation parallel to a detachment plane and constitutes deformation caused by generally basinward-dipping detachments, differential thermal subsidence and tectonic uplift (Fig. 1.1; e.g. Schultz-Ela and Walsh, 2002). Rowan *et al.* (2004) provided a detailed analysis of the role of both processes at passive margins. The thickness of detachment can influence deformation styles and timing in the case of salt (Stewart, 1999). In the case of overpressured shale, current discussions are still assessing the existence of “mobile shale”, which used to be interpreted from poorer-quality seismic data (e.g. Maloney, 2011; Morley *et al.*, 2011). One of the primers for deformation in shale-rich successions is high pore fluid pressures (e.g. Cobbold *et al.*, 2004). Morley *et al.* (2011) also proposed an additional classification of gravity

detachment systems focusing on the orientation of the detachment dip (basinward or not) and the effects of near-field and far-field stresses. This classification notably demonstrates existing similarities between gravity detachment systems at passive and active margins, despite different tectonic stress regimes.

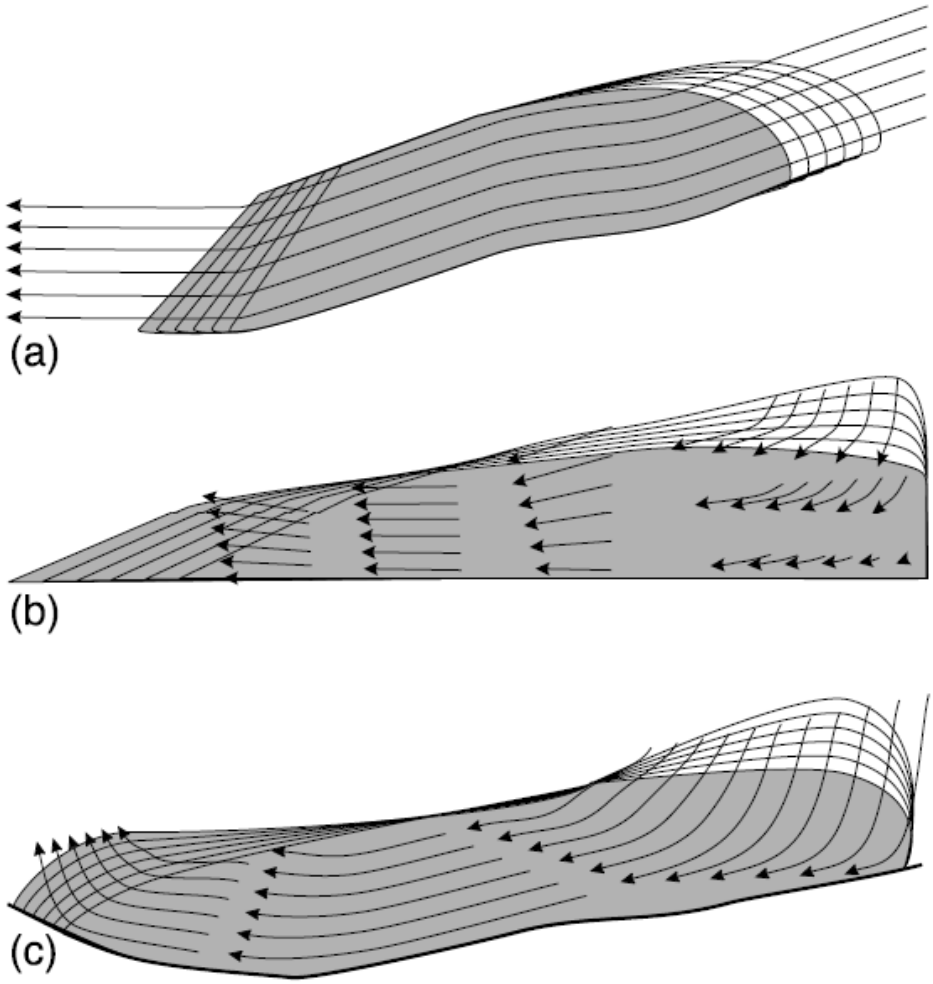

Figure 1.2 - Gravity gliding and spreading, Rowan *et al.* (2004). a. gravity gliding in which a rigid block slides down a detachment; (b) gravity spreading, in which a rock mass distorts under its own weight by vertical collapse and lateral spreading; and (c) mixed-mode deformation.

1.2.2 Overpressure

Overpressure occurs in sedimentary basins around the world (Fig. 1.3). Basins in southeast Asia, offshore Australia, in west Africa, Azerbaijan, off the east coast of north America, in the Gulf of Mexico, in the Caribbean or offshore Brazil show a number of examples of gravity detachment systems taking place over high pore pressure detachment strata in shale-rich successions (e.g. Barbados: Deville *et al.*, 2003; Brunei: Tingay *et al.*, 2009; Niger Delta: Cobbold *et al.*, 2009).

Figure 1.3 - Fluid overpressure around the world. After Yassir and Addis (2002).

Deformation induced by sediment weakening due to overpressure generation has been extensively discussed in the past 30 years and the concepts have evolved a lot as a result of the improvement of seismic data resolution (e.g. Day-Stirrat *et al.*, 2010; Maloney, 2011). Shale is a low permeability sediment which can weaken due to overpressure, its low strength at detachment levels being related to elevated pore-fluid pressure (Maltman, 1994). Detachment levels are potentially generated depending on strata permeability and the distribution of fluid pressure; there can be multiple detachment levels within a given system (e.g. Briggs *et al.*, 2006).

High sedimentation rates and compaction prime overpressure and trigger a number of sediment-remobilization processes such as mud volcanism, fluid escape and associated deformation (Van Rensbergen *et al.*, 2003, Huuse *et al.*, 2010; Moss and Cartwright, 2010). Overpressure is also recognized to influence deformation styles (Mourgues and Cobbold, 2003).

In poorly consolidated materials, mass movement can occur when the shear stress which takes place exceeds the material's shear strength (Maltman and Bolton, 2003), which can be defined as a function of cohesion stress-dependent internal friction and pore-fluid pressure of the material (Terzaghi, 1943), an application to the Mohr-Coulomb relation:

$$\tau = c' + \sigma_n' \tan \varphi' \qquad (1.1)$$

with τ the shear strength, c' the cohesion, σ_n' the stress normal to the plane of shear stress (or, in the case of gravity-driven deformation, the vertical stress, Sv), that is to say the effective stress, and φ' the angle of internal friction of a given material (Maltman, 1994). This state can be produced when overpressure develops. Overpressure occurs when in a given loaded sediment (application of a higher normal stress) pore-fluids have to bear part of the loading as sediment permeability is not high enough to allow fluid escape (Maltman, 1994). Overpressure can be expressed as a fluid pressure ratio (λ) and graphically represented on a Pressure-Depth plot (Fig. 1.4):

$$\lambda = \frac{\textbf{pore fluid pressure}}{\textbf{total burial pressure}} \qquad (1.2)$$

In shale-rich sediment, this ratio characterizes the capacity of the shale to behave as a fluid (Bilotti and Shaw, 2005). The principal cause for overpressure generation is disequilibrium

compaction amongst many other primers, such as chemical reactions due to diagenesis (e.g. illite-smectite transformation), thermal effects (e.g. kerogen formation, etc.) including fluid migration and buoyancy, as well as mechanical changes such as volume changes (Grauls, 1999; Swarbrick *et al.*, 2002). Disequilibrium compaction occurs when pore fluids become trapped during sediment burial as a lithostatic load is imposed on pore-fluids (Osborne and Swarbrick, 1997). The lithostatic load develops as rapid sedimentation provides an increase of sediment load where dewatering does not have time to occur. Thermal and diagenetic effects result from sediment burial either by high sedimentation rate, subsidence or structurally-induced burial. Fluid migration effects are either conducted by fluid buoyancy, especially in the case of hydrocarbons, or by pressure transfer. Transmission of high pressures by fluid flow is termed lateral transfer (Mann and Mackenzie, 1990) and can occur in tilted aquifers embedded in shale-rich successions (e.g. Swarbrick *et al.*, 2002). It has been demonstrated to be at the cause of seal failures, cold seeps and slope failures at margins undergoing sedimentation at high rates (Dugan and Flemings, 2000). Research in this field helped to identify the main triggers for overpressure and to quantify the amount of overpressure potentially in presence (Grauls, 1999).

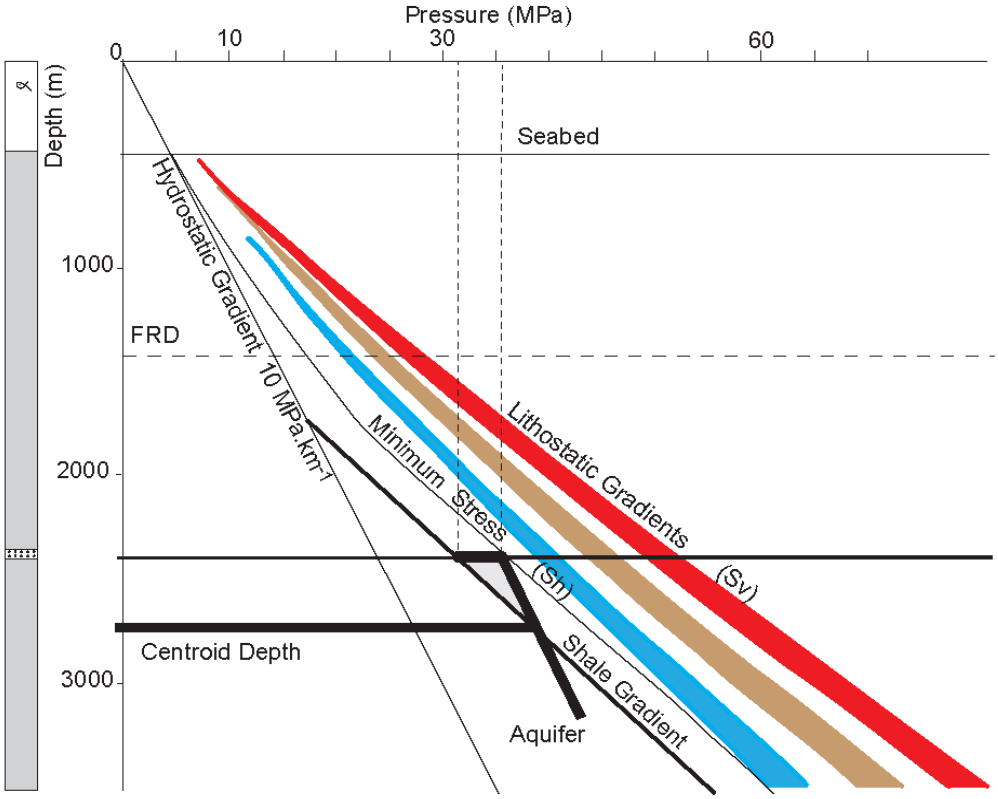

Figure 1.4 - Pressure gradients. Hydrostatic gradient, shale gradient function of the fluid detention depth (FRD, dashed line), minimum stress and lithostatic gradients for different structural settings blue: extension, brown: strike-slip, red: compression). Pressure gradient in a given tilted aquifer is shown by the thick black segment parallel to the hydrostatic gradient and the centroid depth is indicated. Overpressure is displayed in the dashed vertical lines interval. Modified after Grauls (1999) and Yardley and Swarbrick (2000).

A hydraulic fracture should develop perpendicular to the direction of minimum compressive stress (Secor, 1965; Hubbert and Willis, 1972). Fluid conduits will form if sufficient pressure is present to reach the hydraulic fracture pressure and breach the caprock of a given reservoir interval (Fig. 5.1). This mechanism has been recognized in previous studies on vertically-focused fluid flows (Hovland and Judd, 1988; Miller, 1995). Fluid-induced caprock failure implies that the reservoir pressures reaches a value close to the minimum effective stress (Grauls, 1999; Fig 1.4, *Sh*). This minimum effective stress value is function of the tectonic stress regime and thus the lithostatic gradient (Fig. 1.4; e.g. Tingay *et al.*, 2009). In order to predict pressure distribution

at the top of aquifers, an empirical method, the centroid concept has been established and tested (Traugott and Heppard, 1994; Yardley and Swarbrick, 2000; Finkbeiner *et al.*, 2001; Seldon and Flemings, 2005; Tingay *et al.*, 2009). The centroid concept assumes that within a hydrostatically pressured aquifer, there is a specific depth (centroid depth, Fig. 1.4) at which pressure is equally distributed above and below (aquifer segment parallel to the hydrostatic gradient, Fig. 1.4). The centroid is located at the intersection between the centroid depth, the aquifer pressure gradient and the shale gradient which is a given gradient parallel to the minimum stress gradient, and situated below the fluid retention depth (Fig. 1.4). The fluid retention depth (FRD) is dependent on the local sedimentation rate (Swarbrick *et al.*, 2002) and represents the depth at which fluids begin to be retained in the sediment without undergoing dewatering. This process can occur in areas where sedimentation rates are high and where dewatering cannot occur properly.

An increasing number of case studies assessing the role of high pore pressures, reservoir properties and stress regime in fluid escape have been published. For example, Reilly and Flemings (2010) present a case study showing that pore pressures can be predicted using the minimum stress in a connected reservoir. Overpressures can come both from reservoirs and deeper levels through critically stressed faults and open fractures (e.g. Tingay *et al.*, 2009). Another case study from Deville *et al.* (2010) also demonstrated the roles between the formation of deep overpressure in detachment levels and transmission to overburden aquifers and fluid escape through mud volcanism, which can be found in many deepwater environments where high sedimentation rate and structural deformation occur (Fig. 1.5).

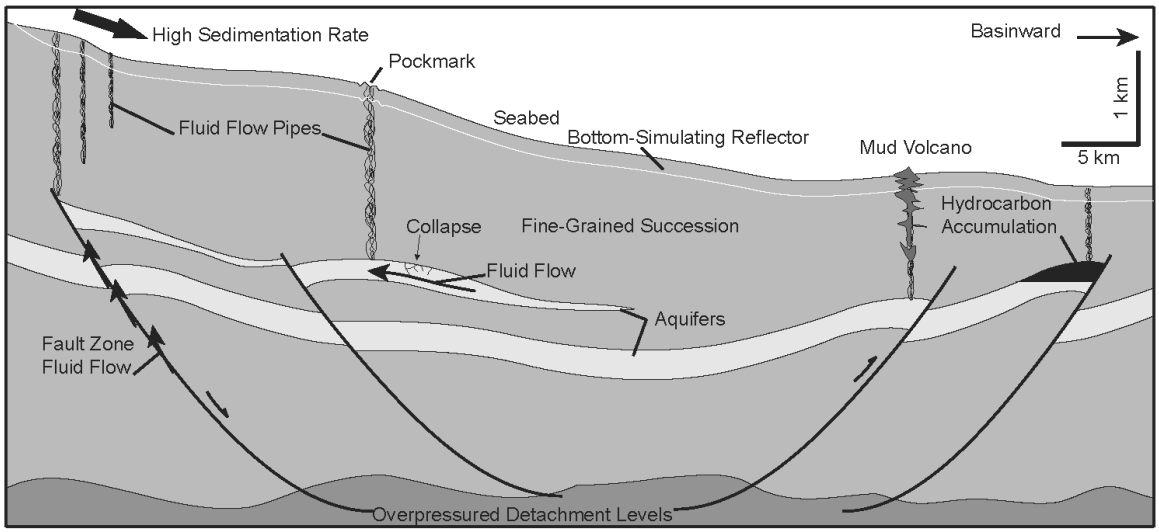

Figure 1.5 - Fluid flow, overpressure and fluid escape in a gravity detachment system. Modified after Huuse *et al.*, (2010) and Deville *et al.*, (2010).

The failure of a seal above an aquifer (water and/or hydrocarbon reservoir) can occur either by capillary seal failure, or by the development of hydraulic fractures (e.g. Cartwright *et al.*, 2007). Capillary seal failure occurs when, in a hydrocarbon-filled unit, the hydrocarbon buoyancy pressure exerted by the increasing column, exceed the top seal capillary entry pressure (Ingram *et al.*, 1999). For both water or hydrocarbon-bearing reservoir, hydraulic fractures can lead to the development of a series of fluid escape such as fluid flow pipes, blowout pipes, mud volcanoes and also sand injectites (Cartwright *et al.*, 2007). These seal bypass systems are often interpreted as direct hydrocarbon indicators in the absence of seabed sampling. However a careful assessment of overpressure development should be undertaken as these systems may not require the presence of a hydrocarbon column to develop (e.g. Bjørkum *et al.*, 1998). The identification of fluid escape is now common from 3D seismic interpretation (e.g. Cartwright *et al.*, 2007) and can help in understanding the development of overpressures and hence the local deformation history of any given gravity detachment systems. Fluid escape, especially through fluid flow pipes, is an important process which conditions to take place are not fully understood yet, and integrated

studies of the structural, stratigraphic and overpressure settings in which they occur may help in better estimating the fluid volumes that can be involved and their relationship to the evolution of gravity detachment systems.

1.2.3 Sedimentation in Deepwater Environments

Driven either by oceanographic research or hydrocarbon exploration, a large number of bathymetry and seismic reflection studies have provided morphological descriptions of Plio-Pleistocene deepwater channel systems around the world (e.g. Normark, 1978; Damuth *et al.*, 1983; Petters, 1984; Morris *et al.*, 1998; Armentrout *et al.*, 2000, Savoye *et al.*, 2000; Babonneau *et al.*, 2002; Krastel *et al.*, 2004; Heiniö, 2007). These observations, added to field studies of geological analogues, provide abundant models for deepwater sedimentary processes, summarized in a series of thorough classifications. Mutti *et al.* (2009) provided a detailed description of the state-of-the-art in turbidite systems, referring to the origins, research progress and current challenges in this research field. Deep-water sedimentary systems depositional models were first published in the early seventies from oceanographic surveys (e.g. Normark, 1978) or outcrop studies in the Appenines (Mutti, 1975). The multiplication of observations contributed to a more complex set of classifications depicting the high variability in turbidite systems. Reading and Richards (1994) proposed a series of static models established regarding their architecture according to grain size and source geometry variations. Dynamic models, which try to predict the lateral and downdip variations of sedimentary facies and architectures, are derived from sequence stratigraphic models (Vail *et al.*, 1977). These models are built within a chronostratigraphic framework of repetitive, genetically related strata bounded by surfaces of erosion or non-deposition, or their correlative conformity (Van Wagoner *et al.*, 1987), due to relative sea-level variations and sediment input. Some models show that sea-level variations only

is sufficient to explain sediment deposition patterns, whereas others use the fact that deepwater depositional controls are driven by climate and tectonic-driven sea-level changes, and sediment supply (e.g. Schlager, 1993; Fig. 1.6.A).

Deepwater fans are the most abundant sedimentary objects in deep-water clastic environments. They often are associated with gravity-driven mass-movement deposits and are formed by non-cohesive density flows, mass movement debrites and pelagic deposits. The fining upward turbidite deposits with interbedded shale were first described in detail by Bouma (1972). Sediment mobilization and deposition occur by specific processes which have been classified according to the mechanical behaviour of flow, transport mechanism and sediment support system, from elastic to plastic to viscous fluid and settling (Stow, 1986). They include creeping, sliding and slumping, debris-flow and grain flow, and eventually turbidite flows. In addition to sediment mobilisation processes, normal bottom currents, pelagic and hemipelagic settling represent the sedimentary processes occurring in deepwater environments (Stow, 1986).

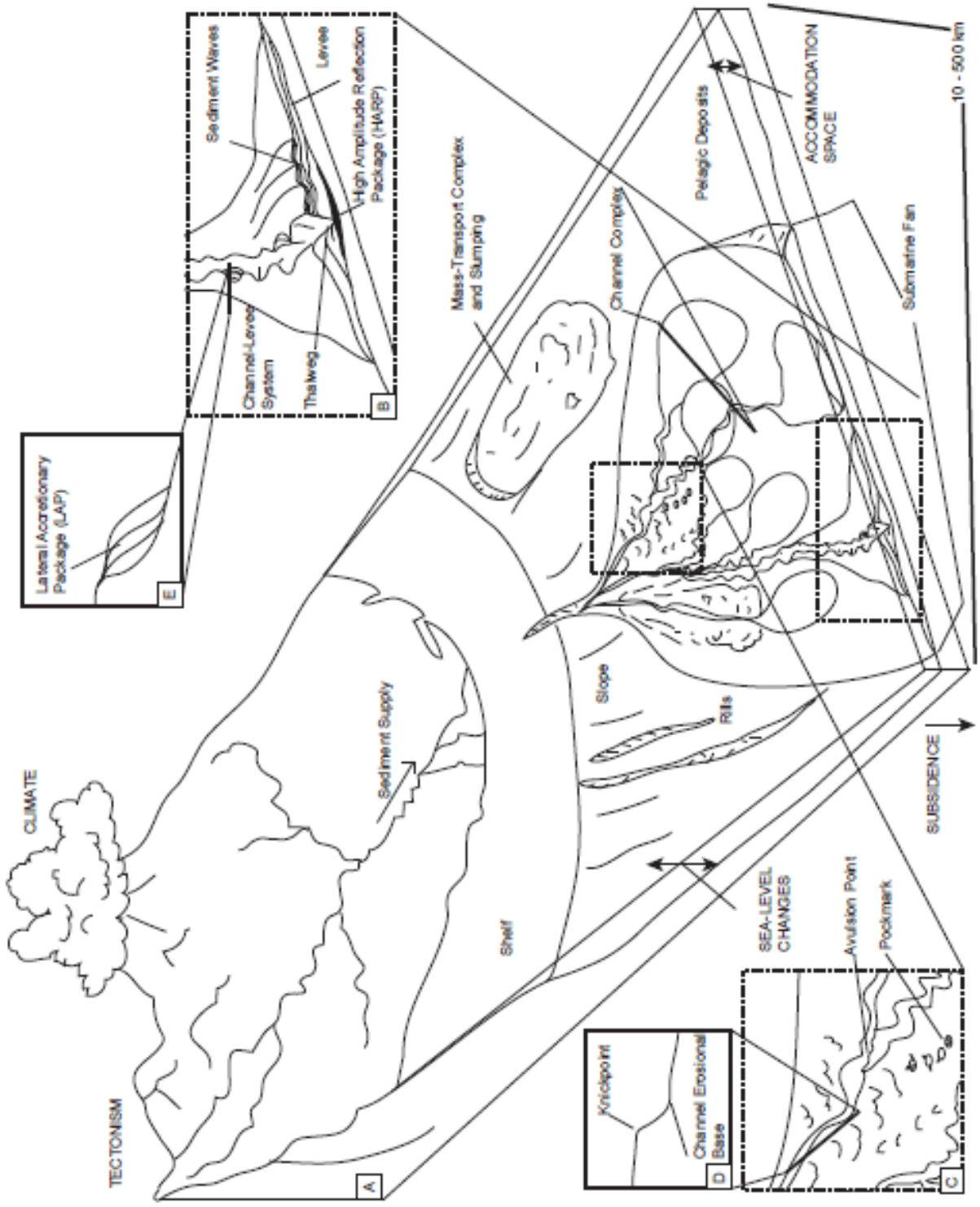

Figure 1.6 - A simplistic compilation of the main architectures and controls of turbidite systems. Compiled and modified after Abreu *et al.* (2003); Arnott (2007); Wynn and Stow (2002); Heiniö and Davies (2009); Jégou *et al.* (2008); Kane *et al.* (2008); Kolla *et al.* (2007); Migeon *et al.* (2006); Posamentier and Kolla (2003); Prélat *et al.* (2010); Schlager (1993); Wynn *et al.* (2000) and Wynn *et al.* (2007).

A lot of predictive models have been developed for turbidite systems (e.g. Stow and Mayall, 2000; Mutti *et al*., 2009). For example, Posamentier and Kolla (2003) described five key architectural elements in submarine fan systems which architecture may show the evolution and controls on the studied systems, including sinuous channel-levee systems (e.g. Kolla *et al.*, 2007; Wynn *et al.*, 2007; Kane *et al.*, 2008) sediment waves and slope failures (e.g. Wynn and Stow, 2002; Migeon *et al.*, 2006 ; Heiniö and Davies, 2009; Kane *et al.*, 2008; Fig. 1.6.B), frontal splays or distributary channels, as well as avulsion points (Fig. 1.6.C), crevasse, splay complexes and debris-flow, channels, distal lobes and sheet sands (e.g. Jégou *et al.*, 2008 ; Prélat *et al.*, 2010). In addition, detailed analyses of deepwater sedimentary systems have also been published from case studies by Wynn *et al.* (2000) and Posamentier (2003). Channel-levee systems are major depositional elements, representing sediment fairways where a basal, central erosional zone is found between levee overbanks where High Amplitude Reflection Packages (HARPs) can be found (fig. 1.6.B). These packages represent heterolithic, conglomeratic depositing after the initial canyon erosion, and pre-dating sand deposition. In the incised channel, sedimentation occurring in sinuous channels can also form terraces and/or Lateral Accretion Packages (LAPs; e.g. Abreu *et al.* (2003); Arnott (2007); fig. 1.6.E) filled with sands and silts. Terraces develop as deposits in the canyon are re-eroded by following flows while LAPs represent successive stages of deposition (e.g. Abreu *et al.*, 2003).

Post-depositional processes such as diagenesis and differential compaction can cause overpressure and fluid flow (e.g. Davies, 2003). They can result in pockmarks (e.g. Loncke *et al.*, 2004) and fluid flow pipes formation (e.g. Davies and Clarke, 2010; Moss and Cartwright, 2010). Other processes affecting the sedimentary record in deepwater settings also include structural deformations (e.g. faulting, folding and salt diapirism) which are also able to create topography and slope instabilities and climate variations controlling sediment supply (e.g. Kneller *et al.*, 2009).

1.2.4 Strike-Slip Faulting

Strike-slip deformation occurs when the vertical stress is equal to the lithostatic stress, so that subvertical deformation on a subvertical plane mainly occurs in a horizontal direction (Christie-Blick and Biddle, 1985). Strike-slip fault zones display a well-defined range of associated structures from synthetic Riedel shears; antithetic, conjugate Riedel shears (R'); P-shears, tension fractures and en-echelon folds (Fig. 1.7.A; Christie-Blick and Biddle, 1985). Structural complexity is extreme and deformation varies from compression (transpression, where a "positive flower structure" can be observed; Harland, 1971; Sylvester and Smith, 1976) to connected extension (transtension, where a "negative flower structure" develops, Fig. 1.7.B, C, D, E and F; Harland, 1971). Fault complexity is also illustrated by strike-slip duplexes (Woodcock and Fischer, 1986). The deformation kinematics, magnitude of the displacement, rock properties and fluid contents as well as pre-existing faulting or lineaments strongly affects the development of strike-slip fault zones complexity (Christie-Blick and Biddle, 1985).

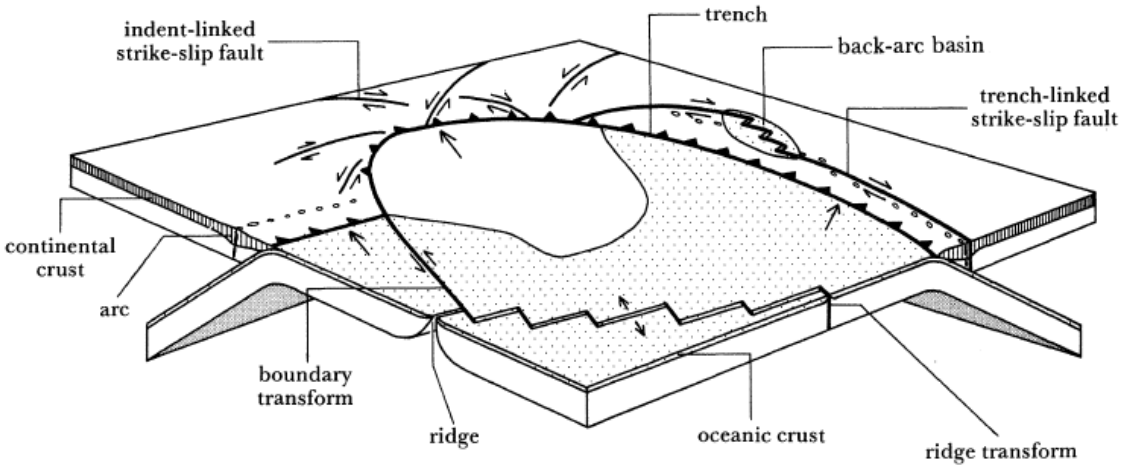

Figure 1.7 - Strike-slip faults in their plate boundary settings. Woodcock and Daly (1986).

Strike-slip faults develop in all kinds of active structural setting (Woodcock and Daly, 1986; Fig. 1.7). When they occur, more rarely, in seismically quiet regions, as a result of loading by crustal thickening and flexural subsidence, they are called wrench or tear faults). In a strike-slip fault zone, both extensional and contractional faults and folds develop in respect to the strain ellipse, and can respectively form releasing and restraining bends in step over areas. Sedimentary basins can develop as a result of this complex deformation (Fig. 1.8.A and B). Basins associated with strike-slip faults are small and the evolution of their fill is strongly linked to structural growth. Sedimentary fill reveals the highly asymmetrical aspect of these basins and subsidence rates are high (e.g. Crowell and Link, 1982; Fig. 1.8.C, D and E). Nilsen and Sylvester (1995) identified the fault bend basins associated with releasing bends (e.g. the Vienna Basin), transrotational basins (Los Angeles Basin) or transpressional basins (Ventura Basin, California) and the overstep basins between the ends of two sub-parallel strike-slip fault segments (e.g. the Dead Sea Basin). Restraining bends and pull-apart basins may develop when different fault segments are sufficiently developed to join and link together, as commonly observed in natural examples and physical experiments, (e.g. Cunningham and Mann (2007); Fig. 1.8.F).

Harding (1974 and 1985) described in detail the seismic identification of hydrocarbon traps in strike-slip settings. Strike-slip faults on seismic data need to be analyzed from both seismic profiles and maps as the structural styles they display along-strike is highly variable. Strike-slip deformation can involve prolific hydrocarbon plays and geometries are fairly predictable.

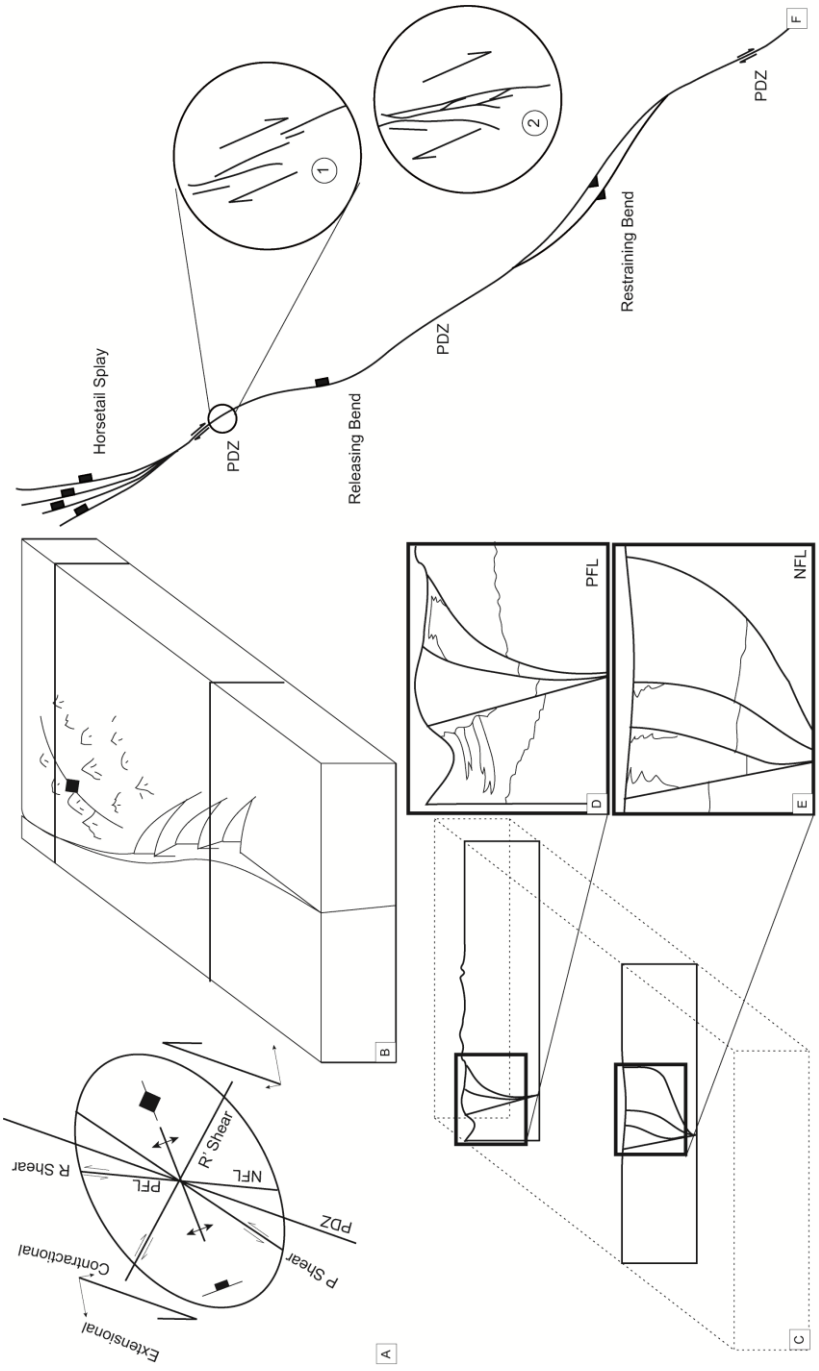

Figure 1.8 –Strike-Slip Fault Zone and Associated Basins. Modified from Crowell (1974), Crowell and Link, (1982), Christie-Blick and Biddle, (1985) and Woodcock and Schubert, (1994). A. Angular relations in right-lateral simple shear and Riedel shears. B. 3D model showing areas of subsidence and uplift along the strike a strike-slip fault zone. C. D. and E. Positive and negative flower structures. F. Evolution of a given strike-slip fault zone and representation of shears (1. Early development; 2. Late development). PDZ stands dor "Principal Displacement Zone"; PFL: Positive Flower structure ; NFL : Negative Flower structure.

The development of tear faults represents a differential displacement within the sedimentary cover between structural units (Christie-Blick and Biddle, 1985). The term "tear fault" may refer either to a crustal fault or flexure linked to either extensional or compressional activity (e.g. Escalona and Mann, 2006) or an individual strike-slip fault in a sedimentary basin. In this thesis, tear faults represent this second type of faulting. It has been reported in gravity detachment settings, for example in the Niger Delta where its potential role in controlling submarine channel systems location was mentioned (Armentrout *et al.*, 2000 and Morgan, 2003 and 2004), and shown on structural maps (Cobbold *et al.*, 2009), and also in the Gulf of Mexico at the edges of "cells" detaching over salt layers and defining the lateral margins of the gravity detachment system (Jackson and Vendeville, 1994; Peel *et al.*, 1995). However their nature and origin in gravitational settings has not been fully analysed, and our current knowledge about tear faults is limited to the fact that they can link extension to compressive domains, and accommodate different behaviour between structural units.

1.2.5. Current Research Issues

Current research in the study of deepwater setting sedimentary processes is still ongoing and has applications in understanding the evolution of sedimentary history of basins as well as predicting reservoir architectures. Looking at near-seabed geological processes can provide insights into depositional processes (e.g. Steffens *et al.*, 2004). Key questions including the significance of sediment record in turbidite beds regarding external, climate-induced controls or local topographic effects are investigated (e.g. Kneller, 1995). The self-confinement in turbidite channel systems is a current major research topic and currently seems to be a result from initial turbidite flow confinement into erosional fabrics or topographic troughs caused by deformation

(e.g. Straub and Mohrig, 2009; Fildani *et al.*, 2012; Brunt *et al.*, 2012). Local structural and topographic controls can also contribute to sediment fairways confinement. They have largely been documented by 3D seismic-based studies in extensional and contractional settings as well as around salt diapirs (e.g. Anderson *et al.*, 2000; Haughton, 2000; Hooper *et al.*, 2002; Broucke *et al.*, 2004; Gee and Gawthorpe, 2006; Hubbard *et al.*, 2007; Clark and Cartwright, 2009 and 2011; Cross *et al.*, 2009; Catterall *et al.*, 2010; Mayall *et al.*, 2010). In this respect the behavior of submarine sediment routing systems in strike-slip settings may have been overlooked in the 3D seismic record.

Deformation mechanisms above multiple detachment levels and triggers for detachment weakening processes, such as overpressure build-up have also recently been analysed (Bilotti and Shaw, 2005; Corredor *et al.*, 2005; Briggs *et al.*, 2006; Mourgues *et al.*, 2006; Gonzales-Mieres and Suppe, 2006; Cobbold *et al.*, 2009) and modelled (e.g. Ings and Beaumont, 2010). Ongoing discussions about overpressure mention potential multiple origins for priming mechanisms of overpressure, such as hydrocarbon cracking (e.g. Cobbold *et al.*, 2009) and at shallower levels in porous reservoirs, generating hydraulic fracturing (Løseth *et al.*, 2010). Lastly, a number of studies evaluated the role of external controls on the development of deepwater fold-and-thrust belts, notably the role of the basement acting as a buttress (e.g. King *et al.*, 2009; Morley *et al.*, 2011; Sellier *et al.*, 2011). Most regional and sub-regional studies on gravity detachment systems concentrate on an updip to downdip analysis (e.g. Cobbold and Szatmari, 1991; Morley and Guerin, 1996; Rowan *et al.*, 2004; Corredor *et al.*, 2005; de Vera *et al.*, 2009). The current knowledge about lateral margins of gravitational collapse is currently limited to a few examples, mostly from mass-transport complexes (e.g. Maltman, 1994; Bull *et al.*, 2009), with an exception to “cells” above salt detachments (Peel *et al.*, 1995). In addition, recent research contributions re-assessed “mobile shale” detachments and overpressure development, showing that deeply buried

shale-cored folds and imbricate thrusts, as well as folds associated with kilometre-scale blowout pipes have previously been misinterpreted (e.g. Day-Stirrat *et al.*, 2010; Morley *et al.*, 2011; Maloney, 2011). These recent observations prove that there is a need to re-examine individual "shale diapirs". Current research interests also concentrate on seismic-based interpretation of individual structures, extensional (e.g. Maloney *et al.,* 2010) and contractional (e.g. Higgins *et al.*, 2007 and 2009; Iacopini and Butler, 2011), in order to reconstruct the deformation kinematics and better model potential hydrocarbon traps geometries and fluid migration pathways (e.g. Cobbold *et al.*, 2009). These studies show the internal complexity and faults linkages within contractional domains of gravitational collapses. Despite the fact that the existence of lateral margins in mass-transport complexes has been demonstrated to be important to understand deformation kinematics (e.g. Bull *et al.,* 2009) and does exists at passive margins (e.g. Rowan, 2009), little work has focused on these lateral margins and their implications for sedimentation and structural styles. Recent works from Morgan in the deepwater Niger Delta (2003 and 2004) relate the potential importance of strike-slip faulting, notably basement-induced (transfer) fault controls for channel systems location and petroleum systems. Further investigations in this direction may therefore be interesting in other areas of the Niger Delta to understand the importance of these zones in gravity detachment systems.

1.3 Thesis Objectives

1.3.1 Focus of the Study

The goal of this study is to characterize specific deformation and sedimentary processes occurring at the lateral margins of gravity detachment systems. Regional seismic mapping is carried out as well as detailed observations of the relationships between sediment routes and deformation. Few studies have focused on gravity-driven strike-slip faulting in deepwater settings

and its consequences on sediment routing systems. Herein we assess the sediment routing response to slope-parallel syn-sedimentary tear faults using examples from the western Niger delta and offshore Mauritania. Close attention is also paid to a case study over a sub-circular antifom where interactions between submarine channel systems, structural deformation and overpressure development are illustrated. Evidence for deformation timing and geometric relationships as well as connections to detachment mechanisms are expected to be found. It can also be assumed that in association to these processes, predictions in terms of channel morphologies and sediment bypass in strike-slip fault zones will be made. The results and implications of this project may improve the current integrated models of gravitational collapse.

1.3.2 Thesis Outline

Further to this introduction chapter, this thesis is organized into five chapters:

- Chapter 2, "Methodology, Data and Geological Settings", provides background information on 3D seismic analysis, the data used in this study and the geology of the Niger Delta and offshore Mauritania;

- Chapter 3 investigates the structural framework of the study area, located at the lateral edge of the Niger delta western deepwater sedimentary lobe, using 3-D seismic reflection data. The work in this chapter has been published as: "The Lateral Strike-Slip Domain at the Margins of Gravity Detachment Systems: A Case Study from the Western Niger Delta", in *AAPG Bulletin*, a copy of which can be found in the Appendix. Over 70 % of the final paper is my own work with remaining 30 % from the other authors. Contributions by the authors to the manuscript are as follows: Leduc (seismic interpretation, manuscript and

figure preparation) Davies, Imber and Densmore (integration of interpretation and manuscript editing advice).

- Chapter 4 describes a potential model for the structural confinement of submarine turbiditic slope channels in tear fault zones. This chapter integrates the results from the region structural assessment in the Niger Delta, presented in chapter 3, and uses additional 3-D seismic data located in another area of the western Niger Delta, as well as from offshore Mauritania. This chapter is based on a manuscript entitled 'Gravity-driven tear faults: a control on sediment routing in deepwater settings', and submitted to *Basin Research* in January 2013, a copy of which can be found in the Appendix). Approximately 85 % of this paper is my own work, with Davies, Densmore and Imber contributing approximately 15 %. Contributions by the authors are as follows: Leduc (original idea, seismic interpretation, manuscript and figure preparation), Densmore (advice for channel morphological analysis and manuscript preparation) and Davies and Imber (manuscript editing advice).

- Chapter 5 investigates the development of kilometre-scale hydraulic fractures and the structural and stratigraphic framework in which they form, and produces an attempt to pore-pressure prediction. The work in this chapter entitled "Fluid Flow Pipe triggered by lateral pressure transfer in the deepwater western Niger Delta" is published in *Marine and Petroleum Geology*, a copy of which can be found in the Appendix. Approximately 60 % of the final manuscript is my own work, with Swarbrick contributing 10 % and Davies, Imber and Densmore contributing the remaining 20 %. Contributions by the authors to the manuscript are as follows: Leduc (seismic interpretation, manuscript and figure preparation), Swarbrick (advice work on overpressure and overpressure theory,

manuscript editing), Davies, Imber and Densmore (advice for structural model and manuscript editing advice).

- Chapter 6 includes a general discussion of key findings and their implications in terms of research and future work, as well as conclusive remarks.

Chapters 3, 4, and 5 cover the main objectives of this thesis and have been written and prepared as manuscripts that have either been published, accepted for publication or are in review in peer reviewed journals. Each of these chapters therefore contains its own *introduction*, *geological setting*, and *data and methodology* section, which cover some of the points from Chapters 1 and 2. In Chapters 3, 4 and 5, pronouns referring to the author (myself) appear in the plural form (*i.e. we* replaces *I*) throughout as an acknowledgement of co-author in the manuscripts. The thesis only contains manuscripts for which I am the first author. Davies, Densmore and Imber conceived the original project, and in Chapters 3, 4, and 5 all authors listed contributed to the development of the ideas during discussions. A full reference list and additional material gathered in the appendices section are provided at the end of this thesis manuscript.

CHAPTER 2: METHOLOGY, DATA AND GEOLOGICAL SETTING

2.1 Background and Overview

This chapter provides background information about the data and methodologies chosen. It then sets the currently known geology of the areas of interest and states the limits of the study. Subsurface geological mapping techniques greatly improved over the 20th century with the advent of seismic reflection surveys. The principles of three-dimensional (3D) seismic data acquisition were set from the 1970s (Tegland, 1977), commercial use for hydrocarbon exploration purposes began in the 1990s (Shell exploration surveys), and it is currently common to acquire, process and interpret seismic data for industry exploration and development, as well as academic research purposes. 3D seismic data represent a major improvement in data resolution and sampling compared to 2D data, but for time volumes, acquisition, processing and interpretation procedures remain the same.

This study is based upon seismic data that were acquired to conduct offshore hydrocarbon exploration where some geological processes are still yet to be understood. A cluster of three adjacent, but not merged, seismic datasets located at the northwest margin of the offshore western Niger Delta was provided by PGS and ENI. Further southwest of these three datasets, another 3D dataset was made available by CGG Veritas with a set of 2D data covering the ultradeep water domain of the Niger delta. In addition, a fifth 3D dataset from offshore Mauritania was provided by Tullow and Petronas; data are of comparable quality and record an analogous succession to the Niger Delta deposits. Data analyses are expected to help building a comprehensive model integrating the structural specificities of the study and their interactions with sediment routing systems.

2.1.1. Seismic Reflection

This section covers some background principles behind seismic data (after Kearey *et al.*, 2002 and Bacon *et al.*, 2007). Seismic reflection data record contrasts in acoustic impedances as the acoustic P-waves propagate at depth through media of varying velocity and density and reflect back at media interfaces (dioptres). The technique relies on an application of the Snell-Descartes law:

$$\frac{\sin i}{v_1} = \frac{\sin t}{v_2}$$

where "i" is the angle of reflection, "t" the angle of incidence, v_1 the velocity of a given medium and v_2 the velocity of a deeper medium, assuming $v_2 > v_1$ (Fig. 2.1).

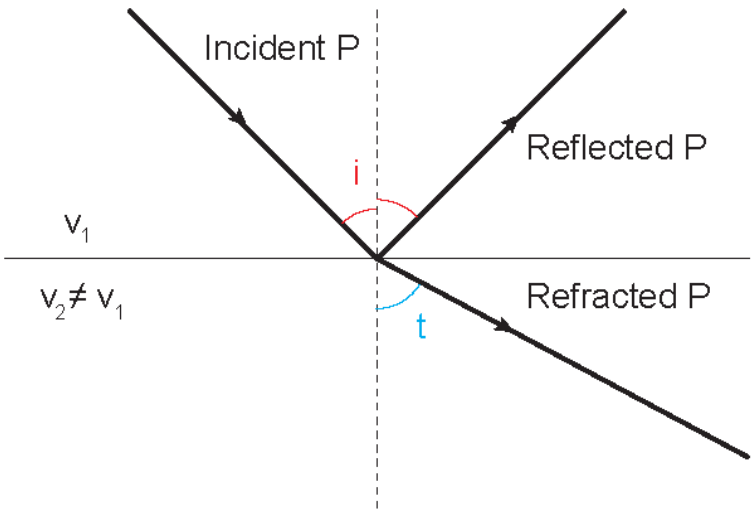

Figure 2.1 - Reflected and refracted P-wave rays associated with a P-wave ray obliquely incident on an interface of acoustic impedance contrast. The red angle is the angle of incidence and the blue angle is the angle of refraction (after Kearey *et al.*, 2002).

In seismic reflection surveys this law is applied in order to acquire an acoustic image of

the sub-surface. In the case of offshore surveys an air gun is used as a source to send elastic waves that penetrate the sub-surface, propagate at depth and reflect at encountered lithological interfaces. These reflected waves are then retrieved by hydrophones on a streamer and recorded as seismic traces. Multichannel seismic acquisition is used in order to reduce potential noise recorded on these traces, which reduces the reflection amplitudes with depth and introduces artifacts (Lansley, 2004). In order to record accurate seismic data, the horizontal reflector sampling distance is typically half of the detector (geophone or hydrophone) spacing. The vertical resolution of the recorded data only remains accurate in the "Fresnel zone", in which seismic waves are returned within half a wavelength of the reflected input. Seismic reflection traces can be considered as the convolution of the input pulse from the source with a time succession of spikes, termed the reflectivity function. Seismic reflection traces are measured in seconds two-way travel time, noted "twt" (Fig. 2.2). In order to obtain 3D seismic data, acquisition is carried out along a grid composed of (downdip) in-lines and cross-cutting traces separated by a defined interval (bin size) of typically 10-20 m. This scaling allows detailed interpretation of geological features. In comparison, 2D data are acquired with a line spacing of 100-1000 m and above that suits regional-scale interpretations. The orientation, extent and frequency parameters of seismic surveys are selected according to the geographical features of the surveyed area. In this research, the provided data were supplied processed and limited information was available to identify the different processing steps done on the datasets.

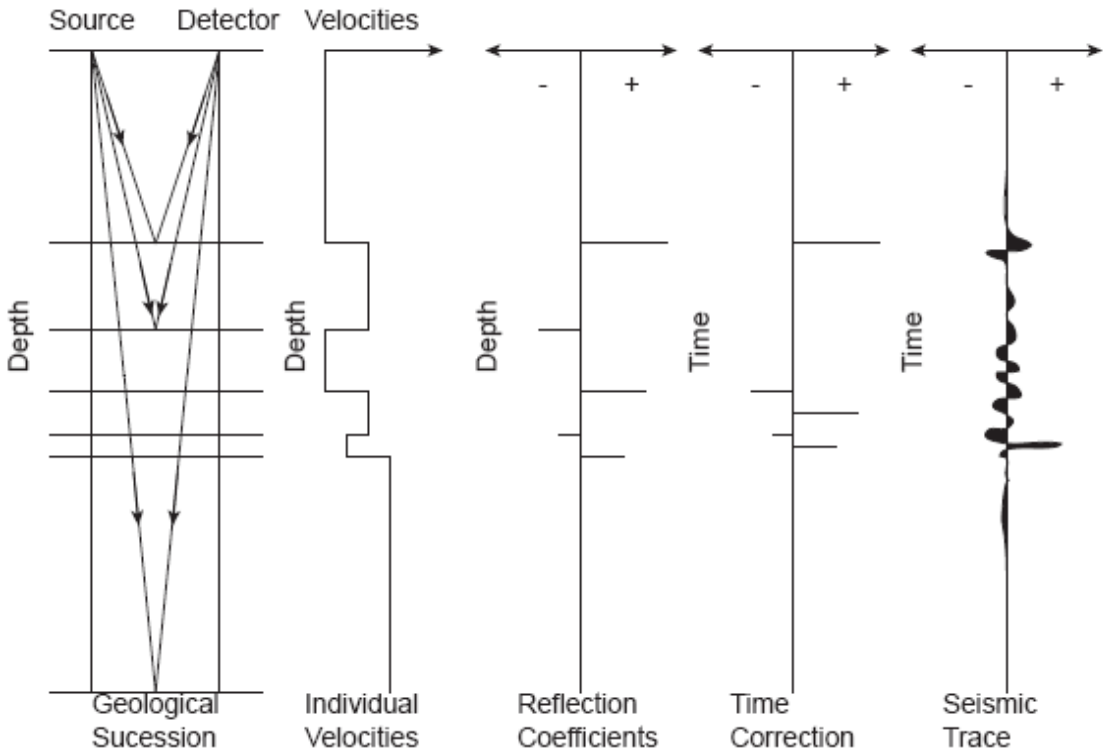

Figure 2.2 – Physical approach to the seismic trace. The trace is composed of seismic wavelets, and is obtained from a record of seismic wave reflection on lithological variations at depth. The wavelets are established with the individual velocities of each reflection, their coefficient and a time correction (e.g. Kearey *et al.*, 2002).

Once the data are acquired and gathered, they go through seismic processing. It consists in a series of binning, spatial filtering and repositioning (including time and spatial migration as well as dip moveout), which are applied on individual seismic traces to maximize the useful signal bandwidth so that accurate geological information is displayed. For 3D seismic data, an additional 3D migration also needs to be done as the initial data acquisition path may not be a straight line and may be disturbed at depth by structural complexities (French, 1975; Brown, 2004). Some filtering, gain, deconvolutions and mutes are also applied to reduce the noise present in the data record, and to calibrate the seismic data frequencies and amplitudes. The processed data are then stacked and can be zero-phased. Data display may differ from one dataset to another: the polarity in which they are displayed can be defined where a trace wavelet indicates a high contrast in

acoustic impedance (Fig. 2.3). This study is based on zero-phased data under both European and American conventions (Brown, 2004), so that an increase in acoustic impedance is represented by a transition from a trough to a peak.

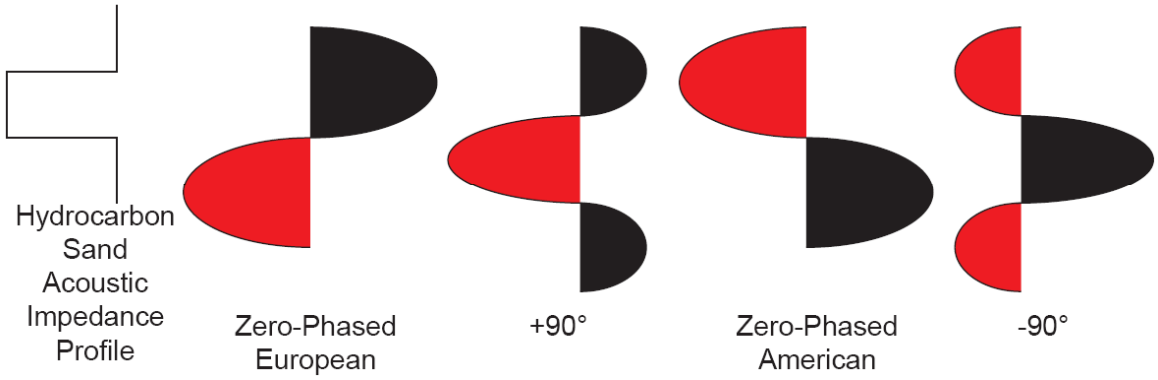

Figure 2.3. Phase and polarity conditions for a low-impedance interval (after Brown, 2004). This example shows a typical response for hydrocarbon sands. In comparison to the illustration, seabed reflections on the same data display would show a reverse signal (high amplitude).

When the frequency content is constant and the data are zero-phased, it is possible to determine the tuning thickness. This is the bed thickness at which two events become indistinguishable in time, and is expressed by:

$$Z = \frac{Vi}{2.8} * fmax$$

Where *Z* is the tuning thickness of a bed, equal to ¼ of the wavelength, *Vi* the internal velocity of the target horizon, and *fmax* the maximum frequency in the seismic section (Bacon *et al*., 2007).

Seismic reflectors indicating contrasts in acoustic impedance can localize a vertical variation

in lithology and/or fluid contents. On a seismic section of multi-trace seismic data, the distribution of seismic reflectors in horizons follows time lines (Vail and Mitchum, 1977). The mapping of seismic reflectors in two-way time can provide accurate geological information from their lateral extent, amplitude, truncations and correlations (Kearey *et al.*, 2002). To establish an accurate geological model, and in the absence of pre-stack depth migrated volumes (psdm) structural and stratigraphic interpretations done in two-way travel time should then be converted to depth below the surface – this can be done via an appropriate seismic velocity model. For basin analysis purposes, seismic velocity models are established from known lithologies and densities encountered in an area, using wells and corrected seismic stacking velocities (Yilmaz, 2011).

2.1.2 Seismic Interpretation

In these sections an overview of the methods used in this study is presented, before introducing the seismic interpretations work which has been done for this study.

2.1.2.1 Horizons Interpretation

In order to interpret the stratigraphic evolution and geometries of a basin sequence stratigraphy (Vail and Mitchum, 1977) is generally used. It is a technique that allows the definition of a global-scale chronostratigraphic framework based upon horizon discontinuities and the correlation of depositional units using the global record of sea-level changes (Van Wagoner *et al.*, 1987). In addition, interpretations in terms of seismic geomorphology (Posamentier, 2004) allow a better understanding of depositional features from 3D seismic data. Seismic geomorphology is defined as the analysis of depositional elements in plan view images extracted from 3D seismic volumes. Such analysis can easily be applied to near-seabed depositional features (Posamentier *et*

al., 2003) in order to model deeper exploration targets. Morphologies reflect the way deposition occurred and became preserved, and can help in interpreting lithologies. In deepwater environments it is possible to identify depositional processes (e.g. sediment waves, mass-transport) their associations and their evolution (channels sinuosity, erosion patterns, fill). As a result, this kind of analysis can be applied of the study in order to understand the deepwater sedimentary processes which took place in the study area and how they evolved with time.

More specifically, the identification of patterns in seismic reflections, or "seismic facies" can depict specific sedimentary architectures (Fig. 2.4) and provide information on the evolution of sedimentary basins. For example, onlapping geometries indicate an aggrading sedimentary fill; toplaps are typical horizon reflection discontinuities found beneath erosion surfaces and downlaps may indicate sediment progradation (Fig. 2.4.A). Similarly, horizontal parallel reflections depict the absence of any disturbance in sedimentary fill; draped facies indicates a sedimentary fill over a topographic or depositional feature; divergent facies shows an increase in accommodation for sediment fill; oblique facies denote a lateral variation in sedimentary fill and thickness; sigmoidal reflections visible as clinoforms represent a prograding and aggrading sediment package ; and chaotic (or hummocky) reflections imply either a complex sedimentary fill, or a structurally disturbed area, or even strong disturbances in seismic reflections caused by a loss in resolution (Fig. 2.4.B). Seismic facies analysis hence helps in studying the internal parameters of the evolution of a sedimentary basin, defining seismic units and understanding facies repartition, and also provides a stratigraphic framework to assess vertical associations and structural features through relative chronology. This kind of interpretation can be done on both 2D and 3D seismic data, and is mainly used in this study to identify specific seismic packages; unit compartmentalization caused by faulting and fracturing; and depositional architectures.

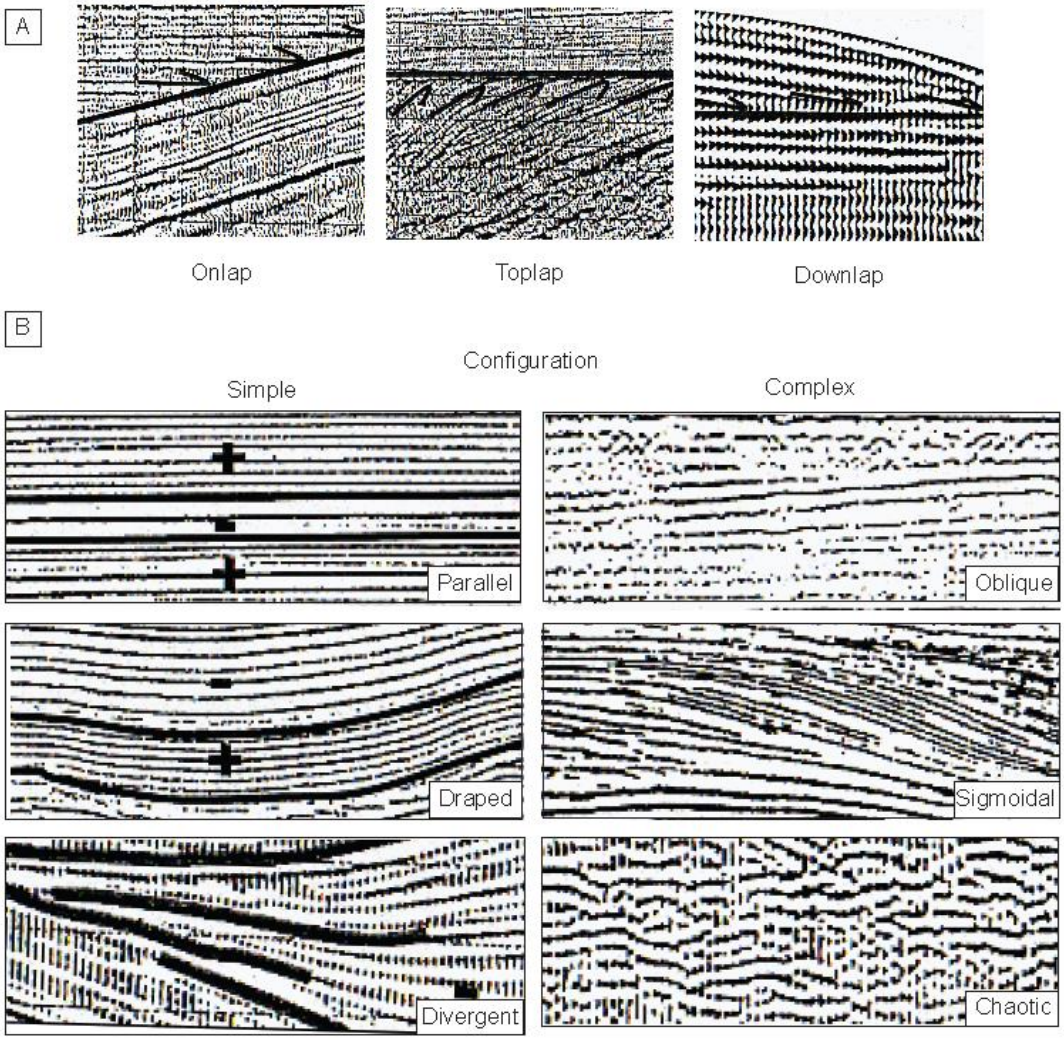

Figure 2.4 - Seismic reflection packages. After Nely (1985), adapted from Sheriff (1980). A. Reflection discontinuities often seen at the boundary between different seismic units. B. Different types of reflection spatial relationships can indicate different depositional processes, environments and lithology.

Interpretation is generally done according to a grid which mesh is defined by the interpreter who can either opt for a loose or tighter "seed" interpretation regarding encountered structural complexities or horizon discontinuities. Ideally the input interpretation grid should be as tight as possible considering the amount of time it takes to obtain a relevant framework. This "seed" interpretation is then laterally propagated using the "Zap" function (Landmark, 2005). Once a horizon is completely interpreted, it is then possible to compute structural maps, including

contours, in order to point out the structural framework of the studied area. Horizons to be interpreted are selected for their extensive lateral continuity and age interpretations are usually only provided once interpretation is complete.

2.1.2.3 Seismic Attributes

Seismic reflection data contain information on basic attributes such as (geological) two-way time and amplitude. Post-stack attributes can also be extracted along one reflection horizon or through a window and displayed on a map view. Attribute maps interpretation is an additional tool in 3D seismic interpretation that again helps in defining more clearly, at a local scale, the structural and depositional environments (Brown, 2004). Time-derived attributes such as isochron or dip magnitude from selected horizon reflections (and windowed coherence for one dataset), as well as horizon amplitude extractions are generally available. The isochron attribute can be computed within a window defined by a top and a bottom horizon. It can be of interest to identify variations in thicknesses. The dip magnitude is computed at the surface of a single horizon and indicates the variation in dip of seismic reflections. It is of interest in the near-seabed to highlight features reliefs and discontinuities at the edges of depositional features or induced by faulting and fracturing (Dalley *et al.*, 1989). At depth its use however becomes limited by additional noise, partly caused by data resolution loss. Coherence is an attribute that can be added to seismic volumes and highlights the variations in seismic reflection continuity. It is used for locating abrupt changes notably caused by the presence of faults. Lastly, amplitude extractions can be computed as a Root Mean Square (RMS) or a Maximum Average Amplitude (MAA). Amplitude extractions display on a map view changes in amplitudes that can be caused in ideal conditions by lithological and fluid contents changes (Brown, 2004). Seismic attributes are largely used both in current 2D and 3D seismic interpretation studies for a variety of purposes, including structural analyses (e.g.

Yilmaz, 2001; Chopra and Marfurt, 2005; Morley, 2009; Iacopini and Butler, 2011) and high-resolution evaluations of sedimentary responses to structural growth (e.g. Frey-Martinez *et al.*, 2005; Heiniö and Davies, 2006 and 2007; Mayall *et al.*, 2010).

2.1.2.3 Artefacts and Pitfalls

Understanding the geophysical principles behind seismic data is essential to make accurate geological interpretations. Data acquisition and processing are assumed to be accurate by the interpreter, but they are not perfect techniques (Brown, 2004). There are many possible sources of misinterpretations from the way seismic data were acquired and processed to the interpreter's choices. Among the issues that can be found in the interpretation process, multiples, seismic pull-up or pull-down are fairly common.

The primary reflections are generally considered as most relevant to geological record. Some raypaths may however return to the surface after incurring more than one reflection during its travel. These reflections are called multiples (Bacon *et al*., 2007). The imprint of multiples is attempted to be removed during processing, but some may remain in the final processed data. These multiples have generally lower amplitudes than primary reflections as they lose energy at each reflection interface. They can also cross cut true strata reflections.

Seismic reflection pull-ups are caused by localized variations in seismic velocities, deforming the reflections in the time domain. This is often encountered in salt successions or when seismic reflections traverse fluid-rich units. Conversely, seismic pull-downs represent a rapid decrease in velocity. They can be seen below extensive erosion surfaces for example. In this study data come from a deepwater environment where steep structures and seabed deep

channel incisions can be encountered and the likelihood to observe pull-downs and associated pull-ups exists. These velocity effects are removed as much as possible with seismic processing but some may remain present in provided seismic volumes (Kearey *et al.*, 2002).

Other issues are related to pitfalls of seismic interpretation. They include mapping across fault zones or "over-interpreting" an area of poor data resolution may corrupt the interpreted seismic model. In addition the resolution of seismic data must be kept in mind when trying to reduce uncertainties (Stewart, 2011). Lastly, direct interpretations of lithology and fluid contents from attribute maps or sections should be done with care, especially with the identification of "direct hydrocarbon indicators" (e.g. escape chimneys; Yilmaz, 2001; Davies *et al.* 2004). This could be a potential issue for this study as it is interested in understanding sediment patterns and their potential for being hydrocarbon reservoirs. In order to avoid the wrong interpretations it is therefore necessary to test the viability of the interpretations (lateral extent, use of different attributes maps) and assess the visibility of the seismic reflections of interests through different vertical scales.

2.2 Datasets

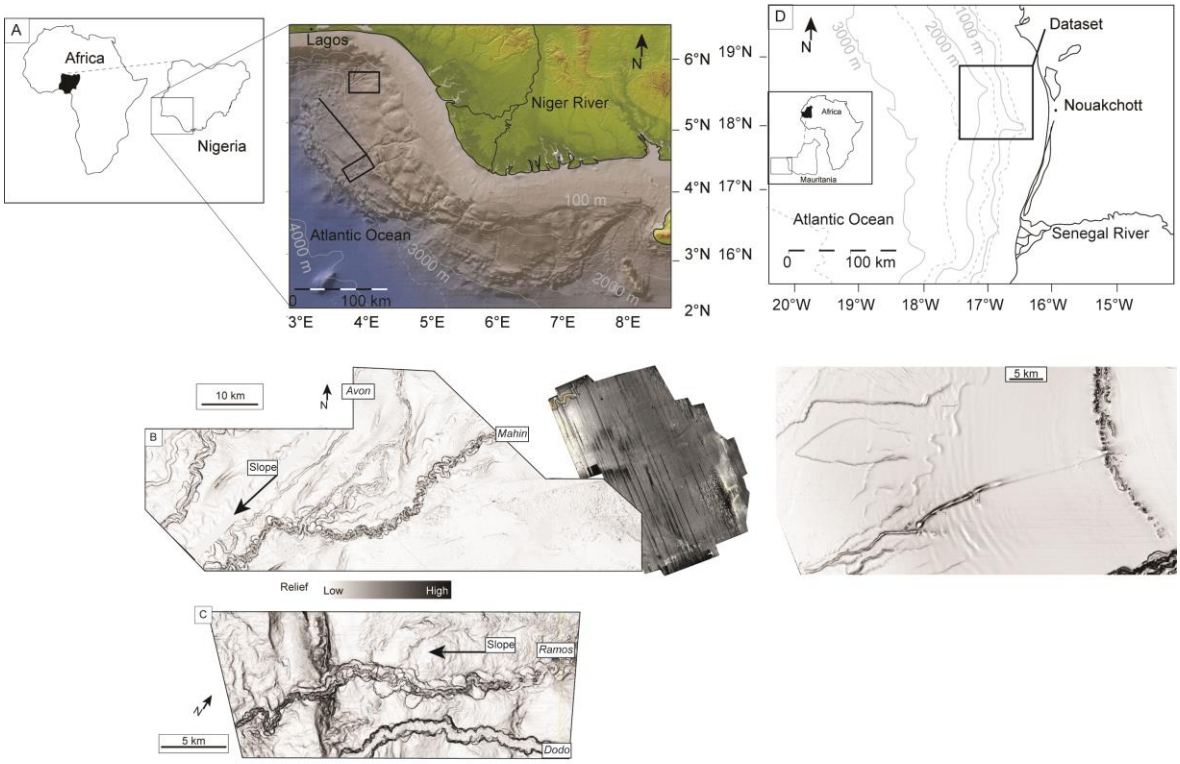

Figure 2.5 - Location of the five 3D datasets and the 2D seismic line used in this thesis. A. Location of OPL 314, 315, 316 and 324, offshore Nigeria. B. OPL 314, 314 and 316 (from west to east) adjacent datasets. C. OPL 324 dataset. D. Offshore Mauritania dataset.

In the Niger Delta a regional 2D and a local 3D dataset (Fig. 2.5; over Oil Prospecting Licence – OPL – 324) from CGG Veritas as well as two adjacent, but not merged, 3D seismic datasets from PGS (over OPL 321 and 323, formerly 314 and 315) were available at Durham. An additional 3D dataset (now called Oil Mining Licence – OML – 125 but formerly covering, and here called OPL 316) was accessible in Milan. "Coherency" volumes were only available in Milan for the 315 and 316 3D datasets. 3D seismic data from offshore Mauritania were also used in Durham in order to supplement observations made in Nigeria.

2.2.1 CGG Veritas Datasets

This dataset is composed of two 2D surveys, VERNG982D and VERNG992D, respectively acquired in 1998 and 1999. A total of 17,800 km of pre-stack migrated data were acquired in the deepwater Niger Delta with a streamer length of 6,000 m and using 12.5 m receiver and 50 m shot point intervals. Southwest-striking lines image the translational domain of the western lobe of the Niger Delta while a few southeast-striking cross-lines form a grid over the downslope structural domains. These seismic lines were used with a view to locate regional NE-striking structural features (Fig. 2.5; see Chapter 3).

OPL 324 (Fig. 2.5) was acquired in 1999 in water depths between 1500 and 3500 m over a surface of 1630 km^2 in the contractional domain of the delta. Data were recorded with a line spacing of 25 m and a 12 s shot interval, and were pre-stack time processed. Data are displayed such that an increase in acoustic impedance appears as a black-red-black trace. The vertical and lateral resolutions in the datasets of interest are estimated to be ~ 8-10 m at the near-seabed interval. Data interpretations as well as isochron, dip and RMS amplitude attributes derived from these data were used in Chapter 5.

2.2.2. PGS Datasets

OPL 314 and 315 (Fig. 2.5) were acquired in 2003 and respectively cover 1878 km^2 and 1600 km^2 of the northwestern margin of the western lobe of the Niger Delta in water depths of 800-2000 m. The data were recorded from a dual source shooting at 135 and 315 degrees in direction and were received on eight 6 km-long streamers. The longest offset is 6300 m, bin dimensions are 12.5 by 18.75 m and the pre-stack time migrated data were processed using a

bent ray Kirchhoff pre-stack time migration process. An increase in acoustic impedance appears as a black-red-black trace. The vertical resolution is 12 m near the sea bed and decreases to 15-20 m in the deepest interpreted intervals. Isochron, dip, RMS amplitude and coherence attributes were extracted from these data, which form the core information of this PhD work and are used in all of the following interpretations.

2.2.3. Eni Dataset

OPL 316 (Fig. 2.5) data cover the producing Abo oil field. They were interpreted in Milan and isochron, dip, coherency and MAA amplitude extractions were used. These 3D data are comparable in dimension and level of processing to the PGS datasets, and cover an area of ~ 800 km^2 located at the updip margin of the PGS datasets, in water depths of 500-1000 m. Their southwestern edge locally overlaps the PGS dataset enabling seismic horizon correlation between both datasets.

2.2.4 Offshore Mauritania Dataset

Provided by Tullow Oil and Petronas and located ~ 100 km away from the Mauritanian coastline in water depths of 300-2000 m, this dataset covers an area of 4000 km^2 (Fig. 2.5). Data were recorded over 3481 lines and 5521 traces with a 25 by 25 m bin spacing. The dominant data frequency is ~50 Hz and vertical resolution is about ~ 10 m in the near-seabed considered interval. These data are not European zero-phased: an increase in acoustic impedance is represented by a red-over-black reflection. In the studied vertical interval, a frequency of 55Hz in the shallow section provides a vertical resolution of ~ 8-12 m. An average velocity of 1481 $m.s^{-1}$ for seawater and 2000 $m.s^{-1}$ in the sediment record can be used with these data (Schultheiss *et al.*, 1987).

Interpretations of these data and use of isochron, dip and RMS amplitude attributes are presented in Chapter 5.

2.3 Regional Geological Setting

2.3.1 Niger Delta

2.3.1.1 Overview

The present day Niger Delta, Gulf of Guinea, equatorial West Africa is one of the largest deltas in the world, and has been explored as a major petroleum province since the 1960s (Allen, 1964; Short and Stauble, 1967; Whiteman, 1982). Its offshore part extends up to 200 km from the coast to the furthest toe-of-slope down to seafloor depths of 3500 m (Fig. 2.6). The present-day delta is sand-rich, with an architecture that is tide and wave-dominated (Allen, 1964). Large quantities of sediments originating from outcropping crystalline basement and Mesozoic to Cenozoic sediments are brought to the offshore basin (Allen, 1964). The delta shelf is ~ 50 to 80 km-wide (Damuth, 1994). The continental slope begins in 85-210 m water depths and extends up to ~ 150 km-long basinward, dipping between 1 and 3° to the southwest in the western delta and to the south in the other regions of the delta (Damuth, 1994). The slope is mantled by clay-rich sediments and numerous slope sedimentary processes (e.g. channel-levee systems and mass-wasting) have taken place (e.g. Allen, 1964; Burke, 1972). Submarine slope canyons developed during sea-level lowstand periods and became sediment-filled during highstands, but the Avon and Mahin canyons are still active at present day (Burke, 1972). Current sedimentary processes still include mass transport complexes (sediment remobilisation) and structurally-controlled turbiditic sedimentation (Damuth, 1994; Morgan, 2004).

Gravity data clearly indicate a separation of the offshore delta deposits into two 7 to 12

km-thick sedimentary lobes on the slope by the southwest-striking Charcot Fracture Zone (Fig. 2.5.B; Evamy *et al.*, 1978; Doust and Omatsola, 1990, and Cobbold *et al.*, 2009). A prominent parallel southwest-striking feature also divides the western lobe into two asymmetric halves: this is the Chain Fracture Zone (Fig. 2.6.B, Briggs *et al.*, 2008). Magnetic data also show NE-SW basement trends which might be associated to fracture zones (Fig. 2.6.C). Deepwater areas of the Niger Delta are therefore presumed to lie over oceanic crust (Morgan, 2003; Briggs *et al.*, 2008) but there is still an active debate on the location of the continental-oceanic crust transition in proximal areas of the delta, where evidence for extended continental crust such as rift geometries (normal faults, tilted blocks and transfer faults) may be encountered (Whiteman, 1982; Damuth, 1994; Bird, 2001; Morgan, 2003; Davies, 2005). An earthquake of magnitude 4.5 and a depth of 10 km was reported on 7th March 2000; it has been speculated that this event occurred on a fracture zone, and be an evidence for far-field activity of the Central Atlantic Ocean (Fig. 2.6.A; Akpan and Yakubu, 2010). It however remains unsure whether to locate a fracture zone (mentioned as the "Okitipupa High") beneath the study area or not (Babalola, 1985; Onuoha, 1999). The presence of these fracture zones is inherited from the Nigerian margin opening history. In the Early Cretaceous, this region was located in the Benue Trough, an opening rift part of a triple junction located in the north-east of the area of interest (Fig. 2.6). Local subsidence is thought to have contributed to focus sediment supply from the early Niger River during the Middle Cretaceous early passive margin stage (Petters, 1984).

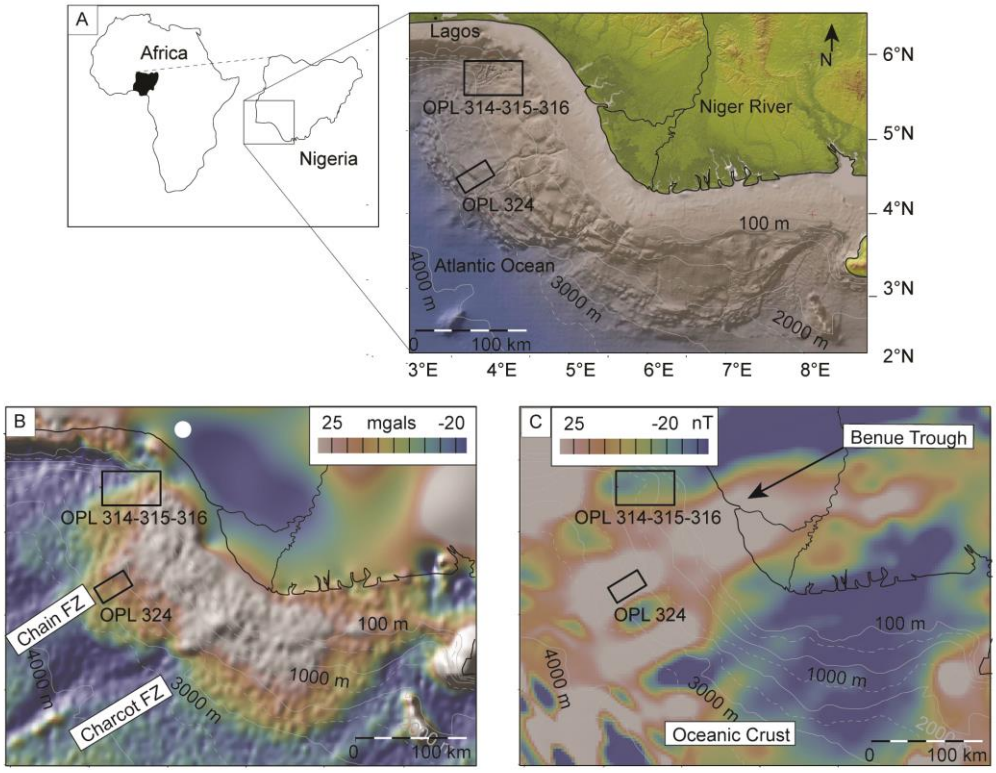

Figure 2.6 - Location of the seismic datasets in offshore Nigeria. A. Geographical location. The approximate locations of the Niger Delta 3D seismic datasets is indicated in the black boxes: from northwest to southeast: OPL 314, OPL 315 and OPL 316 (together) and OPL 324. B. Free-air Gravity anomalies (after Sandwell and Smith, 1997). The white circle indicates the location of the 7 March 2000 earthquake. C. Satellite compilation of magnetic anomalies from EMAG2 (Maus *et al.*, 2009). Source: http://www.geomapapp.org

2.3.1.2 Stratigraphic Setting

The western Niger Delta sedimentary succession overlies the Benue Trough (Doust and Omatsola, 1990; Fig. 2.6.C). This Cretaceous failed rift hosts a Berriasian to Santonian syn-deformational fill overlain by a Campanian to Paleocene marine unit of carbonates and shale (Doust and Omatsola, 1990; Morgan, 2003; Corredor *et al.*, 2005). Delta progradation began

during the Eocene where deltaic sediment including marine shale deposited, and continues at the present day (Burke, 1972; Fig. 2.7.A). The Eocene to present-day sedimentary succession is divided into three main formations that can be defined from seismic facies (Corredor *et al.*, 2005, Fig. 2.7.B), based upon Short and Stauble (1967):

- The Akata Formation is 2 to 7 km thick and represents shale-rich distal marine deposits with some turbidite sands and is Palaeocene to recent. On seismic data, this formation displays low amplitude reflections but internal higher amplitude reflections illustrate the presence of structural markers, which are associated with detachment levels (Corredor *et al.*, 2005; Briggs *et al.*, 2008). At detachments depths seismic velocities suddenly decrease (Bilotti and Shaw, 2001; Morgan, 2003) suggesting high pore pressure at these stratigraphic levels. Structural deformation in the Akata has recently been documented from seismic studies, showing imbricate thrusts and duplexes, as well as smaller-scale deformation within detachment strata (e.g. Cobbold *et al.*, 2009; Maloney, 2011);

- The Agbada Formation overall displays higher amplitude reflections than those in the Akata. These reflections are parallel and occasionally host chaotic events, and have been interpreted as a deltaic succession of sands and shale including mass-transport complexes, submarine channel-levee systems and fans. They represent the delta progradation deposits (delta-front and topset). The Agbada, which started to deposit during Eocene and is still depositing at present day, has channel and fans deposits that form potential hydrocarbon reservoirs in the Niger Delta. It is up to 3.5 km thick and sediment deposition has undergone local structural controls and confinement, impacting on facies and thicknesses locally (e.g. Hooper *et al.*, 2002;

Owoyemi and Willis, 2006; Magbagbeola and Willis, 2007; Pochat *et al.*, 2009). A number of seismic studies in this formation also contributed to an understanding of deepwater sedimentary processes and sediment remobilisation (e.g. Davies, 2003; Deptuck *et al.*, 2003; Fonnesu, 2003; Heiniö and Davies, 2006 and 2007; Deptuck *et al*., 2007; Olabode *et al.*, 2008);

- The Benin Formation represents an up to 2 km thick Upper Eocene to Holocene continental succession (Avbovbo, 1978), including alluvial and coastal-plain deposits. It is overall seen as a high amplitude seismic reflection package caused by its high sand content. Its extent spans from the onshore delta and the coastal regions (Fig. 2.7).

This study concentrates on the Agbada (and Benin) Formation strata.

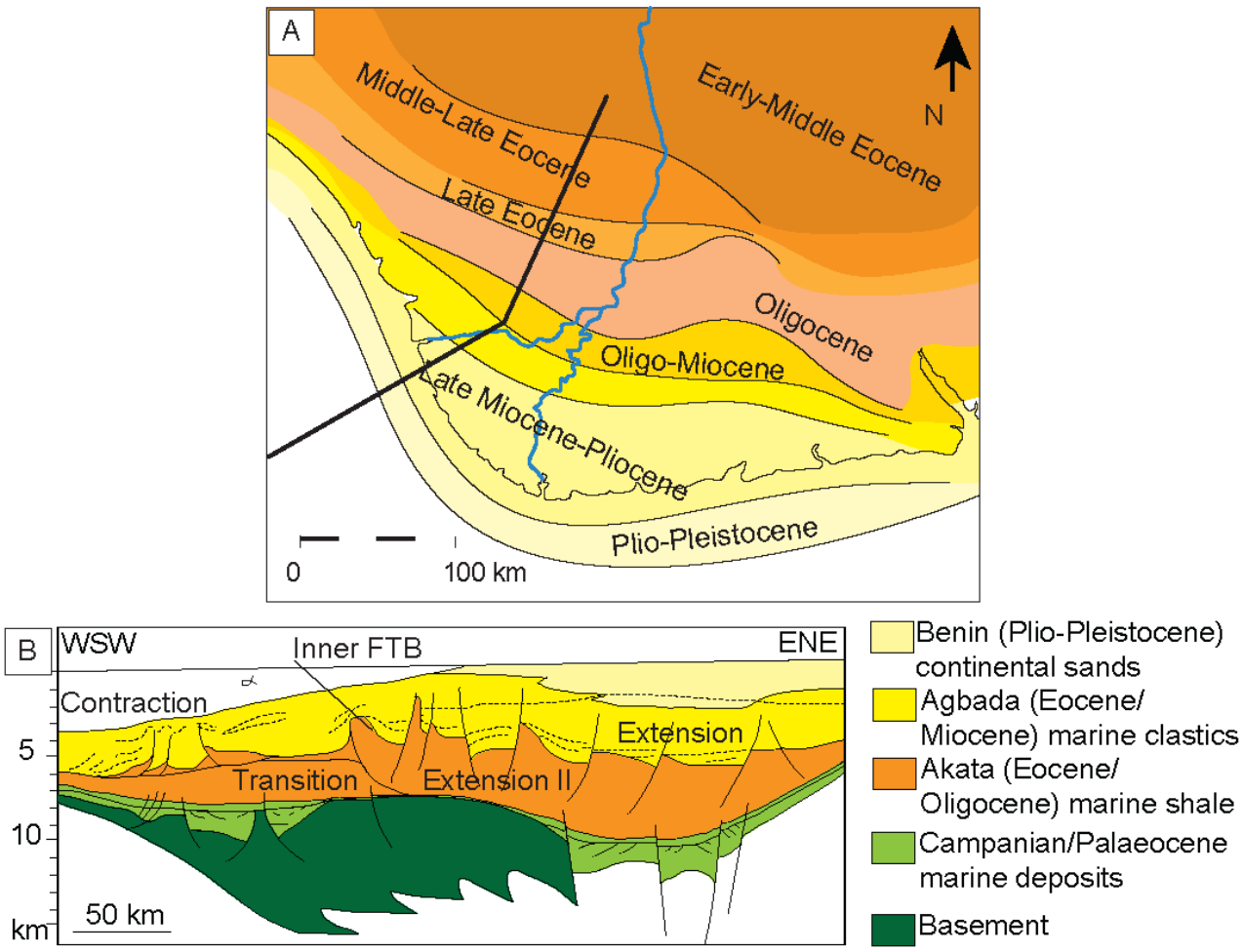

Figure 2.7 –– Delta southeastward progradation with time. A. Map view (modified after Short and Stauble, 1967 and Rouby *et al.*, 2011). B. Cross section modified from Morgan, 2003. FTB stands for "Fold-and-Thrust Belt". The oceanic crust is not indicated in this section. On fig. 2.6, magnetic anomalies are only visible in the most distal parts of the prodelta, while it is sometimes assumed that oceanic crust begins below the delta. Syn-rift fill is not indicated on this section.

The deepwater Plio-Pleistocene record of the Niger Delta was analysed in the southeast deepwater region from a combination of seismic and well data by Jermannaud *et al.* (2010, Fig. 2.8). They established a relationship between the delta sequence stratigraphic interpretation and a climate record in the deepwater southern Niger Delta. Their results indicate that 13 flooding surfaces can be identified in their record and can be correlated to the Plio-Pleistocene climate variations. They also identified two scales of climate feedback loops that affected the regional

sedimentary record through global sea-level changes and drought in the upstream areas where sediments are sourced over the late Pliocene and Pleistocene. This work may provide a tool for correlations around the delta, and has implications for potential relationships between sea-level changes and deformation events (e.g. Rouby *et al.*, 2011). Climate-induced changes in sediment supply, hence in loading rates may have impacted the evolution of gravity-driven structures kinematics (Rouby *et al.*, 2011).

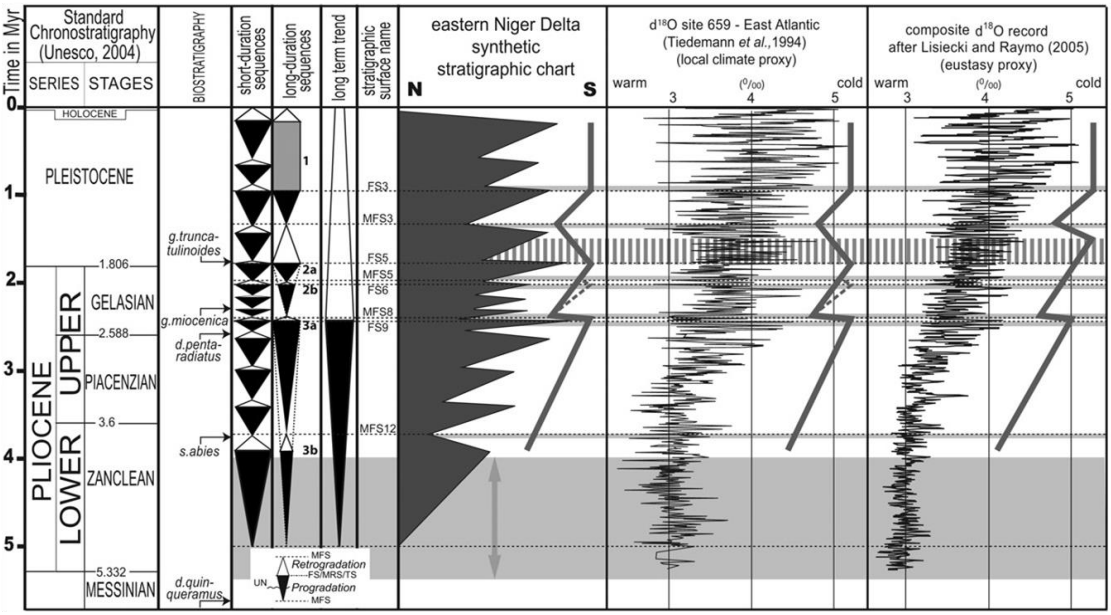

Figure 2.8 - Niger Delta stratigraphic chart compared with the East Atlantic $\delta^{18}O$ record (Tiedemann *et al.*, 1994) and global data (Lisiecki and Raymon, 2005), after Jermannaud *et al.* (2010). Here are correlated the sequence stratigraphic interpretation identified from well and seismic data in the Eastern Niger Delta with the climate and eustacy proxies in order to identify a relationship between sediment deposition and global variations. This correlation indicates that sedimentation and following gravity-driven deformation can be correlated with global events.

2.3.1.3 The Niger Delta Gravity Detachment System

Rapid delta progradation over the mechanically weak Akata Formation generated the Niger Delta gravity detachment system, regional structural interactions of this system with sedimentation have been explained in detail by Damuth (1994), Cohen and McClay (1996), Morley and Guerin (1996), and Corredor *et al.* (2005) after a notably large amount of pre-existing work on

individual structural domains. Deformation styles are important to predict how sedimentation can strongly interacts with individual structures in these domains (e.g. Hooper *et al.* 2002). In the Niger Delta, deformation occurs over multiple levels of detachments occurring in overpressured shale (e.g. Briggs *et al.*, 2006). Detachments dip towards the continent as a result of the sediment load (Morley *et al.*, 2011). Five kinematically linked structural domains have been established from their display of structural styles (Fig. 2.9):

- The proximal extensional domain (Extension I, fig. 2.9) (e.g. Evamy *et al.*, 1978; Rouby and Cobbold, 1996; Koledoye *et al.*, 2003; Pochat *et al.*, 2004; Back *et al.*, 2006; Pochat *et al.*, 2009, Maloney *et al.*, 2011). Large-scale regional (10 – 100 km) and counter-regional arcuate growth faults characterize this domain (Doust and Omatsola, 1990; Cohen and McClay, 1996). Main displacements are assumed to occur on the larger fault traces, whereas later stages of deformation are accommodated by smaller faults (Rouby and Cobboldd, 1996). Synsedimentary strata reveal the different episodes of faulting and topographic fill (Pochat *et al.*, 2004). Faulting occurred in continuously linked events (0.1 $mm.y^{-1}$ over 10 My; Pochat *et al.*, 2009) as depicted by complex fault segmentation (Koledoye *et al.*, 2003) and structural styles indicate several imbricate scales of deformation and the important role played by localized high pore pressures in faults orientation and geometries (Mourgues and Cobbold, 2006; Maloney *et al.*, 2011);

- An intermediate domain comprising reactivated counter-regional normal faults and “shale diapirs” (Extension II, fig. 2.9; e.g. Cohen and Mc Clay, 1996; Hooper *et al.*, 2002). Mud volcanoes over rollover anticlines and shale diapirs (?) are also present in this area (Graue, 2000), as well as km-scale blowout pipes indicating

that seal failure primed by overpressure (Løseth *et al.*, 2010). Some authors state that mobile shale exists in this domain (e.g. Morley and Guerin, 1996; Ajakaiye and Bally, 2002; Ings and Beaumont, 2010; Morley *et al.*, 2011) but this hypothesis is still currently under discussion and disagreements, and the interpretation of shale-cored folds is preferred (e.g. Duerto and McClay, 2002; Maloney *et al.*, 2010; Maloney, 2011);

- The inner fold-and-thrust Belt where regional imbricate thrusting has been observed, a remnant of the paleo fold-and-thrust belt partially buried by delta progradation and an evidence of the complex structures in these structural domains; and a translational domain hosting detachment folds and slope depocentres . Buried paleo-folds are up to 3 km in height and approximately 5 km of extent, and are associated with thrusts (e.g. Hooper *et al.*, 2002). It is now comprised in the translational domain, which extends between the extensional and contractional domains;

- The modern outer fold-and-thrust belt consisting of thrust faults and associated fault-propagation folds (e.g. Bilotti and Shaw, 2005; Corredor, Shaw and Bilotti, 2005; Briggs *et al.*, 2006; Higgins *et al.*, 2007; Cobbold *et al.*, 2009, Maloney *et al.*, 2010). Deformation occurs over thin detachment strata. (E.g. Corredor *et al.*, 2005; Cobbold *et al.*, 2009) It is characterised by imbricate thrusts, pop-ups and triangle zones, and folds wavelengths is between 5 to 10 km (e.g. Morgan, 2003; Higgins *et al.*, 2009; Iacopini and Butler, 2011; Morley *et al.*, 2011).

The OPL 314 and 315 and OML 125 datasets are all located at the margins of the four

downdip structural domains presented above, whereas OPL 324 is located in the outer fold-and-thrust belt (contractional domain, red area in fig. 2.9). It is then expected to observe in the seismic data regional growth faults, detachment folds and contractional structures in the outer thrust belt. Morgan (2003 and 2004) also discussed the occurrence of transfer and tear faults. Transfer faults are strike-slip faults going through the whole sedimentary overburden and may come from transfer faulting occurring between basement normal faults (Morgan, 2003). They are notably observed in the western Niger Delta over the Chain Fracture Zone and may have a role in lateral changes in structural styles in the outer thrust belt (e.g. Briggs *et al.*, 2006 and 2008; Higgins *et al.*, 2007). Strike-slip faulting in the Niger Delta has already been observed (e.g. Morgan, 2003) but has however not been the main focus of recent studies (e.g. Armentrout *et al.*, 2000; Cobbold *et al.*, 2009).

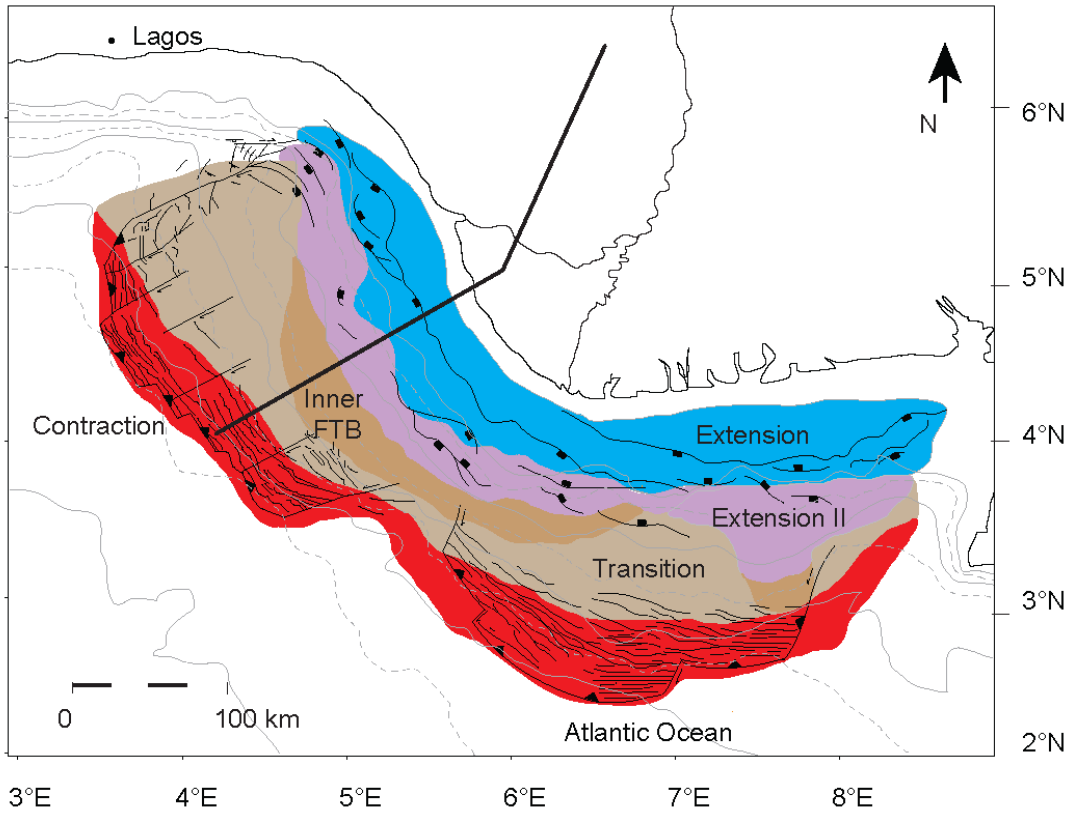

Figure 2.9 - Structural domains in the Niger Delta. Inner FTB stands for "Inner Fold-and-Thrust Belt". Map view adapted from Armentrout *et al.* (2000); Corredor *et al.* (2005); Heiniö and Davies (2006); Deptuck *et al.* (2007); and Cobbold *et al.* (2009). The thick black line locates the cross section in Fig. 2.7.B.

2.3.1.4 Submarine Channel Systems

Hydrocarbon exploration has stimulated a lot of research work on submarine channel systems in the Niger Delta. The study area covers several of these systems. From the northwest to the southwest, they are (Fig 2.10):

- The Avon canyon system (Allen, 1964; Burke, 1972; Petters, 1984), trending NE-SW and identified from the shelf to deepwater areas. At least four stages of development have been associated to sea-level changes and local morphological modifications caused by mass-wasting events (Olabode and Adekoya, 2008). It is assumed to have been in place since the Miocene. Morphologies from seismic reflections include V-shaped incisions into channel fills indicated with basal chaotic reflections overlain by parallel seismic reflections; toplap geometries overlain by parallel reflections at the canyons margins and slope failures on the canyon edges and an overall increase in channel width assumed to be resulting from mass-wasting events. Deposits are assumed to include clastic sediment resulting from local erosion and terrigenous sediment brought from the continent. It is locally affected by syn-sedimentary deformation (Olabode and Adekoya, 2008). Further downslope, the Avon canyon system confluences with the Mahin canyon system;

- The Mahin canyon system is similar in many ways to the Avon canyon (Allen, 1964; Burke, 1972; Petters, 1984; Fonnesu, 2003). It is also a NE-SW long-lived

channel system, displaying low, and then high sinuosity and a characterising depositional succession including: an early-stage aggradation channel-levee system associated with lobe deposits and a second stage of sediment bypass followed by an upslope muddy channel fill and a downslope more sand-rich sediment fill (Fonnesu, 2003);

- Slightly to the south of the study area the Benin system, where have been identified transient fans, in opposition to terminal fans; transient fans representing initial deposition stages followed by channel incision and sediment fill (Adeogba *et al.*, 2005). Further details on the channel morphologies and depositional processes have been published by Deptuck *et al.* (2003);

- In OPL 324, the Ramos/Dodo, or Epe/Ijebu/Iwo canyon systems which interact with active contractional structures (Deptuck *et al.*, 2007; Heiniö, 2007; Heiniö and Davies, 2007).

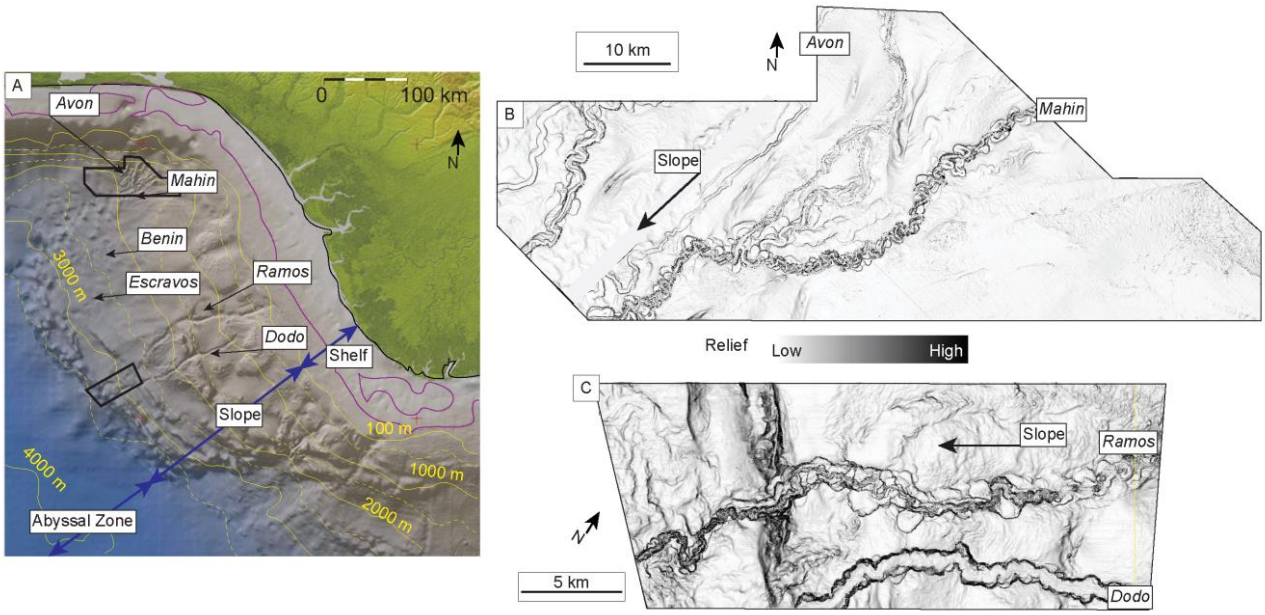

Figure 2.10 - Submarine canyons in the western Niger Delta. Canyons location after Deptuck *et al.* (2007) and Allen (1965). The purple line indicates the location of the "older sands" (Allen, 1965). A. Regional overview, bathymetric map after Rouby *et al.* (2011). Seismic datasets locations are indicated by the black boxes. B. The Avon and Mahin canyons in OPL 314 and 315, seabed dip magnitude maps. C. The Ramos (Ijebu) and Dodo (Ewo) canyons in OPL 324.

An architectural succession of the submarine channel systems in the deepwater western Niger Delta was documented by Fonnesu (2003), Adeogba *et al.* (2005), Deptuck *et al.* (2007), and Heiniö (2007). It is valid for regions where structural deformation did not strongly affect sediment deposition. A first stage of deposition illustrated by a transient sand fan followed by a bypass event of low-relief, low-sinuosity channel has been identified (Adeogba *et al.*, 2005; Fonnesu, 2003). Sedimentary bypass can be triggered by a sea-level fall but also can locally arise from a decrease in base level associated with upslope knickpoint migration (Heiniö and Davies, 2007). Large channels are incised during the bypass and are filled by aggradation of sub-linear to meandering self-confined migrating channels. Progressive channel fill consequently occurs with the vertically and spatially heterogeneous deposition of clastic sediment and mud in the channel

axis (Stage 2 in Fonnesu, 2003; full description in Heiniö, 2007) when sea level rises or when local base level moves upward (Kneller, 2003). Occurrence of sediment waves is also recorded at this stage over the canyon fill (Heiniö, 2007). Sedimentary fill occurring at this stage is also identified as a potential primer for channel migration. This is more likely to occur at sharp bends as accommodation is filled and lateral levee incision is likely to become facilitated in the heterogeneous levee deposits than in the central canyon fill (Deptuck *et al.*, 2007). Frontal splays, or terminal fans, deposit heterogeneous, possibly sand-rich sediment at the channel mouth (Adeogba *et al.*, 2005 and Heiniö, 2007). When a channel system becomes completely sediment-filled and abandoned, trails of hummocky features are often observed (Heiniö, 2007). Channel depositional architecture (terraces, incision valley shapes, etc.) is suggested to be strongly influenced by local topographies. Channel fill is possibly controlled by climate-induced sea-level changes; however deciphering both effects from a single channel system might not be easily done (Deptuck *et al.*, 2007). In terms of autocyclic and allocyclic processes, channel fills can be controlled by relative sea-level changes. In lowstand periods, when the sea level is relatively low, deepwater channels are less likely to develop in comparison to basin floor fans and lobes. A subsequent sea-level rise will not contribute much to the deposition of sediments in deeper water environments since most sediment will be trapped in the upper parts of the basin. Remobilization of sediments is more likely to occur when the sea level falls, as incising canyons can develop and form slope channels in which sediments are transferred to the deeper parts of the basin. Turbiditic sedimentation is expected to best develop in periods of sea-level fall, when more deltaic and shelf sediments are mobilized basinwards.

Understanding the part of sea-level and local controls on deepwater channels may require an extensive detailed knowledge of the whole delta. It would therefore be ideal to carry out this kind of study in all possible channel systems in the study area, but it can be assumed that the

overall channels trends for the deepwater Niger Delta will reproduce similar architectures, unless local structural deformation strongly affects sedimentation. To make sure some channel depositional architectures may be linked to sea-level changes, well data are necessary. The lack of well data in this study prevents a sea-level related sedimentary record analysis in the study area. Depositional changes observed at a local scale can be assumed to be a response to local structural deformation.

2.3.2 Offshore Mauritania

Mauritania is part of the Central African Passive Margin (Fig. 2.11.A). Its geological record is related to the opening of the Central Atlantic, which started in the Late Triassic to the Early Jurassic, earlier than the Nigerian margin, which opened during the Cretaceous. The stratigraphic record spans from the Lias to the present-day including Early Jurassic syn-rift evaporites, carbonate platforms, marine shale and a post-Late Cretaceous clay-rich succession which became incised by canyon systems and complex slope failure processes throughout the Neogene (Davison, 2005; Vear, 2005; Schwab, 2007). Slope failures may either originate from underlying salt deformation or from high slope gradient. Salt deformation, induced by a difference in material density between evaporates and overlying sediments can occur as sediments deposits (e.g. Vendeville and Gaulier, 2005) but also by processes that do not require a rapid and important sediment input. A number of studies have assessed the hydrocarbon potential of this margin (Lane, 2005). This area also provided important examples for the understanding of deepwater turbiditic sedimentary processes (Weaver and Canals, 2003; Wynn *et al.*, 2000; Krastel *et al.*, 2004) and sediment remobilisation with slope failures (Wynn *et al.*, 2000). A thick overall sedimentary cover is seen on free-air gravity data (Fig. 2.11.B). Local variability in this cover is assumed to result from a complex crustal topography including seamounts which origin may be

related to the Cape Verde Islands and is visible on magnetic data (Weaver *et al.*, 2003; Fig. 2.11.C).

At present-day a 25-60 km-wide continental shelf bounds the Mauritanian coast (Seibold and Fütterer, 1982; Fig. 2.11.A). The continental slope extends more than 100 km beyond the shelf edge, dips basinward by 1-6° (occasionally up to 40°; Wynn *et al.*, 2000; Hagen, 2001) and hosts deep water carbonate mounds (Lane, 2005). The study area is located just south of the major Cape Timiris submarine channel system (Krastel *et al.*, 2004). Rapid sedimentation is illustrated by the formation of major turbiditic channel systems (Antobreh and Krastel, 2006). A high-resolution climate record can be identified from bathymetric, seismic and core analyses of these channels architecture (Holtz *et al.*, 2007; Zühlsdorff *et al.*, 2008; Henrich *et al.*, 2010). Complex slope failure processes primed by high pore pressure (Antobreh and Krastel, 2006) and resulting in a varying sediment consolidation (Förster *et al.*, 2010) have also been previously studied. Recent work by Davies and Clarke (2010) showed that these critically pressured stratigraphic fluid traps may also contain episodically released high quantities of methane. Seismic record of channel systems and slope failures from offshore Mauritania therefore presents high quality data of an area where structural deformation is presumably not as important as in the Niger Delta, since little salt deformation is reported to occur where the data are located.

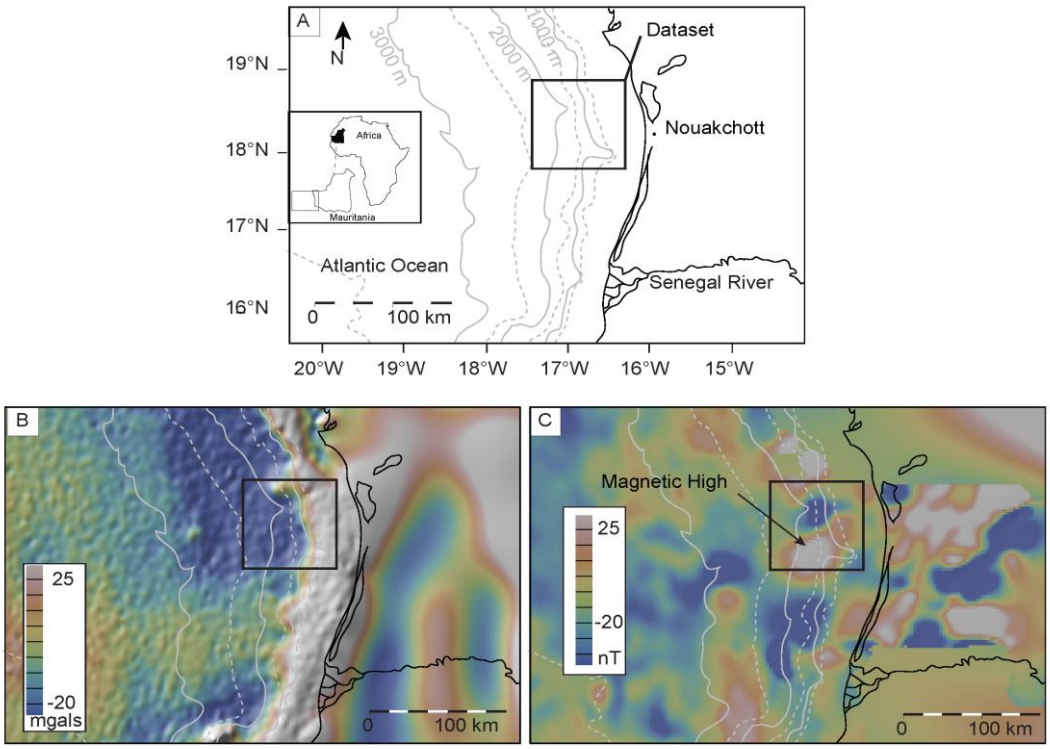

Figure 2.11 - Location of the Mauritania seismic dataset. A. Geographical location. B. Free-air gravity anomalies (after Sandwell and Smith, 1997). C. Magnetic anomalies (EMAG2, Maus *et al.*, 2009) indicating a magnetic anomaly beneath the study area.

2.4 This Study

The aims of this thesis are to establish the stratigraphic, structural and sedimentological relationships at the lateral margins of a regional deepwater gravity detachment system. This study provides a geological and geometrical interpretation as well as a relative timing of events as there was no access to well data. Although both 2D and 3D seismic data were available for this study, the decision was made to focus on the 3D datasets as available 2D data have already supported quite a lot of research studies (Morgan, 2003 and 2004; Briggs, 2006 and 2008 and Maloney, 2010).

Horizon interpretation was carried out across the whole area of interest using eight key strong reflective and continuous horizons. This horizon list was initially provided by the industry

sponsor. Focused interpretations were then done using as many local horizons interpretation as possible. Each chapter illustrated a different study that was carried out independently of the other. A different seismic stratigraphic scheme is therefore used in each study.

Structural interpretation was carried out with the help of structural and contour maps. Details were refined using isochron, dip magnitude, isochron and coherence attributes for some data. The extent of the maps was adapted to the considered geological features. Dip magnitude was also used to interpret near-seabed morphologies as a supplement to amplitude extractions. MAA amplitude extractions were initially preferred for the industry sponsor, whereas choice was made to continue the research using RMS amplitude extractions. Interpretation was performed on Seisworks in picking horizons maximum or minimum trace wavelets according to data polarity, using the "auto-dip" mode. 3D seismic interpretation was carried out on Linux workstations at the Sir Kingsley Dunham Earth Imaging Research Laboratory, Department of Earth Sciences, Durham University and in Eni S.p.A., Divisione Exploration & Production, Milan, using Landmark Openworks Seisworks 2D3D, 3D3D and 3D and StratAmp 2003.12.

Some published material helped in establishing a velocity estimate in order to provide a depth-converted seismic section (Fig. 3.6) using the software Move™. Seismic stacking velocities published by Morgan (2003) helped in building this depth conversion and provided metric depths estimates for the Niger Delta study area (Table 2.1).

Medium	**P-wave Seismic Velocity ($m.s^{-1}$)**
Seawater	1480
Seabed	1800
Poorly compacted clastic sediments and overpressured shale	1900-2100
Compacted clastic sediments	2100-3000

Table 2.1- Average P-wave seismic velocities encountered in the study area (Morgan, 2003).

Stratigraphic mapping was done using a provided list of dated horizons which details are confidential (Table 2.2; Fig. 2.12). Interpretation commenced in collaboration with ENI in Milan with the Late Miocene intervals in OPL 316. Mapping thereafter continued further west over OPL 315 and 314 over the Late Miocene intervals in order to understand the sub-regional structural setting in the study area. Mapping carried on over shallower reflections in OPL 316 in order to better understand the evolution of an identified sub-circular structure. Lastly, sub-regional mapping was done for a series of well-defined reflections in the Plio-Pleiostocene succession in order to track channel system migration and late recent structural activity in the study area. Seismic analysis in the offshore Mauritania dataset and in OPL 324 was then performed in order to obtain several additional examples of interacting channel systems with tear faults as an analogue for the observations made in OPL 314-315-316.

Horizon	**Approximate Age (My)**	**Provided Chronostratigraphic Age**	
seabed	0	Present-Day (Holocene)	
H 050	1.81	Plio-Pleistocene	Piacenzian to Gelasian
H 100	3.6	Pliocene	Zanclean
H 200	5.5	Late Miocene	Messinian
H 300	7.8		Tortonian
H 500	16.4	Early Miocene	Burdigalian
H 700	28	Oligocene	Chattian
H 900	97	Cretaceous	Top Albian

Table 2.2 - Chronostratigraphic ages provided by ENI (2008). These ages are only an approximate indication based on global sea level curves and are not used to precisely estimate ages in this thesis. The corresponding horizon reflection are shown on Fig. 2.12.

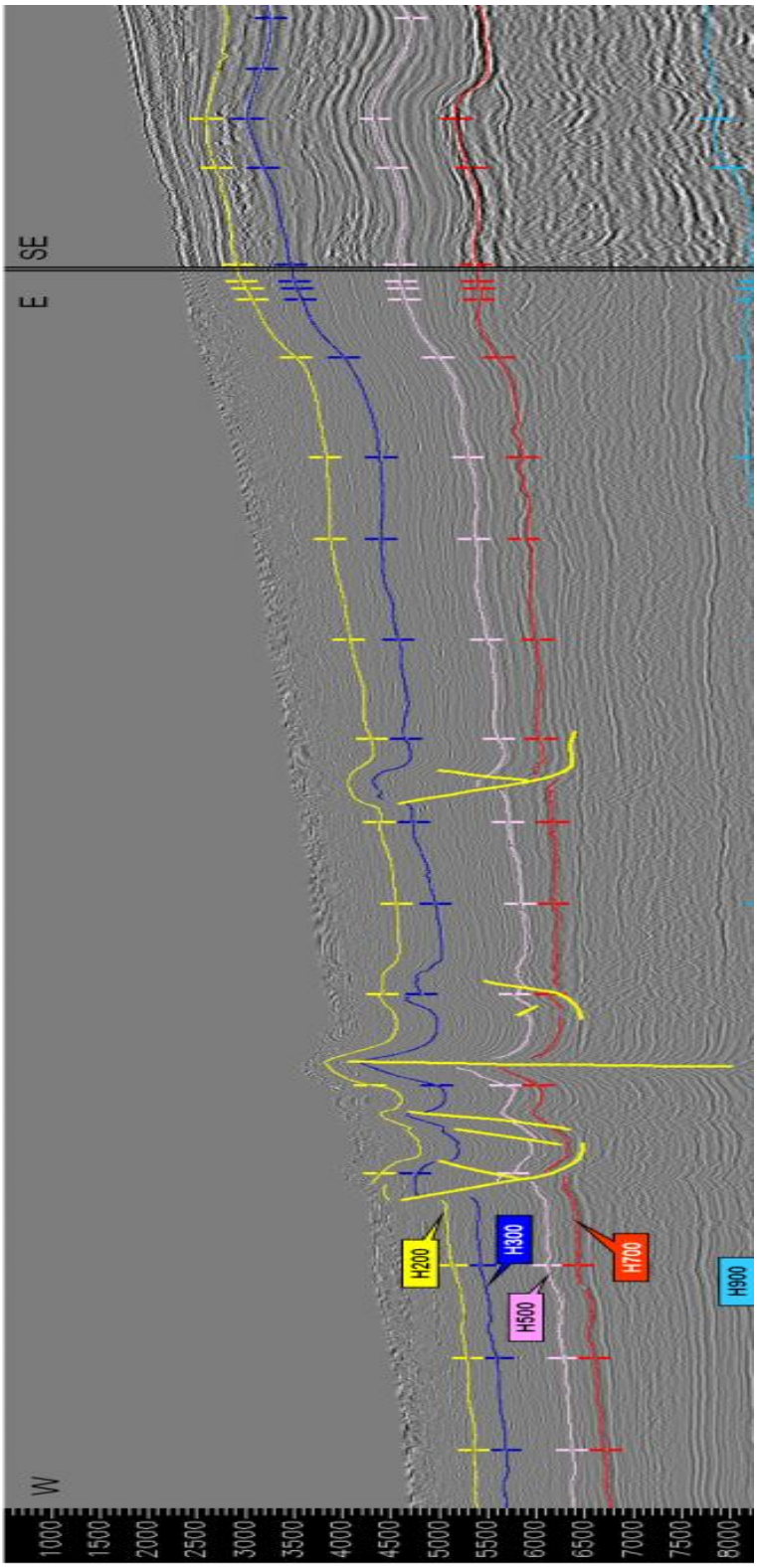

Figure 2.12 - Reference horizon reflections for H200, H300, H500, H700 and H900 on a W-E section from verng99 and a SE-NW section from OPL 315. Horizontal scale: no scale given. Vertical scale given in two way travel time. Source: Eni (2008), reference uninterpreted section not provided.

CHAPTER 3: THE LATERAL STRIKE-SLIP DOMAIN IN GRAVITATIONAL DETACHMENT DELTA SYSTEMS: A CASE STUDY OF THE NORTHWESTERN MARGIN OF THE NIGER DELTA

ABSTRACT

We use two-and three-dimensional seismic data to describe the structural geology of the lateral margin of a deep-water delta lobe within the Niger Delta that has undergone basinward, gravitationally driven translation. We term this region the "lateral strike-slip domain." Deformation is characterized by a strike-slip fault system that can be followed for a distance of approximately 75 km (~47 mi) from the shelf to the slope and toe of slope. On the northwestern side of the fault system, a fold and thrust belt that propagated north to northwest has developed within a large-scale restraining area of 460 km^2 (180 mi^2). On the southeastern side of the strike-slip fault system, widespread extension has occurred, characterized by several graben and kilometer-scale rollover structures. Lateral margins of gravitational collapses give key information on how they deformed. We estimate a minimum horizontal dis-placement on the main strike-slip fault of approximately 7 km (~4 mi). Structural and kinematic evidence, such as present day propagating strike-slip faults, for possible future lateral expansions of the lateral strike-slip domain, is described. We expect to observe similar sets of deformation styles at the margins of other preserved gravitational collapse sliding over a detachment whose efficiency in causing downdip slip may vary laterally.

3.1 INTRODUCTION

Gravitational collapse occurs at a variety of scales from individual landslides and mass-transport complexes up to the dimensions of passive continental margins. Despite this variability, comparable processes and structural features occur (Butler and Turner, 2010). During the last three decades, a focus on describing gravity-driven deformation in large deltas has been observed (Cobbold and Szatmari, 1991; Damuth, 1994; Morley and Guerin, 1996; Gaullier *et al.*, 2000; Gaullier and Vendeville, 2005; Maloney *et al.*, 2010). This deformation is typically expressed as a complex that consists of an updip extensional domain, a translational domain where little internal deformation is observed, and a downdip compressional domain where fold and thrust belts and toe thrusts develop (Damuth, 1994; Stewart, 1999; Morley, 2003; Rowan *et al.*, 2004; Bilotti and Shaw, 2005; Corredor *et al.*, 2005; Cobbold *et al.*, 2009).

A strike-slip domain, located at the lateral margins of a slide mass, has only been described in mass-transport complexes. For example, Frey Martinez *et al.* (2005), in the Levant Basin of the eastern Mediterranean Sea, and Bull *et al.* (2009), on the Storegga slide offshore Norway, provide well imaged seismic examples of the lateral margins of large-scale slumps. Bull *et al.* (2009) illustrated a series of kinematic features that characterize strike-slip deformation on the lateral margins of mass-transport complexes in the translational do-main. These features include en echelon sigmoidal scarps and dragged flow banding (material included in the complex and affected by strike-slip deformation). Important clues to the evolution of the slide, such as evidence for the timing of the deformation, the amount of horizontal downslope displacement of the mass, or the interaction between the slide mass and undeformed material along strike, may be found at the lateral margins. At the delta scale, strike-slip deformation has been documented in the Gulf of Mexico (Peel *et al.*, 1995; Rowan, 2009), in the Nile Delta (Loncke *et al.*, 2006; Clark

and Cartwright, 2009), and in the Amazon Fan (Cobbold and Szatmari, 1991). Recent work from Cobbold *et al.* (2009) and Løseth *et al.* (2010) has shown the presence on the seabed of en echelon kilometer-scale strike-slip faults in the deepwater Niger Delta. Morgan (2004) mentioned the presence of transfer faults in western Niger Delta that control the position of submarine channels, but the geometries and extent of the strike-slip fault zones were not described in detail. Despite these examples, generally, the literature is dominated by examples of strike-slip faults identified from two-dimensional (2-D) seismic data, and most of the focus on strike-slip fault morphology has been on structures in the continental crust instead of those associated with gravitational collapse. Looking into more detail, these strike-slip structures could provide information on how deformation occurs at the margins of gravitational collapses, how fast they will occur and how far the mass moves downslope, and what the controls on their development are.

In this article, we interpret 2-D and three dimensional (3-D) seismic data to describe a set of large-scale structural features at the lateral margin of the northwestern Niger deep-water delta lobe that is undergoing downslope translation driven by gravity. We observe and interpret the structural complexity of coexisting extensional, compressional, and strike-slip deformation in the lateral margin. The lateral strike-slip domain is defined as a discrete structural domain that forms at the margins of a gravity detachment system, linking the extensional, translational, and compressional domains of the system.

3.2 DATA AND METHODS

3.2.1 Geological Setting

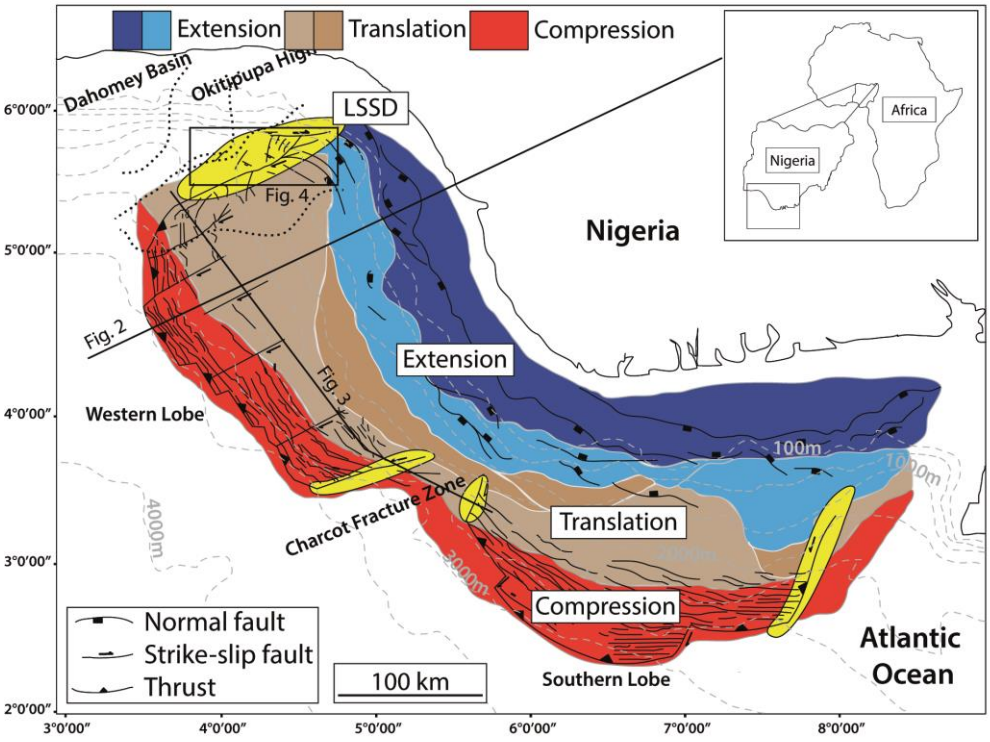

Figure 3.1 – Overview of offshore Niger Delta structural domains (modified from Armentrout *et al.*, 2000; Corredor *et al.*, 2005; Heiniö and Davies, 2006; Deptuck *et al.*, 2007; and Cobbold *et al.*, 2009). Gray dashed lines are bathymetric contours. The structural domains relative to the main structural styles are indicated. The lighter shading corresponds to the potential location of the lateral strike-slip domains. Main canyon positions in the northwest offshore delta are shown by dotted lines; from west to east, these are the Lagos, Avon, Mahin, and Benin canyons. LSSD = lateral strike-slip domain as described in this article. Locations of Figs 3.2 (here mentioned as fig. 3.2) and 3.3 (here mentioned as fig. 3.3) are indicated with thick black lines, and Figure 3.4 (here mentioned as fig. 3.4) is indicated with a rectangle.

The deep-water Niger Delta consists of two lobes in the south and in the west that developed contemporaneously (Fig. 3.1) (Doust, 1990; Damuth, 1994). Deltaic sedimentation began in the Tertiary, and regional seismic lines (Figs 3.2 and 3) show that a 7-to 8-km (4-to 5-mi)-thick sedimentary succession is located above the basement. Immediately above the basement, the Akata Formation is composed of Paleocene to Eocene marine shale. An abnormal decrease of

seismic velocity of 1000 m s^{-1} (3000 ft/s) at the top of the Akata has been interpreted as representing overpressured conditions (Morgan, 2003). The overpressured interval is roughly coincident with the level at which normal and thrust faults sole out to become bedding-parallel detachments, allowing gravity-driven deformation to occur (Damuth, 1994; Cohen and McClay, 1996; Morley and Guerin, 1996; Briggs *et al.*, 2006). The Akata Formation is covered by a succession of turbiditic mass transport and hemipelagic deposits (the Agbada Formation). Over the Agbada Formation, the Benin Formation is sometimes mentioned (Fig 3.2), which has been defined from seismic facies interpretation in the proximal parts of the delta. Deformation is partitioned into three main structural domains: the Extension domain and the Translation domain, both also divided into two other sub-domains and the Compression domain. The Extension domain comprises of an area in extension, and further downslope an area undergoing extension reactivating previous translational and contractional structures. Likewise, the Translation domain now divided in two, includes an inner domain where pre-existing gravity-driven contractional structures are no longer active, and folding linked to the current translation in the gravity detachment system. Both the western and southern lobes are also partitioned by strike-slip faults into several parallel sections sliding at different rates (Morgan, 2004; Cobbold *et al.*, 2009) (Figs 3.1 and 3.3); these faults are visible on seismic data as subvertical reflection terminations and fault-plane reflections.

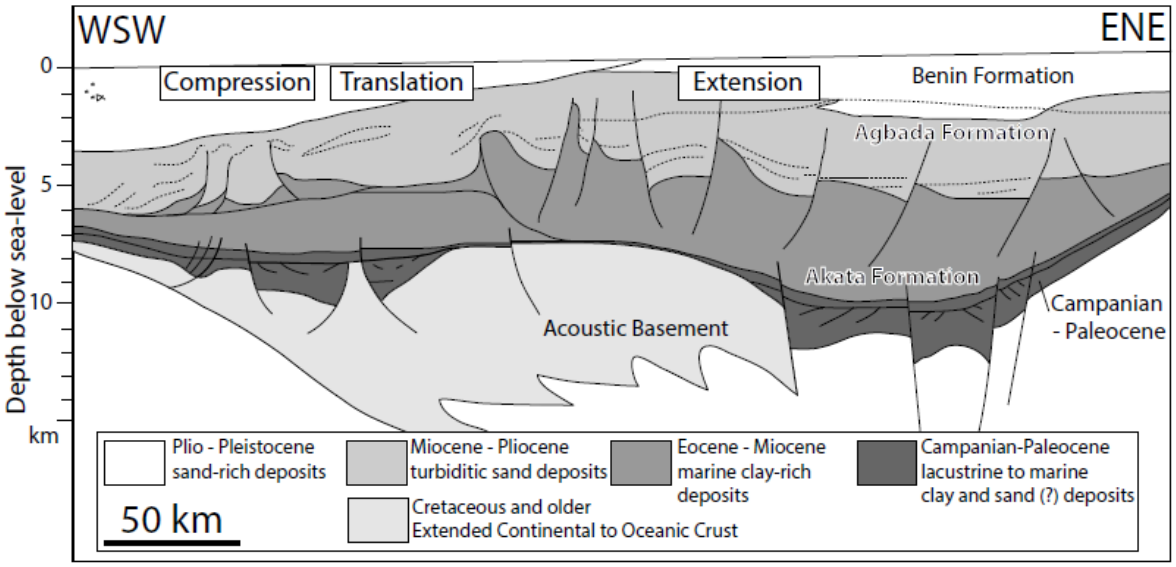

Figure 3.2 – Simplified west-southwest–east-northeast cross section showing the structural features of basement and the sedimentary overburden of the offshore Niger Delta. The structural domains relative to the main structural styles are indicated (modified from Morgan, 2003).

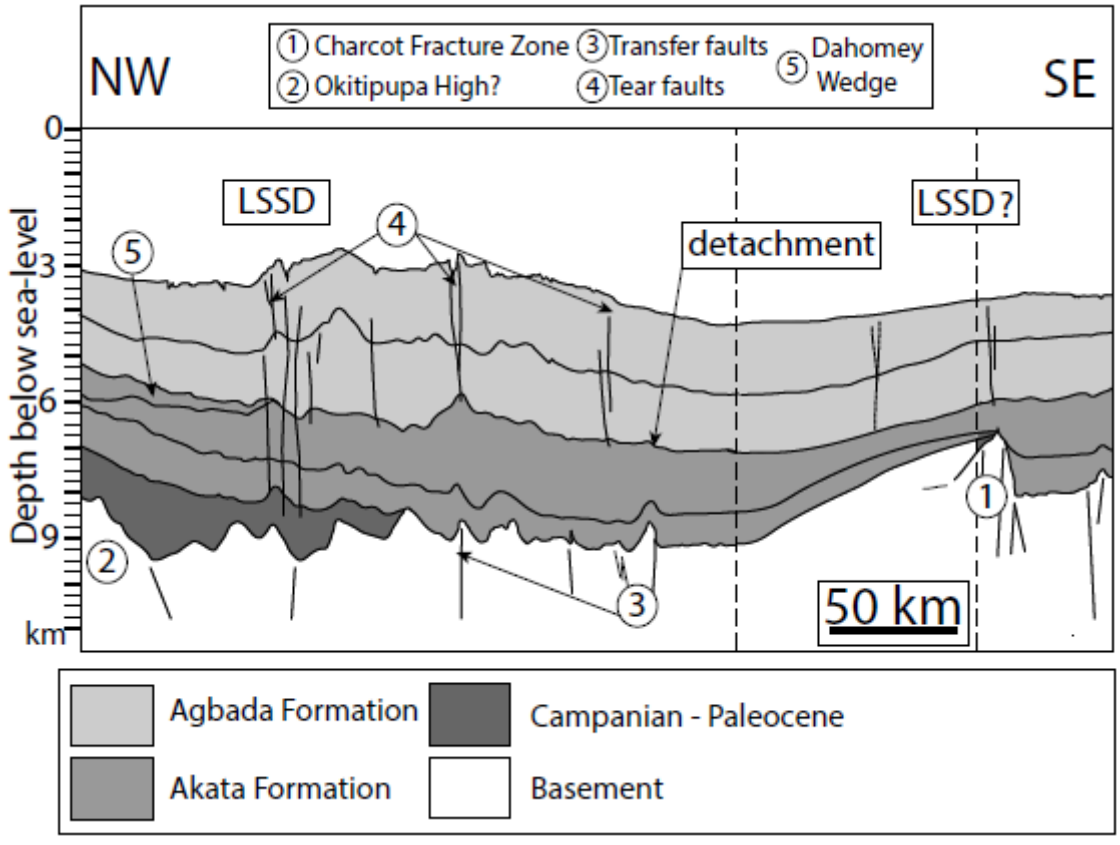

Figure 3.3 – Interpretation of a regional north-northwest–south-south-east two-dimensional seismic section in the western lobe of the Niger Delta. No data between the vertical dotted lines exist; the Charcot fracture zone structure is adapted from Briggs *et al.* (2009). LSSD = lateral strike-slip domain. The Benin Formation is assumed not seen in this section.

We analyze three adjoining 3-D seismic data sets acquired in 2004 that cover most of the area of interest, as outlined on Fig. 3.4. Water depths are between 500 and 2000 m (2000–7000 ft), the seismic surveys cover an area of approximately 4300 km^2 (~1660 mi^2), and bin dimensions are 12.5 × 18.75 m (41.01 × 61.52 ft; see Brown, 2004). At considered depths, frequency bandwidth is estimated to be approximately 30 Hz. Data are zero phased and are displayed in two-way travel time. Combined use of time-structure maps and seismic attributes (coherency, dip, and amplitude extractions) from high-amplitude continuous reflections allows us to identify faults and folds in the area of interest (Fig 3.4). At considered horizon reflections, we extracted windowed amplitude maps (+100 and –100 ms) to observe the main structures. Time-thickness maps were computed between given top-and bottom-interpreted horizon reflections. The succession is subdivided into units A, B, and C based on changes in reflection character and the mapping of four reflections (H1– H4; Fig. 3.5). Ages are roughly estimated based on an assumed uniform sedimentation rate of approximately 100 m/MY (Davies, 2003). A depth conversion of a key seismic section is presented in Fig. 3.6. The description herein starts with an overview of the regional structures and stratigraphic units. We then focus on structural features identified from both map and seismic cross sections. B).

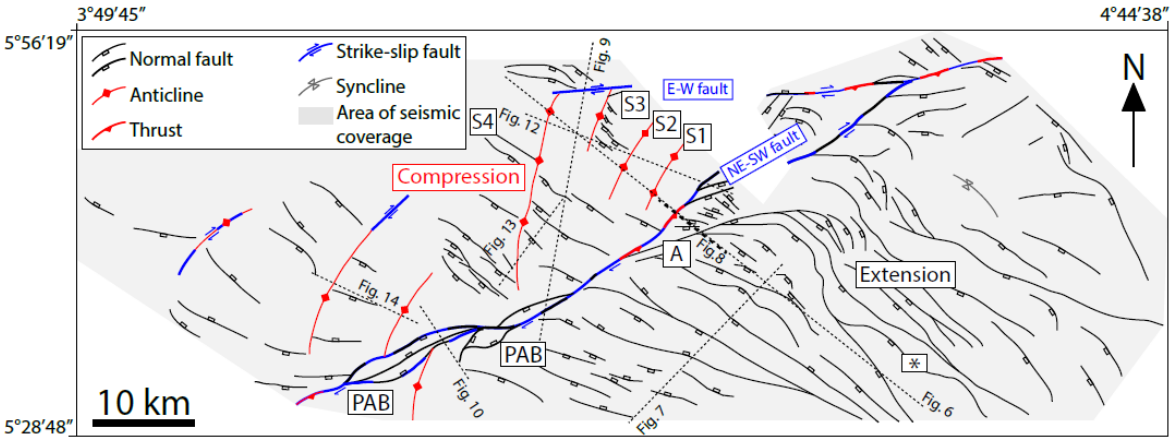

A

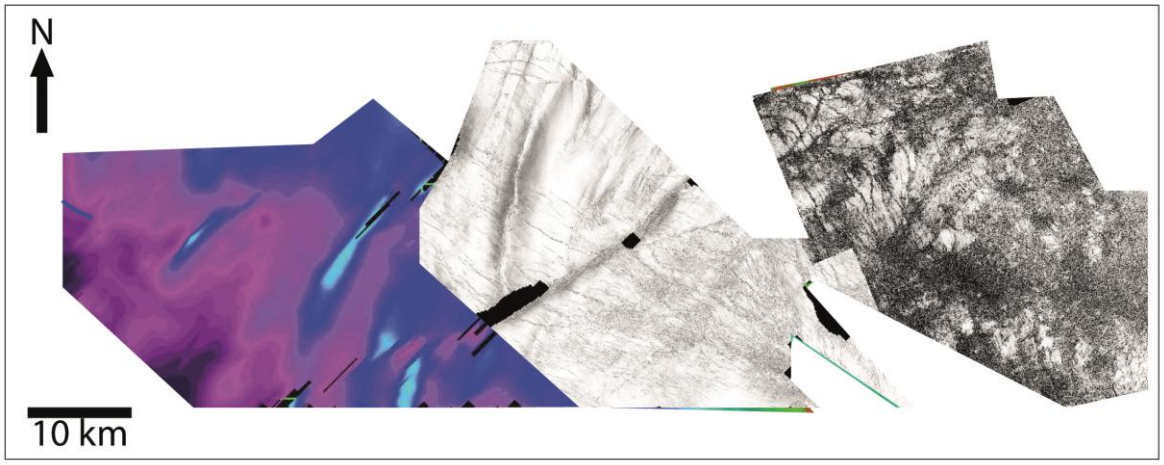

B

Figure 3.4 – A. Detailed structural map of the lateral strike-slip domain from horizon interpretations at 3000 to 4000 ms two-way travel time depth (between interpreted horizons H3 and H4). The positions of Figures 3.6 to 3.10 and 3.12 to 3.14 are indicated by the dotted straight lines. The extensional zone is located in the southeastern part of the map and the compression zone in the northwest. PAB = pull-apart basin. A = fault trace marked A in Figure 3.8. The asterisk indicates the normal fault discussed in the section titled Extensional Zone. Figure numbers are referring to chapter 3 figures (read fig. 3.X). B. Examples of time (west) and coherency (east) maps used for fault mapping. Blue to purple are -2500 to 4000 ms twt; white are high coherency factor, black lower coherency factor.

Unit	Horizon	Min-Max depth (m)*	Inferred Age**	Formation
	seabed	1500 - 2500	Present day	
A		1600 - 2900	Pleistocene	
	H1	1700 - 3300	Pliocene	
B	H2	2400 - 4300	Late Miocene (Messinian)	Agbada
	H3	2600 - 5000	Miocene	
C	H4	3600 - 6800	Late Oligocene ?	
	detachment	5000 - 9000	Oligocene ?	
		7500 - 9000	Eocene?	Akata
	basal strong reflection	8000 - 11000	Palaeocene	

Figure 3.5 – Age and depth of stratigraphic units A, B, and C and horizons used in this article, from the seabed to the basal strong reflection. Depths are estimated from the seismic velocity model of Morgan (2003); velocities and depth are estimated from Morgan (2003). Ages are taken from Morgan (2003) and Lawrence (2002). Unit A, defined between the seabed and the interpreted horizon H1 (Pliocene), is composed of high-amplitude reflections within a background of lower amplitude continuous reflections. These reflections are interpreted to be silts and sands deposited within deep-water channels (e.g., Deptuck *et al.*, 2007). Horizon H2 is estimated to be Messinian based on extrapolation from regional sedimentation rates (Davies, 2003). Unit B (situated between horizons H1 and H3) displays parallel reflections that are lower in amplitude than in those in unit A. It displays a sharp erosive contact with the underlying reflection packages. Unit C lies between H3 and the near top Akata reflection (associated with the top of the Akata Formation). Horizon H4 is another prominent reflection within unit C. Horizons H1 to H4 correspond to H100 to H400 in Table 2.2.

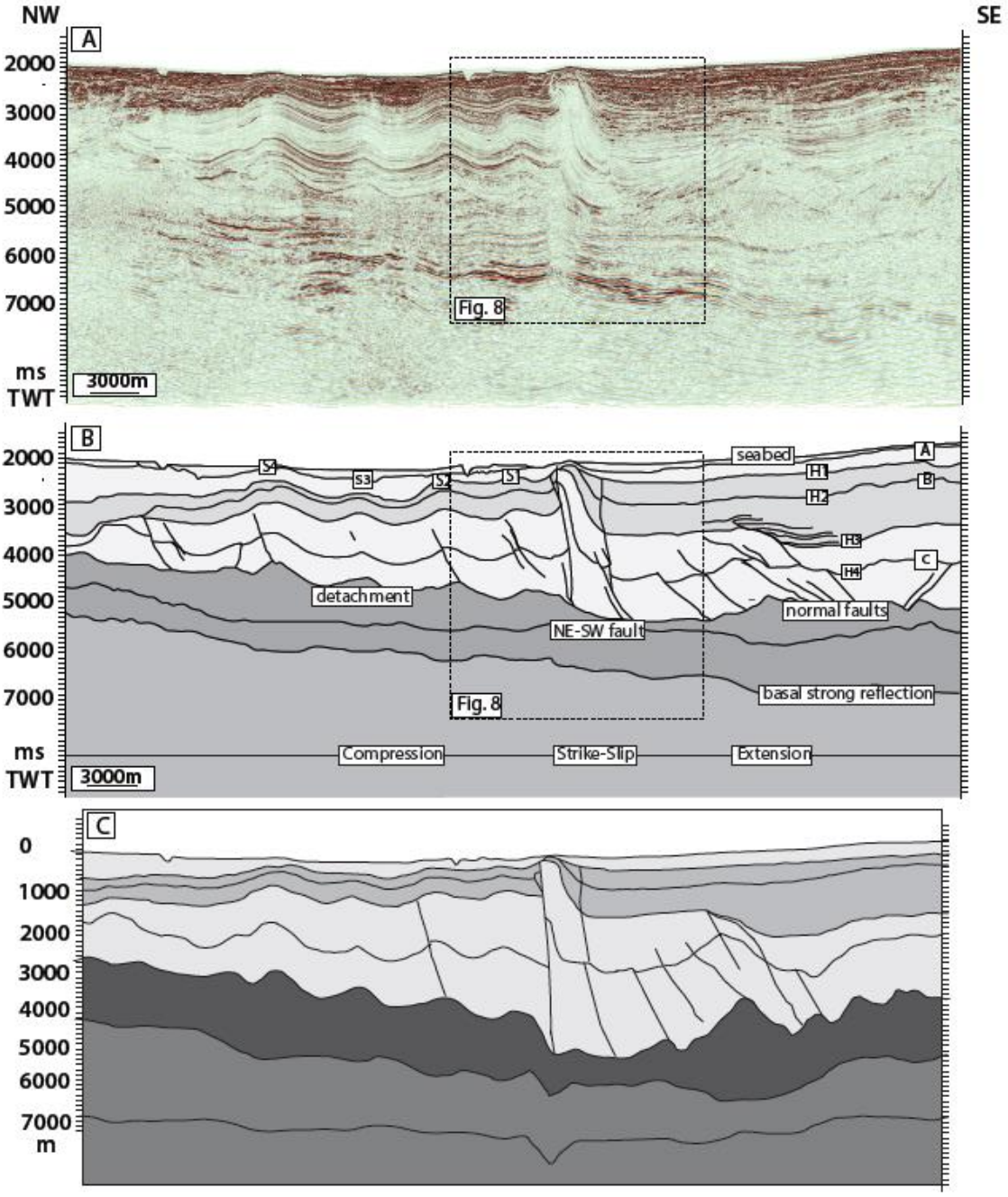

Figure 3.6 – (A, B) Northwest-southeast–oriented interpreted seismic sections selected from a three-dimensional seismic data set crossing the three structural zones of the area of detailed study. Folds are numbered S1 to S4 from the northeast-southwest fault trace to the west. (C) Depth conversion applied to the section displayed in Figure 5.6A and B. The section is depth converted using interval velocities as shown in Figure 5.5. This section shows that the geometries and dips of the structures remain comparable on both time-and depth converted seismic sections. The location of Fig. 3.8 is indicated by the dotted square annotated fig.8. All the following sections are converted. TWT = two-way travel time. Approximate vertical exaggeration x4.

3.3 OBSERVATIONS

Three structural trends are identified both in map view (Fig. 3.4) and in seismic sections (Figs 3.6A and B). A major subvertical northeast-southwest– trending fault marks the boundary between two structural zones located to the northwest (compressional zone) and southeast (extensional zone). This distinction is also clear on a vertical section across the northeast-southwest fault (Figs 3.6A and B). The compressional faults to the northwest of the northeast-southwest fault appear generally much steeper (~60° dips) than the extensional faults to the southeast (~30°). This is only because the section chosen is oblique to the normal faults, whereas it is perpendicular to the shortening structures. Below, we examine each of these trends.

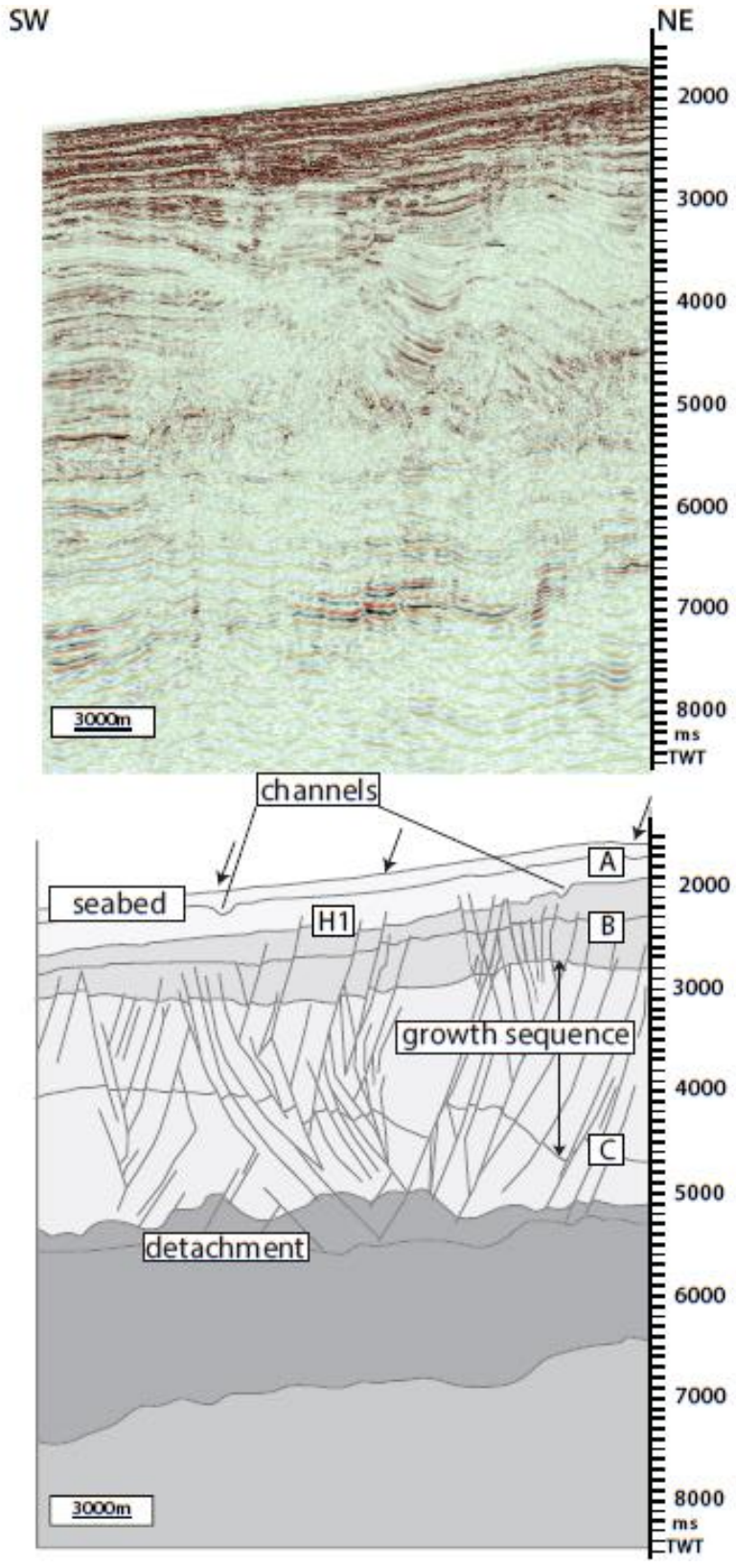

Figure 3.7 – Southwest-northeast–oriented seismic section and interpretation showing a compound graben in the extensional zone. TWT = two-way travel time. Below the detachment, deeper extensional fault corresponds to the pre-Eocene synrift succession.

3.2.1.1 Extensional Zone

Most of the structures in the extensional zone (marked "extension" in Fig. 3.4) are normal faults that strike northwest, dip steeply to the southwest (~60°), and have lengths of as much as 10 to 15 km (6–9mi; Figs 3.4 and 3.7). The largest northwest-striking normal fault is in the east of the study area. It can be traced over a distance of 30 km (20 mi) and connects to a northeast-striking normal fault (marked with an asterisk in Fig. 3.4). The northwest-striking normal fault defines the northeast border of a graben of an approximately 10-km (~6-mi) width (Figs 3.4 and 3.7). A large number of the northwest-striking faults deform H1, H2, H3, H4, and the top Akata reflection. They consist of a series of conjugate normal and growth faults with variable movements and variable length. It is probable that these faults represent several deformation episodes because the related growth sequences appear to have formed during multiple episodes of extension. The main episode of extension is recorded in the upper part of unit C where onlap geometries prograding to the west are found. Other normal faults also exist in the compressional zone, some of which are likely to be the continuation of some northwest-striking normal faults of the extensional zone. They may predate the formation of the strike-slip fault zone. Another hypothesis is to relate these extensional features to a degradation of the fold and thrust belt as they strike perpendicularly to the fold hinges.

3.2.1.2 Strike-Slip Faults

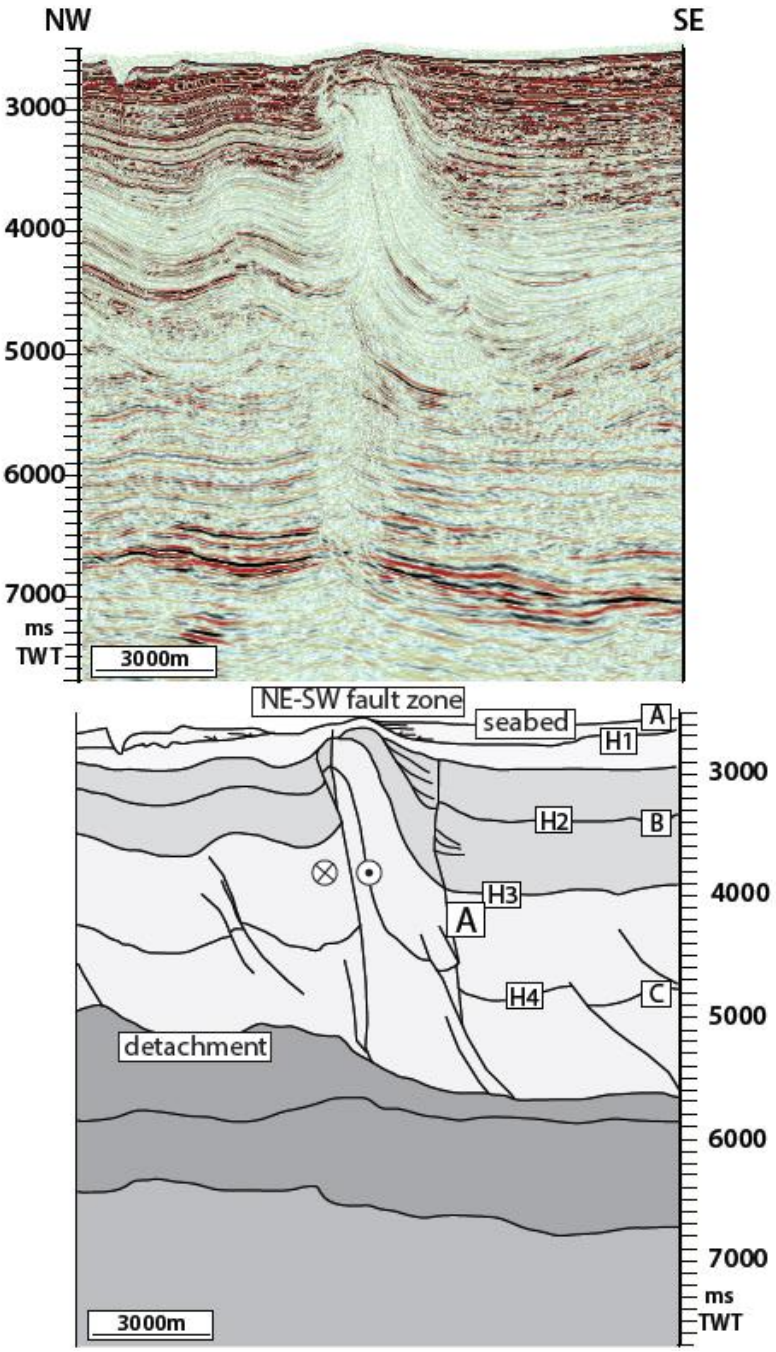

Figure 3.8 – Detailed view of the compressive strike-slip structure shown in the center of Figure 3.6. The steep fault trace at the north western side of the fault zone is bounded by a steep fold. Deformation occurs while sediments are being deposited and eroded. The fault trace marked A represents the southeastern limit of northeast-southwest fault zone. TWT = two-way travel time. Approximate vertical exaggeration x3.

The northeast-southwest fault zone is composed of a variety of faults with geometries that are kinematically linked (Fig. 3.4). The longest fault trace is 75 km (47 mi) long. Because of its

complexity, we describe its main geometries from its northeast mapped tip to the southwest along strike (kilometer 0 is at the northernmost mapped point of the fault; kilometer 75 is at the inferred southwest tip). A northern segment (kilometers 0–10) and a central segment (kilometers 33–43) show contraction. On a seismic section, these segments display two subvertical fault traces, both dipping subvertically to the southeast (Figs 3.6A, B and 3.8), that extend from the top Akata detachment to the seabed. The southeastern fault trace (Fig. 3.8, marked A) is kinematically linked to the fault trace connecting the northeast-southwest fault to a large normal fault in the extensional zone (Fig.3.4). The northwestern fault trace is a thrust fault with pronounced folding in the hanging wall that branches into several segments toward the surface. We interpret this fault system as a compressional strike-slip fault system (Harding, 1985). Unconformable contacts are identified at the base of unit A, on H2 and H3. Variations in the thicknesses of these units suggest the occurrence of three episodes of erosion and/or deposition that can be related to possible pulses of activity on the northeast-southwest fault. Another strike-slip fault, oriented east-west, is located in the north of the study area and connects to the northeast-southwest fault at kilometer 10. Assuming that the fault connects between its eastern and western documented parts, in the area of no seismic coverage, it is approximately 35 km (∼22 mi) long (Fig. 3.4). In a vertical section, the east-west fault is expressed as a subvertical fault array that branches and offsets reflections between the seabed and H3 (Fig. 3.9). The east-west fault displays a negative flower structure (Harding, 1985) with the south-southwestern block downthrown. From kilometer 43 to its southwestern tip, the northeast-southwest fault splays into a series of normal faults that form small pull-apart basins (Fig. 3.4, marked PAB). These basins are bounded on their northwestern side by the northeast-southwest fault zone and by an east-northeast– west-southwest normal fault dipping northwest on its other side. They are, respectively, from northeast to southwest, 8 km (5 mi) long and 2 km (1 mi) wide, 5 km (3 mi) long and 2.5 km (2 mi) wide, and 14.5 km (9 mi) long and 3 km (2 mi) wide. A typical seismic section along the strike of the

northeast-southwest fault in this segment displays a set of high-angle faults that we interpret as a negative flower structure (Harding, 1985) (Fig. 3.10). The horizons within this structure display geometries indicating a rapid subsidence between the border fault lines. The northwestern fault trace (Fig 3.10, marked X) is a steep fault with an apparent down-throw of 200 m (700 ft) to the north on H2 to H3. Offset decreases upsection and goes to zero at the seabed. The other segment branches and cuts reflections between the top Akata reflection and H2. Units B and C are thickening progressively to the south-east, and onlaps suggesting growth sequence are observed in unit C. Extension occurs by the northeast-southwest fault and is likely to occur before and during strike-slip motion. Thus, the same northeast-southwest–striking fault system evolves along strike (on vertical sections) from subvertical fault-propagation fold geometries (Fig. 3.8) to a combination of linked normal faults and pull-apart basins in the southwest (Figs 3.4 and 3.10). This observation is consistent with a strike-slip fault system interpretation (Harding, 1985). An amplitude extraction map of H3 and a time-thickness map of unit C show that areas of high amplitude and previous fault traces are offset along the main northeast-southwest fault zone (Fig. 3.11). They can be restored by a lateral translation of matching blocks of the map that show the state of the region as it probably was in the late Miocene. These blocks are delineated by the northeast-southwest and the east-west strike faults and by the large northwest-southeast normal faults in the south of the study area. A horizontal displacement of as much as 7 km (4 mi) is found on the northeast-southwest fault, and 3 km (2 mi) of displacement is observed on the east-west fault.

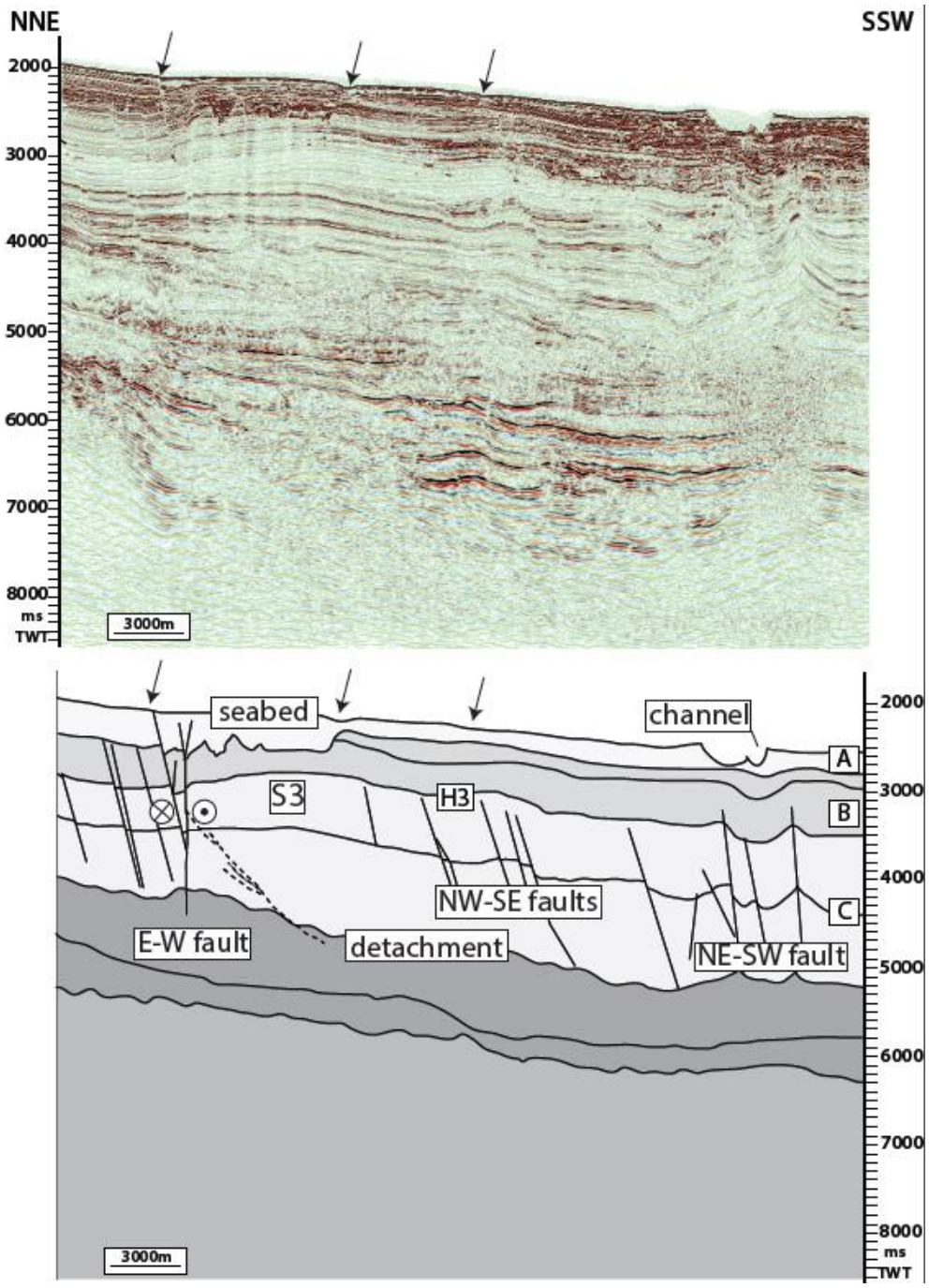

Figure 3.9 – 1North-northeast– south-southwest–oriented seismic section and interpretation showing the east-west strike-slip fault, normal faults dipping southwest, and the northeast-southwest strike-slip fault system. The thickening of the reflection packages in the northeastern part of the figure is caused by the presence of fold S3, obliquely crosscut by this section. The dashed line shows the position of a thrust fault trace (?) associated with fold S3. The arrows above the seabed reflection indicate the location of apparent subsidence at the seabed, suggesting the present-day activity of the underlying fault traces. TWT = two-way travel time. Approximate vertical exaggeration: x3.

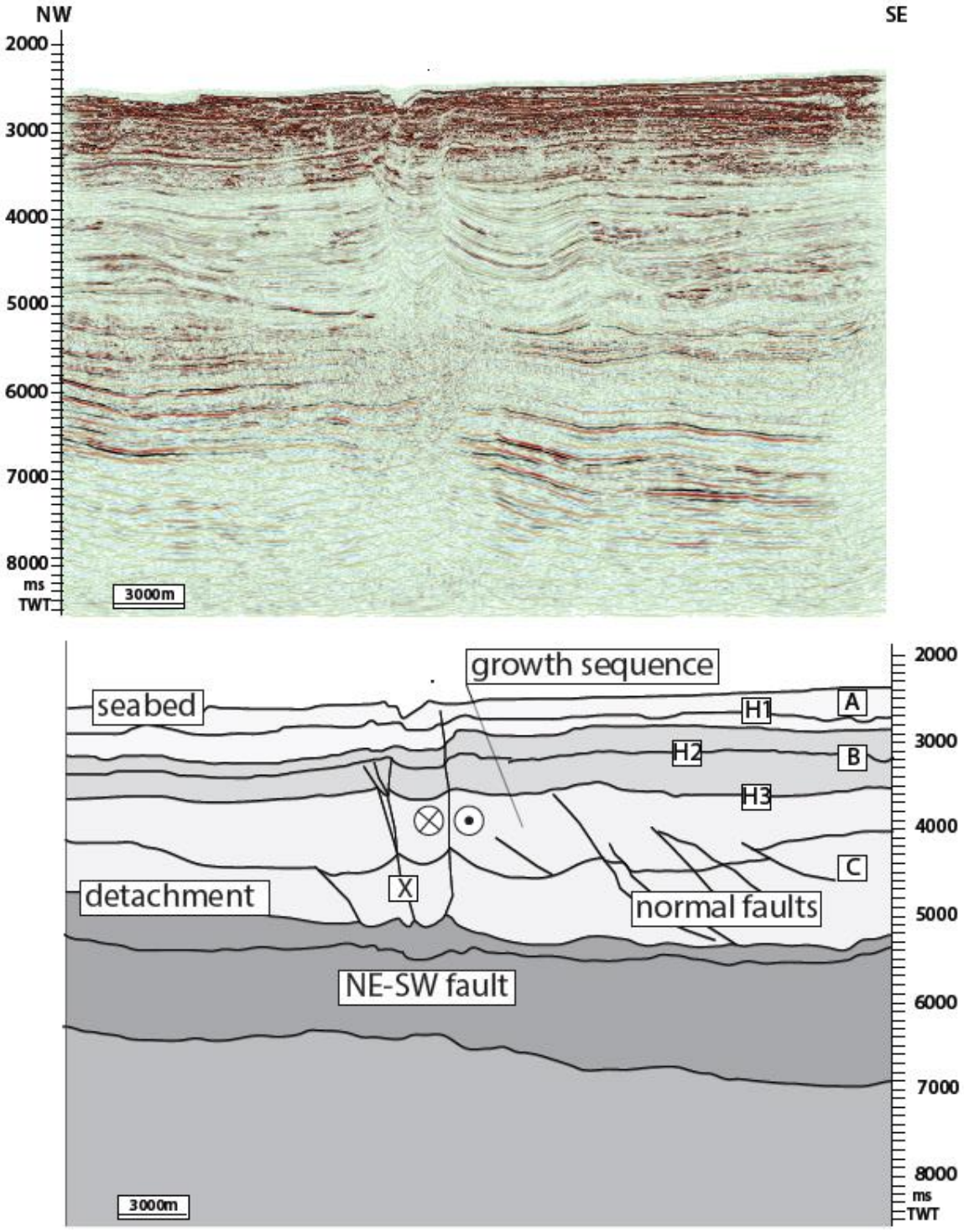

Figure 3.10 – Northwest-southeast– oriented seismic section and interpretation showing a negative flower structure on the northeast-southwest fault. All the fault traces together at the center of the figure are interpreted as a negative flower structure; however, at a smaller scale, the set of fault segments labeled "X" also presents negative flower structure geometries. Approximate vertical exaggeration: x3.

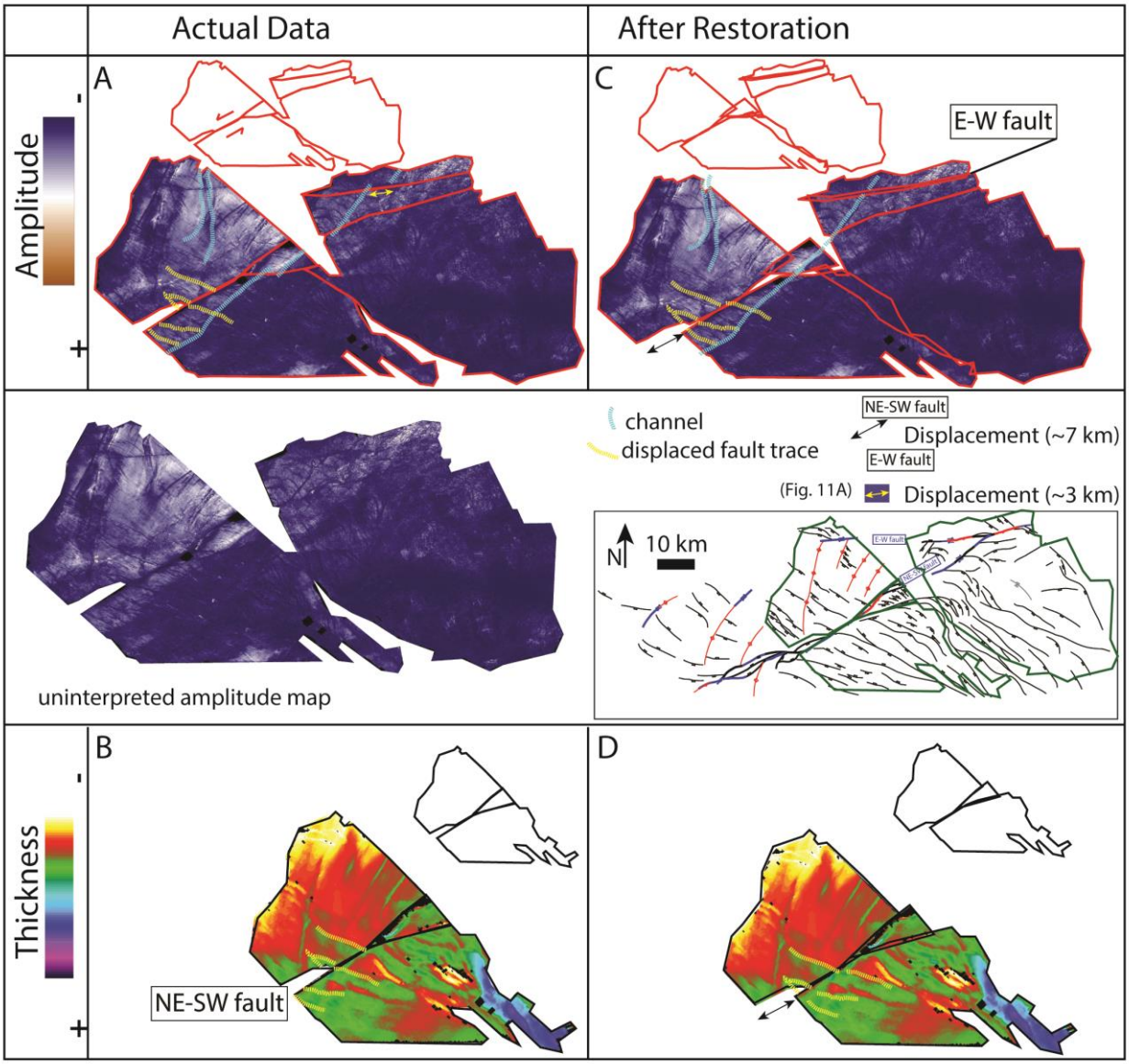

Figure 3.11 – Horizontal displacement on the northeast-southwest and the east-west strike-slip faults. (A, C) Amplitude extractions at H3 (maximum average amplitude, windows 100 ms two-way travel time (TWT) above and 100 ms TWT below H3, top of the figure) show the horizontal displacement on the east-west fault and the normal fault connecting to the northeast-southwest fault from the offset of the channel marked with the blue line. (B, D) Time isopach map between H3 and H4 showing the displacement of two normal faults bounding a graben by the northeast-southwest fault. The displacement on the east-west fault is indicated by a yellow double arrow (Figure 3.11A); the black double arrow indicates the displacement on the northeast-southwest fault (Figure 3.11C).

3.2.1.3 Compressional Zone

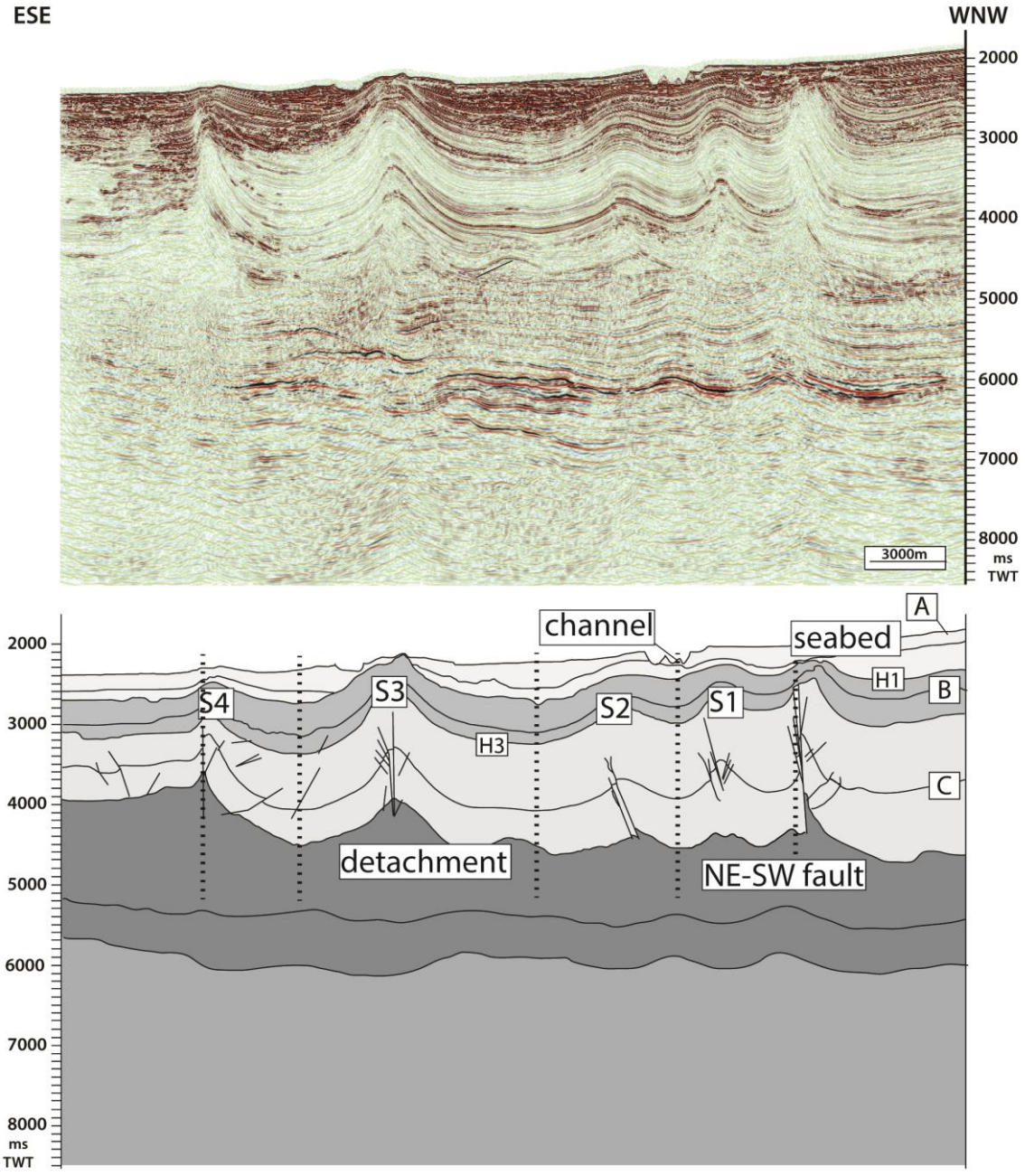

Figure 3.12 – East-west–oriented seismic section and interpretation showing the northeast-southwest fault and the four folds within the area of the restraining bend in the compressional zone. The vertical dashed lines demarcate folds S1 to S4. TWT = two-way travel time. Approximate vertical exaggeration: x3.

The compressional zone lies from kilometer 10 on the northwest flank of the northeast-southwest fault and to the south of the east-west fault (marked “compression” in Fig. 3.4). This

roughly triangular compressional area of approximately 540 km^2 (~210 mi^2) is composed of four arcuate folds numbered S1 to S4. From west to east, the maximum length of their hinge lines is 20, 6.5, 10.4, and 8.5 km (12, 4, 6.5, and 5.3 mi), respectively, at the depth of H1, and the folds have an average wavelength of 5 km (3 mi; Fig. 3.12). Assuming that this was measured on a constant reflection, shortening on each structure is estimated at 2.25, 0.75, 1.5, and 2.2 km (1.40, 0.47, 0.9, and 1.4 mi) for S1 to S4, respectively, yielding a total of 6.7 km (4.2 mi) for the entire system at the depth of H1 (Fig. 3.12). The folds are asymmetric, with a steeper forelimb (near vertical in the case of S4, as displayed on the seismic section). Complex fault traces are visible at the core of the folds, although the fault traces do not extend above H3. Deformation clearly affects the seabed only on folds S3 and S4 (Fig. 3.12), whereas folds 1 and 2 seem to have been buried by the most recent sediment package of unit A. This observation is interpreted as an evidence for a westward propagation of the fold belt, which is perpendicular to the general trend of the continental slope. Folds S3 and S4 gradually die out progressively onto the east-west fault (Fig. 3.4). This suggests that the development of the folds is interrupted by the east-west fault. The folds hinges actually die out onto the east-west fault. In terms of timing relationships, this is interpreted as a contemporaneous development of the strike-slip fault and the shortening features. However, the maximum visible displacement along the east-west fault has been estimated at 3 km (2 mi; Fig. 3.11), which is smaller than the total shortening estimated for the fold and thrust belt. However, the order of magnitude remains similar. It is possible to assess the relative timing of the fold activity by looking at onlap geometries, in particular, around fold S3 (Fig. 3.12). The sediment record is unequal at each fold, suggesting that activity on the folds varies. We suggest that S1 and S2 were active first and that their activity carried on until the present day. Fold S3 is currently buried, which can be interpreted as sedimentation locally overcoming fold growth. Finally, S4 syn-sedimentary activity occurs the latest because onlaps are only found on the top reflections. A timing relationship can be established as follows: (1)

development of the northeast-southwest fault; (2) propagation of the east-west fault to the west; (3) S1 and S2 growth; and (4) S3? and S4 starting to grow, whereas other structures remain active. Because no biostratigraphic data are available, however, prevents us from proposing any absolute age of deformation events in this article.

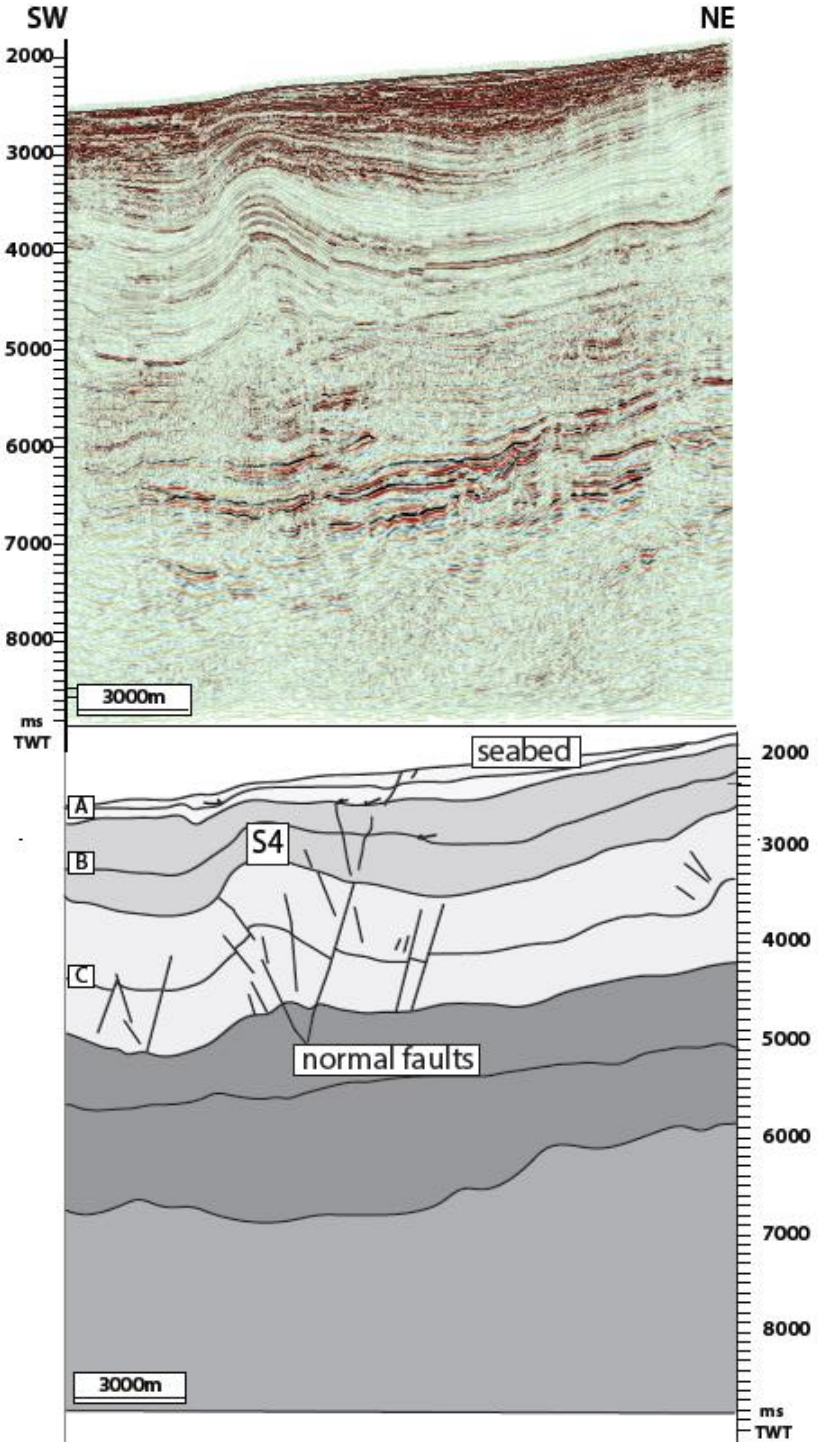

Figure 3.13 – Southwest-northeast–oriented seismic section and interpretation showing rotated normal faults on fold S4. TWT = two-way travel time. Vertical exaggeration: x3.

Whereas the compressional zone is dominated by folding, a few steep northwest-striking normal faults are also observed, with lengths of 2 to 7 km (1–4 mi; Figs 3.9 and 3.14). These faults

strike almost orthogonally to the folds. Normal faults dipping to the southwest are located on both the forelimb and the back limb of fold S4. Conjugate normal faults dipping northeast are also located on the forelimb. Horizon H4 is tilted and offset by these faults, but no offset is observed in the younger horizons. Recent subsidence seems to occur over the tip of the fault traces, whereas onlapping is found in unit A; however, it is hard to distinguish what is controlled by the fold growth or by the activity of the northwest-striking faults. These extensional features could either be interpreted as a marker of preexisting extension before the folding or could be resulting from a perpendicular extension contemporaneous to the folding. As evidence of normal fault offset is observed on both sides of the northeast-southwest fault (Fig. 3.11), we suggest that the steep normal faults (Fig. 3.14) are actually incorporated and rotated within fold S4 during the folding event and are therefore older than the fold.

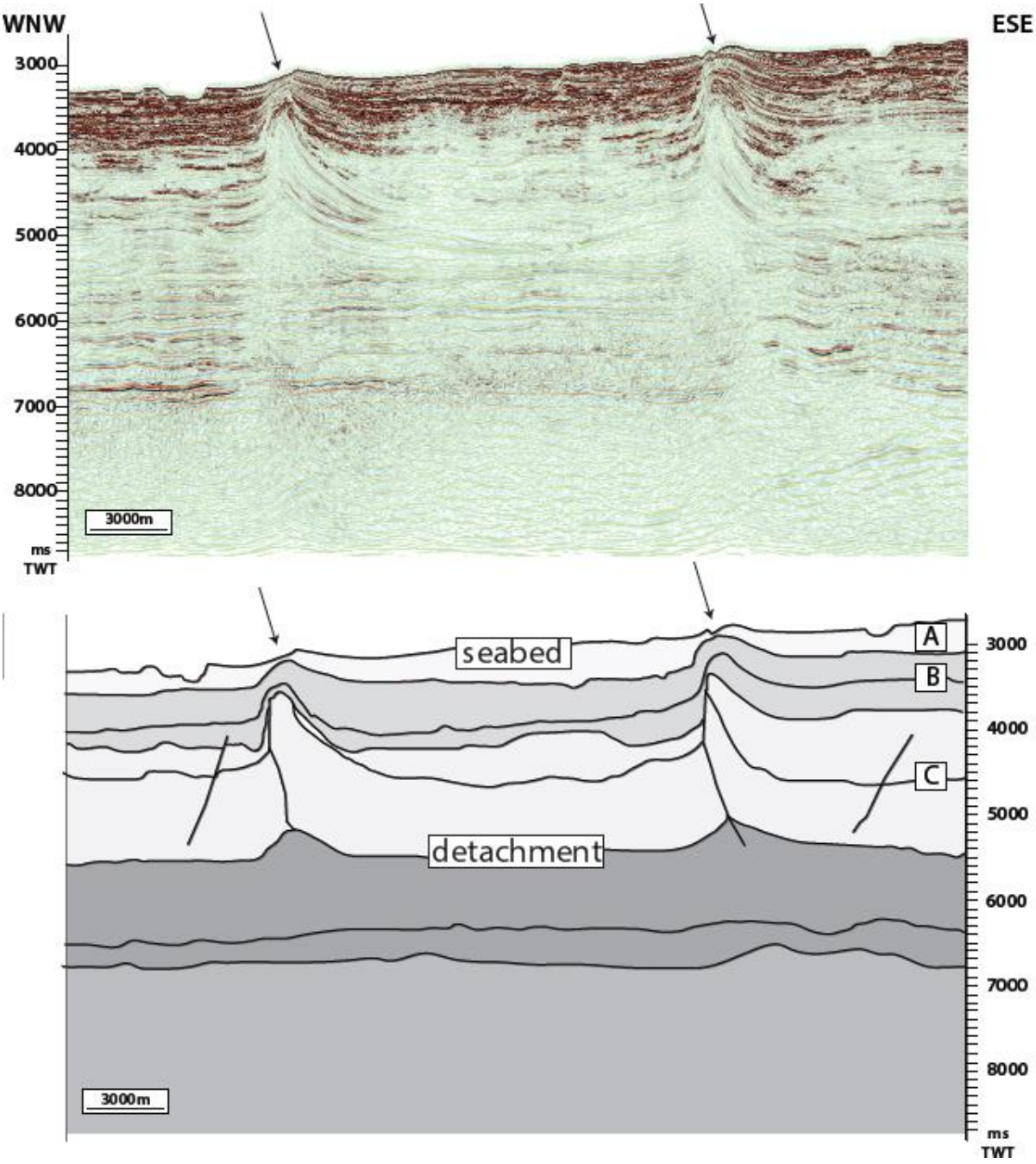

Figure 3.14 – East-west seismic section and interpretation, located west of the lateral strike-slip domain (LSSD), show two present-day developing northeast-southwest–oriented possible strike-slip faults that are just beginning to slip at present; therefore, no offset can yet be observed west of the LSSD. They display fault-propagating fold geometries. They could represent similar geometries to what used to be the earliest segments of the northeast-southwest fault geometries in its compressional part. TWT = two-way travel time. Vertical exaggeration: x5.

Two other compressional structures are observed in the western end of the studied area (Figs 3.4 and 3.14). They are west-vergent thrust faults associated folds. These structures create topography of approximately 300 m (~1000 ft) at the seabed and are responsible for the localized

erosion of unit A. Channels are localized at the front of the western structure and over the back limb of the eastern structure (Fig. 3.14). The faults within the folds are very recent features because no evidence for previous structural control of sedimentation is observed at the periphery of the folds. The folds are parallel with the northeast-southwest trend, and their shape is comparable to the compressional features of the strike-slip fault zone (Fig. 3.8). As a result, we suggest that these structures are associated with a compressional bend within the overall strike-slip domain.

3.3 DISCUSSION

3.3.1 Structural Relationships

Christie-Blick and Biddle (1985), Woodcock and Fischer (1986), Woodcock and Schubert (1994), and Cunningham and Mann (2007) provided 3-D models of the various geometries of strike-slip faults. The strike-slip nature of deformation on the northeast-southwest fault system is indicated by the wide range of structural features observed along strike. These features include a horsetail splay at the northeast end of the studied area, linking extensional features to strike-slip features (Fig. 3.4). The angle and the shape of the strike-slip features we described appear to be slightly different to what is found in the literature (Harding, 1985). For instance, the strike-slip compressive structure we present (Fig. 3.8) is comparable to a steep fault-propagation fold, its branching out appearing very asymmetric as the structure tilts westward. These changes in shape could be explained by the fact that sedimentation is syntectonic and will influence the shape of the final structure, as demonstrated in sandbox experiments (Casas *et al.*, 2000), or that braided geometries correspond to an advanced stage of growth.

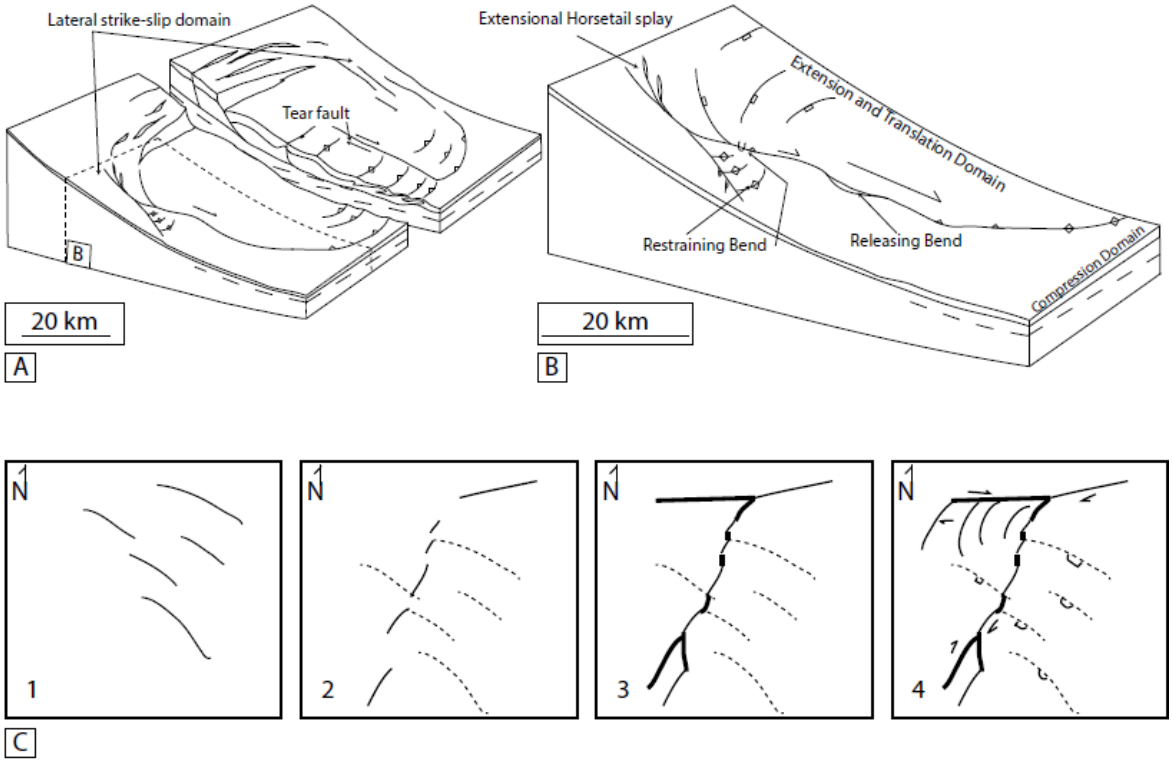

Figure 3.15 – The theoretical model proposed for the lateral strike-slip domain. (A) Three-dimensional block diagram to the scale of the deep-water deltaic lobe showing the geometric interplay between the main structures of each structural domain. (B) Cutaway from A, focusing on the lateral strike-slip domain. (C) Summary of the development of the main structures. 1 = extensional faults; 2 = early stages of strike-slip deformation; 3 = propagation of strike-slip faults; 4 = "restraining bend" area development, including the westward verging fold and thrust belt as a later stage of regional strike-slip deformation.

The northeast-southwest fault and the east-west fault define a major structural boundary at the lateral margin of the sedimentary lobe (Fig. 3.15) (Cobbold *et al.*, 2009), with the east-west fault representing a secondary continuation of the main fault to the west. This fault system is defined as a tear-fault system because it accommodates differential sliding between one sedimentary compartment included in the lobe and another outside the lobe. The dextral sense of slip is compatible with the downdip sliding of the margins of the delta lobe. The northeast-southwest fault thus links and transmits deformation caused by the normal faults in the extensional domain to the outer thrust belt in the compression zone over the detachment surface. The northeast-southwest fault zone was probably used to separate the slide mass from a relatively unfailed material. As it appears at present day, de-formation has expanded to the northwest (via the development of the fold belt) so that the active mass has grown in a second

more recent episode of deformation.

3.4.2 Relative Timing of Deformation

We can assess the relative timing of activity on the different structures associated with the lateral margin by interpreting crosscutting relationships between the different geometries and sediment growth packages. The complex braided geometries and widespread linkage displayed on the northeast-southwest fault indicate a mature stage in the faulting (Fig. 3.4). The east-west fault shows evidence for only recent stages of deformation in its westernmost segment (onlapping in the youngest packages). We therefore think that the western part of the east-west fault is younger than the northeast-southwest fault. The northeast-southwest fault system is developed as a vertical fault in the east where highly deformed structures similar to inversion structures are sometimes identifiable along strike seismic sections (Figs 3.6A and B). We suggest that the northeast-southwest fault has therefore locally become a factor both in extension and in compression during strike-slip deformation.

The combined east-west and northeast-southwest tear-fault system shows varying styles of de-formation and amount of displacement. Evidence for erosion caused by an uplift of the footwall on the northeast-southwest fault indicates that this fault has been active in the past and is still partly active at present day as uplifted zones (Figs 3.6A and B, 3.9 and 3.12) and subsiding zones (Figs 3.7, 3.9 and 3.10) occur on the seabed. The evidence for the deformation of the seabed by the western, but not by the eastern, folds is consistent with a very young age of deformation on the east-west fault. Complementary evidence for this comes from the tilting of units A, B, and C caused by the deformation on the east-west fault (Fig. 3.9), which shows that activity on the western part of the fault occurred very recently. This part of the fault likely developed after deposition of H1 (above which are observed the first growth strata; Figs 3.9 and 3.12).

Furthermore, we do not observe any sedimentary growth packages in the deposits on the footwall of this structure, indicating again very recent deformation. The east-west fault is still propagating westward at the present day. The fold hinges in the compressional zone are kinematically connected to the east-west fault, whereas no direct geometrical relationship can be established between the fold belt and the northeast-southwest fault. The curved shape of the fold hinges could indicate a decreasing anticlockwise rotation of the deformation front from the east-west fault to the northeast-southwest fault. Shortening in the west occurred at the same time as the east-west fault began to propagate to the west, building up what we interpret as a restraining bend area. We suggest that this area would be controlled by the growth of the east-west fault (Fig. 3.15C). This restraining bend is thought to be formed once the northeast-southwest fault and the east-west fault linked and developed contemporaneously to the propagation of the east-west fault to the west.

The extensional zone consists of numerous extensional fault traces, some of which display growth packages (Figs 3.4, 3.6A and B and 3.7). Growth sequences are visible in the seismic data and are probably associated with successive stages of de-formation (Figs 3.6A and B). We therefore show that this area does not undergo simple compression as it would be thought for a regional deep-water compressional domain (Fig. 3.1). We suggest that the northwest-striking normal faults in the compressional zone (Figs 3.9 and 3.13) developed contemporaneously to the faults with the same trend in the extensional zone, that is to say before H1. They then probably became inactive and have been reactivated as the fold belt grew in the compressional zone at very recent stages. The deposits over the detachment surface underwent a first phase of extension. During this period, extension was very limited in the compressional zone, and only a few small faults developed. A second phase of extension started after H2 to H3 and has continued to the present day. Strike-slip deformation on both the east-west fault and the northeast-

southwest fault probably began before the end of the first phase of extension but became predominant after H2. In fact, most of the structures related to strike-slip deformation seem to control post-H2 sediments. Deformation occurred at different stages along the strike of the strike-slip faults. Numerous smaller normal faults also indicate several ages of faulting. These fault traces are likely to be rotated by later shortening structure (e.g. Fig. 3.13).

3.4.3 Evolution of the Lateral Strike-Slip Domain

A schematic block diagram (Figs 3.15A and B) including the location of the lateral strike-slip do-main in a gravity-driven detachment system shows the geometric interrelations between the extensional, translational, and compressional domains using the analogy of a mass-transport complex. At the scale of 100 m (300 ft) to 10 km (6 mi), lateral margins are mostly documented, and their geometries are comparable to what we observe in the western Niger Delta. Extensional faults evolving to transfer faults and to purely strike-slip deformation have been reported from field examples. For instance, pure strike-slip deformation occurs on slumps of constant width (Martinsen and Bakken, 1990). This evolution in the structures illustrates, in the case of slides, a lateral expansion of the margins, leading to a change in their width.

The compressive structures linked to the lateral strike-slip domain are younging westward, which shows that the structural domain is getting wider with time. Deformation is more likely to propagate laterally over a previously unfailed margin because it has no constraint to stop its propagation, leading to the development of the lateral strike-slip domain. This increase in width may also indicate that the local overburden cannot effectively slide downslope compared with other areas. This may be because the detachment surface is less conducive to sliding or because the sediment overburden at the lateral margin is relatively thin and less prone to downslope motion. We speculate that a local change in effective stress caused by overpressure development in the lateral variations of sediment thicknesses could cause a control on stress

patterns, leading to the expansion of this structural domain. Alternatively, an abrupt increase in the regional sediment input, coupled with spatially non-uniform accumulation, could also trigger the regional partitioning of the slide mass. Therefore, the slope angle would be expected to increase in areas of greater sedimentation and the more central parts of the sedimentary lobes would be more likely to become unstable and begin to slide basinward. The origin and development of tear faults is likely to be common in any gravitational system driven by a high sedimentation (or sediment supply) rate.

Irregularities within the detachment such as a change in the nature or thickness, therefore, rheology of the sediments, such as the Dahomey wedge, a thinner shale unit included in the Akata Formation (Morgan, 2004) (Fig. 3.3), may explain the development of strike-slip stresses in this particular region. Otherwise, Treviño and Vendeville (2008) provided an example of a normal fault in the hanging wall of a major growth-fault complex with a strike line that is perpendicular to the direction of deformation. They suggested that a slight convergence or divergence of the stresses from the center of the structure could lead to the growth of coast-perpendicular structures in the sedimentary cover as coast-parallel convergent stresses occur in the detachment unit. A similar process can be suggested for our strike-slip fault zone because its general strike is perpendicular to coast-parallel extensional features.

Finally, the position of the northeast-southwest strike-slip fault zone could also be controlled by a preexisting basement structure (transfer faults from the rifting event associated with the formation of the underlying oceanic crust). The basement in this area is shallower (~5km[~3 mi]) than that in the central part of the deep-water delta (up to 10–12 km [6–7 mi]) because the sedimentary overburden is wedging to the northwest and therefore becomes thinner than areas farther to the southeast on the delta lobe. The higher basement could act as a buttress that would

confine the slide and control its dimensions.

Tear-fault systems in such a setting may provide structural traps for hydrocarbons and localize syn-deformation sedimentation in a similar way to continental tear-fault systems. Deepwater sedimentation may be controlled by such structures and additional migration pathways could be created through deformed strata.

3.5 CONCLUSIONS

A complex strike-slip fault zone in the northwestern deep-water Niger Delta is composed of extensional, strike-slip, and reverse faults. The complex forms the northwestern lateral margin of the deepwater western Niger Delta, but comparable structures may occur at the margins of both sedimentary lobes of the Niger Delta, as well as in similar deep-water delta settings on other gravity-driven detachment systems. Situated at the lateral boundary of the translation domain, the lateral strike-slip domain links deformation between the extensional and compressional domains.

This article shows that the lateral margins of a regional-scale gravitational collapse provide clues in understanding the kinematics and timing of deformation between the extensional and compressional parts of such features. Regional lateral margins are structurally complex, but heir evolution is predictable. They can also provide structural traps for hydrocarbon accumulations. We suggest that the position of the lateral strike-slip domain is either controlled by a modification of the underlying detachment properties and efficiency or that preexisting basement elements still influence the sedimentation and compartmentalization of gravitational collapse.

CHAPTER 4: GRAVITY-DRIVEN TEAR FAULTS: A CONTROL ON SEDIMENT ROUTING IN DEEPWATER SETTINGS

Abstract

We use a number of three-dimensional seismic datasets from offshore of Mauritania and offshore Nigeria to assess the interactions between tear faults and deepwater submarine channel systems on continental margins. Structural observations combined with channel analysis are performed in four case studies in order to illustrate a variety of local settings and stages of development. Based upon the Mauritania data we propose that new gravity-driven tear faults are the sites for the early stages of canyon and channel development, leading to a long-lived canyon. Low sinuosity and a deep incision thalweg are characteristics of these stages. The Mahin and Ijebu channels, offshore Nigeria, help to describe the submarine channels migration history around strike-slip related structures that are parallel to the continental slope. The analysis of the Mahin channel depositional patterns also provides an illustration to the evolution of channel systems and focus points at the periphery of pull-apart basins. The spatial relationships we observe in both datasets suggest that: (1) tear fault zones can strongly influence submarine channel development, sinuosity and lateral migration in causing a strong structural confinement; (2) this control persists over successive stages in the evolution of the fault and channel systems; (3) we propose that there is a complex interplay between deformational processes along the fault and the development of the channel systems. More generally, these Interrelationships can be observed from the scale of depositional elements to regional trends. Since gravitational faults and deepwater channel and canyons occur in similar settings our synoptic model should have application elsewhere.

Keywords: tear fault; sediment; bypass; sinuosity; slope; submarine; channel; syn-sedimentary ; deformation.

4.1 Introduction

4.1.1 Gravity detachment systems and tear faults

Gravity detachment systems occur at a variety of scales and geological settings (e.g. Farrell, 1984; Morley and Guerin, 1996; Rowan *et al.*, 2004; de Vera *et al.*, 2010). They are generally divided into upslope extensional, translational and downslope contractional domains (e.g. Damuth, 1994). Passive margins undergo gravity-driven structural deformation as a result of high sedimentation rates and slope instabilities (e.g. Cobbold and Szatmari, 1991; Rowan *et al.* 2004). They are found at continental margins all around the world and have been of interest for their potential in hosting major hydrocarbon plays over the past forty years.

Tear faults allow a differential displacement between adjacent structural units (Biddle and Christie-Blick, 1985). In gravity detachment systems, tear faults may occur at the lateral boundaries of the sliding systems over detachment levels (Rowan, 2011; Leduc *et al.*, 2012) as a result of a variation in slope orientation and gradient, or due to variations in the rheological properties of the detachment unit (e.g. Leduc *et al.*, 2012). Examples of these faults are currently documented from the Niger Delta (Morgan, 2003 and 2004; Cobbold *et al.*, 2009; Maloney *et al.*, 2010; Leduc *et al.*, 2012), but are expected to be found in many other regions (e.g. Montgomery *et al.*, 2009). They are larger-scale geometric equivalents to the lateral margins of mass-transport complexes, where the differential displacement and rate of development are very diverse (Maltman, 1994; Leduc *et al.*, 2012). They can provide information on the deformational mechanisms of regional slope failures and have a potential to contribute to the formation of hydrocarbon traps.

The role of strike-slip deformation has been extensively studied for tectonic strike-slip settings in both fluvial and marine environments (e.g. California: Christie-Blick and Biddle, 1985; Dead Sea: Manspeizer, 1985; Spain: Haughton, 2000). Although it has been proposed by Damuth (1994), Armentrout *et al.* (2000) and Morgan (2003 and 2004) that tear fault zones could have a greater influence on channel location than ramp anticlines in the Niger Delta as they are slope-parallel and potentially ubiquitous, the importance of tear faults for sediment routing has not been thoroughly investigated. Gravitational tear faults could influence contemporaneous sedimentation in a similar way to what is observed in active tectonic strike-slip settings and slope-parallel, confined submarine channels could be important sediment bypass areas.

In this study we assess the role of slope-parallel, syn-sedimentary tear faults in influencing channel systems migration and depositional architecture. Four areas of interest are chosen (Fig. 4.1) for the quality of the information they provide: one of shows near-seabed geometries of a tear fault, a second illustrates the paleo-record of submarine channels in a contractional zone of a slope-parallel tear fault zone, whereas the third example displays tear fault – channel interactions in extensional regime. A fourth example provides support for local migration controls induced by tear fault activity.

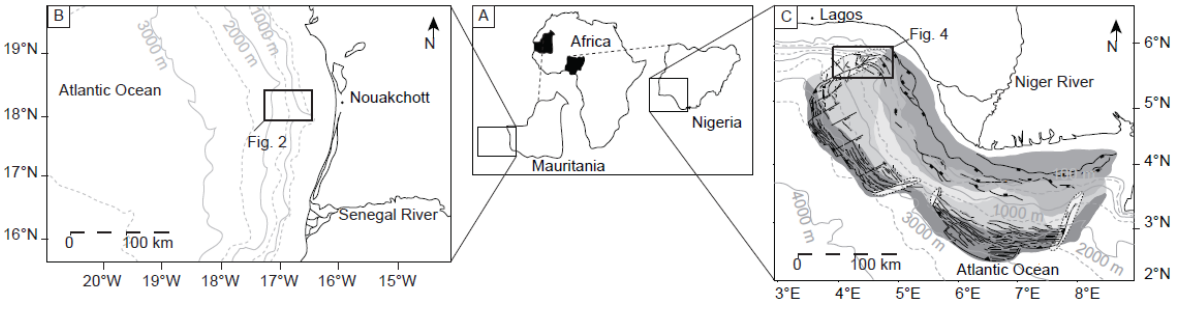

Figure 4.1 A. Location map of the four areas of interest, West Africa. B. Seismic data coverage, area 1, offshore Mauritania. C. Seismic data coverage, areas 2, 3 and 4, deepwater western Niger Delta.

4.1.2 Submarine channel systems

An extensive range of submarine channel geomorphological studies have been published using 2D and 3D seismic data (Piper and Normark, 1983 and 2001; Babonneau *et al.*, 2002; Deptuck *et al.*, 2003; Posamentier and Kolla, 2003; Robinson *et al.*, 2004; Adeogba *et al.*, 2005; Wynn *et al.*, 2007; Cross *et al.*, 2009; Catterall *et al.*, 2010), and these have helped in identifying many depositional elements and processes that are specific to these environments. Classifications of submarine channels by sedimentological and geomorphological records have also been established (e.g. Piper and Normark, 2001) in order to understand the relationships between morphologies, structural settings and sediment patterns. Depositional patterns in submarine channels imaged with 3D seismic data have been used extensively as indicators of structural faults and folds growth in deepwater settings (e.g. Beaubouef *et al*, 2000; Hooper *et al.*, 2002; Abreu *et al.*, 2003; Deptuck *et al.*, 2003; Morley, 2009; Clark and Cartwright, 2009 and 2011). However the efficiency of this method is limited to settings where the sediment record is not heavily affected by erosion or deformation. 3D seismic analysis can provide data at a variety of scales (10 m to 10 km) which can offer accurate information on how these systems would interact and their potential importance for regional sediment routing systems and stratigraphic patterns.

Seismic analysis of modern and buried submarine channels is used to better understand structural growth in gravity detachment systems (e.g. Morley, 2009). Clark and Cartwright (2009 and 2011) proposed a detailed methodology to assess the interaction between submarine channel morphologies and adjacent growing folds. They analysed channel and levee depositional patterns as well as quantitative data from the spatial variation in sinuosity and channel fill and erosional depth. Channel diversion and confinement were found in tectonically active strike-slip fault zones, resulting in an increase in channel sinuosity when channel course was diverted, and aggradation where confinement occurred. In their results, diversion differs from deflection.

Diversion is characterized by a change in channel path as it meets a pre-existing structure whereas deflection illustrates a process of channel migration during the growth, for instance of a fold, over time. In addition, Jerolmack and Paola (2007) modelled avulsion processes and their relationship to long-term channel pathway migration. Their results show that once the extent of a floodplain is defined, the later channel avulsions will take place within this floodplain; that is to say the channel pathways remain persistently in a nearby location, illustrated by stacked channel patterns.

4.1.3 Geological settings

4.1.3.1 Area 1: offshore Mauritania

We focus on the area of the present-day partially filled Nouakchott-North channel system (Fig. 4.2A). Plio-Pleistocene deposits are affected by turbiditic sedimentation (Holtz *et al.*, 2007; Zühlsdorff *et al.*, 2008). Deposits undergo remobilization by slope processes such as mass-transport (Wynn *et al.*, 2002; Antobreh and Krastel, 2006; Henrich *et al.*, 2010; Förster *et al.*, 2010) and fluid escape. Numerous gas chimneys, pockmarks and gas hydrate accumulations, as well as associated slope instabilities have been documented in the area of interest (Lane, 2005; Davies and Clarke, 2010; Yang and Davies, 2013). The study area is located above a structural high and the sedimentary succession of interest is recent to Pliocene in age (Vear, 2005). Deepwater sediments are mud-rich, punctuated with episodes of turbiditic coarse-grained sedimentation, as well as carbonate build-ups in the upper part of the slope (Henrich *et al.*, 2010; Vear, 2005).

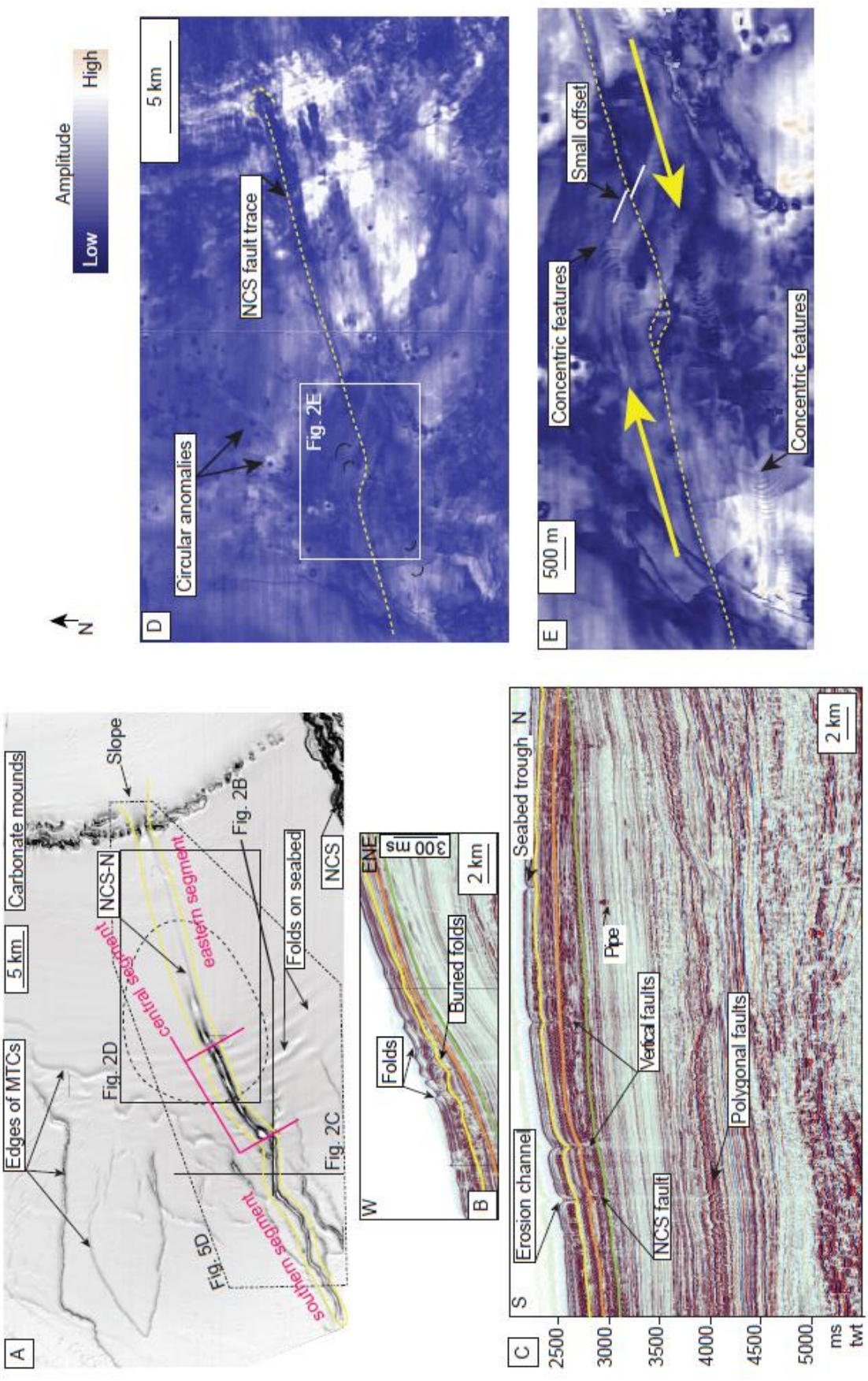
A
Edges of MTCs
Carbonate mounds
5 km
Slope
Fig. 2B
NCS-N
Fig. 2D
Transect 1
Central segment
eastern segment
Folds on seabed
NCS
Fig. 2C
Fig. 5D
southern segment
B
W
Folds
Buried folds
2 km
ENE
300 ms
C
S
Seabed trough_N
Erosion channel
Pipe
Vertical faults
NCS fault
Polygonal faults
2 km
2500
3000
3500
4000
4500
5000
ms
twt
N
D
Amplitude
High
Low
5 km
NCS fault trace
Circular anomalies
Fig. 2E
E
500 m
Small offset
Concentric features
Concentric features

Figure 4.2 Area 1, offshore Mauritania, showing the Nouakchott Channel System-North (NCS-N) and the Nouakchott fault. A. Seabed map. The dashed sub-circular outline indicates the location of the buried Khop structure. The Nouakchott tear fault lies below the channel system, outlined in yellow; the three segments of the NCS-N are separated by pink lines. "Folds" on the sea bed are interpreted as due to concentric shallow slope failures, described as "folds caused by creep" or contourites in the text. B. W-ENE seismic profile across the NCS-N showing transversal geometries of these concentric folds over pre-existing buried ones. C. N-S seismic profile across the Nouakchott tear fault. The yellow horizon is H1, the orange is H2 and the green is Z. Vertical exaggeration 4x. D. Amplitude extraction map of horizon Z showing a releasing bend structure and braided geometries at depth in the tear fault zone, indicated by a thin dashed yellow line. The upslope fault tip is highlighted by the thicker dashed yellow line. E. Close-up of the tear fault trace geometry (thin dashed yellow line) showing the dextral sense of slip. White segments on each side of the fault highlight the small offset observed.

4.3.1.2 Areas 2, 3 and 4: deepwater western Niger Delta

These data are approximately central to the western lobe outer thrust belt (Fig. 4.1B) which is characterized by up to 12 km of syn-deformational Miocene to Holocene clastic sediment (Doust and Omatsola, 1990) that was deposited in a gravity detachment system (Morley and Guerin, 1996). Downslope deformation occurred over multiple detachment levels caused by overpressured shale (Briggs *et al.*, 2006). The north-western area of coverage (areas 2 and 3) includes the Avon and the Mahin channel systems (Deptuck *et al.*, 2003; Adeogba *et al.*, 2005; Olabode and Adekoya, 2008), and a 75 km strike-slip fault zone, oriented in a NE-SW direction (Leduc *et al.*, 2012). Submarine channel systems in the Niger Delta are often confined by structural growth of faults, either normal or reverse, and folds and their morphological evolution relies on the evolution of the local structural setting (Adeogba *et al.*, 2005; Heiniö and Davies, 2006 and 2007). These areas of interest display larger channel systems than in offshore Mauritania and a NE-SW tear fault zone which hosts a variety of strike-slip related structures along strike (Leduc *et al.*, 2012). It is selected to analyse interactions between active strike-slip structures and channel location and depositional patterns. The second dataset in area 4 covers the Ijebu and Iwo channel systems in a contractional domain characterized by thrusts and back thrusts (Heiniö, 2007). In this area tear faults are present but they seem to be of less importance

in the morphological evolution of the area. One of these tear faults is however located nearby a recent channel system, and the lateral migration of channels in this region is assessed.

4.2 Data and methods

4.2.1 3D seismic datasets

4000 km^2 of seismic data cover the offshore Mauritania study area with a survey bin size of 25 x 25 m. These data were processed using multiple suppression and post-stack time migration and are minimum phased. An increase in acoustic impedance is represented by a red-over-black reflection. Seismic profiles from offshore Mauritania are displayed with a vertical exaggeration of ~ 3 in order to better display subtle vertical features. The second dataset, in the Niger Delta was acquired by PGS in 2003 and covers 3678 km^2. It is a pre-stack time migrated volume, with a line spacing of 12.5 m and 18.75 m. The third dataset (area 4) covers 1630 km^2 of the deepwater Niger Delta. Line spacing is 12.5 m in both directions. Datasets are zero-phase migrated and an increase in acoustic impedance is displayed as a red-black-red reflection loop. Water depths are between ~ 450 m to 2500 m for the seismic data covering areas 1, 2 and 3; area 4 is located under water depths of 2000 m to 3000 m. In this paper, seismic profiles are displayed in milliseconds two-way-time (ms twt) for the vertical scale, with an average velocity of 1481 $m.s^{-1}$ for seawater and 2000 $m.s^{-1}$ in the sediment record (Schultheiss *et al.*, 1987). In the studied vertical interval, a frequency of 55 Hz provides a vertical resolution of ~ 8-12 m.

4.2.2 Channel system analysis

Area 1 is located over the Nouakchott Channel System-North (NCS-N), offshore

Mauritania. This area is 56 km long downdip and 29 km wide (Figs. 4.1A and 4.2A). Here we analyse a modern channel system and its interaction with a minor tear fault. Continuous horizon reflections were interpreted at the seabed, at the current erosional base (horizon H1.0), and the inferred previous maximum erosion surface at the base of the channel (horizon H1.1) of the NCS-N, and on an underlying undisturbed reflection (horizon Z).

In the Niger Delta region, two areas where the Mahin channel system (MCS) and the NE-SW tear fault interact were selected for the difference in structural style in place. Area 2 is ~ 13 km (east-west) by ~ 9 km long (north-south) and is located over an antiform along the NE-SW fault (Fig. 3A; Leduc *et al.*, 2012). At the present day the Mahin channel system flows next to the related bathymetric high. Area 3 is 14 x 8 km and is positioned over a pull-apart basin located further downslope on the same NE-SW fault zone (Fig. 4.3A, Leduc *et al.*, 2012). Area 4 was used for comparison with the other examples; it is located in a compressive setting and includes tear faults developing between active folds that behave as potential lateral ramps. It presents local channel migration against growing structures near the seabed (Fig. 4.4A).

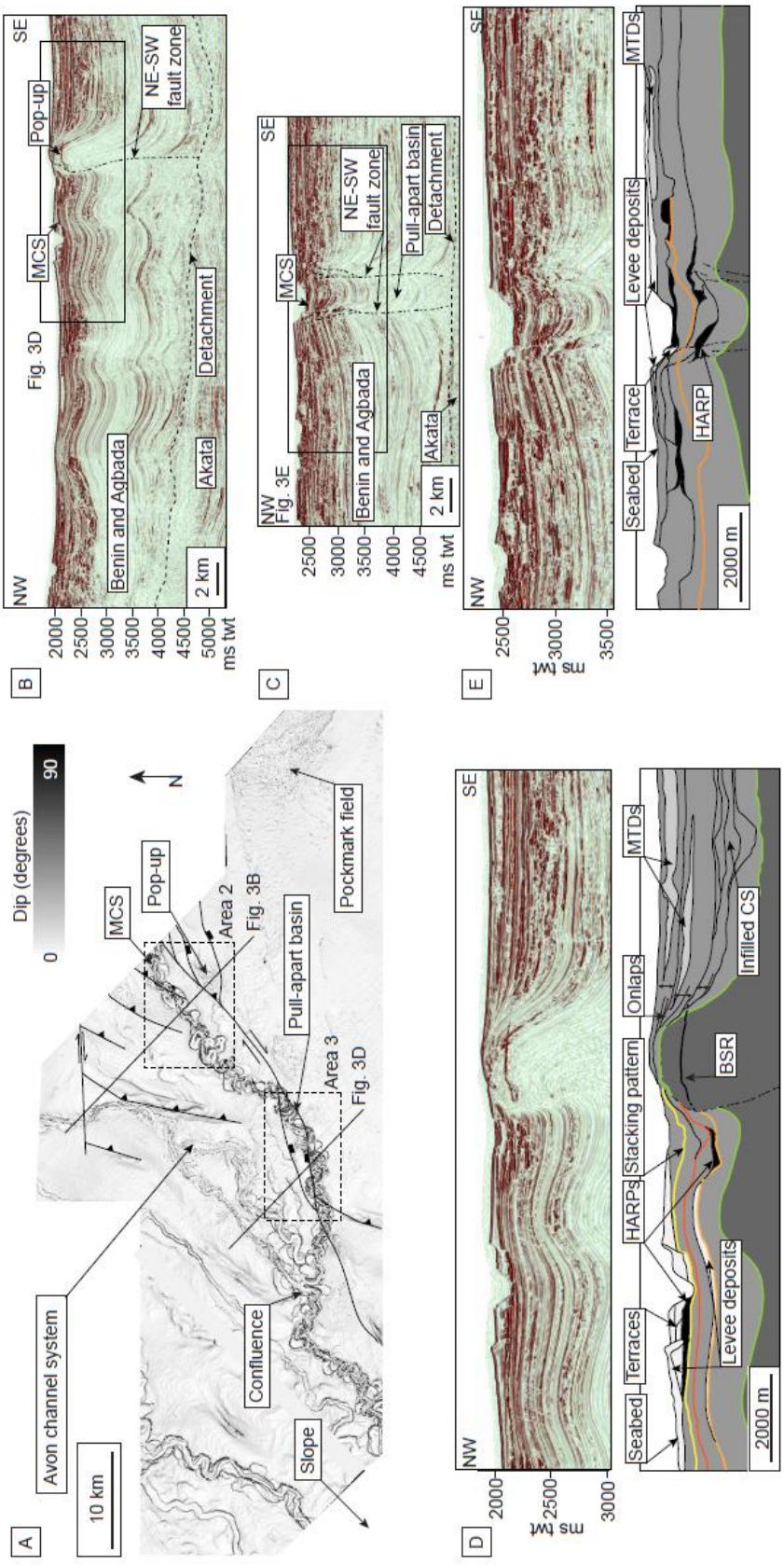
A
Avon channel system
10 km
Dip (degrees)
0
90
N
MCS
Pop-up
Area 2
Fig. 3B
Pull-apart basin
Area 3
Fig. 3D
Pockmark field
Confluence
Slope
B
NW
SE
Fig. 3D
MCS
Pop-up
NE-SW fault zone
Benin and Agbada
Akata
Detachment
2 km
ms twt
C
NW
SE
Fig. 3E
MCS
NE-SW fault zone
Pull-apart basin
Detachment
Benin and Agbada
Akata
2 km
ms twt
D
NW
SE
ms twt
MTDs
Onlaps
Stacking pattern
HARPs
Terraces
Seabed
Levee deposits
BSR
Infilled CS
2000 m
E
NW
SE
ms twt
MTDs
Levee deposits
Terrace
Seabed
HARP
2000 m

Figure 4.3 Areas 2 and 3, western deepwater Niger Delta, showing the Mahin Channel System (MCS) and the NW-SE tear fault. A. Seabed map. B. NW-SE oriented seismic profile across the MCS in area 2, showing the pop-up structure. The yellow horizon is H1.1, the dark orange is H1.2, the light orange is H2 and the green is Z. Vertical exaggeration x4. C. NW-SE oriented seismic profile showing the fault traces geometries across the pull-apart basin, area 3. D. Detail of seismic profile and interpretation across the MCS in area 2 showing channels location and confined depositional architecture near the pop-up. A succession of stacked and filled paleo-channels is observed near the pop-up. The oldest paleo-channel (d) as well as the current seabed channel system (a) display preserved levees geometries, whereas the intermediate stacked and filled paleo-channels (c; c' and b) do not show obvious levee deposits. E. Detail of seismic profile and interpretation across the MCS in area 3. MTD stands for mass-transport deposit; HARPs stand for high amplitude reflection packages. (e) indicates the location of the southern paleo-channel.

Horizon interpretations were performed on the seabed, at the base of the present-day MCS (horizons H1.1 and H1.2, channel systems a) towards the top of the paleo-MCS fill, at the base of the paleo-MCS (H2, channel system (c)) and at its base (Z, channel system (d)). For each area we first assessed the present-day channel and levee depositional patterns and the relationship between onlap reflections associated with levees and neighbouring strike-slip related faults. Lateral migration of the channel systems through time due to local structural growth was analysed using amplitude and horizon dip maps (Brown, 2004). These maps were also used to study the downdip sinuosity variation of the paleo and present-day channels, measured as a ratio between the channel length and the downslope distance and using intervals of measurement of 1.5 km. Isochron maps were also computed between the erosional base of the most recent channel and the seabed reflection to depict the current channel geometries and fill. In this paper, a channel system is a slope depositional element characterised by a complex cut-and-fill architecture. A channel refers to a sub-element of the channel system defined between an erosional base and consequent passive and active channel fill volume, itself being part of a channel complex (Posamentier and Kolla, 2003).

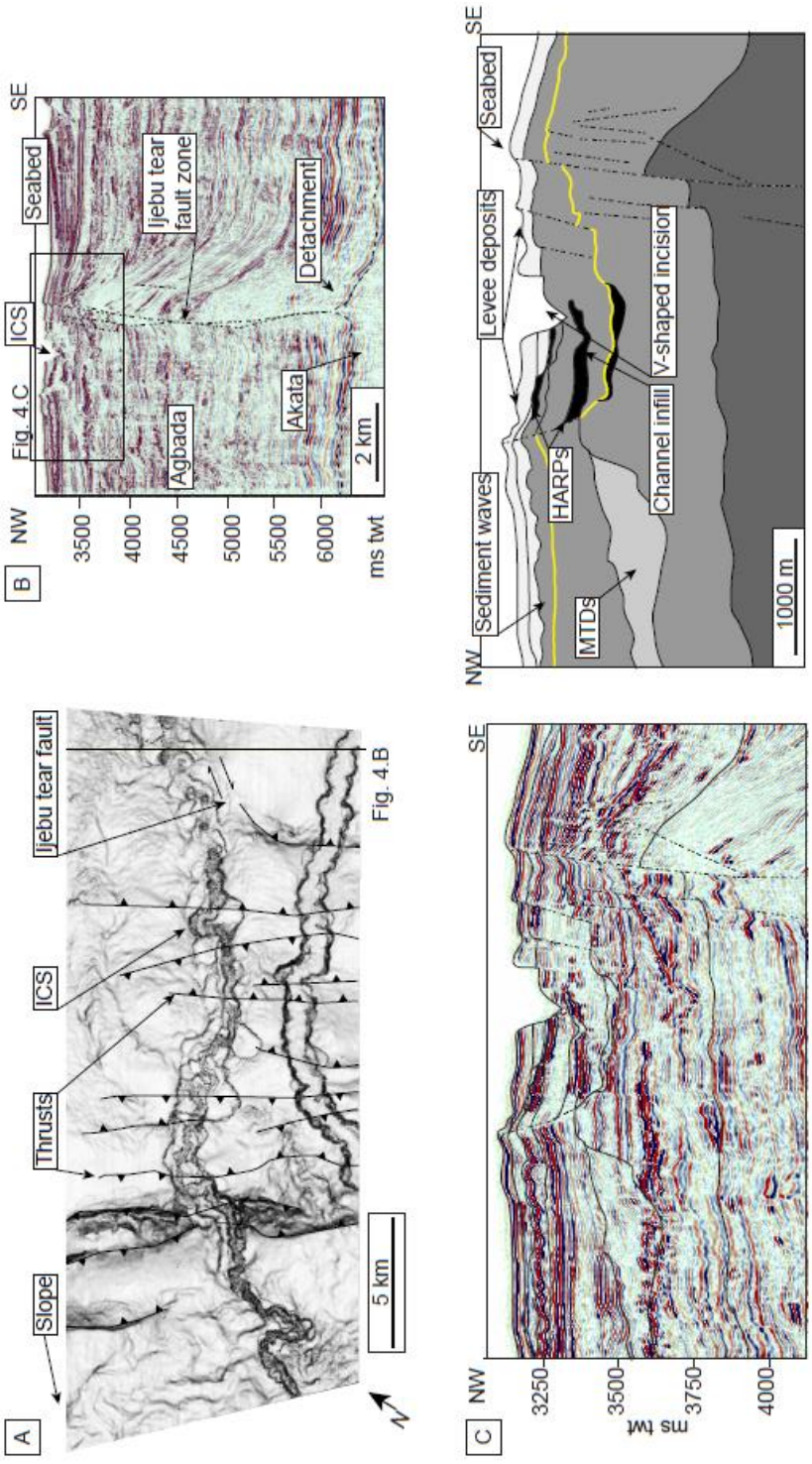

Figure 4.4 Area 4, deepwater Niger Delta, showing the Ijebu Channel System (ICS) and the Ijebu fault. A. Seabed map. Vertical exaggeration x4. B. NW-SE oriented seismic profile showing the tear fault. The yellow horizon is H1. C. Detail of the same seismic profile and interpretation showing the depositional patterns of the ICS against the tear fault traces.

4.3 Observations

4.3.1 Gravity driven structures

4.3.1.1 Area 1, offshore Mauritania.

In area 1, numerous ridges (~ 100 m up to 30+ km long) with an asymmetric relief (~ 20 m) mark the seabed (Fig. 4.2A). For example one of these seabed ridges shows along-strike wavelength of ~ 3 km and can be followed downslope for over ~ 20 km. Another set of ridges are interpreted as the edges of mass-transport complexes (Fig. 4.2A; e.g. Förster *et al.*, 2010; Yang and Davies, 2013). A third set of seabed ridges are parallel to one another, with an across-strike wavelength of less than 1 km, and have similar morphology to small-scale "folds" caused by creep (e.g. Jansen *et al.*, 1987). These "folds" develop in a limited belt, parallel to the strike of the slope. They could also be interpreted as contourite deposits. A seismic profile shows their internal architecture (Fig. 4.2B) which consists of internal reflections within the folds that are parallel and continuous over ~ 500 m of wavelength and a two-way-travel time amplitude of 70 ms, but the reflections stop below troughs. The troughs are asymmetric, with a gentler downslope side and a steeper upslope side. Individual, sub-circular depressions are also occasionally observed on the seabed within these folds (Fig. 4.2A and B). They can be up to ~ 800 m in diameter and are occasionally sediment-filled (Fig. 4.2B). Finally, vertical zones of disturbed reflections, 600 to 800 ms deep are also observed (Fig. 4.2C). They are spatially associated to a relatively dense cluster of buried, circular anomalies at depth (Fig. 4.2D) and probably represent vertical pipes.

There are also lineaments identified from the seabed reflection down to ~ 500 ms twt below the seabed (Fig. 4.2C), extending E-W parallel to the slope direction. On seismic profile these features appear to be vertical fault traces, or tear faults that extend from the seabed

reflection down to ~ 500 ms twt below the seabed (Fig. 4.2C). A trough on the present seabed down to a depth of ~ 50 m is identified on the top of each one (Fig. 4.2C). High amplitude anomalies are found underlying these troughs, possibly indicating a locally focused higher concentration in fluids (Yang and Davies, 2013). At horizon Z, one of the fault traces appears as a ~ 31.3 km-long, ~15 m to 1000 m wide, low-amplitude linear feature. It has a WSW strike (Fig. 4.2D). It is located well above an enigmatic, roughly circular basement high called the "Khop structure" (Vear, 2005). A slight change in slope dip occurs across the trace of this boundary in separate northern and southern seismic reflection packages with a seabed offset of ~50 ms (down to the south) occur across the trace of this fault (Fig. 4.2C). The northern package is ~ 50 ms thicker than the southern package, and the seabed occurs at 2450 ms twt in the northern package, whereas in the southern package it is at > 2500 ms twt (Fig. 4.2C). The fault tip coincides with a circular morphology, and braided geometries over ~ 14 km along strike are seen. A ~ 1.5 km step-over (Fig. 4.2D and E) is observed over this braided section. The step-over is associated with concentric amplitude anomalies (Yang and Davies, 2013) which seem to develop parallel to the step-over and are offset by the fault. These observations suggest that the fault is a tear fault of higher importance than the near-seabed, smaller-scale, faults, and is here referred to as the NCS tear fault. The observation of the downdip expression of the fault and variations in amplitude around the fault zone suggest a right-lateral sense of slip (Fig. 4.2E).

4.3.1.2 Areas 2, 3, and 4, deepwater Niger Delta

A full description of the NE-SW striking tear fault in areas 2 and 3 is provided in Leduc *et al.* (2012). Faults in these areas extend from the seabed down to 5000 ms twt (or ~ 6000 m; Fig. 4.3C). Area 2 is defined around an oval bathymetric high, stretching for 8 km NE-SW and 2 km NW-SE (Fig. 4.3A and B). The high is defined by an asymmetric subvertical fault-propagating fold

propagating westward, in the NE-SW fault zone (Fig. 4.3B, Leduc *et al.*, 2012). Reflection geometries vary across the fold: onlapping reflection packages indicate recent local structural growth on the southeast flank, whereas more diverse reflection geometries, including high amplitude reflection packages (HARPs), parallel reflections, onlaps and truncations (e.g. Posamentier and Kolla, 2003) are found to the northwest (Fig. 4.3D). A bottom simulating reflection (BSR) is identified across the fold over an area of ~ 15 km². The BSR progressively disappears to the southeast whereas it abruptly stops on the NE-SW fault to the northwest (Fig. 4.3D).

Area 3 is dominated by straight, near-vertical fault traces spanning 13.5 km from the north-western edge of the area to the southwest, which link together towards the east and the west (Fig. 4.3A). Near-seabed seismic reflections geometries are more complex than in area 2. High amplitude reflection packages are located around the high-angle fault. A drop in reflection depth of ~ 200 m (or 200 ms twt) occurs against the fault, indicating subsidence (Fig. 4.3E).

In area 4 a ~ 5 km-long, northeast-southwest striking, subvertical fault zone is observed (Fig. 4.4A and B). It is located at the western margin of a fold to which it is linked. At the seabed the fault trace is detected by the presence of *en echelon* sigmoids. In seismic profile, the fault zone can be seen from the seabed down a strong reflection located at ~ 6000 ms twt and hence propagates over ~ 6 km of sediments (Fig. 4.4B). In the top 1000 ms three high-angle fault traces, dipping westwards, are identified. Offset reflections indicate a throw of 50 m to 100 m on each fault trace, down to the west (Fig. 4.4C). Below 4000 ms twt the seismic reflectivity loss prevents observation of much detail on the fault trace.

4.3.2 Channel systems position and morphology

4.2.3.1 Area 1

A partially filled incision, interpreted as a channel, is associated with the WSW-striking fault (Fig. 4.2A). A seismic profile (Fig. 4.5A) shows that it is comprised of three fault segments (Figs 4.2A and 4.5A). The upslope limit of the channel on the seabed coincides with the location of steep, high amplitude reflections interpreted as carbonate mounds (Lane, 2005, Fig. 4.2A). Its first upslope segment, which has a WSW strike and continues for ~ 20 km, is barely visible on the seabed, and stops at a bathymetric high. This segment, referred as the "eastern segment", has incised by up to ~ 200 m into the underlying parallel reflections, and some sedimentary filling has occurred as indicated by parallel reflections within the erosional incision (Fig. 4.5B).The second segment, referred as the "central segment" has an E-W orientation and is ~10 km long, ending at a sub-circular depression. The fault path from this point becomes more erratic with directions trending parallel to the slope parallel to locally oblique (Fig. 4.2A). Further downslope, the channel remains erosional as suggested by an absence of reflections onlapping the channel form and a seabed expression (Fig. 4.5C). These linked elements compose the Nouakchott Channel System-North (NCS-N).

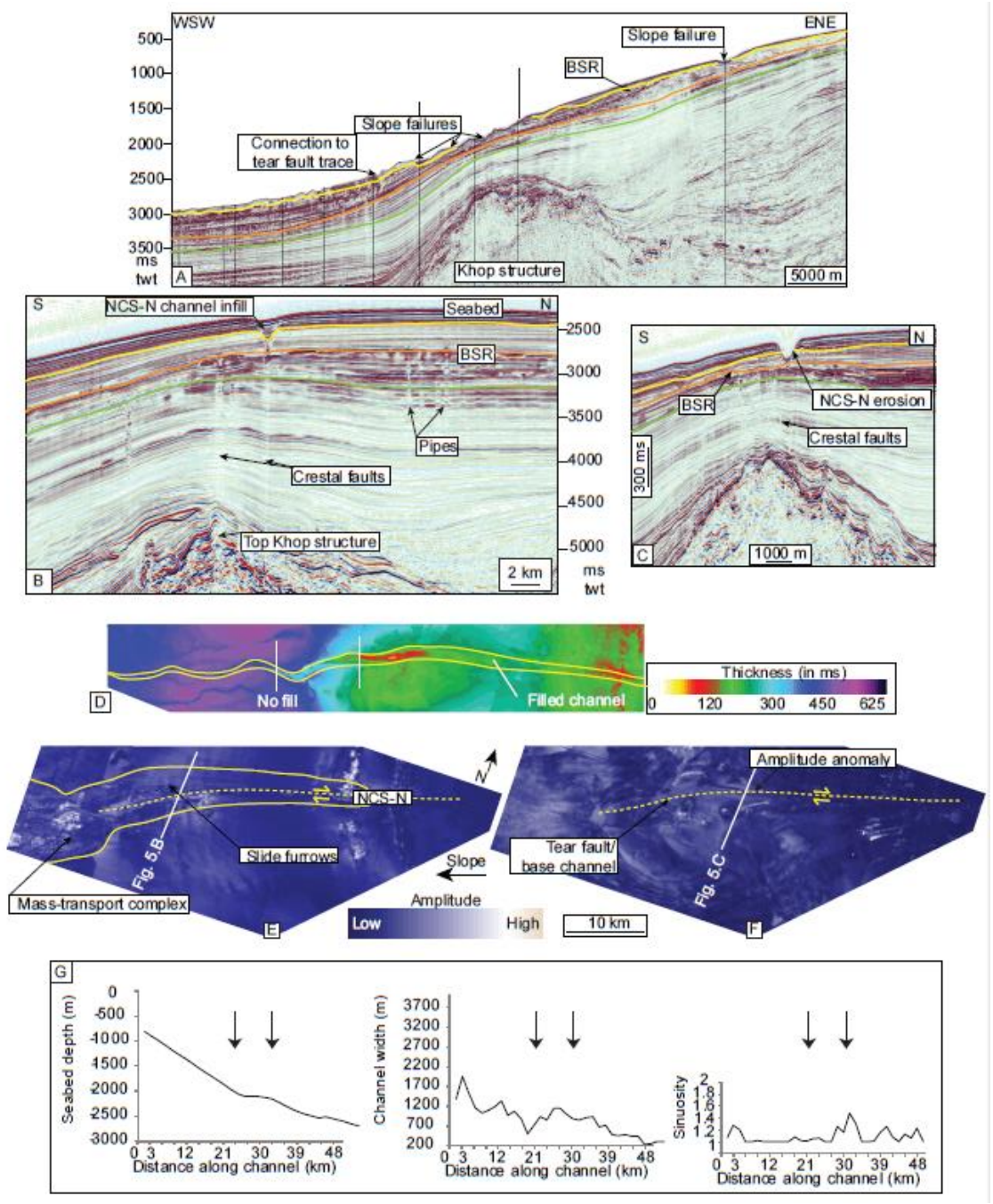

Figure 4.5 The NCS-N in area 1. A. Seismic profile along the NCS-N showing the slope setting and surface morphologies encountered by the channel system. Vertical exaggeration 6x. The yellow horizon is H1.0, the orange is H2, and the green is Z. The vertical black lines above the profile delineate the channel segments. B. N-S oriented seismic profile showing the NCS-N channel infill and the location of the BSR. Vertical exaggeration x6. C. N-S seismic profile across the NCS-N in an area with no sedimentary fill. Vertical exaggeration x5. D. Isochron map between the seabed and H1.2 indicating the areas of erosion and channel fill. Channel form edges are highlighted in yellow. E. Amplitude extraction of horizon H1.0 showing regional-scale slide furrows and associated mass-transport complex, highlighted by the yellow lines. F. Amplitude extraction of horizon H1.2 showing the base of the NCS-N and the tear fault, highlighted by the yellow dashed line. G. Channel morphological analysis: seabed depths along the channel trace and downslope patterns of channel width and sinuosity. The two vertical arrows indicate the limits of the three channel segments, labeled 1-3.

An isochron map computed between H1.0 and the seabed indicates a partial fill in the NCS-N eastern section and erosion occurs throughout the rest of the channel path (Fig. 4.5D). An amplitude extraction from H1.0 (Fig. 4.5E) shows > 30 km-long lines than fan out from the upslope end of the NCS-N down to the start of the central segment. These lines are interpreted to be slide furrows - linear erosion traces on an incised surface left by the mobilization of a mass-transport complex (e.g. Haflidason *et al.*, 2004; Fig. 4.5E). Chaotic reflections associated with a mass-transport complex are found downslope of these furrows. In addition, H1.1 amplitude extraction shows a linear fault, the NCS tear fault, interrupting circular concentric amplitude anomalies at the base of the NCS-N (Fig. 4.5F). Where it coincides with the tear fault trace, the NCS-N shows a narrow average width of ~1000 m over a steep slope of 3°s (Fig. 4.5G). The overall sinuosity remains low (1 to 1.2) but an increase in sinuosity and a slight decrease in channel width occur at km 30-35 (Fig. 4.5G).

4.3.2.2 Mahin channel system, Area 2

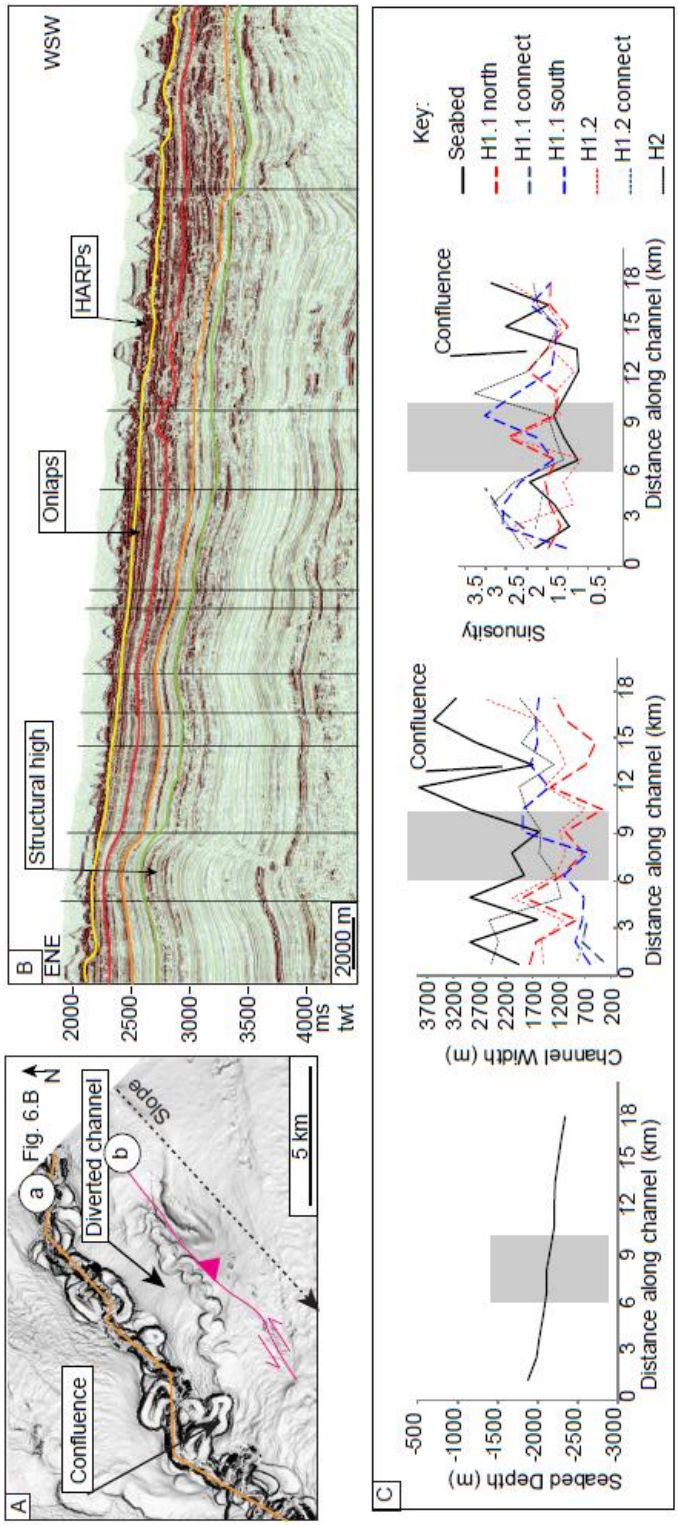

Figure 4.6 The MCS in area 2. A. Seabed map showing the current Mahin channel system and seabed remnants of the paleo-channel position. B. Seismic profile along the present-day channel trace showing topography related to meanders at the surface. Vertical exaggeration x4. The yellow horizon is H1.1, the red is H1.2, the orange is H2, and the green is Z. C. Channel morphological analysis: present-day channel seabed depths along the channel trace and downslope patterns of paleo- and current channel width and sinuosity. The grey rectangles highlight the position of the structural high.

On the seabed the active MCS is a meandering channel (Fig. 4.6A, (a) and Fig 4.6B). Along a smooth bathymetric gradient, the MCS has a width of up to 2000 m and a sinuosity of 1.4 to 2 (Fig. 4.6C). The current MCS exhibits a basal high amplitude reflection package, as well as onlapping and parallel reflections associated with meandering geometries, over occasional toplapping reflections (Fig. 4.6B). The presence of low amplitude, parallel reflections indicating levee and terrace deposits (also called lateral accretion packages, e.g. Abreu *et al.*, 2003) are also commonly found as part of the present-day channel system (Fig. 4.6B, (a)). A parallel, inactive, filled channel section is seen south-east of this currently active channel system (Fig. 4.6A, (b)). Three other erosional surfaces associated to paleo-systems, located on H2 (b), H1.2 (c') and H1.1 (c) also suggest the presence of a long-lived channel complex in the area, in the western part of the fault system (Fig. 4.3D). The oldest evidence in the area is found SE of the restraining bend in the tear fault at the vicinity of horizon Z (Fig. 4.3D, (d)). The migration of the MCS is also imaged in map view from amplitude extractions and near-seabed dip maps (Fig. 4.7). On horizon Z a subtle ridge can be followed on the amplitude extraction (Fig. 4.7A). This ridge is associated with higher amplitude reflections that are probably due to a mass-transport complex that lies across the NE-SW tear fault zone, and may indicate an ENE-WSW axis of transport (Fig. 4.7A). The interpretation of a mass-transport complex is based on the chaotic character of the seismic reflections and the amplitudes they display on map view, as well as the geometry of the body seen on sections and maps. The complex is in two parts, interpreted as originating from the same body that was later dislocated by slip on the fault zone. Dip magnitude map of H2 shows (c), overall striking in the same orientation and location as the mass-transport complex (Fig. 4.7B). The systems (c and c') are visible at H2 and H1.2 depths and are buried and sediment-filled. They both display sharp erosional reflection geometries and HARPs at the channel base. Levee deposits are also identified on the rim opposite to the restraining bend (Fig. 4.3D). Over the first 4000 m of the path, starting

from the east they display meandering geometries and gradually bends to flow ESE-WNW in the next 4000 m. Downslope of these two segments, (c) readopts an ENE-WSW pathway. A decrease in channel width from ~600 to 200 m is observed between (c) and (a) (Fig. 4.3D and 4.6C). This decrease is also associated with a decrease in sinuosity at the vicinity of the bathymetric high (Fig. 4.6C). These decreasing trends seem to correlate with a progressive fill of (c). The H1.2 dip magnitude map shows similar channel trends to those observed on the map of H2 (Fig. 4.7C). An amplitude extraction on H1.2 shows that there is change in flow direction (diversion) at a sharp angle as the system encounters the positive topography of the NE-SW fault zone (Fig. 4.7D). This is associated with a decrease in channel width and sinuosity between 0 and 9 km (Fig. 4.6C). The channel system (c) coexists with another channel system, developing to the northwest, and away from the structural high (Figs. 4.7C and 4.7E). In addition, a new system (b) appears at this horizon to the northwest of (c), which is partially filled. The system (b) connects to (c) after ~6000 m (Fig. 4.7D). The development of (b) can be tracked from amplitude extraction maps H1.2 and H1.1 (Figs 4.7D and E). The channel system (b) is located 3 km north and parallel to (c) (Fig. 4.7D). It is between 500 and 1000 m in width, about 100 m in depth, and shows a sinuosity around 2.5, which is comparable to (c) (Fig. 4.6C). The channel system (c) is deflected to the northwest of the structural high. It connects to b 6 km downslope as (c) develops along the structural high, and forms a confluence point. While (b) develops, the partial fill of (c) can be seen with lower amplitudes in the channel path and a smoothed morphology on the surface of (c) at H1.1 (Fig. 4.7E). The current MCS then develops over the trace of (b) and displays similar channel width and sinuosity (Figs. 4.6A and 4.7E). It also re-uses the location of (c) further downslope, past the structural high. These observations suggest a channel fill and abandonment succession towards the northwest and indicate a long-lasting deviation of the pre-existing channel path towards the northwest, and likely to be initiated by the uplift of the neighbouring structural high.

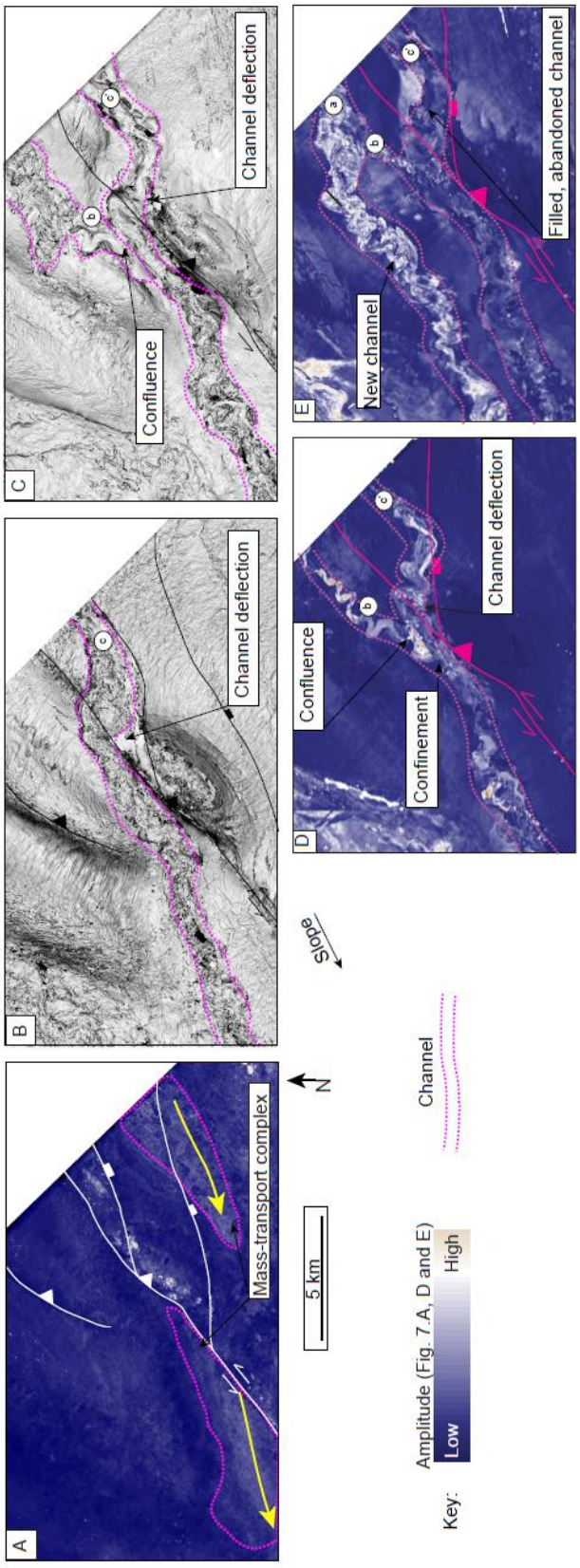
A
Mass-transport complex
B
Channel deflection
C
Confluence
Channel deflection
D
Confluence
Confinement
Channel deflection
E
New channel
Filled, abandoned channel
N
Slope
5 km
Channel
Key:
Amplitude (Fig. 7.A, D and E)
Low
High

Figure 4.7 Paleochannels in the MCS, area 2. Note that successive panels indicate progressively younger horizons. A. Horizon Z amplitude extraction showing the location of a mass-transport complex (circled) and the paleo-axes of sediment fairways (yellow arrows). B. Map of H2 showing the location of the paleo-MCS. C. Map of H1.2 showing the location of the paleo-MCS around the strike-slip fault restraining bend. D. Amplitude extraction map of H1.2 showing the diversion of the MCS around the growing fold and the existence of a dual channel system. E. Amplitude extraction map of H1.1 showing the abandonment of the paleo-MCS southern channel and the greater activity of the paleo-MCS northern channel.

4.3.2.3 Mahin channel system (MCS), area 3

The continuation of the MCS into area 3 also displays intense meandering and is located to the south of an abandoned channel system (Figs. 4.8A and B, (c)). The channel systems (a) and (c) are connected at an apparent avulsion point in the northeast corner of area 3 (Fig. 4.8A). On-lapping and top-lapping reflections are seen at all the studied levels (Fig. 4.8B). In this area, a variation in horizon interval thicknesses, from ~ 50 m around structural highs to ~ 400 m in thicker deposits, at the vicinity of normal faults, is observed. In addition, numerous chaotic, high amplitude reflections indicate intense erosion and a poorly preserved sediment record over time into the pull-apart basin area (Fig. 4.8B). At ~ 3 km north of the fault zone the location of another channel system (Fig. 4.8C, (e)) is inferred. This pattern is confirmed on H2 dip and amplitude maps where two meandering channel systems, referred as (c) and (e) are identified (Figs. 4.8C and D). Of these two, (c) appears more clearly than the southern channel e and shows higher amplitude reflections. This amplitude effect may be related to erosion and deposition of coarser-grained sandy sediments and enhanced by fluid content. This trend is however inverted on the current seabed as c appears to be smooth and partially filled, whereas actively eroding meanders and levee deposits are visible along the channel to the south, e (Fig. 4.8A). The overall channel bed slope is very low (~ 0.8°) in area 3 (Fig. 4.8E), and the paleo-channel (e) is narrower than the modern MCS (around 1500 to 1800 m in comparison with a current width of around 2000 m). Sinuosity is similar for the modern MCS and the southern paleo-channel (e), and is lower for the northern paleo-channel (c) (Fig. 4.8E). Measured sinuosities are high (between 1.5 and 2.5).

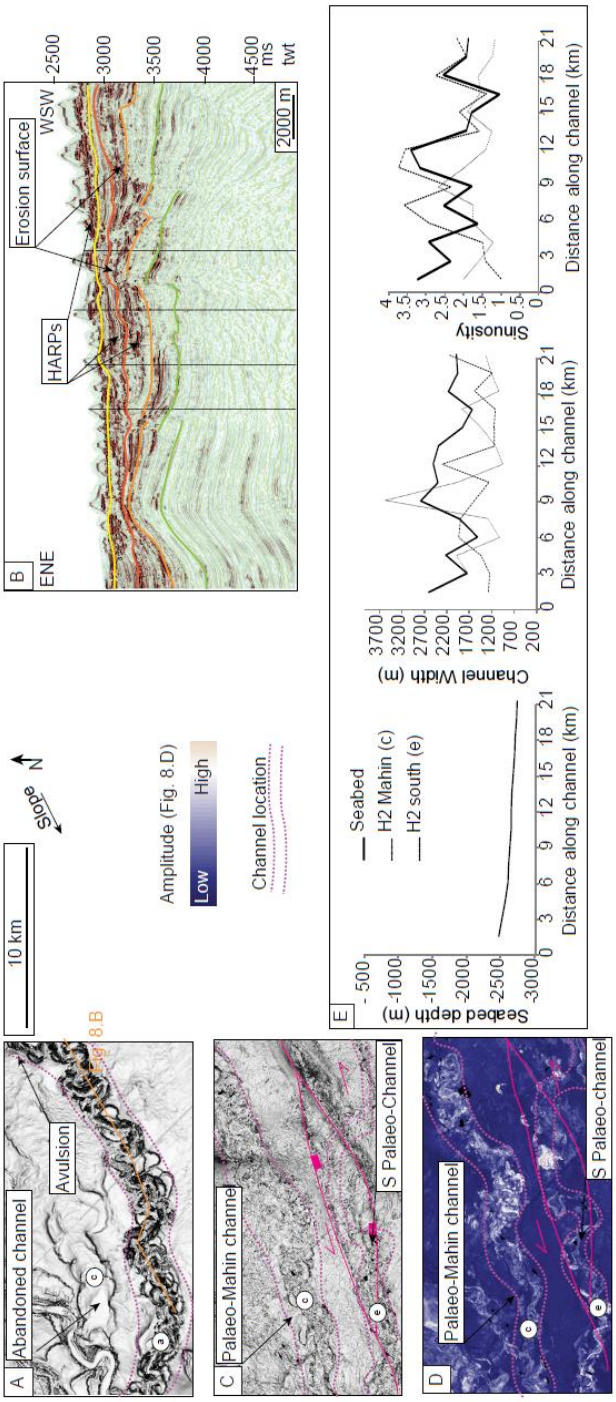

Figure 4.8 Evolution of the MCS in area 3. A. Seabed map indicating the position of the paleo and current MCS. B. WSW-ENE seismic profile along the MCS. Vertical exaggeration x4. The yellow horizon is H1.1, the red horizon represents H1.2, the orange indicates H2, and the green horizon represents Z. C. Map of horizon Z showing the location of the strike-slip releasing bend and the position of the paleo-MCS. D. Amplitude extraction map of H2 showing the location of the paleo-channels. E. Channel morphological analysis: present-day channel seabed depths along the channel trace and downslope patterns of paleo- and current channel width and sinuosity.

4.3.2.4 Ijebu channel system (ICS)

The studied section of the modern ICS in area 4 is 25 km in length (Fig. 4.4A). The ICS displays several high amplitude reflection packages (HARPs) at various depths over a ~ 300 to 400 m-thick interval (Fig. 4.4C). At the present day the visible upslope segment of the ICS is adjacent to the Ijebu tear fault zone. A V-shaped channel incision in this interval demonstrates that fill previously occurred along that portion of the channel before undergoing incision again (Fig. 4.4C). This pattern of partial filling is confirmed on an isochron map between the seabed and H1, which also shows that erosion becomes progressively greater downstream in the channel system (Fig. 4.9A). The modern ICS is developed over a buried paleo-channel system (Fig. 4.9B, C and D). H1 dip and amplitude extraction maps show that this paleo-channel system is located ~ 6 km to the northwest of the current ICS toward the downstream end of the study reach, but is nearly coincident near its upstream end (Fig. 4.9A and B). It is suggested that this paleo-channel represents a former location of the ICS, which has undergone diversion of up to ~6 km between H1 time and the present day. Patterns of channel width and sinuosity on both the modern and paleo-channel systems are similar, with a notable decrease in channel width of several hundred meters and a decrease in sinuosity where both systems diverge from the tear fault zone (Fig. 4.9E). Channel bed slope also decreases where the channel departs from the tear fault zone, which could explain the changes in channel morphologies (Fig. 4.9E).

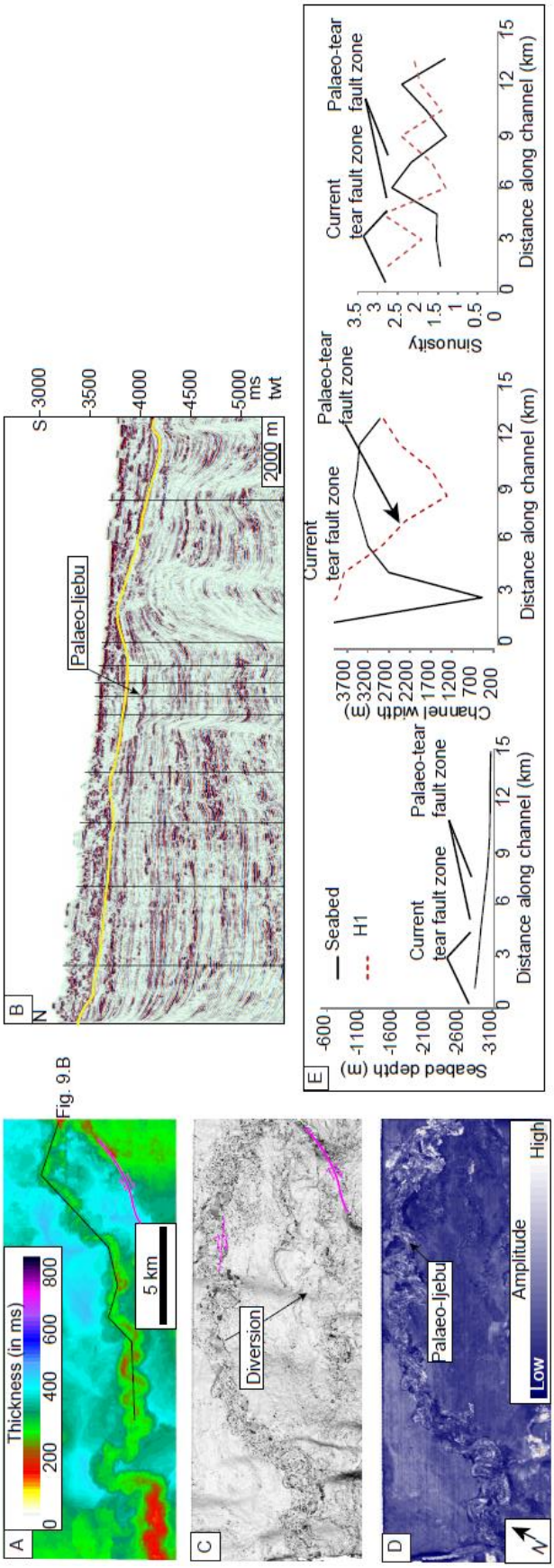
A
Thickness (in ms)
0
200
400
600
800
5 km
Fig. 9.B
B
N
S
Palaeo-Ijebu
2000 m
3000
3500
4000
4500
5000
ms
twt
C
Diversion
D
Palaeo-Ijebu
Amplitude
Low
High
E
Seabed depth (m)
-600
-1100
-1600
-2100
-2600
-3100
Seabed
H1
Current tear fault zone
Palaeo-tear fault zone
Distance along channel (km)
Channel width (m)
3700
3200
2700
2200
1700
1200
700
200
Sinuosity
3.5
3
2.5
2
1.5
1
0.5
0
0
3
6
9
12
15

Figure 4.9 Evolution of the ICS in area 4. A. Isochron map between H1 and the seabed in the ICS area. B. Seismic profile along the ICS. Vertical exaggeration 4x. The yellow horizon is H1. C. Map of H1 showing the former position of the ICS. D. Amplitude extraction map of H1 showing the former position of the ICS. E. Channel morphological analysis: present-day channel seabed depths along the channel trace and downslope patterns of paleo- and current channel width and sinuosity.

4.4 Interpretation and Discussion

4.4.1 Interactions between sedimentary processes and structural setting

In offshore Mauritania, tear faults bound localized slope failures (Fig. 4.2D and E, and Fig. 4.5A and E). We argue that overpressure and seal failure associated with these failures are evidenced by the presence of fluid escape pipes spatially coincident with tear faults (Fig. 4.2B and C; Yang and Davies, 2013). Slope failures are also more likely to occur more often over the Khop structural high. These slope failures, in turn, lead to local erosion and changes in slope gradient coincident with the tear fault trace, generating a preferential path for channel initiation or steering of existing channels (e.g. Heiniö and Davies, 2009; Fildani *et al.*, 2006). This hypothesis is confirmed by the fact that the NCS-N develops over pre-failed mass-transport units (e.g. Fig. 4.5A and F). Patterns of channel sinuosity increase can be linked to variations in the slope gradient and channel direction of propagation over the Khop high (Fig. 4.5A). Low sinuosity and narrow channel width are interpreted to indicate an early stage of channel development (Stage 1, Gee *et al.*, 2007), and a typical illustration of early interactions between slope-parallel tear faults and channel systems. In the same area, Antobreh and Krastel (2006) described vertical fault traces underlying the Cap Timiris canyon. These faults were interpreted as pre-existing stratigraphic discontinuities exploited by the initial turbiditic currents. We interpret this whole suite of observations as indicating an early stage of channel development over the NCS fault (Fig. 4.10A).

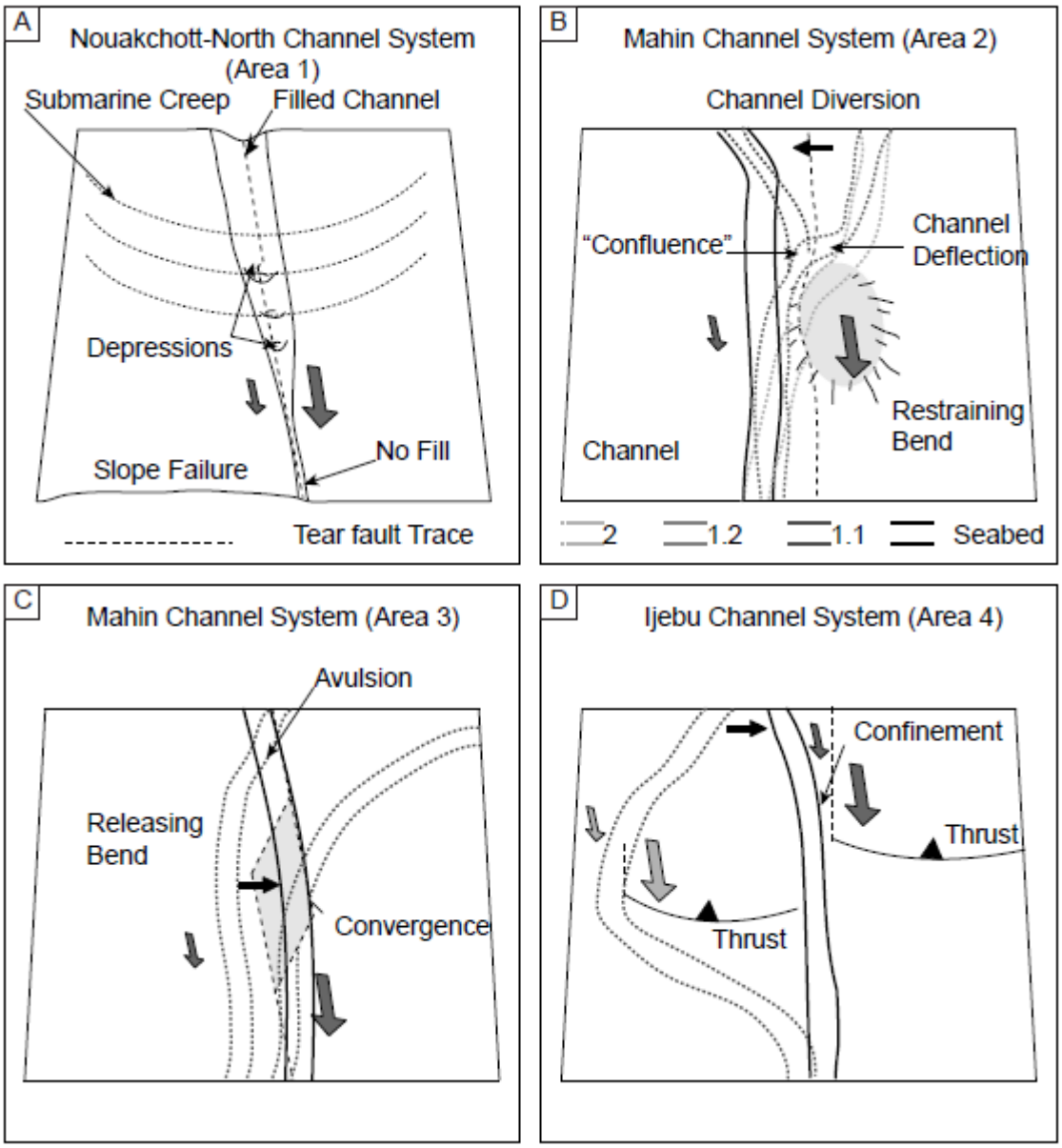

Figure 4.10 Summary model of the evolution of channel systems in tear fault zones in the areas of interest. A. NCS-N in area 1. B. MCS in area 2. MCS in area 3. D. ICS in area 4. The small black arrows highlight directions of channel migration. The large arrows illustrate the horizontal displacement along the strike-slip fault.

In area 2, positive topography is induced by the development of a restraining bend in the regional-scale strike-slip fault zone (Leduc *et al.*, 2012). We interpret the MCS as a structurally confined system. Channel migration between horizons Z and H2 is a response to structural growth that outpaces the local sedimentation rate (Fig. 4.6). Observations on younger horizons H1.1 and H1.2 show that the structural growth has continued until present-day. The channel has been

diverted northward away from the high created by the restraining bend (Fig. 4.10B). This diversion and structural confinement resulted in a decrease in channel width, channel deflection around the existing or growing fold, and deviation. These observations illustrate the local channel system response to a change in slope gradient at the vicinity of the high (flow-stripping).

The avulsion process observed in area 3 may have occurred as local subsidence due to the development of a pull-apart basin (Leduc *et al.*, 2012), while uplift was ongoing upslope, in area 2. Abandonment of the paleo-channel system (c) through avulsion and capture by the paleo-channel system (e) in the south led to establishment of a sediment routing pathway coincident with the present-day MCS (Fig. 4.10C). From these data little evidence is present to indicate the detailed process of this capture. It is however suggested that the ongoing subsidence increases the slope gradient and therefore decreases channel width and sinuosity by causing an hydraulic jump (Fig. 4.9D; e.g. Anderson *et al.*, 2000). This increase in channel width may have occurred on (e). The local width decrease may have generated a trough at the vicinity of the palaeo-channel system (c), which would have initiated the avulsion process. Normal fault growth still controls the migration of segments of the current MCS (a) towards these locally subsiding areas. The interactions between the MCS and the along-strike structural variety of the NE-SW tear fault thus represent potential examples of how to predict the evolution of a submarine channel system in a tear fault zone at a regional scale, and through time (Fig. 4.9D).

In area 4, a decrease in channel width and sinuosity is observed at the vicinity of tear faults for both the paleo-ICS and the present-day ICS (Fig. 4.9E). This may be due to a structural confinement of the channels by the tear faults. The fact that the channel system is seen to divert away from its initial path suggests a change in the local structural activity, potentially linked to a change in relative fold growth rates between the different structures coexisting in the area, and

consequent development of tear faults. In addition, the ICS in area 4 shows that a channel system can be diverted by the activity of a recent tear fault, regardless the fact that it has an extensional, or contractional component (Fig. 4.10D). It is assumed that the formerly active structures that confined the paleo-ICS are no longer growing. As activity may have occurred further south, and slightly downslope, the ICS would have followed the tear fault trace against the growing fold structures of the restraining bend (Fig. 4.7) and may have become structurally confined late in its evolution as normal faults associated with the pull-apart were developing (Fig. 4.4C).

4.4.2 Conceptual model

The observations described in this paper show that slope-parallel tear fault development can interact with the translation of sediment downslope. An overview model (Fig. 4.11) summarises the different steps in the structural confinement of submarine channel systems from early stages (Fig. 4.11A to C) to later stages (Fig. 4.11D) of evolution. Local, near-seabed slope failures combined with pre-existing highs can generate tear faults and encourage slope-parallel incision along the fault trace (Fig. 4.11A). This early incision can represent preferential path for downslope sediment transfer, either through the initiation of new channels or through steering of existing sediment transport pathways (Fig. 4.11B and C). Hence the surface expression of a young tear fault trace may be hidden by sedimentation, particularly in more distal locations (Fig. 4.11C and D).

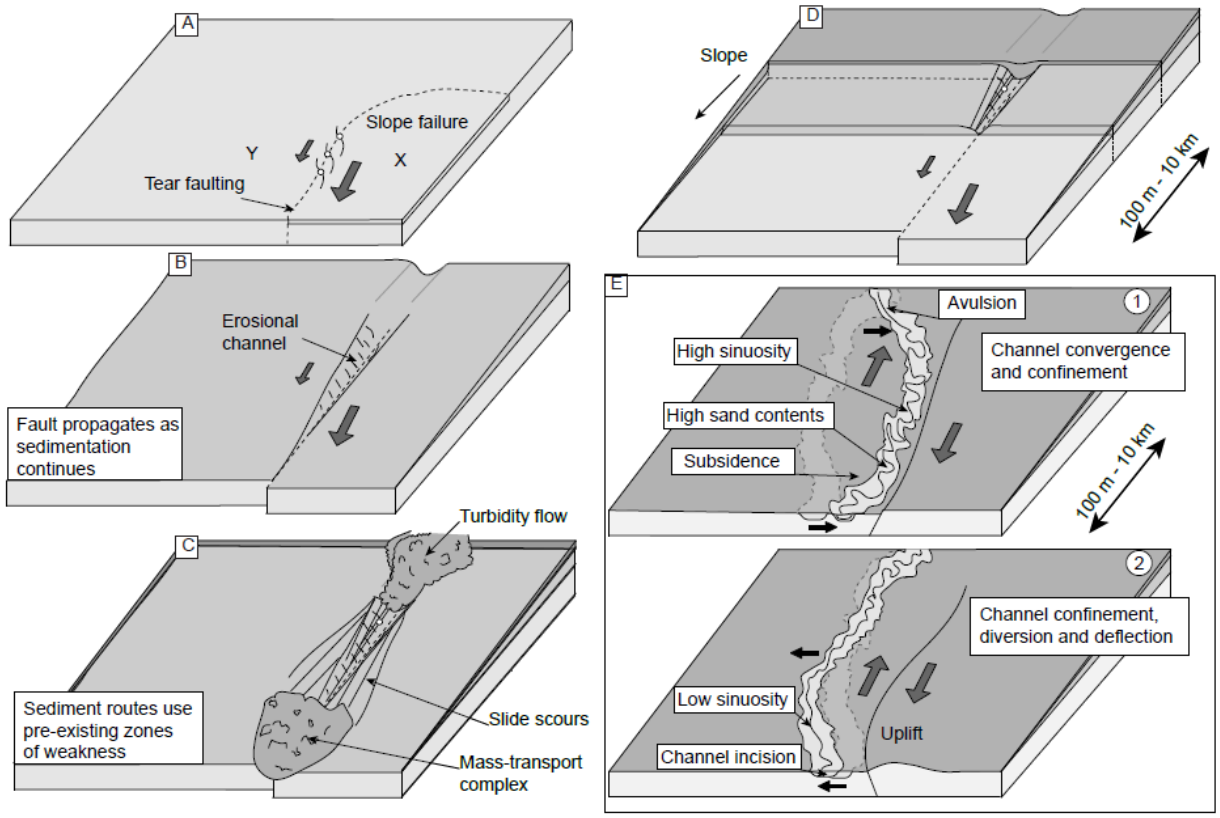

Figure 4.11 Model for the interaction between tear fault development and controls on deepwater channels. A. Potential initial stage of development, in which overpressure or differential compaction (?) generates tear faulting. X and Y indicate sedimentary deposits for which degree of compaction and rheological properties may differ. B. Fluids migrate up to the surface using these stratigraphic discontinuities. Tear faults propagate and contribute to local slope-parallel erosion as sedimentary processes continue to occur in the area. C. Downslope erosion and sediment transport occurs by turbiditic flow and mass-transport over the tear fault zone, defining a preferential sediment route. D. Overall summary of the spatial relationships between tear faulting, sedimentation, and potential fluid pathways indicated by "bubble" escape to the top. E. Possible structural controls on sediment pathways and depositional architecture. The small black arrows highlight directions of channel migration. Panel 1 shows a transtensional setting, while panel 2 shows a transpressional setting.

Other interactions are possible where the seabed expression of the tear fault is more complex than a simple linear fault trace (Fig. 4.11E). This can be the case if the tear fault develops from deeper detachment levels, for example, or by linkage of multiple pre-existing fault segments. In these settings channel system depositional architectures can record the topographic effects of fault displacement. If the tear fault is locally transtensional, then local subsidence can "pull" the channel system against the fault zone (Fig. 4.11E). The resulting lateral migration of the system towards the subsiding area (i.e. channel convergence) would be associated with the

creation of an avulsion point upslope, indicating channel abandonment (Fig. 4.11E, 1). Local subsidence would also result in an increase in slope gradient, driving a channel sinuosity increase. This kind of area is expected to become a depocentre (Fig. 4.11E part 1). Conversely, uplift along a transpressional segment in the tear fault zone would contribute to the confinement of the channel system and diversion (or deflection if the uplift occurred over the pre-existing channel path) away from the uplifted area (Fig. 4.11E, part 2). This diversion creates a potentially long-lived sediment pathway, and an overall increase in sinuosity and potential sediment starvation (due to efficient throughput) can be expected (Fig. 4.11E, part 2).

4.4.3 Implications

Slope-parallel tear fault zones are areas of strong sediment bypass. They can easily be used as preferential routes for sediment transfer over long time scales, as they form localised zones of weakness and encourage incision and channel confinement, constraining the spread of turbidity currents and debris flows. As a result erosion should be intense in these areas, particularly in young systems on a steep slope as observed offshore Mauritania. Our observations also confirm that channel system geometries and deposits can be preserved in more mature systems (Niger Delta). Erosional processes and mass transport can still occur, but the persistence of sediment supply and a gentler slope makes it more likely to preserve a palaeo-channel record in the stratigraphy. Interactions may begin early in the development of faults and channels (e.g. area 1) and persist for extended periods of time.

In transpressional settings, channel paths undergo deflection and diversion and contribute to changes in the locus of deposition. Conversely, channel segments confined against a structural high are expected to have a lesser capacity for sediment transfer. In contrast, transtensionally-induced subsidence contributes to an increase in channel width, an increase in

slope gradient and consequently a sinuosity decrease. This would imply a higher sand/shale ratio in the subsiding areas, similarly to what can be observed in extensional settings (e.g. Pochat *et al.*, 2009). As a result there is potential for good reservoir development and preservation in tear fault zones, but local-scale fault compartmentalization is important to consider. In addition, the syn-sedimentary development of tear faults may contribute to generate fluid migration pathways in the near-surface (e.g. Calvès *et al.*, 2008; Yang and Davies, 2013).

It is also important to remember that, in tear fault settings, structural deformation styles and growth rates are expected to be strongly affected by sedimentation. Intense deposition rates may decrease the growth rate of tear fault-related folds (e.g. Morley, 2009), and high erosion rates would reduce the vertical load in comparison to the rate of the fold growth. In addition, sediment aggradation and loading in subsiding surroundings of the growing fold would enhance structural growth. Conversely, an increase in the rate of normal faulting may correspondingly be produced by sediment segregation, with higher local erosion followed by potential deposition of locally coarser-grained sediment in the hangingwall and finer-grained, more marginal sediment deposition at the footwall (e.g. Pochat *et al.*, 2009). The structural evolution of different segments within a given tear fault zone may thus vary according to local sedimentation rate.

4.5 Conclusions

Gravity-driven tear faults can significantly affect submarine channel system migration and channel-fill architectures at different stages of development. Three-dimensional seismic data allow us to document the tear fault geometries and their effects on early channel confinement. Near-seabed, slope-parallel tear faults at the continental margin of offshore Mauritania are interpreted to underlie young submarine channels, and form preferential erosional pathways for

submarine channel initiation. The location of new channel systems may therefore depend on an increased slope gradient formed by pre-existing tear faults. Comparable examples from the deepwater western Niger Delta show that later submarine channel evolution is also affected by tear fault growth. Channel pathway deflection, channel confinement as indicated by vertically stacked, incised channel fills, and a decrease in sinuosity all characterise the effect of the growth of a local strike-slip restraining bend. Likewise, a strike-slip releasing bend triggers channel diversion and an increase in sinuosity. Channels can respond to structural growth through time by remaining confined in tear fault zones or by avulsing and creating major bypass zones, thus creating specific depositional patterns associated with channel migration. These patterns are likely to change along the channel and fault zone with different fault segment growth rates and local sedimentation rates. We also infer that these interactions have important implications for preserving sands and trapping fluids, and are expected to be found at many other continental margins. Future work may involve detailed investigation on the sedimentary facies record of tear fault activity, local overpressure generation and required conditions to create tear faulting, and the geographical extent of these processes over time.

CHAPTER 5: FLUID FLOW PIPES TRIGGERED BY LATERAL PRESSURE TRANSFER IN THE DEEPWATER WESTERN NIGER DELTA

5.0. Abstract

Using three-dimensional (3D) seismic data, we establish a simple model for the development of vertical fluid flow pipes in the deepwater western Niger Delta. We analyze two examples of fluid flow pipes that form vertical seismic chimneys that are 400 to 600 m wide and ~ 2000 to 2500 m in height, terminate at the current seabed and have bases located at the crest of rollover anticlines. In both cases we identify buried deepwater channels-complexes located below the pipes that formed prior to the growth of the rollover anticlines. The development of the anticlines caused tilting of these channel complexes and differential loading. We propose the channel complexes represent connected permeable reservoir intervals and that lateral pressure transfer caused the pore pressure at the crest of the structures to reach critical levels, leading to hydraulic fracturing of the overburden. Although hydrocarbons may migrate upwards through the chimney systems, they are not necessarily indicators that the channel complexes were gas or oil charged.

Keywords: Niger Delta, 3D seismic, syn-sedimentary deformation, vertical pipes, overpressure, lateral pressure transfer

5.1. Introduction

The occurrence of fluid flow pipes is often linked to the presence of an active petroleum system (Grauls and Baleix, 1994; Ingram and Urai, 1999; Davies and Stewart, 2005; Cartwright *et al.*, 2007) and therefore could be used as a potential hydrocarbon indicator (Grunau, 1987). Vertical fluid conduits above folds commonly occur in basins with high sedimentation rates (Huuse *et al.*, 2010) on both active margins (Caspian Sea – Stewart and Davies, 2006; Trinidad – Deville *et al.*, 2010; Brunei: Van Rensbergen and Morley, 2003) and passive continental margins, such as the Atlantic Ocean and Gulf of Mexico (Dugan and Flemings, 2000; Seldon and Flemings, 2005; Reilly and Flemings, 2010), the Nile delta (Loncke *et al.*, 2004; Feseker *et al*., 2010), west Africa (Moss and Cartwright, 2010), and the Niger Delta (Graue, 2000).

Recent research has been focusing on the recognition of fluid flow pipes, mainly from seismic data (Cartwright, 2007; Cartwright *et al*., 2007, Moss and Cartwright, 2010). Løseth *et al*. (2010) also compared kilometer-scale fluid flow pipes in the Niger Delta to field examples in Greece. In such environments, it is generally considered that vertical escape pipes result from an escape of buoyant hydrocarbons (Cobbold *et al*., 2009; Løseth *et al.*, 2010). But vertical conduit systems may be primed and triggered by pressure in reservoir intervals that develops due to the existence of structural relief and connected permeable strata (Bjørkum *et al.*, 1998). The assumption that vertical conduits are the result of hydrocarbons causing seal failure may be erroneous (Bjørkum *et al.*, 1998; Nordgard Bolas and Hermanrud, 2003; Heggland, 2005).

This paper considers the structural and stratigraphic setting of two significant fluid flow pipes in a deepwater environment in order to assess the geological processes leading to critical pressuring and vertical fluid flow. We develop a simple, generally applicable model for a how fine

grained deepwater sedimentation, channel development and fold growth, can lead to the establishment of overpressure and catastrophic seal failure without the requirement for a hydrocarbon column.

5.1.1 Overpressure

High sedimentation rates cause a rapid increase in the vertical stress that is applied onto the stratigraphic column and leads to sediment compaction. In low permeability sediments, pore fluid is prevented from escaping as the lithostatic load is imposed upon it. This process is known as disequilibrium compaction (Dickinson, 1953) and is the main cause of overpressure in mudstone-rich Tertiary basins deltas (Swarbrick and Osborne, 1998). Tilting of permeable reservoir intervals can also cause overpressure due to lateral pressure transfer from the base to the crest (Yardley and Swarbrick, 2000), otherwise known as the centroid model (Traugott and Heppard, 1994, Finkbeiner *et al*., 2001). Lateral pressure transfer is characterized by an upward increase in the pressure gradient, in a sealed reservoir at hydrostatic pressure, as a response to the reservoir interval tilt. In this case study, permeable reservoirs are preserved sands from deepwater turbidite channels and structural deformation is a potential source of lateral pressure transfer.

Fluid flow due to lateral pressure transfer in permeable reservoirs can contribute significantly to increasing pore pressure at the crest of the reservoir (Reilly and Flemings, 2010). At a depth termed the centroid depth, pressure is balanced within the reservoir, between the section of the reservoir that is above and below the centroid depth (Traugott and Heppard, 1997). Pressures can reach the pressure required to cause hydraulic fracturing (Fig. 5.1). Pore pressure

and horizontal stress are coupled (Mourgues and Cobbold, 2003) and can be quantified from well data (Mourgues *et al.*, 2010). Well data were not available for publication in this study, we therefore use estimated pressure values based upon well-known and established gradients, such as the hydrostatic gradient, and the shale gradient combined with the minimum stress gradient, estimated from geological analogues (Heppard *et al.*, 1998; Nashaat, 1998; Swarbrick and Osborne, 1998; Tingay *et al.*, 2009).

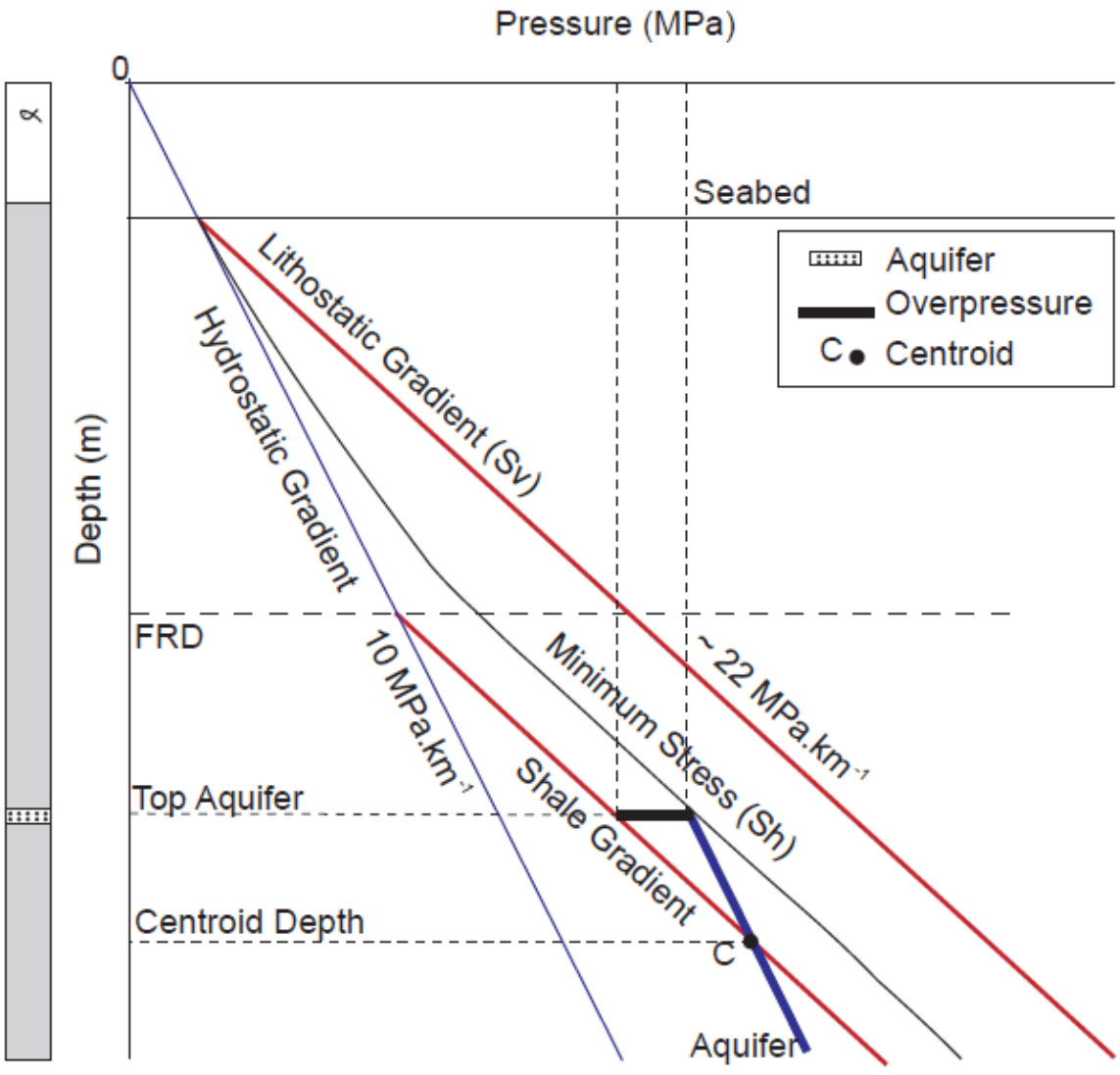

Figure 5.1 Theoretical pressure-depth plot showing the parameters taken into account to determine overpressure in this case study showing hydrostatic, lithostatic and shale gradient The shale gradient is drawn from the fluid retention depth (FRD), representing the top of overpressure in the overburden and is a function of the local sedimentation rate. The minimum horizontal stress (Sh) is indicated for a structural setting in extension; gradient is obtained from Grauls (1999) and Deville *et al.* (2010).

5.1.2 Fluid flow pipes

A hydraulic fracture should develop perpendicular to the direction of minimum compressive stress (Secor, 1965; Hubbert and Willis, 1972). Fluid conduits will form if sufficient pressure is present to reach the hydraulic fracture pressure and breach the caprock of a given reservoir interval (Fig. 5.1). This mechanism has been recognized in previous studies on vertically-focused fluid flows (Hovland and Judd, 1988; Miller, 1995). However, in hydrocarbon-rich environments, such as Tertiary delta systems, escape features do not systematically require hydraulic fracturing to develop. Capillary seal failure also commonly occurs (e.g. Ingram *et al.*, 1999).

Fluid flow pipes can be identified on 3D seismic data as subvertical zones of disturbed reflection or stacked amplitude anomalies (Cartwright, 2007). They can bypass hydrocarbons seals (Cartwright *et al.*, 2007). They were first described in the Niger Delta by Løseth *et al.* (2000), and literature in the past decade has considered how to recognize fluid flow pipes from 3D seismic data and their morphological, lithological and seismic character (Davies, 2003; Cartwright, 2007; Cartwright *et al.*, 2007 Huuse *et al.*, 2010; Moss and Cartwright, 2010; Løseth *et al*., 2010).

5.1.3 Geological setting

The deepwater western Niger Delta, Gulf of Guinea (Fig. 5.2A) is a mud-rich Cenozoic prograding sedimentary accumulation, where updip extension expressed by regional-scale growth

faults is linked to downdip compression with fold-and-thrust belts (Doust and Omatsola, 1990; Morley and Guerin, 1996). This historically has been considered to occur at the first development of overpressure coincident with detachment faults (e.g. Briggs *et al.*, 2006). The 7 to 10 km-thick succession was deposited from the middle Miocene to the Holocene (Short and Stauble, 1967). It is part of the Agbada and the Benin Formations. In cross-section, the seismic signature is characterized by mid to high amplitude reflection packages, including, high amplitude parallel to chaotic lenses associated with channel-levees complexes. Deposition of sediments at high rates leads to rapid loading and in low permeability sediment can cause overpressure. Unpublished well data in the study area provide an estimate of about 2000 m of decompacted sediments in 11.6 Ma (approximately 160 $m.My^{-1}$). Overburden undergoes gravity-driven deformation above deeply buried, overpressured strata (Cobbold *et al.*, 2009). Smaller-scale deformation caused by overpressure and sediment remobilization also occurs, for instance fluid flow pipes and mud volcanoes (Graue, 2000; Heggland *et al.*, 2001; Kopf, 2002) and kilometre-scale fluidization features (Davies, 2003) have been described.

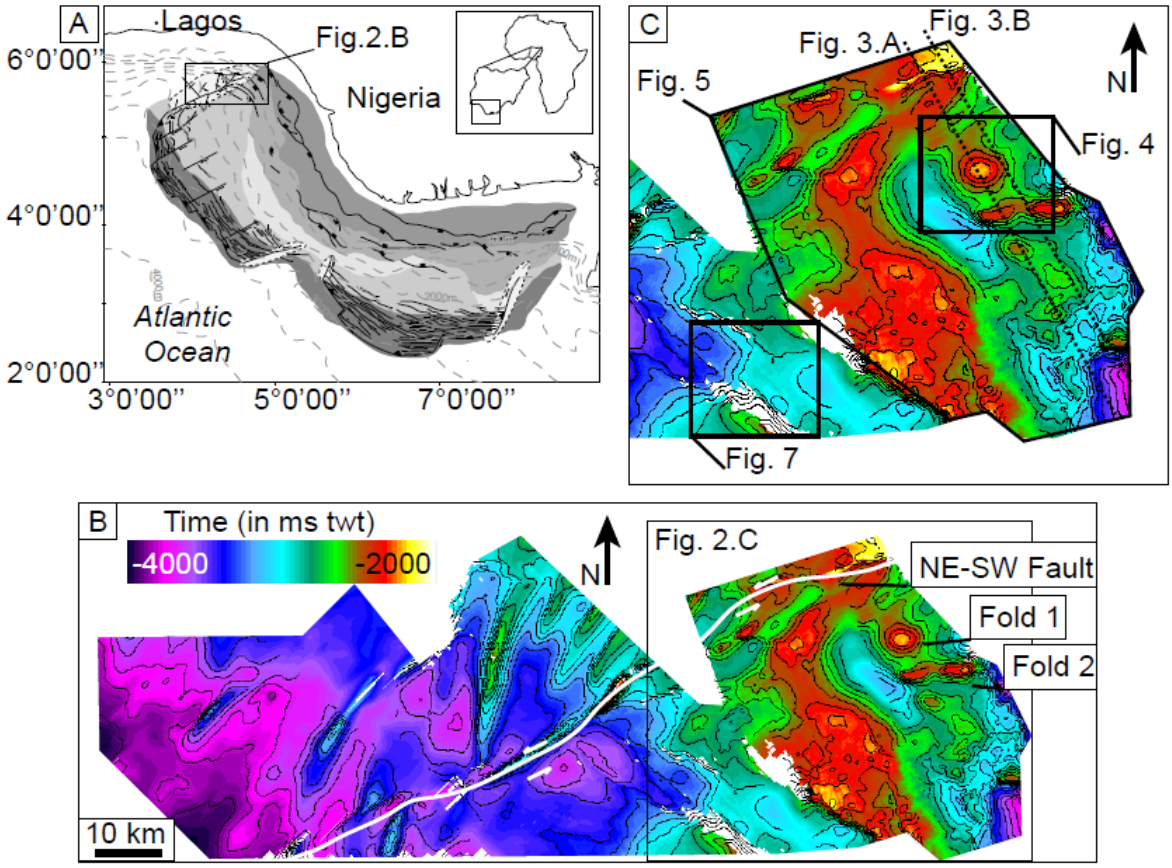

Figure 5.2 Location maps. A. Location of the study area in the western Niger Delta. B. Time contour map (at depth of horizon 2) showing the structural setting of the area and the location of fold 1 and fold 2. "ms twt" in this and subsequent figures - milliseconds two-way time. C. Location of Figs 5.3, 5.4, 5.5 and 5.7 indicated on the figure respectively as figs 3, 4, 5 and 7.

5.1.4. Structural setting

The area of study is located at the periphery of a major growth fault and a lateral strike-slip fault that developed contemporaneously (Fig. 5.2B). Here extension, strike-slip deformation and compression are kinematically linked (Leduc *et al.*, 2012). Deformation occurred in several stages as the study area was located within the contractional domain of a regional gravity detachment system in the Miocene. A period of reorganization of the regional system then resulted in the development of strike-slip faulting at the margins of the gravitational detachment lobes, resulting in the growth of E–W to NE–SW oriented elongated structures. Finally, more

recent delta progradation and resulting structural evolution triggered regional, coast-parallel normal and growth faulting which structures orientation is approximately WNW-ESE.

5.2. Data and methodology

We use three seismic volumes located in water depths of between 500 and 2000 m on a southwest-dipping slope and cover an area of 4300 km^2. The surveys were acquired in 1998 with a bin spacing of 12.5 m by 18.75 m. Data are zero-phase migrated and are displayed in two-way travel time (twt), with a vertical resolution of about 10 to 20 m at the depth of our seismic interpretation. The dominant frequency is ~ 45-50 Hz. We interpret four regional horizon reflections (numbered 1, 2, 3 and 4 from the deepest to the shallowest (Figs 5.3A and B) mapped around a sub-circular structural high, and corresponding to horizons H100 to 400 in table 2.1). These horizons delineate five stratigraphic units from a regional detachment level to the seabed (A, B, C, D and E from the deepest to the shallowest units). Mapping has been carried out by auto-dip tracking of maximum (high amplitude) reflections. A full stack amplitude volume is available for all the seismic surveys. We use interpreted time-structure and time thickness maps (isochron maps) and seismic attributes such as RMS (Root Mean Square) windowed (-20 to +20 ms) amplitude extractions along the selected horizons with a view to interpret the structural evolution and locating channel migration pathways (Brown, 2011).

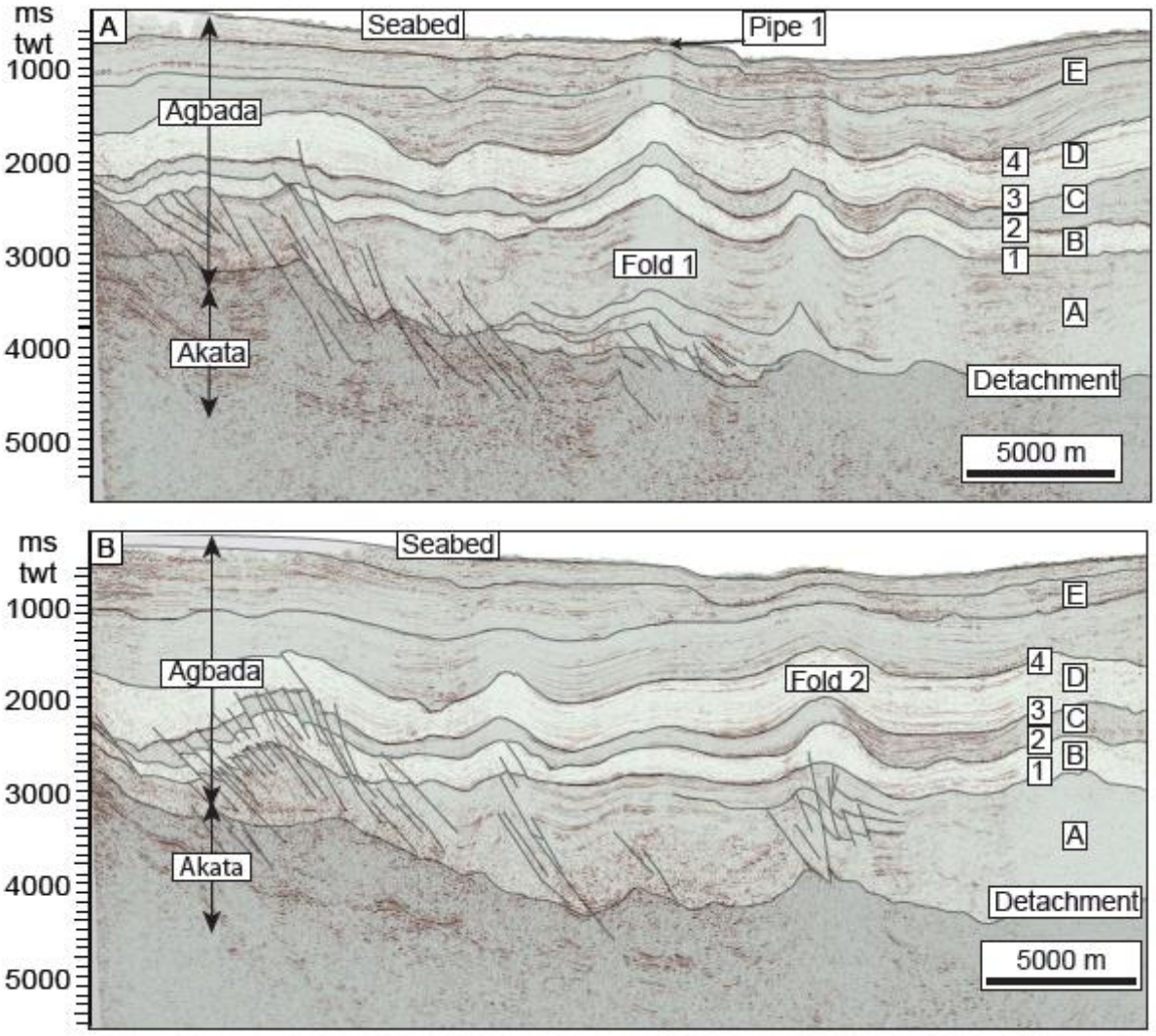

Figure 5.3 A. Seismic section across fold 1, perpendicular to dip direction. B. Seismic section parallel to Fig. 5.3A, across fold 2 and perpendicular to dip direction. Both seismic sections show the general structural trends and units A, B, C, D and E which time-thickness (isochron) maps are shown on Fig 5.6.

To estimate overpressure, we need to know: (1) the lithostatic and hydrostatic gradient; (2) the sedimentation rate, and as a result, the fluid retention depth (FRD), obtained from the empirical relationship established by Swarbrick *et al*. (2002). This allows one to locate the shale gradient, which represents the pore pressure within the shale, a lithostatic-parallel gradient originating from the FRD (Fig. 5.1). The numbers used to build the graphical interpretations were obtained by converting the measured depths (in ms twt) into metres (Table 5.1). In this chapter we use the term reservoir to refer to porous and permeable strata where the pore fluid is either

gas or water.

TWT interval	Velocity used ($m.s^{-1}$)
Seabed	1800
Near seabed →1000 ms below	2100
-1000 to -1500 ms below the seabed	2500
-1500 to -2800 ms and below	3000

Table 1- Velocity and depth estimates used in this chapter.

5.3. Observations

5.3.1 Folds 1 and 2

Fold 1 is a buried sub-circular structure located approximately 12 km southwest of a major listric normal fault and ~ 10 km south of the lateral boundary of the sedimentary lobe defined by a NE–SW trending strike-slip fault system (Figs 5.2A and B). The fold is a symmetrical, positive structure ~ 5000 m in diameter, with a relief of ~ 800 m, occurring between 2500 m and the seabed (Figs 5.3A and 5.4). Seismic imaging of the core of the fold is poor below horizon reflection "1"; however we identify fault traces and a stratigraphic package that suggest a structural thickening of the deepest units (Fig. 5.3A, package A, and Maloney *et al.*, 2010). Onlaps indicating growth of the structure are observed above horizon reflection "4" and the seabed. High amplitude reflections at the crest of the structure suggest the presence of an escape feature at the seabed (Figs 5.3A and 5.4).

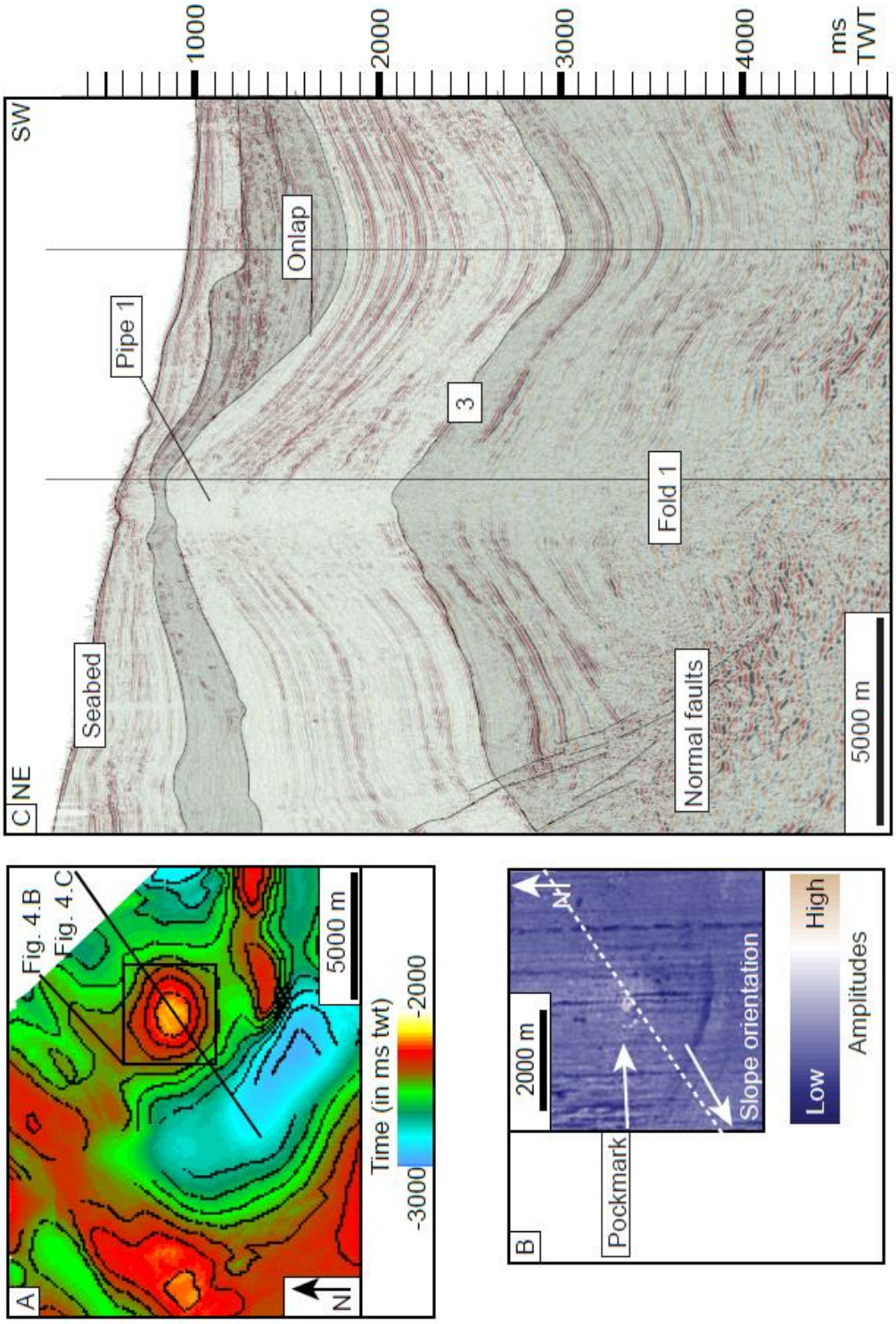

Figure 5.4 Seismic section showing the fluid flow pipe 1, at the top of fold 1. A seabed amplitude extraction map shows the pockmark at the top of pipe 1 (high amplitude is white to brown; lower amplitudes are shown in blue). "3" refers to the nomenclature presented in Fig 5.3; this horizon embeds

"channel 2" shown on Fig 5.7. Vertical exaggeration: x5.

A second anticline (fold 2) is located to the south of fold 1 (Fig. 5.3B) in a comparable structural setting, although its geometries are more elongated in a NE-SW direction. Its hinge is 15 km-long and it is 3 km wide from north to south (Fig. 5.2C). A low-reflectivity unit disturbed by sub-vertical features is found at the base of fold 1. They are interpreted as either compressive or strike-slip, east-west oriented, fault traces that develop over the detachment (Leduc *et al.*, 2012).

5.3.2 Channel complexes at folds 1 and 2

In the absence of more precise information, we assume that sedimentation rates are spatially uniform. Isochron maps from packages A to E show the evolution of the position of depocentres in the area of folds 1 and 2 (Fig. 5.5). Contemporaneous with the development of the NE–SW strike-slip fault zone, deposit progressively thin out northwards (Fig. 5.5, isochron maps A to E). Similarly the development of a syncline to the southwest of folds 1 and 2 is observed at later stages (Figs 5.3A and B, packages C to E). Areas where the youngest package E is thinner suggest that a bathymetric high prevented sediment deposits from being deposited or preserved above folds 1 and 2 (Fig. 5.5, unit E).

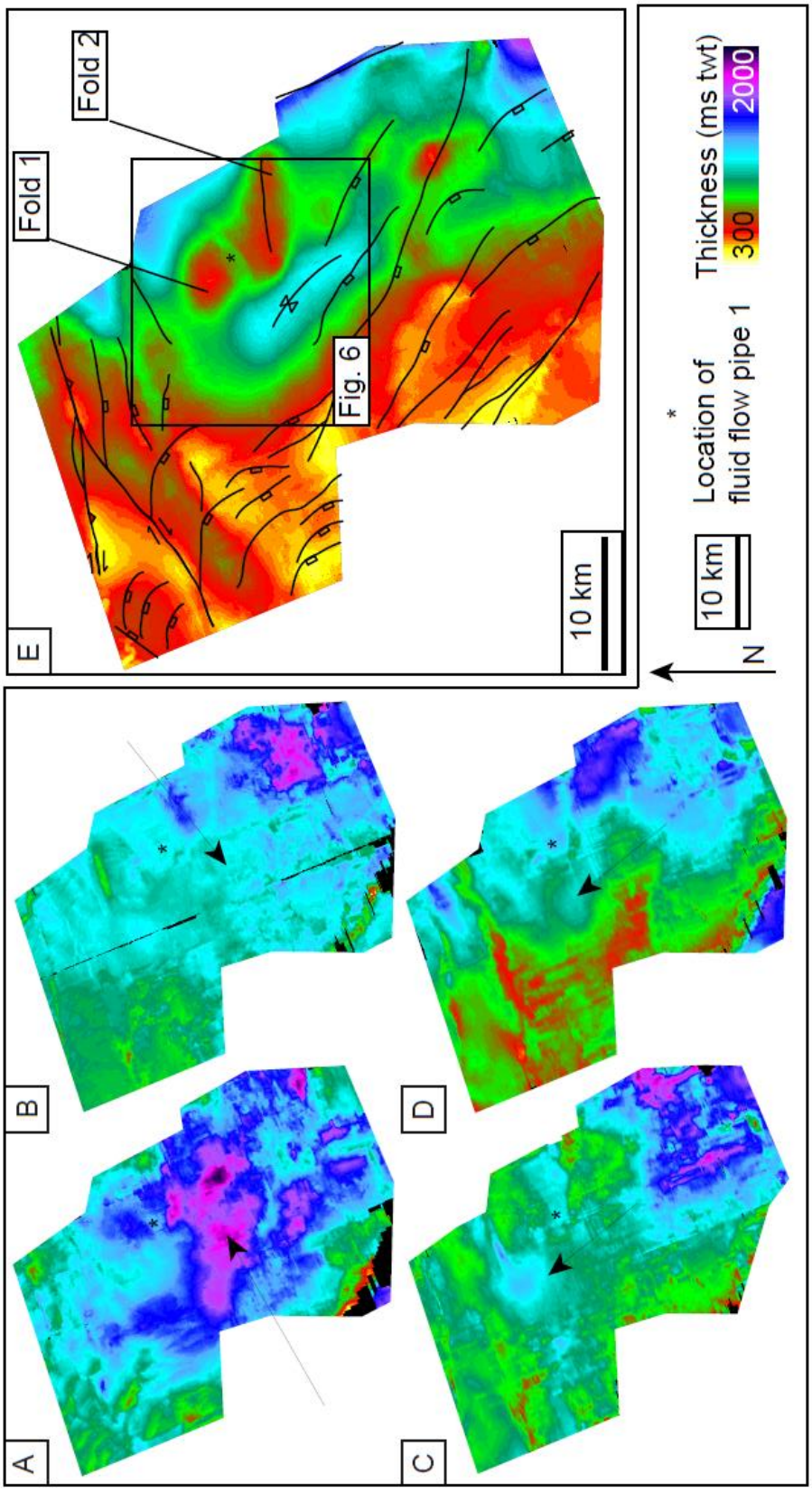
A
B
C
D
E
Fold 1
Fold 2
Fig. 6
10 km
Thickness (ms twt)
2000
300
Location of
fluid flow pipe 1
10 km
N

Figure 5.5 Time thickness maps in the folds 1 and 2 areas for each unit (A, B, C, D and E, over which are represented the main structural trends) defined in figures 5.3A and B. Red to yellow indicates thinner areas, blue to purple shows thicker areas. The asterisk shows the location of the fluid flow pipe; the arrows indicate areas where an important change in thickness trend is observed between the previous and the actual map.

Five channels are identified to the north and south of fold 1 (Fig. 5.6). Two different types of sediment pathways developed. At earlier stages all channels are low-sinuosity (Fig. 5.6, map A). These channels are mud-filled and levee deposits are fine-grained (Fonnesu, 2003). No deflections of the sediment routes are found around fold 1 (Fig. 5.6, maps A and B). A reorganization of the channels network appears at later stages (Fig. 5.6, maps C and D) and channels were clearly deflecting around a bathymetric high.

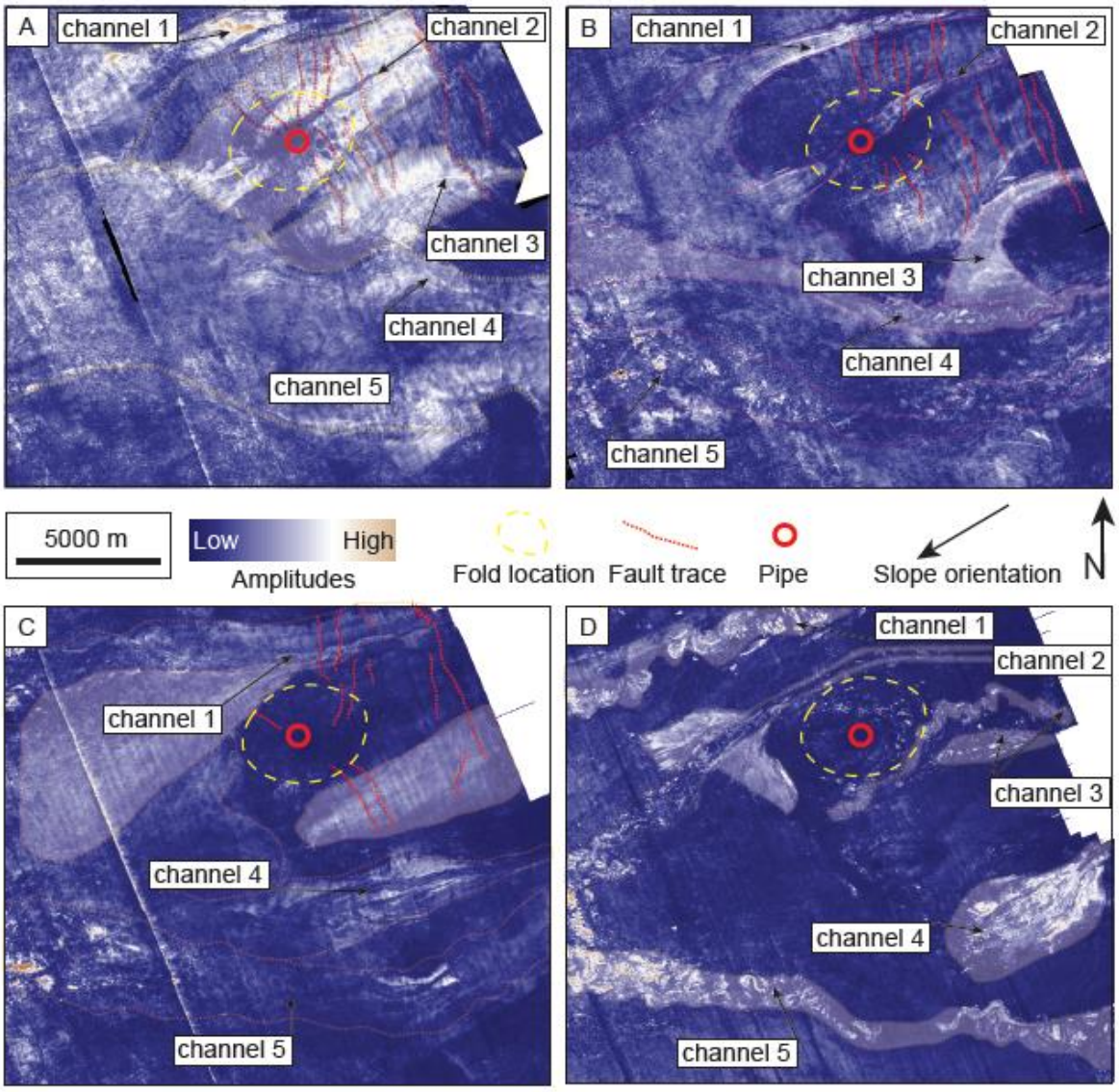

Figure 5.6 Amplitude extraction maps of horizons A, window: -100+100 ms twt, B, window: -10+80 ms twt, C, window: -10+60 ms twt and D, window: -0+80 ms twt. Red circle indicates the position of the fluid flow pipe 1. Dashed red lines indicate faults and dashed yellow line the position of fold 1.

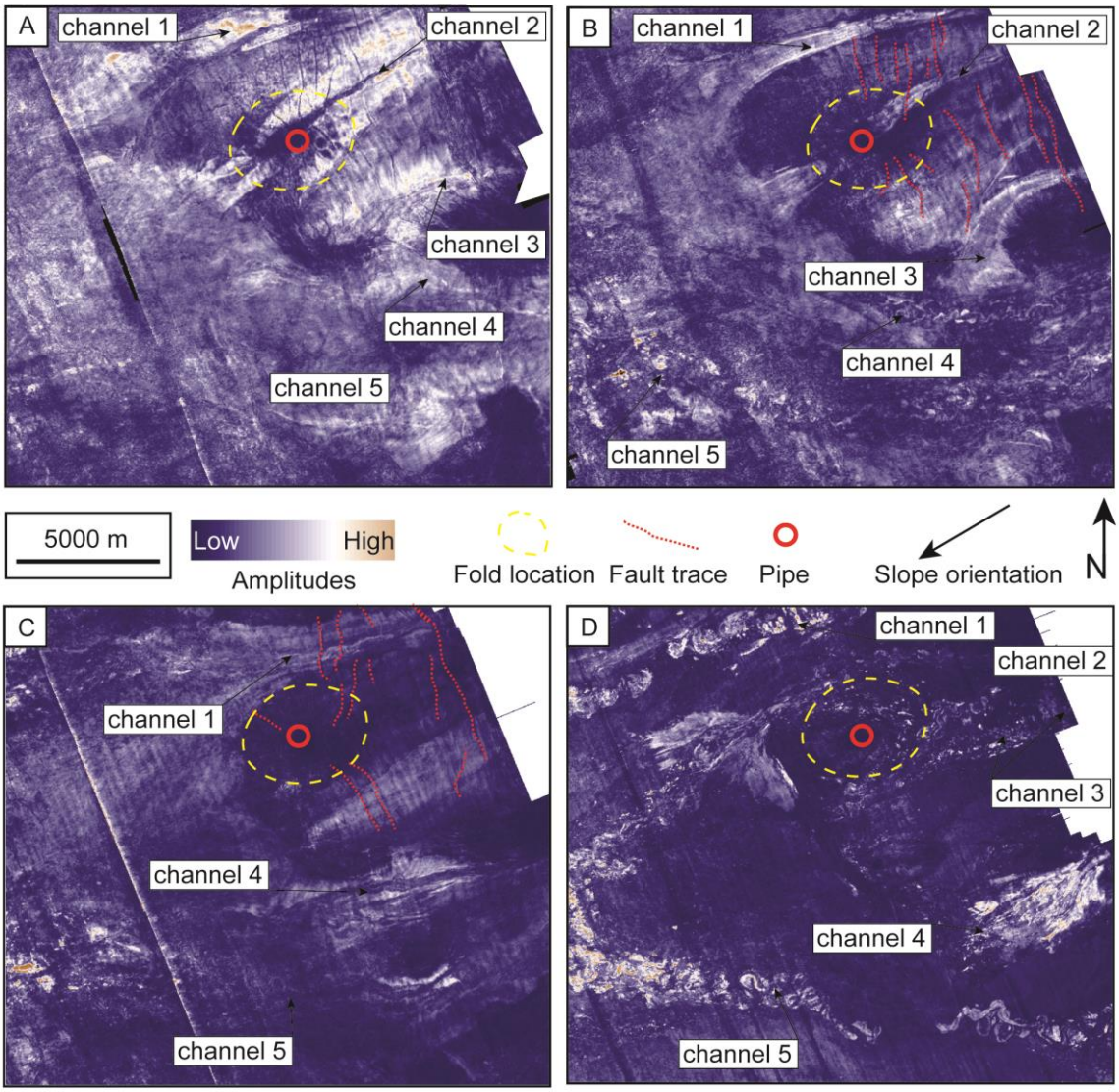

Figure 5.6 Same maps without colouring.

5.3.3 Pipes 1 and 2

A roughly circular high amplitude region of the seabed is apparent at the crest of fold 1 (Figs 5.2C and 3). It is underlain by a vertical area of low-reflectivity that extends from the seabed to a depth of 2100 ms twt (approximately 2625 m). A lack of seismic reflectivity is interpreted as an indicator for the presence of gas. Evidence for bottom-simulating reflections and similar amplitude anomalies can be observed at the periphery of the pipe, occurring at depths of approximately 495 m (or 400 ms twt) below the seabed (Fig. 5.4). It is an approximately cylindrical

feature ~ 650 m in diameter. A similar feature is observed downdip (pipe 2, Fig. 5.7). Their structural and stratigraphic setting are comparable, as well as their dimensions (~ 450 m diameter at the seabed; ~ 1965 m in height). Both are also located above an anticline structure. At pipe 1, the flexure generated a relief of 1340 m between the lowest point (at 3050 ms twt, or 3965 m depth burial, Fig. 5.4C and Fig. 5.6A) and the highest point (at 2100 ms twt, or 3965 m depth burial) of the channel complex (Fig. 5.8A). At pipe 2, a relief of ~ 800 m is measured between the top of the reservoir interval located 2500 ms twt or 3250 m depth burial) and the lowest point (at 3000 ms twt or 4050 m depth burial, Fig. 5.7 and 5.8B). The channel located below pipe 2 appears as a package of high amplitude, chaotic reflections (Fig. 5.7). RMS amplitude extraction of the channel shows meandering geometries with low amplitude reflection, indicative of a mud fill in the core of the channel complex and high amplitudes on each side (levee deposits, Fig. 5.8B).

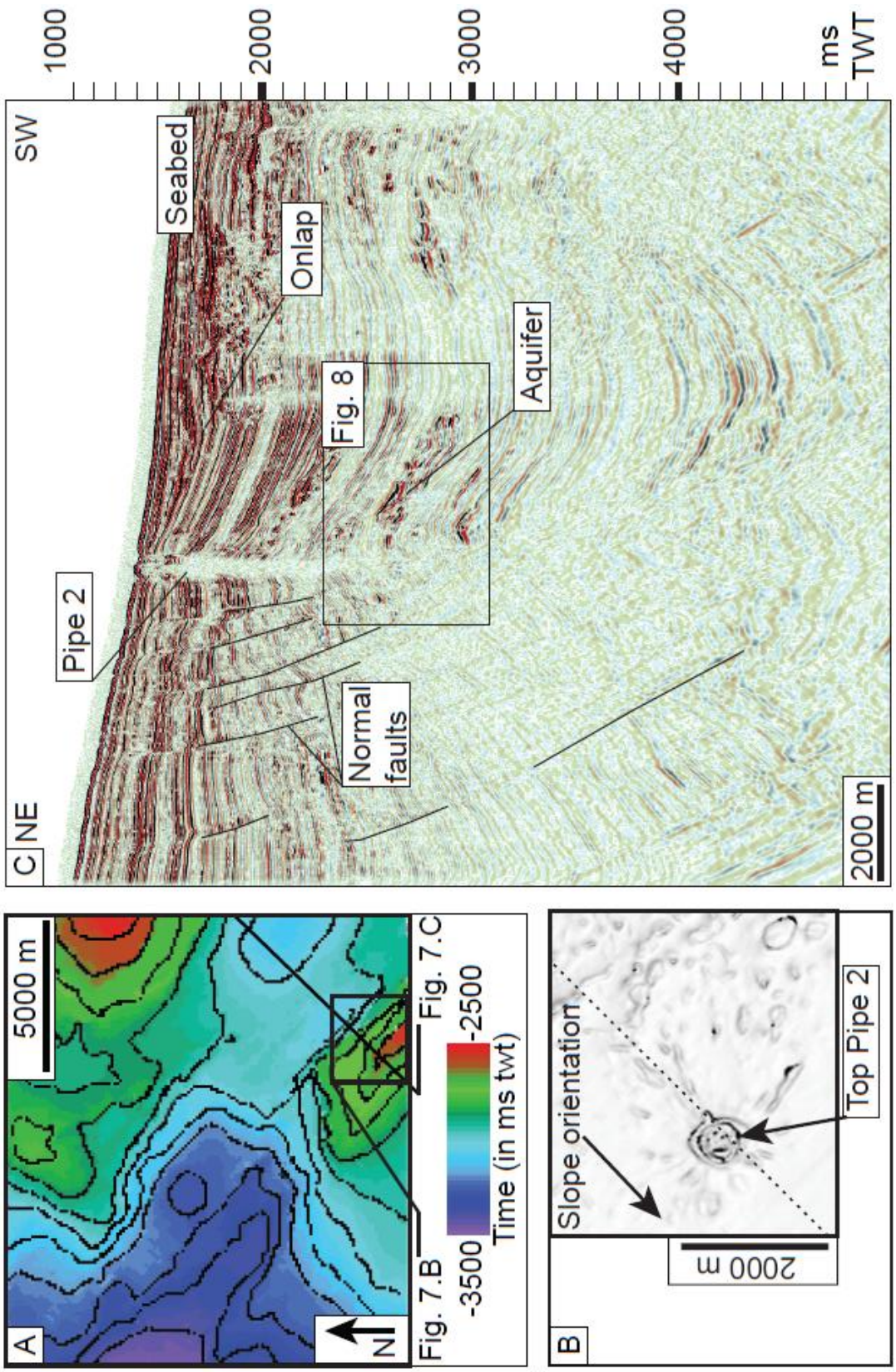
1000
2000
3000
4000
ms
TWT
SW
NE
C
Seabed
Onlap
Fig. 8
Aquifer
Pipe 2
Normal faults
2000 m
A
5000 m
N
Fig. 7.B
Fig. 7.C
-2500
-3500
Time (in ms twt)
B
Slope orientation
Top Pipe 2
2000 m

Figure 5.7 Pipe 2. A. Time contour map (see Fig. 5.2) locating the following sections. B. Seabed dip map showing the pockmark at the top of pipe 2. C. Seismic section across pipe 2. The potential source of overpressured fluids for this pipe is inferred to be the tilted reservoir interval shown in details in Fig. 5.8 (indicated as Fig. 8).

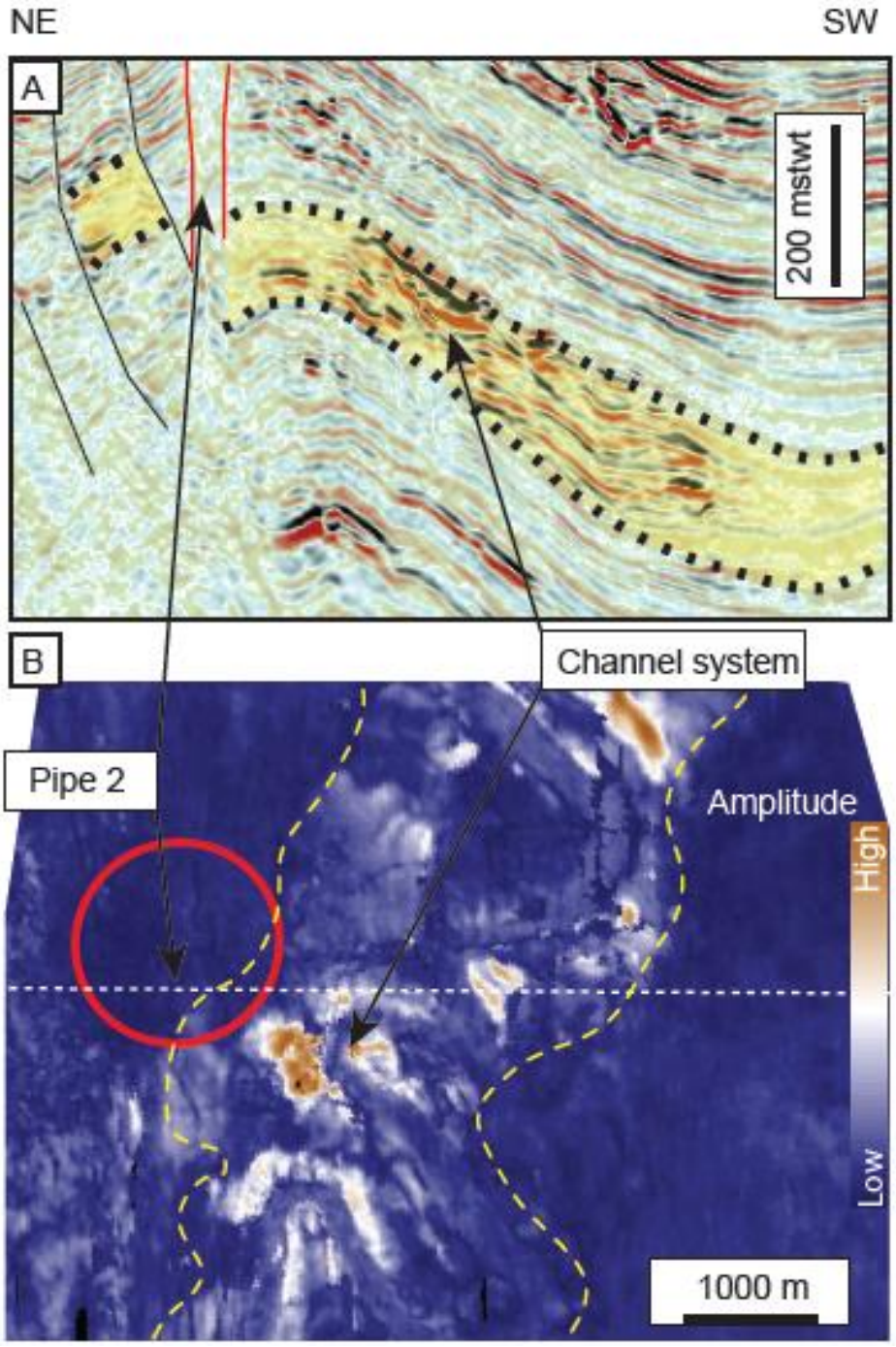

Figure 5.8 A. Details of the reflections at the level of the reservoir below pipe 2 (area colored in red; see full section on Fig. 5.7). B. Amplitude extraction map from a window between the top and the bottom reservoir interval reflections (indicated with dashed lines and highlighted in yellow). High amplitudes are shown in white to brown; lower amplitudes in blue. A meandering channel-levee system can be identified; high amplitudes being located in the potential channel-fill deposits. The fluid flow pipe stands just east of the high amplitude pattern; a discrete fault network possibly links the two. Reverse polarity high amplitudes could suggest the presence of a hydrocarbon-water contact in the reservoir.

5.4. Interpretation

5.4.1 Fluid flow pipes

These observations argue for a fluid escape feature (Cartwright *et al.*, 2007), however there is no evidence for mud flows at the near-surface and no evidence for a buried or active edifice. We herein term the feature a fluid flow pipe (pipes 1 and 2, Figs 5.4 and 5.7) although we recognize that this term does not reflect the likely complexity of the structure (e.g. Morley 2003). At the seabed a high amplitude reflection may indicate the development of a chemosynthetic community, gas hydrates, or a local seabed diagenetic effect at the summit of the pipe, arguing for gas escape. In both cases a growth package and the presence of normal fault traces support the hypothesis that these structures are rollover anticlines. We propose that there were a series of deformation episodes within this strike-slip domain, and then extension led to the formation of this sub-circular feature. Near-seabed growth packages suggest recent activity of the growth fault (onlapping reflections marked on Figs 5.4 and 5.7, growth strata visible in packages D and E). The vertical pipes then develop in an analogous structural setting and over similar pre-existing depositional features. High amplitude reflection packages, interpreted as channels, are found at the base of the vertical zones of low reflectivity in both cases. In plan view, a low-sinuosity channel located at the base of pipe 1 is identified. Internal low amplitude reflections indicate a mud fill whereas the channel body is interpreted to be fine-grained sand (Fonnesu, 2003). The associated levee deposits display high amplitude reflections (channel 2, Fig. 5.6).

5.4.2 Development of fold 1

Fold 1 is sub-circular. Several geological mechanisms can form circular structures, for example diapirs (salt or "mobile shale"), volcanic calderas (magmatic or mud volcanism as a result of overpressure), rollover anticlines, compressive or strike-slip pop-ups (Stewart, 1999). Similar structures have been termed "shale diapirs" (Cohen and McClay, 1996; Kopf, 2002), but with higher-resolution data, it is possible to identify an east-west compressive or strike-slip structure at the core of fold 1. We propose that the slight east-west elongate irregularity may be inherited from early stages of strike-slip deformation as seen in fold 2. It could have formed as the region underwent the early stages of strike-slip deformation, evidenced by the development of the NE–SW strike-slip fault to the northwest. This deformation event may be followed by a regional extensional event which took place to the northeast of the study area. This later event resulted in the development of growth fault-related rollovers, which may modify the overall geometries of pre-existing structures. Finally, the occurrence of pipe 1 postdates the development of the fold, but is contemporaneous with normal fault growth. It is thought to be contemporaneous to mud volcanism activity, which has been reported in the Pliocene and at present day in other locations of the deepwater delta (Kopf, 2002).

The structural development of fold 1 can be explained in two steps. Evidence for the existence of a growing positive topographic feature is found from seismic reflection amplitude attribute maps (Fig. 5.6). A channel (marked channel 2, Fig. 5.6) is identified from a series of time thickness maps calculated between the interpreted horizons. It is deflected around the position of Fold 1 between maps B and C, and that trend is even cleared during the later stages of deposition (Fig. 5.6, map D). Time thickness maps (Fig. 5.5) confirm a localized thinning in the area of Fold 1 but only seen on the isochron map for the most recent sedimentation (Fig. 5.5E). This observation

matches the observations from seismic data showing onlap geometries in the overlying sediment package (Fig. 5.7). However, deposition of sediment packages is not strongly disturbed and the structure is shallow enough for sedimentation to continue at its crest. As a result two episodes of growth are identified, one in the Late Miocene and one between the Pliocene and present day. These observations suggest the following three hypotheses. Either folds 1 and 2 start to grow after the channels deposition, or their rate of uplift is much lower than the rate of burial.

We associate the early stage of fold 1 growth with an earlier stage of the evolution of the gravitational collapse when this area was located in a compression setting. In a second stage, as a result of the delta progradation seaward the structural domains migrate to deeper parts of the basin and the area from then on is in the position of the translational domain, close to the extensional domain. Fold 1 is incorporated at the northern tip end of a large rollover anticline (Fig. 5.6E) and updip growth strata (Fig. 5.4) indicate the presence of a large associated normal fault.

5.4.3 Pore pressure

The porosity of the generally fine-grained sediments is estimated to be 60-70% at the seabed, and is reduced to 40% by compaction at a depth of 800 m (Janik *et al.*, 1998).The density of mud is taken to be 2.1 $g.cc^{-1}$ (Janik *et al.*, 1998) and the density of water is 1.03 $g.cc^{-1}$. The hydrostatic gradient is approximately 10 $MPa.km^{-1}$; the lithostatic gradient is estimated to be 22 $MPa.km^{-1}$ and the horizontal stress at ~18.2 $MPa.km^{-1}$, as the ratio between the horizontal to the vertical effective stress are estimated to give a fracture gradient of 0.85 which is typical for a basin that is undergoing little extension, similar to Trinidad (Heppard *et al.*, 1998; Deville *et al.*, 2010), the Nile delta (Nashaat, 1998), and Brunei (Tingay *et al.*, 2009). This value is also predicted from the model of Grauls (1999), who proposed that a predictable correlation exists for the maximum

fluid pressure value, between the minimum principal stress and depth, for a given tectonic regime, which is, for this study extensional. Finally, the fluid retention depth (FRD) is expected to be found in a depth interval between 700 – 1400 m below the seabed given the sedimentation rate of approximately 160 m.My^{-1} (Swarbrick *et al.*, 2002; Davies, 2003).

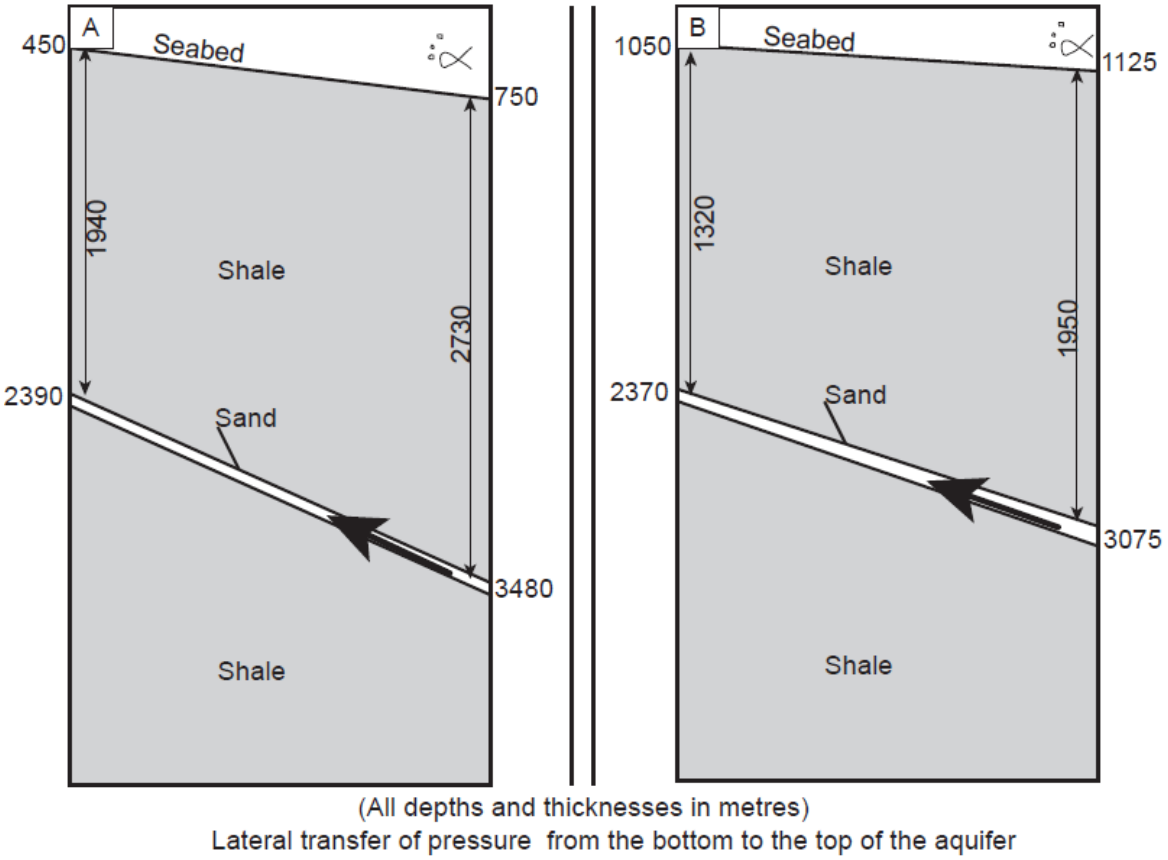

Figure 5.9 Lateral pressure transfer in a given reservoir. A. values measured for pipe 1. B. values measured for pipe 2. In this model, the reservoir is inferred to be a tilted sand body confined in a shale succession. Black arrow denotes lateral pressure transfer. Depths are calculated after Morgan (2003).

Development of fold 1 generated uplift. This uplift, associated to the tilting of the reservoir interval is thought to cause an increase in pore pressure within the reservoir at the base of pipe 1, within channel 2 (Fig. 5.7, horizon 3; Fig. 5.6B, marked “channel 2”), assuming internal channel connectivity. Uplift by the tilting of the footwall is a likely cause for lateral pressure transfer (Yardley and Swarbrick, 2000). In addition, no significant evidence for erosion is found at

the crest of the anticline, which does not allow arguing for a significant change in reservoir pressures before the pipes formation. For both pipe 1 and pipe 2 systems, it is possible to calculate the amount of overpressure required in each reservoir interval to come sufficiently close to the minimum horizontal stress to generate a fracture (Fig. 5.9). A graphic construction is proposed in order to define the centroid depth. We present results for pipe 1 (Fig. 5.10A) and pipe 2 (Fig. 5.10B). A centroid depth between 3000 m (for a FRD located 700m below the seabed)and 3850m (for a deeper FRD, Fig. 5.10A) is required for Sh min to be reached at the base of pipe 1 escape system, and of at least 3600 m for pipe 2 escape system (Fig. 5.10B). A difference in overpressure of about 4 to 13 MPa is required to reach hydraulic fracturing for pipe 1 (Fig. 5.10A), and 5 MPa of additional overpressure are required for pipe 2 to reach fracturing. In this estimation we do not include the role of extensional faults close to the crest of the fold as their role in the release of fluid and lowering of overpressure cannot be estimated from our available data. However, if one assumes these faults could also be used for fluid circulation, the estimated required overpressure for pipe 1 and 2 would be inferior to the above estimated figures. In our case study the lack of relevant data prevents from specifying the role of fault as conduits, which can be estimated in analogue studies, and may help in carrying a full forward model (e.g. Hustoft *et al.*, 2009).

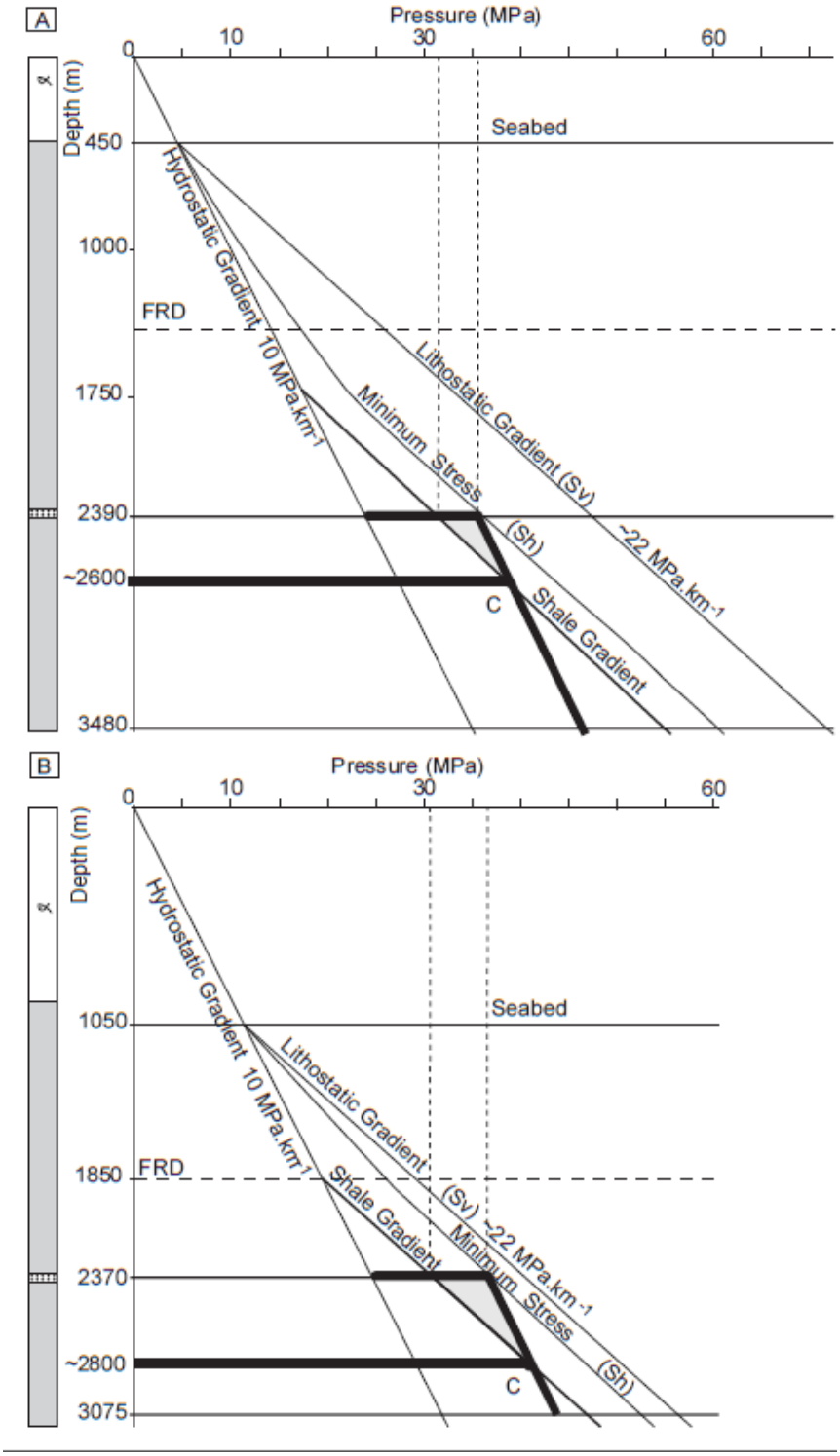

Figure 5.10 Pressure (MPa) versus depth (m) plot showing the position of the reservoir and the amount of overpressure required to reach the fracture pressure for the case of pipe 1 (A) and pipe 2 (B). FRD (1) – the shallowest estimated fluid retention depth. – FRD (2) – the deepest estimated fluid retention depth. The thick, longer horizontal line represents the estimated depth of the centroid (C), located at the intersection between the shale gradient and the hydrostatic-parallel gradient within the reservoir. The thick, shorter horizontal line indicates in case A, the maximum amount of overpressure required to reach seal fracture (~ 13 MPa), with a FRD located at its deepest, whereas case B shows the opposite situation where a minimum of 4 MPa are required to reach fracture pressure, with the FRD given at its shallowest.

5.5. Discussion

5.5.1 Source of overpressured fluids

There are at least two potential sources of overpressured fluids. A deep source of overpressured fluids had been discussed by previous works (Graue, 2000; Cobbold *et al.*, 2004; Cobbold *et al.*, 2009; Løseth *et al.*, 2010). They suggested that, in the Niger Delta, hydrocarbon cracking at depth would provide a suitable source to generate overpressure in deep reservoir intervals. It is possible that fluids coming from deeper strata migrate to shallower reservoirs in the overburden through a connected detachment fault network (Maloney *et al.*, 2010). However, a combination of disequilibrium compaction and lateral pressure transfer processes could also well explain the presence of shallower overpressure without the need of a large amount of overpressured fluids migrating from deep strata. This shallower source of overpressured fluids would be more likely to generate the studied fluid flow pipes.

5.5.2 Role of gas

Two main hypotheses can be taken into account. The first hypothesis we discuss is about hydraulic fracturing. We also discuss a second hypothesis taking into account capillary seal failure. There is evidence for the presence of gas in the pipe and at its periphery. At depth, hydrocarbon accumulation, and specifically gas, is likely to be trapped in sandstone reservoirs which were deposited within deepwater channel deposits. The presence of hydrocarbon accumulations can easily be observed from high amplitude reflections associated with a flat spot on seismic section (Fig. 5.8). If a vertical failure occurs at the top of these hydrocarbon-filled reservoirs, then this accumulation could escape through a fluid escape pipe. It does however not demonstrate that the

hydrocarbon accumulation actually caused the initiation of the failure at the reservoir-caprock interface Hydrocarbon buoyancy, as well as water within a given reservoir modifies the effective stresses by increasing the fluid pressure equidirectionally, but to breach the seal, the failure conditions must be met. An increase in fluid pressure can drive a fluid-filled fracture (e.g. Flemings *et al.*, 2003). Under such conditions grains can separate, allowing seal breaching and fluid escape. Caprock hydraulic fracturing can then occur once the pore fluid pressure exceeds the minimum stress, added to the tensile strength perpendicular to the direction of minimum stress (Hubbert and Willis, 1972; Jolly and Lonergan, 2002, Reilly and Flemings, 2010). Lateral pressure transfer (the centroid model) can help predicting higher pore pressures in a fluid-filled sand body included in a sealing, impermeable shale-rich environment, when structural relief (e.g. caused by tilting) triggers a differential sedimentary loading over the sand body. As a result a hydrostatic pressure gradient parallel to the slope of the hydrostatic gradient develops in the sand body (Traugott and Heppard, 1994; Yardley and Swarbrick, 2000). The lateral transfer of pressure then can locally enhance pore pressures at structural crests (Swarbrick and Osborne, 1998). Mechanically, the lateral transfer of pressure within a tilted reservoir interval can explain the initiation of a vertical failure in this presented case study, with or without the presence of hydrocarbon. The role of hydrocarbon, and gas in particular, in this model, would be limited to the actual propagation of the vertical pipe towards the surface, by escaping of buoyant gas initially present in the reservoir. Rodgers (1999) also suggest that, as an application to Newton's third law of conservation, it can be predicted that hydraulic fracturing is not more likely to occur in gas reservoirs than in water-filled reservoirs. As a result the role of gas is limited to bring the overpressured fluids through the pipe towards the surface. This would explain how the pipe propagates vertically to the surface, and why leaking gas may be observed within and at the top of the pipe. This model thus suggests that the effect of hydrocarbon buoyancy needs not be involved to create the pore pressure required for failure (Bjørkum *et al.*, 1998).

However, the presence of hydrocarbons suggests a capillary seal failure. This is a common process found in west African margins (e.g. Ingram *et al*., 1999). This alternative process assumes that shales act as leaky valves. They cannot support gas columns so all the fields are saturated oils directly overlying the oil kitchen. The instant a gas cap is formed the gas escapes by capillary failure and the oil is retained, since gas has larger molecules than oil. Residual gas only is found over the gas kitchen due to seal failure, and no hydrocarbons are present where the source rocks are immature. In this paper, we choose to highlight the first hypothesis, the hydraulic fracture, since evidence for the presence of gas is not found in clusters in the overburden, but in vertical chimneys, which would argue for a focused flow. A practical way of testing both hypotheses would be to develop a basin model to test the fluid migration. However, in the absence of well data and seismic stacking velocities, we prefer not to conclude on this topic.

Hydrocarbons present in the pores are also buoyant and an increase in volume triggered by their cracking can contribute to an increase in overpressure (Osborne and Swarbrick, 1997; Swarbrick and Osborne, 1998; Grauls, 1999). They are thought to be the main cause of regional overpressure in the deepwater Niger Delta (Cobbold *et al*., 2009). In this study, however, hydrocarbon accumulation at these depths would not reach a temperature high enough to generate hydrocarbon cracking. We therefore prefer the lateral pressure transfer mechanism for the formation of such large scale fluid flow pipes. Numerous other smaller vertical pipes (less than 1 km long in cross-section) are present; however their formation is not specifically assigned to lateral pressure transfer. Pipes 1 and 2 share two main location characteristics: above a potential reservoir and at the crest of a steep structural high. This has implications in terms of reservoirs integrity as, even though such reservoir intervals may constitute interesting prospects in oil and gas exploration, it is necessary to be careful about the critically pressured state of these objects.

5.5.3 Model

The chronology of deposition, structural deformation and overpressure development is: (a) first, sedimentation through deepwater clastic-filled channels, including fine sand deposits in a shale-rich succession occurs, and deepwater channels become quickly buried due to rapid loading; (b) overpressure builds up and regional-scale gravitational collapse triggers structural deformation, including rollover anticlines. Local subsidence or uplift causes a local rearrangement of sediment pathways at the periphery of the structure; (c) as structures grow, tilting of the underlying sediments increases and potential overpressured reservoirs – bearing water with or without hydrocarbon accumulation – undergo a redistribution of pressure, a lateral transfer towards the highest point of the reservoir. Structural deformation might also generate a fracture network allowing fluids from deeper reservoir intervals to migrate to a higher position in the stratigraphic succession, which is not seen on the interpreted data. Finally the pressure gradient between the reservoir and the caprock at the highest point of the reservoir becomes high enough to reach hydraulic fracturing, and large, vertical fluid flow pipes develop. A later resulting local deformation and sediment redistribution is likely to occur, and the pipe may remain an active fluid migration pathway as long as overpressure remains in the connected underlying compartments (Fig. 5.11).

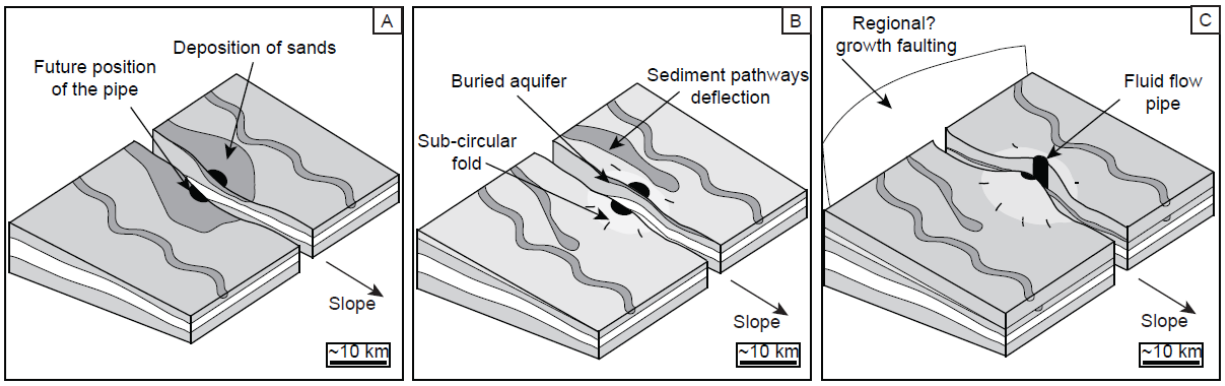

Figure 5.11 Summary block diagram. A. Deposition of channel complexes downslope. B. Early stage of uplift (i.e. first stage of folding for fold 1; this stage is not observed on the structure of pipe 2). C. Late stage of folding generating enough tilting for the fluid flow pipe to form at the crest of the structure.

5.6. Conclusions

We propose that large-scale vertical pipes need not be related to hydrocarbon buoyancy and can form above porous and permeable strata with no hydrocarbon charge. In this study we presented pipes that develop at the crest of anticlines as a result of the following succession of events: (1) rapid sedimentation and loading; (2) uplift; (3) lateral pressure transfer in the reservoir intervals; (4) hydraulic fracturing of the caprock at the shallowest point in the reservoir interval; (5) vertical fluid escape through the overburden to the seabed. Our results suggest that this process, lateral pressure transfer, added to regional-scale disequilibrium compaction is sufficient to generate enough overpressure (~ 5-10 MPa) to initiate the two kilometer-scale fluid flow pipes located right above these water-filled sand bodies. This model could have general applicability to other deepwater settings where vertical fluid pipes are common.

This case study provides complementary information on the nature of low-reflectivity vertical features in a gravity detachment system, which have commonly been interpreted as shale diapirs with lower-resolution data. Appropriate seismic interpretation around each fluid flow

pipes allows the mapping the source of fluids escaping through the pipes and the structural setting in which they develop. The results show that kilometer-scale vertical fluid flow pipes can develop as a result of interacting sedimentary, structural and overpressure mechanism and need not be a direct hydrocarbon indicator**.**

CHAPTER 6: GENERAL DISCUSSION AND CONCLUSIONS

Chapters 3, 4 and 5 all include a discussion section. This discussion and conclusion chapter summarizes the main results of the previous chapters. Links between the three chapters are then considered. More general implications of this work are also discussed including the limitations of this study and potential field analogues. Lastly, I discuss potential further work.

6.1 Main conclusions

Through three case studies based on the deepwater Niger Delta and offshore of Mauritania, this research project has investigated the structural evolution of the lateral margin of a deepwater gravitational detachment system, the interaction between sedimentation, deformation and overpressure and folding in the vicinity of the lateral margins, and the interaction between faults and sediment routing systems. Three adjacent 3D seismic datasets located in the deepwater western Niger Delta, with water depths of 500 m and 3500 m were interpreted (chapter 2). Selected seismic stratigraphic horizons from the Late Miocene and Plio-Pleistocene fine-grained succession were mapped in a ~ 4500 km² area. Seismic interpretation, including the derivation of seismic attributes such as dip and amplitude, allowed one to establish the structural setting of the area of interest in the Niger Delta. Detailed case studies from the lateral margin of the western lobe and structural elements of the transitional domain were also carried out in order to identify linked processes between structural growth, sedimentation and overpressure. An integrated analysis of the structural evolution of tear fault zones and the migration of submarine channels was also performed between various parts of the study area and with a fourth 3D seismic dataset situated offshore Mauritania, in order to create a model for the evolution of tear fault zones in deepwater margins gravity detachment systems.

Key results include:

- *(Chapter 3) The identification and interpretation of a lateral strike-slip domain in a gravity detachment system of a continental margin.*

The lateral strike-slip domain in the deepwater western Niger delta represents a 75 km long tear fault system that has been occurring over the last 5 to 7 million years. This structural domain located at the edge of the gravitational system links the updip extensional domain to the downdip contractional domain. A wide variety of strike-slip-related structures are identified. They include transtensional faults such as horsetail splays, and pull-apart basins, as well as transpressional faults and fault-related folds in a restraining bend. Questions however remain on the origin and constraints of tear faulting in the study area. This is important to understand the fluid flow history in the area of interest, as well as the implications for tear fault development at continental margin gravity detachment systems and implications for sediment routing. Similar lateral strike-slip domains may exist in other gravity detachment systems around the world.

- *(Chapter 4) Characterization of the role of tear faults in controlling sediment routing.*

In gravity detachment systems, slope-parallel tear faults can provide an initial canyon path followed by the routing of sediment. These fault systems can then locally control channel migration and depositional architectures in channel complexes by channel confinement, or deflection in contractional parts of tear faults, and also migration and diversion in extensional parts of the fault zones. Conversely, sedimentary processes, such as the long-term development of canyons or lateral variability in sedimentation rates during the gravity-driven deformation

events may impact deformation styles. For example, localized increased erosion rates may contribute to an increase in the rate of growth of folds and increased sedimentation rates may involve increased subsidence and differential compaction (e.g. chapter 4). This model implies for the long-term evolution of gravity-detachment systems, the formation of major focused sediment bypass areas.

- *(Chapter 5) A case study of fluid flow pipes triggered by lateral pressure transfer.*

In the transitional domain of the deepwater western Niger delta, a case study located at the vicinity of the tear fault system integrates the regional structural and stratigraphic framework where > 1 km-long blowout pipes develop above sub-circular structures. This work is an attempt at predicting the local pore pressure history of a given area from basic structural and stratigraphic interpretations. The concept of lateral pressure transfer is shown to be a key process in overpressure build-up and seal failure on folds within the Niger Delta. It also suggests that km-scale blowout pipes are not necessarily direct hydrocarbon indicators since their formation is not necessarily caused by a hydrocarbon column accumulation. This case study over a sub-circular structure also questions previous seismic characterization of “shale diapirs”.

The interactions identified in this study characterize the fundamental links between sedimentary processes and structural deformation that occur in the transitional domain of a gravity detachment system and at its lateral margins. Overpressure was studied in a case study, but its processes at the scale of the regional gravity detachment system have not been studied in detail in this thesis. Overpressure is a process occurring both in the detachment levels and locally in the sedimentary overburden. The detachment levels of the Niger Delta gravity system are made of overpressured shale. This overpressure is a result of high sedimentation rates, rapid loading, and causes a weakening of these levels. Gravity-driven tructural deformation then takes place

over these strata that behave like detachments and the sedimentary overburden is affected by an upslope to downslope regional gravity deformation. I demonstrated in this thesis that this deformation occurs in 3D and is responsible for the development of lateral strike-slip faulting. The case study presented in chapter 5 illustrates local interactions between sediment deposition, structural deformation, lateral pressure transfer and fluid escape. In this case study it was shown that lateral pressure transfer is a process that can occur in porous and permeable sediment units that are structurally tilted. This process can result in hydraulic fracturing of the overlying stratigraphic units and cause fluid escape.

6.2 Discussion

The case studies presented in chapters 3, 4 and 5 show evidence for linked geological processes in the transitional domain of a gravity detachment system. The following relative succession of linked events and processes, for most of them seen in this thesis are proposed: (1) initially, the locus of sedimentation was controlled by the pre-existing basin geometry, prior to gravity-driven deformation. One can speculate that earlier structural relief that existed prior to progradation of the delta had a control on the later position of the lateral margins of the delta lobes, where the lateral strike-slip domain occurs. Then, (2) as the gravity detachment system developed, the structural growth of gravity-driven folds and strike-slip faults may have begun to have a local impact on sedimentation rates. For example, the thesis shows evidence for the close relationship between deformation (e.g. folding) and the location and migration of long-term sediment routing system. Folding and tear faulting may also contribute to submarine channels confinement and enhance the downslope transfer of sediment through tear fault zones, or sediment could pond between contractional structures (chapter 4). Since overpressure development by disequilibrium compaction is linked to rapid deposition of fine-grained sediment

(e.g. Swarbrick *et al*., 1998), it can be speculated that the local variations in sedimentation rates could also induce local changes in overpressure distribution. The differential distribution of overpressures, combined with the pre-existing structural trends, could then speculatively control the later evolution of gravity-driven structural units and influence deformation rates and structural styles (4). In addition, in the sedimentary succession overlying the detachment units, structural deformation and fluid flow interact with the local stratigraphic pattern for processes such as the lateral pressure transfer, where in an aquifer comprised in a fine-grained succession, the distribution of the pressure gradient can be modified by tilting of the units during an uplift event. This may then cause a top seal failure at the crest of the aquifer and generate fluid escape features such as large blowout pipes (5). These linked processes and interactions described in this thesis are part of a great variety of geological features and morphologies observed in the study area at present day.

The five given examples of interactions between structural deformation, sedimentary and fluid flow processes have a relative timing of development which suggests that tear fault zones occurred relatively late when compared to the longer developmental history of the extensional faults and late compression of the gravity detachment system (chapter 3). This is consistent with tear faulting being a response to mechanical changes between gravity-driven sliding blocks or at lateral margins. These mechanical changes may be due to a difference in rheology of the detachment levels, possibly due to variations in magnitude of disequilibrium compaction-induced overpressure, which is itself linked to sedimentation rates.

In chapter 4 interactions between tear fault zones development and submarine channel systems were characterized. Repeated activity of strike-slip faults in the accommodation of gravity-driven deformation was previously assumed to bring channel systems confinement within these long-lasting active faults in the western Niger Delta (Morgan, 2004), and this research

confirmed the existence of this spatial relationship on several channel systems in the Niger Delta and offshore Mauritania. Moreover, the importance of tear fault zones in controlling channel systems evolution occurs not only at channel initiation stage, but also at later stages of channel development (chapter 4). This spatial relationship can exist when tear faults develop in a similar downslope orientation as submarine sediment routing systems. This is a pattern that is likely to develop as soon as tear faults start to form, whether they are present early or not in the building up of the gravity detachment system. The likelihood can depend on the local relief and subsidence occurring along the fault trace.

6.3 Limitations

The timing relationships, pore pressure history and present-day stress regime of the study area could have been better constrained with the use of well data. However, the closest well data available were from the ODP leg 159 over the Côte d'Ivoire-Ghana transform margin, hundreds of kilometres from the area of interest and could only be used for an estimation of the sedimentation rate and approximate sediment properties (e.g. Janik *et al.*, 1998). Some wells exist in the area of interest (e.g. Abo-1) but were not available for this study. Well data would have provided material for more accurate, detailed and quantifiable interpretations about the lithology and their response to seismic amplitude changes, fluid contents and sedimentation rates. Mud weight from drilling reports and sample from cuttings would have contributed to more accurate pore-pressure predictions and implications in terms of structural growth, lateral pressure transfer, overpressure development, and fluid escape. Wireline logs would also have added information about the lithology and fluid contents, helping in better understanding sediment deformation mechanics. In addition, an integration of the results from biostratigraphic analyses would have helped better defining the time frame in which deformation took place and would have contributed to establish regional correlations with published work in the area (Cobbold *et al.*,

2009; Jermannaud *et al.*, 2010).

It is also difficult to conclude whether or not there is an underlying basement structure controlling the formation of the tear fault. This problem could have better assessed with access to 2D, coast-parallel seismic lines, located updip the contractional domain and over the area covered by 3D data. Their deeper penetration could provide a better imaging of the basement geometries and in the overlying sediment succession. Higher resolution gravity data in this area could also help in further investigating the basement properties and the presence of basement features that could impact the evolution of the overlying structural domains of the gravity detachment system. In chapter 3, a key seismic line was converted into depth using published stacking velocities from another area of the Niger Delta (Morgan, 2003) as it represented the most accurate estimate for seismic stacking velocities in the study area. This however represents an extrapolation and potentially adds uncertainties to the structural interpretations. Accurately depth-converted 3D seismic volumes could provide more correct images of the study areas key structures for the first hundreds to thousand meters below the seabed and provide more precise description of the near-seabed strike-slip related structures.

The realization of a numerical 2D basin model would have also strongly helped in the scientific test of the hypotheses presented in chapter 5. They remain highly speculative but in the absence of any available well data to tie the interpretation, it was not possible to carry on this kind of analysis.

In addition, a limited access to 3D visualization tools during the project also prevented integrated detailed analysis of near-seabed features (e.g. channels and fluid escape structures). The complexity of mapping seismic reflections through highly deformed strike-slip fault zones interacting with long-lived channel systems caused a potential mapping quality loss for detailed

features. This limited the analysis of geological process at local scale (i.e. at the scale of individual structures). A better understanding of these complex zones would require an interpretation fitting to an analogue model, either from the field of laboratory experiments, which would provide a driving model for the interpretation.

6.4 Analogues

Lateral margins and their associated strike-slip fault zones in gravity detachment systems are still poorly documented around the world. Using field analogues may provide essential information on detailed fault geometries and the pattern and degree of deformation within these fault zones. A field-scale analogue would allow assessing the local processes where slope changes occur and how faults geometries and sedimentation patterns interact. Another application would be test how ubiquitous the links between tear faults and sediment patterns are. Smaller scale land analogues could also provide a relevant image of larger-scale processes (100 m – 1 km, Butler and Turner, 2010; e.g. western Ireland: Martinsen and Bakke, 1990). These smaller-scale analogues would allow understanding the exact timing relationships of the development of lateral margins geometries in comparison to the updip and downdip structural domains. In addition, the inner structural complexity of tear faults can be assumed to be analogous to thrust fault zones, for example in the steep transpressional areas of restraining bends (e.g. Homza and Wallace, 1997; Iacopini and Butler, 2011; Maloney, 2011). Illustrations from such complex structures and associated rock types in shale-rich successions are also found in active tectonic settings (e.g. Barbados: Deville *et al.*, 2003; Borneo: Morley *et al.*, 2003; Indus Fan: Calvès *et al.*, 2008). These field analogues would provide higher resolution data in order to assess the intensity of deformation and shear strains in place. Applications would be found in fluid flow models through this complex zone. Lastly, field examples of sediment routing control by tectonic strike-slip faulting are numerous (e.g. San Andreas Fault, Crowell, 1974 or strike-slip faulting in a deepwater succession, e.g. James and James, 1969). The concept of structural confinement of sediment

routing systems in tear fault zones is comparable, and can be used to predict sedimentary facies location near a strike-slip fault zone.

Examples of similar lateral margins and tear faults may be present in other submarine regions (e.g. Gulf of Mexico: Peel *et al.*, 1995; Orange Basin: de Vera *et al.*, 2010) and they have also been observed on Mars (Montgomery *et al.*, 2009). Access to these analogues however still remains difficult. Analogues are also likely to exist in many other gravity detachment systems associated with high sedimentation rates (a review of these other potential analogues is presented in Morley *et al.*, 2011). In addition, King *et al.* (2009) worked on a preserved gravity detachment system in a deepwater setting from the Karoo Basin, and this research may show that some field examples could be available for the study of their subaqueous analogues, but may be still poorly known.

6.5 Potential future research

Since access to field analogue remains difficult, physical and numerical models could help to study tear fault zone. An issue with previous and current attempts to physically experiment detachment levels structural evolution in gravity detachment systems is the difficulty of making brittle-ductile multilayer detachment levels. Some fairly accurate analogue models have recently been developed for gravity detachment systems on a basal overpressured shale detachment (Lecomte *et al.*, 2008; Mourgues *et al.*, 2009; Lacoste *et al.*, 2011). Results include strike-slip lateral faulting which however might be related to a lateral friction effect, and this lateral faulting is not represented nor analysed accurately enough to be compared to natural case studies. There are currently few models focusing on the evolution of tear faults (e.g. Hindle and Vietor, 2006). Recent input in modelling strike-slip fault zones include modelling of pull-apart basins, which brought a 4D vision of such regions (e.g. Wu *et al.*, 2009). It would be of interest to focus a study on the development of tear faulting over a weak detaching layer in order to confirm the

predictability of such structural elements, and possibly to include the influence of basement topography (pre-existing compartmentalization, basement highs, etc.). In addition, current numerical models provide relevant upslope to downslope sections, in a dip direction, that help in better understand the timing relationships between the different structural elements of a gravity detachment system (e.g. Ings and Beaumont, 2010). Similarly, it would be of interest to carry out such simulations in a strike direction, or in 3D, in order to observe in plan view the 3D structural evolution in the area, and to predict its interactions with sedimentation.

A focused analysis of the evolution of strike-slip fault zones in gravity detachment systems is a potential way forward to delineate the geographical extent of gravity detachment system and characterize in more details how these structural domains interact with others, what their exact timing relationship is and how fluids behave through them. This study also demonstrates the importance of looking at the evolution of gravity detachment systems in 3D, both in dip and strike directions since a variety of different processes occur at lateral margins of the systems, which can be different to other areas of a gravity detachment system. In the western Niger Delta, analysis of basement and near-basement deposits (syn-rift and early post-rift successions), perhaps from shallower areas, should, if possible, also be carried out in order to provide a more accurate model for the offshore Nigeria margin. This would help in defining the succession of processes that lead to a compartmentalization of the margin and set the extent of the gravity detachment system. The results from such study may also help to predict the geological settings required for specific structural and sedimentological patterns, such as strike-slip zones in gravity detachment systems, or long-term focused sediment routes. In addition, a re-interpretation of previously interpreted "shale diapir" might be of interest, using 3D seismic data and coast-parallel seismic lines in order to better define hydrocarbon traps in this kind of settings (e.g. Cohen and Mc Clay, 1996; Morley and Guerin, 1996; Morley, 2003). Focused studies in tear fault zones, comparable to those carried on folds and fault-propagating folds in the contractional domain (e.g. Higgins *et al.*, 2009) could

be done using high resolution 3D seismic data and integrating strike-slip faulting mechanisms. This would help to determine the geometrical constraints and fluid overpressure conditions required for these fault zones to develop and evaluate a precise timing of deformation linked to updip normal faulting and downdip contraction. Numerical and analogue models might help in understand deformation processes (e.g. Hindle and Vietor, 2006; Lecomte *et al.*, 2008; Mourgues *et al.*, 2009).

A step further might be to correlate deformation to stratigraphic events such as sea-level changes (e.g. Rouby *et al.*, 2011), in also assessing and quantifying the role of sedimentary processes and external controls in conditioning structural growth in integration a full 3D regional vision of gravity detachment systems. This would help in establishing a more accurate stratigraphic setting for finer-scale interactions between gravity-driven structures, sediment deposition and overpressure development. This further research could contribute to improve prediction models in hydrocarbon exploration and build more accurate reservoir models (depositional processes, facies, fractures and fluid flow), as well as providing a more complete vision of gravity-driven processes at continental margins.

The characterization of these interactions is also important for hydrocarbon exploration purposes in an area where commercial drilling successes occurred in the late 1990s (e.g. Bosi discovery, 1996; Abo discovery, 1997). Understanding these processes may help in further investigations of the extent and nature of structural traps, in predicting the localization of potential reservoir accumulations and raise the importance of fluid barriers and escape routes. Exploration seismic surveys now also extend in the west of the Niger Delta study area, and it may be of interest to establish how relevant this study can be for these further regions.

REFERENCES

ABREU, V., SULLIVAN, M., PIRMEZ, C. and MOHRIG, D. (2003) Lateral accretion packages (LAPs): an important reservoir element in deep water sinuous channels. *Marine and Petroleum Geology*, 20 (6-8), p. 631-648.

ADEOGBA, A.A., McHARGUE, T.R. and GRAHAM, S.A. (2005) Transient fan architecture and depositional controls from near-surface 3-D seismic data, Niger Delta continental slope. *AAPG Bulletin*, 89, p. 627-643.

AJAKAIYE, D. E., and BALLY, A. W. (2002) *Course manual and atlas of structural styles on reflection profiles from the Niger Delta* (No. 41). American Association of Petroleum Geologists.

ALLEN, J. R. L. (1964). Sedimentation in the modern delta of the River Niger, West Africa. *Deltaic and Shallow Marine Deposits*, p. 26-34.

ANDERSON, J., CARTWRIGHT, J., DRYSDALL, S. and VIVIAN, N. (2000) Controls on turbidite sand deposition during gravity-driven extension of a passive margin: examples from Miocene sediments in Block 4, Angola. *Marine and Petroleum Geology*, 17, p. 1165-1203.

ANTOBREH, A.A. and KRASTEL, S. (2006) Morphology, seismic characteristics and development of Cap Timiris Canyon, offshore Mauritania: a newly discovered canyon preserved off a major arid climatic region. *Marine and Petroleum Geology*, 23, p. 37-59.

ARMENTROUT, J.M.,K. M.KANSCHAT,K. E.MEISLING, J. J. TSAKMA, L. ANTRIM, and MCCONNELL, D. M. (2000) Neogene turbidite systems of the Gulf of Guinea continental margin slope, offshore Nigeria: Fine-grained turbidite systems. In: *Fine-grained turbidite systems:* (Ed. By BOUMA, A. H. and STONE, C. G.), *AAPG Memoir 72/SEPM Special Publication 68,* p. 93-108.

ARNOTT, R. W. C. (2007) Stratal architecture and origin of lateral accretion deposits (LADs) and conterminuous inner-bank levee deposits in a base-of-slope sinuous channel, lower Isaac Formation

(Neoproterozoic), East-Central British Columbia, Canada. *Marine and Petroleum Geology*, *24*, 6, p. 515-528.

AVBOVBO, A. A. (1978) Tertiary Lithostratigraphy of Niger Delta: GEOLOGIC NOTES. *AAPG Bulletin*, *62*, 2, p. 295-300.

BABONNEAU, N., SAVOYE, B., CREMER and M., KLEIN, B. (2002) Morphology and architecture of the present canyon and channel system of the Zaire deep-sea fan. *Marine and Petroleum Geology*, 19, p. 445-467.

BACON, M., SIMM, R. and REDSHAW, T. (2007) *3-D Seismic Interpretation*. 212 pp. Cambridge, New York, Melbourne: Cambridge University Press.

BEAUBOUEF, R. T. and FRIEDMAN, J. (2000) High resolution seismic/sequence stratigraphic framework for the evolution of Pleistocene intra-slope basins, Western Gulf of Mexico: depositional models and reservoir analogs. In: *Deep Water Reservoirs of the World* (Ed. By WEIMER, P., SLATT, J., COLEMAN, N., ROSEN, C.H., NELSON, A., BOUMA, A.H., STYZEN, M.J. and LAWRENCE, D.T.), *GCSSEPM Foundation*, Houston, p. 40-60.

BIDDLE, K.T. and CHRISTIE-BLICK, N. (1985) *Strike-Slip Deformation, Basin Formation and Sedimentation.* SEPM, Tulsa, OK 386 p.

BILOTTI, F., and SHAW, J. H. (2005) Deep-water Niger Delta fold and thrust belt modeled as a critical-taper wedge: The influence of elevated basal fluid pressure on structural styles. *AAPG Bulletin*, v. 89, no. 11, p. 1475-1491.

BOUMA, A. H. (1972). Recent and ancient turbidites and contourites, *Gulf Coast Association of Geological Societies Transactions*, 22, p. 205-221.

BJØRKUM, P.A., WALDERHAUG, O., and NADEAU, P.H. (1998) Physical constraints on hydrocarbon leakage and trapping revisited*. Petroleum Geoscience,* 4, p. 237-239.

BRIGGS, S. E., CARTWRIGHT, J., DAVIES, R.J., and MORGAN, R. (2006) Multiple detachment levels and their control on fold styles in the compressional domain of the deepwater west Niger Delta. *Basin Research*, v. 18, p. 435-450.

BRIGGS, S. E., CARTWRIGHT, J., and DAVIES, R. J. (2009) Crustal structure of the deep-water west Niger Delta passive margin from the interpretation of seismic reflection data. *Marine and Petroleum Geology*, v. 26, no. 2, p. 404-410.

BROWN, A. R. (2004) *Interpretation of three-dimensional seismic data*, 6th ed.: AAPG Memoir 42, 541 p.

BRUNT, R. L., DI CELMA, C. N., HODGSON, D. M., FLINT, S. S., KAVANAGH, J. P., and VAN DER MERWE, W. C. (2013) Driving a channel through a levee when the levee is high: an outcrop example of submarine down-dip entrenchment. *Marine and Petroleum Geology*, 41, p.134-145.

BULL, S., CARTWRIGHT, J., and HUUSE, M. (2009) A review of kinematic indicators from mass-transport complexes using 3-D seismic data. *Marine and Petroleum Geology*, v. 26, no. 7, p. 1132-1151.

BURKE, K. (1972) Longshore drift, submarine canyons, and submarine fans in development of Niger Delta. *AAPG Bulletin*, *56*, 10, p. 1975-1983.

BUTLER, R. W. H., and TURNER, J.P. (2010) Gravitational collapse at continental margins: Products and processes: An introduction. *Journal of the Geological Society* (London), v. 167, p. 569-570.

CALVÈS, G., HUUSE, M., SCHWAB, A. and CLIFT, P. (2008) Three-dimensional seismic analysis of high-amplitude anomalies in the shallow subsurface of the northern Indus fan: sedimentary and/or fluid origin. *Journal of Geophysical Research*, 113, B11103, 16p.

CARTWRIGHT, J., (2007) The impact of 3D seismic data on the understanding of compaction, fluid flow and diagenesis in sedimentary basins. *Journal of the Geological Society*, 164, p. 881-893.

CARTWRIGHT, J., HUUSE, M., and APLIN, A., (2007) Seal bypass systems. *AAPG Bulletin,* 91, p. 1141-1166.

CASAS, A.M., GAPAIS, D., NALPAS, T., BESNARD, K., and ROMAN- BERDIEL, T. (2000) Analog models of transpressive systems. *Journal of Structural Geology*, v. 23, p. 733–743.

CATTERALL, V., REDFERN, J., GAWTHORPE, R., HANSEN, D. and THOMAS, M. (2010) Architectural style and quantification of a submarine channel-levee system located in a structurally complex area: offshore Nile Delta. *Journal of Sedimentary Research*, 80, p. 991-1017.

CHILDS, C., NICOL, A., WALSH, J. and WATTERSON, J. (2003) The growth and propagation of synsedimentary faults. *Journal of Structural Geology*, 25, 4, p. 633-648.

CHOPRA, S., and MARFURT, K. J. (2005) Seismic attributes—A historical perspective. *Geophysics*, *70*, 5, 3SO-28SO.

CHRISTIE-BLICK, N. and BIDDLE, K.T. (1985) Deformation and basin formation along strike-slip faults. In: BIDDLE, K.T. & CHRISTIE-BLICK, N. (editors), *Strike-Slip Deformation, Basin Formation and Sedimentation*, 37, SEPM, Tulsa, OK, p. 1-34.

CLARK, I. R., and CARTWRIGHT, J. A. (2009) Interactions between submarine channel systems and deformation in deepwater fold belts: Examples from the Levant Basin, eastern Mediterranean Sea. *Marine and Petroleum Geology*, v. 26, no. 8, p. 1465-1482.

CLARK, I.R. and CARTWRIGHT, J.A. (2011) Key controls on submarine channel development in structurally active settings. *Marine and Petroleum Geology*, 28, 7, p. 1333-1349.

COBBOLD, P. R., and SZATMARI, P. (1991) Radial gravitational gliding on passive margins. *Tectonophysics*, v. 188, p. 249-289.

COBBOLD, P. R., CLARKE, B.J., and LØSETH, H. (2009) Structural consequences of fluid overpressure and seepage forces in the outer thrust belt of the Niger Delta. *Petroleum Geoscience*, v. 15, p. 3-15.

COBBOLD, P.R ., GILCHRIST, G., SCOTCHMAN, I., CHIOSSI, D., FONSECA CHAVES, F., GOMES DE SOUZA, F. and LILLETVEIT, R. (2010) Large submarine slides on a steep continental margin (Camamu Basin, NE Brazil). *Journal of the Geological Society*, 167, p. 583-592.

COBBOLD, P.R., MOURGUES, R., and BOYD, K. (2004) Mechanism of thin-skinned detachment in the Amazon Fan: assessing the importance of fluid overpressure and hydrocarbon generation. *Marine and Petroleum Geology*. 21, p. 1013-1025.

COHEN, H. A., and MCCLAY, K. (1996) Sedimentation and shale tectonics of the northwestern Niger Delta front. *Marine and Petroleum Geology*, v. 13, p. 313-328.

CORREDOR, F., J. H. SHAW, and BILOTTI, F. (2005) Structural styles in the deep-water fold and thrust belts of the Niger Delta. *AAPG Bulletin*, v. 89, p. 753-780.

CUNNINGHAM, W. D., and MANN, P. (2007) Tectonics of strike-slip restraining and releasing bends. In: *Tectonics of strike-slip restraining and releasing bends* (ED. By: W. D. CUNNINGHAM and MANN, P.)*, Journal of the Geological Society* (London), v. 290, p. 1-12.

CRANS, W., MANDL, G. and HAREMBOURE, J. (1980) On the theory of growth faulting: a geomechanical delta model based on gravity sliding. *Journal of Petroleum Geology*, 2, 3, p. 265-307.

CROSS, N.E., CUNNIGHAM, A., COOK, R.J., TAHA, A., ESMAIE, E. and EL SWIDAN, N. (2009) Three-dimensional seismic geomorphology of a deep-water slope-channel system: the Sequoia field, offshore West Nile Delta, Egypt. *AAPG Bulletin*, 93, p. 1063-1086.

CROWELL, J. C. (1974) Origin of late Cenozoic basins in southern California.

CROWELL, J. C., and LINK, M. H. (1982) *Geologic history of Ridge Basin, southern California: Los Angeles, Pacific Section, Society of Economic Paleontologists and Mineralogists*, *304*.

DALLEY, R.M., GEVERS, E.E.A., STAMPLI, G.M., DAVIES, D.J., GASTALDI, C.N., RUIJTENBERG, P.R. and VERMEER, G.J.D. (1989) Dip and azimuth displays for 3-D seismic interpretation. *First Break*, 7, p. 86-95.

DAMUTH, J. E., KOLLA, V., FLOOD, R.D., KOWSMANN, R.O., MONTEIRO, M.C., GORINI, M.A., PALMA, J.J. C. and BELDERSON, R.H. (1983) Distributary channel meandering and bifurcation patterns

on the Amazon deep-sea fan as revealed by long-range side-scan sonar (GLORIA). *Geology*, 11, 2, p. 94.

DAMUTH, J. E. (1994) Neogene gravity tectonics and depositional processes on the deep Niger Delta continental margin. *Marine and Petroleum Geology*, v. 11, p. 320-346.

DAVIES, R. J. (2003) Kilometer-scale fluidization structures formed during early burial of a deep-water slope channel on the Niger Delta. *Geology*, v. 31, p. 949-952.

DAVIES, R.J. and CLARKE, A.L. (2010) Methane recycling between hydrate and critically pressured stratigraphic traps, offshore Mauritania. *Geology,* 38, p. 963-966.

DAVIES, R. J., MACLEOD, C.J., MORGAN, R., and BRIGGS, S.E. (2005) Termination of a fossil continent-ocean fracture zone imaged with three-dimensional seismic data: The chain fracture zone, eastern equatorial Atlantic. *Geology*, v. 33, p. 641-644.

DAVIES, R.J., STEWART, S.A., CARTWRIGHT, J.A., LAPPIN, M., JOHNSTON, R., FRASER, S.I. and BROWN, A. (2004) *3D Seismic Technology: Are We Realising Its Full Potential?* Geological Society Memoirs, 29, p. 1-10.

DAVISON, I. (2005) Central Atlantic margin basins of North West Africa: geology and hydrocarbon potential (Morocco to Guinea). *Journal of African Earth Sciences*, *43*, 1, p. 254-274.

DAY-STIRRAT, R.J., MCDONNEL, A. and WOOD, L.J. (2010) Diagenetic and seismic concerns associated with interpretation of deeply buried “mobile shales”. In: *Shale tectonics* (ed. By: WOOD, L.) AAPG Memoir 99, p. 5-27.

de VERA, J.*,* GRANADO, P. and McCLAY, K. (2010) Structural evolution of the Orange Basin gravity driven system, offshore Namibia*. Marine and Petroleum Geology,* 27, p. 223-237*.*

DEPTUCK, M.E., STEFFENS, G.S. BARTON, M. and PIRMEZ, C. (2003) Architecture and evolution of upper fan channel-belts on the Niger Delta slope and in the Arabian Sea. *Marine and Petroleum Geology*, 20, p. 649-676.

DEPTUCK, M. E., SYLVESTER, Z., PIRMEZ, C. and O'BYRNE, C. (2007) Migration-aggradation history and 3-D seismic geomorphology of submarine channels in the Pleistocene Benin-Major Canyon, western Niger Delta slope. *Marine and Petroleum Geology*, v. 24, p. 406-433.

DEVILLE, E., MASCLE, A., GUERLAIS, S.-H., DECALF, C., and COLLETTA, B. (2003) Lateral changes of frontal accretion and mud volcanism processes in the Barbados accretionary prism and some implications. In: *The Circum-Gulf of Mexico and the Caribbean: Hydrocarbon habitats, basin formation, and plate tectonics* (ed. By: BARTOLINI, C., BUFFLER, R.T. and BLICKWEDE, J.) AAPG Memoir 79, p. 656-674.

DEVILLE, É., GUERLAIS, S.H., LALLEMANT, S., and SCHEINER, F. (2010) Fluid dynamics and subsurface sediment mobilization processes: an overview from southeast Caribbean. *Basin Research,* 22, p. 361-379.

DICKINSON, G. (1953) Geological aspects of abnormal reservoir pressures in Gulf Coast Louisiana. *AAPG Bulletin,* 37, p. 410-432.

DOUST, H. (1990) Petroleum geology of the Niger Delta. In: *Classic petroleum provinces* (Ed. By: BROOKS, J.), Geological Society (London) Special Publication 50, p. 365.

DOUST, H., and OMATSOLA, E. (1990) Niger Delta. In: *Divergent/Passive Margin Basins* (Ed. by: EDWARDS J.D. and SANTOGROSSI, P.A.), AAPG Memoir, 48, p. 201-238.

DUERTO, L., and MCCLAY, K. (2002) 3D geometry and evolution of shale diapirs in the Eastern Venezuelan Basin. *American Association of Petroleum Geologists, Search and Discovery Articles*, *10026*.

DUGAN, B., and FLEMINGS, P.B. (2000) Overpressure and fluid flow in the New Jersey continental slope: implications for slope failure and cold seeps. *Science*, 289, p.288-291.

ESCALONA, A., and MANN, P. (2006) Tectonic controls of the right-lateral Burro Negro tear fault on Paleogene structure and stratigraphy, northeastern Maracaibo Basin. *AAPG bulletin*, *90*, 4, p. 479-504.

EVAMY, B. D., HAREMBOURE, J., KAMERLING, P., KNAAP, W. A., MOLLOY, F. A., and ROWLANDS, P. H. (1978) Hydrocarbon habitat of Tertiary Niger delta. *AAPG bulletin*, *62*, 1, p. 1-39.

FARRELL, S.G. (1984) A dislocation model applied to slump structures, Ainsa Basin, South Central Pyrenees, *Journal of Structural Geology*, 6, 6, p. 727-736.

FESEKER, T., BROWN, K.R., BLANCHET, C., SCHOLZ, F., NUZZO, M., REITZ, A., SCHMIDT, M., and HENSEN, C. (2010) Active mud volcanoes on the upper slope of the western Nile deep-sea fan — first results from the P362/2 cruise of R/V Poseidon. *Geo-Marine Letters,* 30, p. 169-186.

FILDANI, A., HUBBARD, S. M., COVAULT, J. A., MAIER, K. L., ROMANS, B. W., TRAER, M., and ROWLAND, J. C. (2012) Erosion at inception of deep-sea channels. *Marine and Petroleum Geology*, 41, p. 48-61.

FILDANI, A., NORMARK, W.R., KOSTIC, S. and PARKER, G. (2006) Channel formation by flow stripping: large-scale scour features along the Monterey East channel and their relation to sediment waves. *Sedimentology*, 53, p. 1265-1287.

FINKBEINER, T., ZOBACK, M., FLEMINGS, P., and STUMP, B. (2001) Stress, pore pressure, and dynamically constrained hydrocarbon columns in the South Eugene Island 330 field, northern Gulf of Mexico. *AAPG Bulletin*, 86, 6, p. 1007-1031.

FONNESU, F. (2003) 3D seismic images of a low-sinuosity slope channel and related depositional lobe (west Africa deep-offshore). *Marine and Petroleum Geology*, 20, p.615-629.

FÖRSTER, A., ELLIS, R., HENRICH, R., KRASTEL, S. and KOPF, A. (2010) Geotechnical characterization and strain analyses of sediment in the Mauritania slide complex, NW-Africa. *Marine and Petroleum Geology*, 27, p. 1175-1189.

FRENCH, W. S. (1975). Computer migration of oblique seismic reflection profiles. *Geophysics*, *40*, 6, p. 961-980.

FREY MARTINEZ, J. F., J. CARTWRIGHT, and HALL, B. (2005) 3-D seismic interpretation of slump complexes: Examples from the continental margin of Israel. *Basin Research*, v. 17, p. 83–108.

GALLOWAY, W.E. (1989) Genetic stratigraphic sequences in basin analysis I: architecture and genesis of flooding-surface bounded depositional units. *AAPG Bulletin*, 73, 2, p. 125-142.

GAULLIER, V., and VENDEVILLE, B.C. (2005) Salt tectonics driven by sediment progradation: Part II. Radial spreading of sedimentary lobes prograding above salt. *AAPG Bulletin*, v. 89, p. 1081-1089.

GAULLIER, V., Y. MART, G. BELLAICHE, B. C. VENDEVILLE, T. ZITTER, and Second Leg Prismed II Scientific Party (2000) Salt tectonics in an around the Nile deep-sea fan: Insights from the PRISMED II cruise: Geological Society (London) Special Publication 174, p. 111-129.

GEE, M.J.R., GAWTHORPE, R.L., BAKKE, K. and FRIEDMANN, S.J. (2007) Seismic geomorphology and evolution of submarine channels from the Angolan continental margin. *Journal of Sedimentary Research*, 77, p. 433-446.

GEE, M. J. R., GAWTHORPE, R. L., and FRIEDMANN, S. J. (2006) Triggering and evolution of a giant submarine landslide, offshore Angola, revealed by 3D seismic stratigraphy and geomorphology. *Journal of Sedimentary Research*, *76*, 1, p. 9-19.

GONZALES-MIERES, R. and SUPPE, J. (2006) Relief and shortening in detachment folds. *Journal of Structural Geology*, 28, 10, p. 1785-1807.

GRANDO, G. and MCCLAY, K. (2010) Morphotectonics domain and structural styles in the Makran accretionary prism, offshore Iran. *Sedimentary Geology*, 196, p. 157-179.

GRAUE, K. (2000) Mud volcanoes in deepwater Nigeria. *Marine and Petroleum Geology,* 17, p.959-974.

GRAULS, D. (1999) Overpressures: causal mechanisms, conventional and hydromechanical approaches. *Oil & Gas Science and Technology – Rev. IFP,* 54, p. 667-678.

GRAULS, D.J., BALEIX, J.M. (1994) Role of overpressures and in situ stresses in fault-controlled hydrocarbon migration: a case study. *Marine and Petroleum Geology*, 11, p. 734-742.

GRUNAU, H.R. (1987) A worldwide look at the cap-rock problem. *Journal of Petroleum Geology*, 10, p. 245-265.

HAFLIDASON, H., SEJRUP, H.P., NYGÅRD, A., MIENERT, J., BRYN, P., LIEN, R., FORSBERG, C.F., BERG, K. and MASSON, D. (2004) The Storegga slide: architecture, geometry and slide development. *Marine Geology*, 213, p. 201-234.

HARDING, T. P. (1974) Petroleum traps associated with wrench faults. *AAPG Bulletin*, v. 58, p. p. 1290-1304.

HARDING, T. P. (1985) Seismic characteristics and identification of negative flower structures, positive flower structures, and positive structural inversion. *AAPG Bulletin*, v. 69, p. 582-600.

HARLAND, W. B. (1971) Tectonic transpression in Caledonian Spitsbergen. *Geological Magazine*, *108,* 1, p. 27-41.

HAUGHTON, P.D.W. (2000) Evolving turbidite systems on a deforming basin floor, Tabernas, SE Spain. *Sedimentology*, 47, p. 497-518.

HEGGLAND, R., HOVLAND, M., GRAUE, K., and GALLAGHER, J.W. (2001) Mud volcanoes and gas hydrates on the Niger Delta Front. Conference Abstract Book: *Subsurface Sediment Mobilization*. University Of Gent, Belgium, Sept, 44 p.

HEGGLAND, R. (2005) Using gas chimneys in seal integrity analysis: a discussion based on case histories. In: *Evaluating Fault and Cap Rock Seals* (Ed. By: BOULT P. and KALDI, J.), AAPG Hedberg Series, 2, p. 237-245.

HEINIÖ, P. (2007) *3D Seismic Analysis of Sedimentary Processes on Deepwater Continental Margins*. PhD Thesis, Cardiff University.

HEINIÖ, P. and DAVIES, R.J. (2006) Degradation of compressional fold belts: Deep-water Niger Delta. *AAPG Bulletin*, v. 90, p. 753-770.

HEINIÖ, P. and DAVIES, R.J. (2007) Knickpoint migration in submarine channels in response to fold

growth, western Niger Delta. *Marine and Petroleum Geology*, 24, p. 434-449.

HEINIÖ, P. and DAVIES, R.J. (2009) Trails of depressions and sediment waves along submarine channels on the continental margin of Espirito Santo Basin, Brazil. *Geological Society of America Bulletin*, 121, p. 698-711.

HENRICH, R., CHERUBINI, Y. and MEGGERS, H. (2010) Climate and sea level induced turbidite activity in a canyon system offshore the hyperarid western Sahara (Mauritania): the Timiris canyon. *Marine Geology*, 275, p. 178-198.

HEPPARD, P., CANDER, H.S., and EGGERTSON, E.B. (1998) Abnormal pressure and the occurrence of hydrocarbons in offshore Eastern Trinidad, West Indies. In: *Abnormal Pressures in Hydrocarbon Environments* (Ed. By: LAW, B. E., ULMISHEK, G.F. and SLAVIN, V.I.), AAPG Memoir, Tulsa, OK, 70, p. 215-246.

HOLZ, C., STUUT, J.B.W., HENRICH, R. and MEGGERS, H. (2007) Variability in terrigenous sedimentation processes off northwest Africa and its relation to climate changes: inferences from grain-size distributions of a Holocene marine sediment record. *Sedimentary Geology*, 202, p. 499-508.

HOOPER, R.J., FITZSIMMONS, R.J., GRANT, N. and VENDEVILLE, B.C. (2002) The role of deformation in controlling depositional patterns in the south-central Niger Delta, West Africa, *Journal of Structural Geology*, 24, 4, p. 847-859.

HOVLAND, M. and JUDD, A.G. (1988) Seabed pockmarks and seepages: impact on geology, biology and the marine environment. Graham and Trotman, London.

HUBBERT, M.K. and WILLIS, D.G. (1972) *Mechanics of hydraulic fracturing*. AAPG Memoir, 18, p. 239-257.

HUSTOFT, S., DUGAN, B. and MIENERT, J., Effects of rapid sedimentation on developing the Nyegga pockmark field: Constraints from hydrological modeling and 3-D seismic data, offshore mid-Norway. *Geochemistry, Geophysics, Geosystems,* 10, 6, 17 p.

HUUSE, M., JACKSON, C.A.L., VAN RENSBERGEN, P., DAVIES, R.J., FLEMINGS, P.B. and DIXON, R.J. (2010) Subsurface sediment remobilization and fluid flow in sedimentary basins: an overview. *Basin Research*, 22, 342-360.

IMBER, J., CHILDS, C., NELL, P.A.R., WALSH, J., HODGETTS, D. and FLINT, S. (2003) Hanging wall fault kinematics and footwall collapse in listric growth fault systems. *Journal of Structural Geology*, 25, 2, p. 197-208.

INGRAM, G.M. and URAI, J.L. (1999) Top-seal leakage through faults and fractures: the role of mudrock properties. In: *Muds and Mudstones: Physical and Fluid-Flow Properties* (Ed. By: APLIN. A.C., FLEET, A.J. and MACQUAKER, J.H.S.), Geological Society, Special Publications, London, 158, p. 125-135.

HAGEN, E. (2001) Northwest African upwelling scenario. *Oceanologica Acta*, *24*, p. 113-128.

HIGGINS, S., CLARKE, B., DAVIES, R. J., and CARTWRIGHT, J. (2009) Internal geometry and growth history of a thrust-related anticline in a deep water fold belt. *Journal of Structural Geology*, *31*, 12, p. 1597-1611.

HIGGINS, S., DAVIES, R. J., and CLARKE, B. (2007) Antithetic fault linkages in a deep water fold and thrust belt. *Journal of Structural Geology*, *29*, 12, p. 1900-1914.

HINDLE, D., and VIETOR, T. (2006) 3D numerical modelling of tear faults. In *Geophysical Research Abstracts* (Vol. 8, p. 06761).

HOMZA, T. X., and WALLACE, W. K. (1997) Detachment folds with fixed hinges and variable detachment depth, northeastern Brooks Range, Alaska. *Journal of Structural Geology*, *19*, 3, p. 337-354.

HUBBARD, S. M., ROMANS, B. W., and GRAHAM, S. A. (2007) An outcrop example of large-scale conglomeratic intrusions sourced from deep-water channel deposits, Cerro Toro Formation, Magallanes basin, southern Chile, AAPG Memoir, 87.

IACOPINI, D., and BUTLER, R. W. (2011) Imaging deformation in submarine thrust belts using seismic attributes. *Earth and Planetary Science Letters*, *302,* 3, p. 414-422.

INGRAM, G.M. and URAI, J.L. (1999) Top-seal leakage through faults and fractures: the role of mudrock properties. *Geological Society, London, Special Publications*, vol. 158, no 1, p. 125-135.

INGS, S. J., and BEAUMONT, C. (2010) Continental margin shale tectonics: preliminary results from coupled fluid-mechanical models of large-scale delta instability. *Journal of the Geological Society*, *167*, 3, p. 571-582.

JACKSON, M. P. A., and VENDEVILLE, B. C. (1994) Regional extension as a geologic trigger for diapirism. *Geological Society of America Bulletin*, *106*, 1, p. 57-73.

JAMES, D. M., AND JAMES, J. (1969) The influence of deep fractures on some areas of Ashgillian-Llandoverian sedimentation in Wales. *Geol. Mag*, *106*, 6, p. 562-582.

JANIK, A.G., HOOD, J.A., ASK, M.V. (1998) Physical properties data at hole 959d: comparison of core and log measurements and a proposed revision of lithologic units. In: *Proceedings of the Ocean Drilling Program, Scientific Results* (Ed. By: MASCLE, J., LOHMANN, G.P., MOULLADE, M*., et al.*), Ocean Drilling Program, College Station, Texas, 159, p. 241-248.

JANSEN, E., BEFRING, S., BUGGE, T., EIDVIN, T., HOLTEDAHL, H. and SEJRUP, H.P. (1987) Large submarine slides on the Norwegian continental margin: sediments, transport and timing. *Marine Geology*, 78, p. 77-107.

JEGOU, I., SAVOYE, B., PIRMEZ, C., and DROZ, L. (2008) Channel-mouth lobe complex of the recent Amazon Fan: The missing piece. *Marine Geology*, *252,* 1, p. 62-77.

JERMANNAUD, P., ROUBY, D., ROBIN, C., NALPAS, T., GUILLOCHEAU, F. and RAILLARD, S. (2010) Plio-Pleistocene sequence stratigraphic architecture of the eastern Niger Delta: A record of eustasy and aridification of Africa. *Marine and Petroleum Geology*, 27, 4, p. 810-821.

JEROLMACK, D.J. and PAOLA, C. (2007) Complexity in a cellular model of river avulsion, *Geomorphology*, 91, 3-4, p. 259-270.

JOLLY, R.J.H. and LONERGAN, L. (2002) Mechanisms and controls on the formation of sand intrusions. *Journal of the Geological Society*, 159, p. 605-617.

KANE, I. A., MCCAFFREY, W. D., and PEAKALL, J. (2008) Controls on sinuosity evolution within submarine channels. *Geology*, *36*, 4, p. 287-290.

KEAREY, P., BROOKES, M., and HILL, I. (2002) An introduction to geophysical exploration, Third Edition, Blackwell Science, Oxford.

KING, R. C., HILLIS, R. R., TINGAY, M. R., and MORLEY, C. K. (2009) Present-day stress and neotectonic provinces of the Baram Delta and deep-water fold–thrust belt. *Journal of the Geological Society*, *166,* 2, p. 197-200.

KNELLER, B. (1995) Topographic controls on turbidite sandstones reservoirs: Facies models with a physical basis. *AAPG Bulletin*, *79*(CONF-950995--).

KOLLA, V., POSAMENTIER, H. W., and WOOD, L. J. (2007) Deep-water and fluvial sinuous channels—Characteristics, similarities and dissimilarities, and modes of formation. *Marine and Petroleum Geology*, *24*, 6, p. 388-405.

KOLEDOYE, B. A., AYDIN, A., and MAY, E. (2003) A new process-based methodology for analysis of shale smear along normal faults in the Niger Delta. *AAPG bulletin*, *87*, 3, p. 445-463.

KOPF, A.J. (2002) Significance of Mud Volcanism. *Review of Geophysics*, 40, 2.

KRASTEL, S., HANEBUTH, T. J. J., ANTOBREH, A. A., HENRICH, R.; HOLZ, C.; KÖLLING, M., SCHULZ, H. D., WIEN, K., MORRIS, S.A., KENYON, N.H.,LIMONOV, A.H. and WYNN, R. B (1998) Cap Timiris canyon: a newly discovered channel system offshore of Mauritania. *EOS Transactions, AGU*, 85, 42, p. 417–423.

LACOSTE, A., VENDEVILLE, B. C., and LONCKE, L. (2011) Influence of combined incision and fluid overpressure on slope stability: Experimental modelling and natural applications. *Journal of Structural Geology*, *33*, 4, p. 731-742.

LANE, A. (2005) Overcoming deepwater geohazards in west Africa. *Offshore Technology Conference*, Houston, TX, U.S.A.

LANSLEY, M. (2004) AAPG Memoir 42 and SEG Investigations in Geophysics, No. 9, Appendix A: Considerations for Optimum 3-D Survey Design, Acquisition and Processing.

LAWRENCE, S. R., MUNDAY, S. and BRAY, R. (2002) Regional geology and geophysics of the eastern Gulf of Guinea (Niger Delta to Rio Muni). *The leading edge*, v. 21, p. 1112-1117.

LECOMTE, E., and VENDEVILLE, B. (2008) Analogue modelling and numerical simulations of gravitational spreading along passive margin under fluid overpressure. In *International Geological Modelling Conference. Florence, Italy. Abstract. CD-ROM.*

LEDUC, A. M., DAVIES, R.J., IMBER, J. and DENSMORE, A.L. (2012) The lateral strike-slip domain in gravitational detachment delta systems: a case study of the northwest margin of the Niger Delta. *AAPG Bulletin,* 96, 4, p. 709-728.

LEDUC, A. M., DAVIES, R. J., SWARBRICK, R. E., and IMBER, J. (2012) Fluid flow pipes triggered by lateral pressure transfer in the deepwater western Niger Delta. *Marine and Petroleum Geology*, 43, p. 423-433.

LONCKE, L., GAULLIER, V., MASCLE, J., VENDEVILLE, B. and CAMERA, L. (2006) The Nile deep-sea fan: An example of interacting sedimentation, salt tectonics, and inherited subsalt paleotopographic features. *Marine and Petroleum Geology*, v. 23, p. 297-315.

LONCKE, L., MASCLE, J. and FANIL Scientific Parties (2004) Mud volcanoes, gas chimneys, pockmarks and mounds in the Nile deep-sea fan (Eastern Mediterranean): geophysical evidences. *Marine and Petroleum Geology*, 21, p. 669-689.

LØSETH, H., L.WENSAAS, B. ARNTSEN, N.-M. HANKEN, C. BASIRE and K. GRAUE (2010) 1000-m-long gas blowout pipes. *Marine and Petroleum Geology*, v. 28, no. 5, p. 1047-1060.

MAGBAGBEOLA, O. A., and WILLIS, B. J. (2007) Sequence stratigraphy and syndepositional deformation of the Agbada Formation, Robertkiri field, Niger Delta, Nigeria. *AAPG bulletin*, *91*, 7, p. 945-958.

MALONEY, D., DAVIES, R., IMBER, J., HIGGINS, S. and KING, S. (2010) New insights into deformation mechanisms in the gravitationally driven Niger Delta deep-water fold and thrust belt. *AAPG Bulletin*, v. 94, p. 1401-1424.

MALONEY, D., DAVIES, R., IMBER, J. and KING, S. (2011) Structure of the footwall of a listric fault system revealed by 3D seismic data from the Niger Delta. *Basin Research*, 24, 1, p. 107-123.

MALTMAN, A. (1994) *The Geological Deformation of Sediments*. Chapman and Hall, London, 362 p.

MALTMAN, A.J. and BOLTON, A. (2003) How sediments become mobilized. *Geological Society (London), Special Publications*, 216, p. 9-20.

MANN, D.M., MACKENZIE, A.S. (1990) Prediction of pore fluid pressures in sedimentary basins. *Marine and Petroleum Geology*, 7, p. 55–65.

MANSPEIZER, W. (1985) The Dead Sea rift: impact of climate and tectonism on Pleistocene and Holocene sedimentation. In: *Strike-Slip Deformation, Basin Formation and Sedimentation* (Ed. by BIDDLE, K.T. and CHRISTIE-BLICK, N.), *SEPM Special Publication*, Tulsa, OK, 37, p. 143-158.

MARTINSEN, O. (1989) Styles of soft-sediment deformation on a Namurian (Carboniferous) delta slope, Western Irish Namurian Basin, Ireland. *Geological Society (London) Special Publications*, 41, p. 167-177.

MARTINSEN, O. J., and B. BAKKEN (1990) Extensional and compressional zones in slumps and slides in the Namurian of County Clare, Ireland. *Journal of the Geological Society* (London), v. 147, p. 153-164.

MAUS, S., BARCKHAUSEN, U., BERKENBOSCH, H., BOURNAS, N., BROZENA, J., CHILDERS, V. et al. (2009) EMAG2: A 2–arc min resolution Earth Magnetic Anomaly Grid compiled from satellite, airborne, and marine magnetic measurements. *Geochemistry, Geophysics, Geosystems*, *10*(8).

MAYALL, M., LONERGAN, L., BOWMAN, A., JAMES, S., MILLS, K., PRIMMER, T., POPE, D., ROGERS L. and SKEENE, R. (2010) The response of turbidite slope channels to growth-induced seabed topography. *AAPG Bulletin*, 94, p. 1011-1030.

MIGEON, S., MULDER, T., SAVOYE, B., and SAGE, F. (2006) The Var turbidite system (Ligurian Sea, northwestern Mediterranean)—morphology, sediment supply, construction of turbidite levee and sediment waves: implications for hydrocarbon reservoirs. *Geo-Marine Letters*, *26,* 6, p. 361-371.

MILLER, T.W. (1995) New insights on natural hydraulic fractures induced by abnormally high pore pressures. *AAPG Bulletin*. 79, p. 1005-1018.

MONTGOMERY, D.R., SOM, S.M., JACKSON, M.P.A., CHARLOTTE SCHREIBER, B., GILLESPIE, A.R. and ADAMS, J.B. (2009) Continental-scale tectonics on Mars and the origin of Valles Marineris and associated outflow channels. *GSA Bulletin*, 121, 1-2, p. 117-133.

MORGAN, R. (2003) Prospectivity in ultradeep water: The case for petroleum generation and migration within the outer parts of the Niger Delta apron. In: *Petroleum geology of Africa: New themes and developing technologies* (Ed. By: ARTHUR, T.J., MACGREGOR, D.S., and CAMERON, N.R.) Geological Society (London) Special Publication 207, p. 151-164.

MORGAN, R. (2004) Structural controls on the positioning of submarine channels on the lower slopes of the Niger Delta. In: *3-D seismic technology: Application to the exploration of sedimentary basins* (ed. By: DAVIES, R.J., CARTWRIGHT, J.A., STEWART, S.A., LAPPIN, M. and UNDERHILL, J.R.) Geological Society (London) Memoirs 29, p. 45-51.

MORLEY, C. K. (2003) Mobile shale-related deformation in large deltas developed on passive and active margins. In: *Subsurface sediment mobilization* (ed. By: VAN RENSBERGEN, P., HILLIS, R.R., MALTMAN, A.J. and MORLEY, C.K.) Geological Society (London) Special Publication 216, p. 335-357.

MORLEY, C. K. (2003) Outcrop examples of mudstone intrusions from the Jerudong anticline, Brunei Darussalam and inferences for hydrocarbon reservoirs. In: *Subsurface sediment mobilization* (ed. By: VAN RENSBERGEN, P., HILLIS, R.R., MALTMAN, A.J. and MORLEY, C.K.) Geological Society (London) Special Publication 216, p. 381-384.

MORLEY, C. K. (2009) Growth of folds in a deep-water setting. *Geosphere*, 5, 2, p. 59-89.

MORLEY, C. K., and GUERIN, G. (1996) Comparison of gravity driven deformation styles and behavior associated with mobile shale and salt. *Tectonics*, v. 15, p. 1154-1170.

MORLEY, C.K., KING, R., HILLIS, R., TINGAY, M. and BACKE, G. (2011) Deepwater fold and thrust belt classification, tectonics, structure and hydrocarbon prospectivity: A review. *Earth-Science Reviews*, 104, p. 41-91.

MORRIS, S.A., KENYON, N.H.,LIMONOV, A.H. and ALEXANDER, J. (1998) Downstream changes of large-scale bedforms in turbidites around the Valencia channel mouth, north-west Mediterranean: implications for palaeoflow reconstruction. *Sedimentology*, 45, p. 365–377.

MOSS, J.L. and CARTWRIGHT, J. (2010) 3d seismic expression of km-scale fluid escape pipes from offshore Namibia. *Basin Research*, 22, p. 481-501.

MOURGUES, R. and COBBOLD, P.R. (2003) Some tectonic consequences of fluid overpressures and seepage forces as demonstrated by sandbox modelling. *Tectonophysics*, 376, p.75-97.

MOURGUES, R., and COBBOLD, P. R. (2006) Thrust wedges and fluid overpressures: Sandbox models involving pore fluids. *Journal of Geophysical Research: Solid Earth (1978–2012)*, *111*(B5).

MOURGUES, R., GRESSIER, J.B., BODET, L., BUREAU and D., GAY, A. (2011) "Basin scale" versus "localized" pore pressure/stress coupling - implications for trap integrity evaluation. *Marine and Petroleum Geology*, 28, 5, p. 1111-1121.

MUTTI, E. (1975). *Examples of turbidite facies and facies associations from selected formations of the Northern Apennines*.

MUTTI, E., BERNOULLI, D., LUCCHI, F.R. and TINTERRI, R. (2009) Turbidites and turbidity currents from Alpine `flysch' to the exploration of continental margins. *Sedimentology, AGU*, 56, 1, p. 267–318.

NORDGARD BOLAS, H.M. and HERMANRUD, C. (2003) Hydrocarbon leakage processes and trap retention capacities offshore Norway. *Petroleum Geoscience*, 9, p. 321-332.

NORMARK, W.R. (1978) Fan Valleys, Channels, and Depositional Lobes on Modern Submarine Fans: Characters for Recognition of Sandy Turbidite Environments. *AAPG Bulletin*, 62, 6, p. 912-931.

NASHAAT, M. (1998) Abnormally high fluid pressure and seals Impacts on hydrocarbon accumulations in the Nile Delta and North Sinai Basins, Egypt. In: *Abnormal Pressures in Hydrocarbon Environments* (Ed. By: LAW, B. E., ULMISHEK, G.F. and SLAVIN, V.I.), AAPG Memoir, Tulsa, OK 70, p. 161-180.

NELY, G., COUMES, F. and CREMER, M. (1985) La réussite exemplaire d'une exploration en mer par des méthodes complémentaires: l'éventail du Cap-Ferret (Golfe de Gascogne, France), *Bulletin Centre Recherche Exploration Production Elf-Aquitaine*, Pau, 9, p. 253-334.

NILSEN, T. H., and SYLVESTER, A. G. (1995) Strike-slip basins. *Tectonics of sedimentary basins. Blackwell Science*, p. 425-457.

OSBORNE, M.J. and SWARBRICK, R.E. (1997) Mechanisms for generating overpressure in sedimentary basins: a reevaluation. *AAPG Bulletin*, 81, p. 1023-1041.

OLABODE, S.O. and ADEKOYA, J.A. (2008) Seismic stratigraphy and development of Avon canyon in Benin (Dahomey) Basin, southwestern Nigeria. *Journal of African Earth Science*, 50, p. 286-304.

OWOYEMI, A. O., and WILLIS, B. J. (2006) Depositional patterns across syndepositional normal faults, Niger Delta, Nigeria. *Journal of Sedimentary Research*, *76*, 2, p. 346-363.

PEDERSEN, S.A. (1987) Comparative studies of gravity tectonics in Quaternary sediments and sedimentary rocks related to fold belts. *Geological Society (London), Special Publications*, 29, p. 165-179.

PEEL, F. J., TRAVIS, C.J. and HOSSACK, J.R. (1995) Genetic structural provinces and salt tectonics of the Cenozoic offshore U.S. Gulf of Mexico: A preliminary analysis. In: *Salt tectonics: A global perspective* (ed. By: JACKSON, M.P.A., ROBERTS, D.G. and SNELSON, S.) AAPG Memoir 65, p. 153-175.

PETTERS, S.W. (1984) An ancient submarine canyon in the Oligocene—Miocene of the Western Niger Delta . *Sedimentology*, 31, 6, p. 805-810.

PIPER, D.J.W. and NORMARK, W.R. (1983) Turbidite depositional patterns and flow characteristics, Navy submarine fan, California Borderland. *Sedimentology*, 30, p. 681-694.

PIPER, D.J.W. and NORMARK, W.R. (2001) Sandy fans—from Amazon to Hueneme and beyond. *AAPG Bulletin*, 85, p. 1407-1438.

POCHAT, S., CASTELLTORT, S., CHOBLET and VAN DEN DRIESSCHE, J. (2009) High-resolution record of tectonic and sedimentary processes in growth strata*. Marine and Petroleum Geology*, 26, p. 1350-1364.

POCHAT, S., CASTELLTORT, S., VAN DEN DRIESSCHE, J., BESNARD, K., and GUMIAUX, C. (2004) A simple method of determining sand/shale ratios from seismic analysis of growth faults: An example from upper Oligocene to lower Miocene Niger Delta deposits. *AAPG bulletin*, *88*, 10, p. 1357-1367.

POSAMENTIER, H. W. (2004) Seismic geomorphology: imaging elements of depositional systems from shelf to deep basin using 3D seismic data: implications for exploration and development. *Geological Society, London, Memoirs*, *29*, 1, p. 11-24.

POSAMENTIER, H.W. and KOLLA, V. (2003) Seismic geomorphology and stratigraphy of depositional elements in deep-water settings. *Journal of Sedimentary Research*, 73, p.367-388.

PRELAT, A., COVAULT, J. A., HODGSON, D. M., FILDANI, A., and FLINT, S. S. (2010) Intrinsic controls on the range of volumes, morphologies, and dimensions of submarine lobes. *Sedimentary Geology*, *232*, 1, p. 66-76.

READING, H. and RICHARDS, M. (1994) Turbidite systems in deep-water basin margins classified by grain size and feeder system. *AAPG bulletin*, *78,*5, p.792-822.

REILLY, M.J. and FLEMINGS, P.B. (2010) Deep pore pressures and seafloor venting in the Auger Basin, Gulf of Mexico. *Basin Research*, 22, p. 380-397.

ROBINSON, A.M., CARTWRIGHT, J.A., BURGESS, P.M. and DAVIES, R.J. (2004) Interaction between topography and channel development from 3D seismic analysis: an example from the Tertiary of the Flett Ridge, Faroe-Shetland Basin, UK. In: *3D Seismic Technology: Application to the Exploration of Sedimentary Basins,* (Ed. by: R. J. DAVIES, J.A. CARTWRIGHT, S.A. STEWART, M. LAPPIN & J.R. UNDERHILL), *Geological Society Memoirs*, London, 29, p. 45-51.

RODGERS, S., BJØRKUM, P., WALDERHAUG, O. and NADEAU, P. (1999) Discussion: physical constraints on hydrocarbon leakage and trapping revisited' by P.A. BJØRKUM *et al*. – Further aspects. *Petroleum Geoscience*, 5, 421-423.

ROUBY, D., and COBBOLD, P. (1996) Kinematic analysis of a growth fault system in the Niger Delta from restoration in map view. *Marine and Petroleum Geology*, 13, 5, p. 565-580.

ROUBY, D., NALPAS, T., JERMANNAUD, P., ROBIN, C., GUILLOCHEAU, F. and RAILLARD, S. (2011) Gravity driven deformation controlled by the migration of the delta front: The Plio-Pleistocene of the Eastern Niger Delta. *Tectonophysics*, 513, p. 54-67.

ROWAN, M. G. (2009) Lateral boundaries in deep-water, salt detached fold and thrust belts: AAPG Hedberg Conference on deep-water fold and thrust belts: Tirrenia, Italy, October 4–9, 2009, http://www.searchanddiscovery .com/abstracts/pdf/2011/2009hedberg-italy/index.htm (accessed October 2011).

ROWAN, M. G., PEEL, F.J. and VENDEVILLE, B.C. (2004) Gravity-driven fold belts on passive margins, in K. R. McClay, ed., Thrust tectonics and hydrocarbon systems: AAPG Memoir 82, p. 157-182.

SANDWELL, D. T., and SMITH, W. H. (1997) Marine gravity anomaly from Geosat and ERS 1 satellite altimetry. *Journal of Geophysical research*, *102*(B5), 10039-10.

SAVOYE, B., COCHONAT, P., APPRIOUAL, R., BAIN, O., BALTZER, A., BELLEC, V., BEUZART, P., BOURILLET, J.F., CAGNA, R., CREMER, M., CRUSSON, A., DENNIELOU, B., DIEBLER, D., DROZ, L., ENNES, J.C., FLOCH, G., GUIOMAR, M., HARMEGNIES, F., KERBRAT, R., KLEIN, B., KUHN, H., LANDURE, J.Y., LASNIER, C., LE DREZZEN, E., LE FORMAL, J.P., LOPEZ, M., LOUBRIEU, B., MARSSET, T., MIGEON, S., NORMAND, A., NOUZE, H., ONDREAS, H., PELLEAU, P., SAGET, P., SERANNE, M., SIBUET, J.C., TOFANI, R., VOISSET, M. (2000) Downstream changes of large-scale bedforms in turbidites around the Valencia channel mouth, north-west Mediterranean: implications for palaeoflow reconstruction. *Comptes rendus de l'Académie des sciences. Série 2. Sciences de la terre et des planètes*, 331, 3, p. 211–220.

SCHLAGER, W. (1993) Accommodation and supply—a dual control on stratigraphic sequences. *Sedimentary Geology*, *86*,1, p. 111-136.

SCHULTHEISS, P. and MIENERT, J. (1987) Whole core P-wave velocity and gamma ray attenuation logs from ODP Leg 108 (Sites 657-668). *Proc. DSDP, Ini. Rep,* 108, p. 1015-1017.

SCHULTZ-ELA, P.P. and WALSH, P. (2002) Modeling of grabens extending above evaporates in Canyonlands National Park, Utah. *Journal of Structural Geology*, 24, 2, p. 247-275.

SCHWAB, A. M., TREMBLAY, S., and HURST, A. (2007) Seismic expression of turbidity-current and bottom-current processes on the Northern Mauritanian continental slope. *Geological Society (London) Special Publication, 277,* p. 237.

SECOR, D.T. (1965) Role of fluid pressure in jointing. *American Journal of Science*, 263, 8, p. 633-646.

SEIBOLD, E., and FÜTTERER, D. (1982) Sediment dynamics on the Northwest African continental margin. *The Ocean Floor. John Wiley & Sons, Chichester*, p. 147-163.

SELLIER, N. C., VENDEVILLE, B. C., and LONCKE, L. (2011) Post-Messinian evolution of the Florence Rise area (Western Cyprus Arc) Part II: Experimental modeling. *Tectonophysics*, 591, p. 143-151.

SELDON, B. and FLEMINGS, P.B. (2005) Reservoir pressure and seafloor venting: predicting trap integrity in a Gulf of Mexico deepwater turbidite minibasin. *AAPG Bulletin*, 89, p. 193-209.

SHERIFF, R. E., (1980). *Seismic stratigraphy*. Boston, Mass.: International Human Resources Development Corporation.

SHORT, K. and STAUBLE, A. (1967) Outline of geology of Niger Delta. *AAPG Bulletin*, 51, p. 761-779.

SIMPSON, G. (2004) Role of river incision in enhancing deformation. *Geology*, 32, p. 341-344.

STEFFENS, G. S., SHIPP, R. C., PRATHER, B. E., NOTT, J. A., GIBSON, J. L., and WINKER, C. D. (2004) The use of near-seafloor 3D seismic data in deepwater exploration and production. *Geological Society, London, Memoirs*, *29*, 1, p. 35-43.

STEWART, S. (1999) Geometry of thin-skinned tectonic systems in relation to detachment layer thickness in sedimentary basins. *Tectonics*, v. 18, p. 719-732.

STEWART, S.A. (1999) Seismic interpretation of circular geological structures. *Petroleum Geoscience*, 5, p. 273-285.

STEWART, S. A. (2011) Vertical exaggeration of reflection seismic data in geoscience publications 2006–2010. *Marine and Petroleum Geology*, 2011, vol. 28, no 5, p. 959-965.

STEWART, S.A. and DAVIES, R.J. (2006) Structure and emplacement of mud volcano systems in the South Caspian Basin. *AAPG Bulletin*, 90, p. 771-786.

STOW, D. A. V. (1986) Deep clastic seas. *Sedimentary environments and facies*, *2*, p. 399-444.

STOW, D. A., and MAYALL, M. (2000) Deep-water sedimentary systems: New models for the 21st century. *Marine and Petroleum Geology*, *17*, 2, p. 125-135.

STRAUB, K. M., and MOHRIG, D. (2009) Constructional canyons built by sheet-like turbidity currents: observations from offshore Brunei Darussalam. *Journal of Sedimentary Research*, *79*, 1, p. 24-39.

SWARBRICK, R.E. and OSBORNE, M.J. (1998) Mechanisms that generate abnormal pressures: an overview. In: *Abnormal Pressures in Hydrocarbon Environments* (Ed. By: LAW, B. E., ULMISHEK, G.F. and SLAVIN, V.I.), AAPG Memoir, Tulsa, OK, 70, p. 13-34.

SWARBRICK, R.E., OSBORNE, M.J. and YARDLEY, G.S. (2002) Comparison of overpressure magnitude resulting from the main generating mechanisms. In: *Pressure Regimes in Sedimentary Basins and their Prediction*, AAPG Memoir, Tulsa, OK, 76, p. 1-12.

SYLVESTER, A. G., and SMITH, R. R. (1976) Tectonic transpression and basement-controlled deformation in San Andreas fault zone, Salton Trough, California. *AAPG Bulletin*, *60*, 12, p. 2081-2102.

TEGLAND, E. R. (1977) 3-D seismic techniques boost field development. *Oil and Gas Journal*, *75*, 37, p. 79-82.

TERZAGHI, K. (1943) *Theoretical Soil Mechanics*, Wiley and Sons, New York.

TINGAY, M.R.P., HILLIS, R.R., SWARBRICK, R.E., MORLEY, C.K. and DAMIT, A.R. (2009) Origin of overpressure and pore-pressure prediction in the Baram Province, Brunei. *AAPG Bulletin*, 93, p. 51-74.

TRAUGOTT, M.O. and HEPPARD, P. D. (1994) Prediction of pore pressure before and after drilling - taking the risk out of drilling overpressured prospects In: *Abnormal Pressures in Hydrocarbon Environments* (Ed. By: LAW, B. E., ULMISHEK, G.F. and SLAVIN, V.I.), AAPG Hedberg Research Conference, Abnormal Pressures in Hydrocarbon Environments: Golden Colorado, June 8-10 (extended abstract).

TRAUGOTT, M.O. and HEPPARD, P.D. (1997) Pore/fracture pressure determination in deep water. Deep water supplement to World Oil.

TREVIÑO, R. H. and B. C. VENDEVILLE (2008) Origin of coast-perpendicular extensional faults, western Gulf of Mexico: The relationship between an early-stage ridge and a late stage fault: *AAPG Bulletin*, v. 97, p. 951-964.

VAIL, P. R., MITCHUM JR, R. M., and THOMPSON III, S. (1977) *Seismic Stratigraphy and Global Changes of Sea Level: Part 4. Global Cycles of Relative Changes of Sea Level.: Section 2. Application of Seismic Reflection Configuration to Stratigraphic Interpretation.*

VAN RENSBERGEN, P. and MORLEY, C.K. (2003) Re-evaluation of mobile shale occurrences on seismic sections of the Champion and Baram Deltas, Offshore Brunei. In: *Subsurface Sediment Mobilization* (ed. By: VAN RENSBERGEN, P., HILLIS, R.R., MALTMAN, A.J. and MORLEY, C.K.) Geological Society, London, Special Publication 216, p. 395-409.

VAN WAGONER, J. C., MITCHUM JR, R. M., POSAMENTIER, H. W., and VAIL, P. R. (1987). Seismic Stratigraphy Interpretation Using Sequence Stratigraphy: Part 2: Key Definitions of Sequence Stratigraphy, p. 11-14.

VEAR, A. (2005) Deep-water plays of the Mauritanian continental margin. In: *Petroleum Geology: North-West Europe and Global Perspectives – Proceedings of the 6th Petroleum Geology Conference* (Ed. by: A.G. DORÉ and B.A. VINING), *Petroleum Geology Conference series*, 6, Geological Society of London.

WEAVER, P. P. E., and CANALS, M. (2003) The Iberian and Canaries Margin including NW Africa. In *European Margin Sediment Dynamics*, Springer Berlin Heidelberg, p. 251-260.

WOODCOCK, N. H., and DALY, M. C. (1986) The Role of Strike-Slip Fault Systems at Plate Boundaries [and Discussion]. *Philosophical Transactions of the Royal Society of London. Series A, Mathematical and Physical Sciences*, *317*, 1539, p. 13-29.

WOODCOCK, N. H., and FISCHER, M. (1986) Strike-slip duplexes. *Journal of Structural Geology*, v. 8, p. 725-735.

WOODCOCK, N. H. and C. SCHUBERT (1994) Continental strike-slip tectonics. In: *Continental deformation* (ed. By: P. L. HANCOCK) Oxford, Pergamon Press, p. 251–263.

WU, J. E., MCCLAY, K., WHITEHOUSE, P., and DOOLEY, T. (2009) 4D analogue modelling of transtensional pull-apart basins. *Marine and Petroleum Geology*, *26*, 8, p. 1608-1623.

WYNN, R.B., CRONIN, B.T. and PEAKALL, J. (2007) Sinuous deep-water channels: genesis, geometry and architecture. *Marine and Petroleum Geology*, 24, p. 341-387.

WYNN, R. B., MASSON, D. G., STOW, D. A., and WEAVER, P. P. (2000) Turbidity current sediment waves on the submarine slopes of the western Canary Islands. *Marine Geology*, *163*, 1, p. 185-198.

WYNN, R.B. and STOW, D.A.V. (2002) Classification and characterisation of deep-water sediment waves. *Marine and Petroleum Geology*, 192, p. 7-22.

YANG, J. and DAVIES, R.J. (2013) Gravity-driven faults: migration pathways for recycling gas after the dissociation of marine methane hydrate, *Marine Geology*, 336, p. 1-222.

YARDLEY, G.S. and SWARBRICK, R.E. (2000) Lateral transfer: a source of additional overpressure? *Marine and Petroleum Geology*, 17, p. 523-537.

YASSIR, N.A., ADDIS, M.A. and HENNIG, A. (1998) Relationships between pore pressure and stress in different tectonic settings. *American Association of Drilling Engineers Industry Forum on Pressure Regimes in Sedimentary Basins and their prediction*, Del Lago Resort, Lake Conroe, Texas, Sep. 2-4, 6p.

YILMAZ, Ö., DOHERTY, S.M. (1987) *Seismic data processing*. Society of Exploration Geophysicists, Tulsa, OK.

ZÜHLSDORFF, C., HANEBUTH, T.J.J. and HENRICH, R. (2008) Persistent quasi-periodic turbidite activity off Saharan Africa and its comparability to orbital and climate cyclicities. *Geo-Marine Letters*, 28, p. 87-95.

APPENDICES

The appendices are presented in digital format only. The enclosed DVD provides the following information:

- *Appendix_01:* Thesis in PDF format;
- PDF files of published papers :

    - *Appendix_02:* LEDUC, A. M., DAVIES, R.J., IMBER, J. and DENSMORE, A.L. (2012) The lateral strike-slip domain in gravitational detachment delta systems: a case study of the northwest margin of the Niger Delta. *AAPG Bulletin,* 96, 4, p. 709-728.

    - *Appendix_03:* LEDUC, A. M., DAVIES, R. J., SWARBRICK, R. E., and IMBER, J. (2012) Fluid flow pipes triggered by lateral pressure transfer in the deepwater western Niger Delta. *Marine and Petroleum Geology*, 43, p. 423-433.

- Some supporting material from the in-house Eni 3D seismic datasets (OPL316) and PGS datasets (314 ad 315) used in chapters 3, 4 and 5:

    - *Appendix_04* to *Appendix_06*: A selection of seismic sections that were used for the research in OPL316 (chapters 3 and 5).
    - *Appendix_07:* Isochron maps of the key horizons H400 and H300 interpreted in Eni and in Durham across OPL314, 315 and 316, and used for research in chapters 3 - 5.
    - *Appendix_08*: Isochron maps of horizon H200 interpreted in Eni and in Durham used for research in chapters 3, 4 and 5.
    - *Appendix_09*: Isochron maps of the horizons “H250, H150, H100”, and the seabed interpreted in Eni and used for research in chapter 5.

- *Appendix_10*: Parameters used in 2D Move for the depth conversion of Fig.3.6C (chapter 3).

- *Appendix_11:* A seismic section from the 3D dataset OPL324 (CGG Veritas) used in chapter 4 and showing the Ijebu channel and an underlying tear fault.

- *Appendix_12:* Seismic sections of the "Khop" structure, a basement high located below the NCS-N channel where the relationship between the basement geometry, overburden deformation and fluid escape can be seen.

- *Appendix_13*: Provides a glossary of terms used in this thesis.

The lateral strike-slip domain in gravitational detachment delta systems: A case study of the northwestern margin of the Niger Delta

Amélie M. Leduc, Richard J. Davies, Alexander L. Densmore, and Jonathan Imber

ABSTRACT

We use two- and three-dimensional seismic data to describe the structural geology of the lateral margin of a deep-water delta lobe within the Niger Delta that has undergone basinward, gravitationally driven translation. We term this region the "lateral strike-slip domain." Deformation is characterized by a strike-slip fault system that can be followed for a distance of approximately 75 km (~47 mi) from the shelf to the slope and toe of slope. On the northwestern side of the fault system, a fold and thrust belt that propagated north to northwest has developed within a large-scale restraining area of 460 km^2 (180 mi^2). On the southeastern side of the strike-slip fault system, widespread extension has occurred, characterized by several graben and kilometer-scale rollover structures. Lateral margins of gravitational collapses give key information on how they deformed. We estimate a minimum horizontal displacement on the main strike-slip fault of approximately 7 km (~4 mi). Structural and kinematic evidence, such as present-day propagating strike-slip faults, for possible future lateral expansions of the lateral strike-slip domain, is described. We expect to observe similar sets of deformation styles at the margins of other preserved gravitational collapse sliding over a detachment whose efficiency in causing downdip slip may vary laterally.

Manuscript received March 3, 2011; provisional acceptance May 5, 2011; revised manuscript received August 16, 2011; final acceptance September 14, 2011.
DOI:10.1306/09141111035

AUTHORS

AMÉLIE M. LEDUC ~ *Center for Research in Earth Energy Systems, Department of Earth Sciences, Science Laboratories, Durham University, United Kingdom; amelie.leduc@durham.ac.uk*

Amélie Leduc is a Ph.D. research student at the Center for Research in Earth Energy Systems, Durham University, United Kingdom. She received her M.Sc. degree in 2008 from the University of Lille, France. Her current research focuses on the interaction between deformation and sediment dispersal in the western Niger Delta.

RICHARD J. DAVIES ~ *Center for Research in Earth Energy Systems, Department of Earth Sciences, Science Laboratories, Durham University, United Kingdom; richard.davies@durham.ac.uk*

Richard Davies is a professor at Durham University, United Kingdom. He is the director of the Durham University Energy Institute and recently led the Carbon Capture and Storage Research Group. His interests include the seismic interpretation of fluid flow; gas hydrates; diagenetic, structural, and igneous phenomena; as well as natural and man-made mud volcanoes.

ALEXANDER L. DENSMORE ~ *Institute of Hazard, Risk, and Resilience, and Department of Geography, Science Laboratories, Durham University, United Kingdom; a.l.densmore@durham.ac.uk*

Alex Densmore is a lecturer at Durham University, United Kingdom. He received his Ph.D. from the University of California, Santa Cruz, and held lectureships at Trinity College Dublin and Eidgenössische Technische Hochschule Zürich before joining Durham University in 2006. His current research includes aspects of tectonic geomorphology, efforts to understand sediment routing systems, and work on the role of mass wasting in shaping mountain belts.

JONATHAN IMBER ~ *Center for Research in Earth Energy Systems, Department of Earth Sciences, Science Laboratories, Durham University, United Kingdom; jonathan.imber@durham.ac.uk*

Jonathan Imber is a StatoilHydro lecturer in structural geology at Durham University. He received his B.Sc. degree in 1984 and his Ph.D. in

1988 from Durham University before joining the Fault Analysis Group in 1988. He returned to Durham University as a lecturer in 2005. His work is mainly concerned with investigating the growth of faults using three-dimensional seismic data.

ACKNOWLEDGEMENTS

We thank CGG Veritas and PGS for making the data available, as well as Dave Stevenson and Gary Wilkinson at Durham University. The support of this research and/or project by the Landmark Graphics Corporation via the Landmark University Grant program is acknowledged by Durham University. We also thank Eni S.p.A., Divisione Exploration and Production, Marco Orsi, Franco Fonnesu, and Juan Di Croce for their help and for providing access to their data in S. Donato Milanese. We also thank Eni for funding this Ph.D. project and the Center for Research into Earth Energy Systems, Durham Energy Institute, Durham University, for hosting the project.

The AAPG Editor thanks the following reviewers for their work on this paper: David Iacopini and Graham Yielding.

INTRODUCTION

Gravitational collapse occurs at a variety of scales from individual landslides and mass-transport complexes up to the dimensions of passive continental margins. Despite this variability, comparable processes and structural features occur (Butler and Turner, 2010). During the last three decades, a focus on describing gravity-driven deformation in large deltas has been observed (Cobbold and Szatmari, 1991; Damuth, 1994; Morley and Guerin, 1996; Gaullier et al., 2000; Gaullier and Vendeville, 2005; Maloney et al., 2010). This deformation is typically expressed as a complex that consists of an updip extensional domain, a translational domain where little internal deformation is observed, and a downdip compressional domain where fold and thrust belts and toe thrusts develop (Damuth, 1994; Stewart, 1999; Morley, 2003; Rowan et al., 2004; Bilotti and Shaw, 2005; Corredor et al., 2005; Cobbold et al., 2009).

A strike-slip domain, located at the lateral margins of a slide mass, has only been described in mass-transport complexes. For example, Frey Martinez et al. (2005), in the Levant Basin of the eastern Mediterranean Sea, and Bull et al. (2009), on the Storegga slide offshore Norway, provide well-imaged seismic examples of the lateral margins of large-scale slumps. Bull et al. (2009) illustrated a series of kinematic features that characterize strike-slip deformation on the lateral margins of mass-transport complexes in the translational domain. These features include en echelon sigmoidal scarps and dragged flow banding (material included in the complex and affected by strike-slip deformation). Important clues to the evolution of the slide, such as evidence for the timing of the deformation, the amount of horizontal downslope displacement of the mass, or the interaction between the slide mass and undeformed material along strike, may be found at the lateral margins. At the delta scale, strike-slip deformation has been documented in the Gulf of Mexico (Peel et al., 1995; Rowan, 2009), in the Nile Delta (Loncke et al., 2006; Clark and Cartwright, 2009), and in the Amazon fan (Cobbold and Szatmari, 1991). Recent work from Cobbold et al. (2009) and Løseth et al. (2010) has shown the presence on the seabed of en echelon kilometer-scale strike-slip faults in the deepwater Niger Delta. Morgan (2004) mentioned the presence of transfer faults in western Niger Delta that control the position of submarine channels, but the geometries and extent of the strike-slip fault zones were not described in detail. Despite these examples, generally, the literature is dominated by examples of strike-slip faults identified from two-dimensional

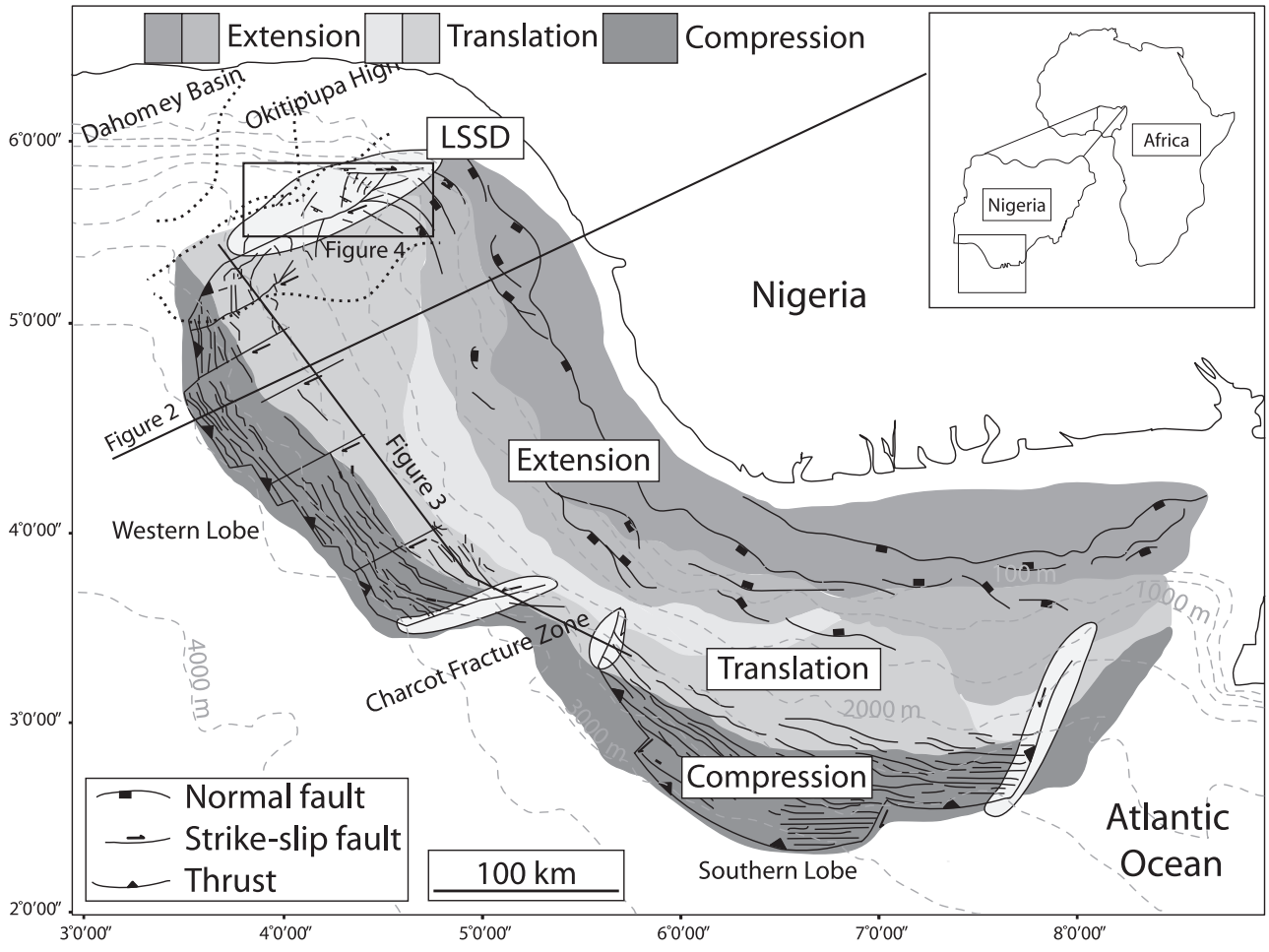

Figure 1. Overview of offshore Niger Delta structural domains (modified from Armentrout et al., 2000; Corredor et al., 2005; Heiniö and Davies, 2006; Deptuck et al., 2007; and Cobbold et al., 2009). Gray dashed lines are bathymetric contours. The structural domains relative to the main structural styles are indicated. The lighter shading corresponds to the potential location of the lateral strike-slip domains. Main canyon positions in the northwest offshore delta are shown by dotted lines; from west to east, these are the Lagos, Avon, Mahin, and Benin canyons. LSSD = lateral strike-slip domain as described in this article. Locations of Figures 2 and 3 are indicated with thick black lines, and Figure 4 is indicated with a rectangle.

(2-D) seismic data, and most of the focus on strike-slip fault morphology has been on structures in the continental crust instead of those associated with gravitational collapse. Looking into more detail, these strike-slip structures could provide information on how deformation occurs at the margins of gravitational collapses, how fast they will occur and how far the mass moves downslope, and what the controls on their development are.

In this article, we interpret 2-D and three-dimensional (3-D) seismic data to describe a set of large-scale structural features at the lateral margin of the northwestern Niger deep-water delta lobe that is undergoing downslope translation driven by gravity. We observe and interpret the structural complexity of coexisting extensional, compressional, and strike-slip deformation in the lateral margin. The lateral strike-slip domain is defined as a discrete structural domain that forms at the margins of a gravity detachment system, linking the extensional, translational, and compressional domains of the system.

DATA AND METHODS

Geologic Setting

The deep-water Niger Delta consists of two lobes in the south and in the west that developed

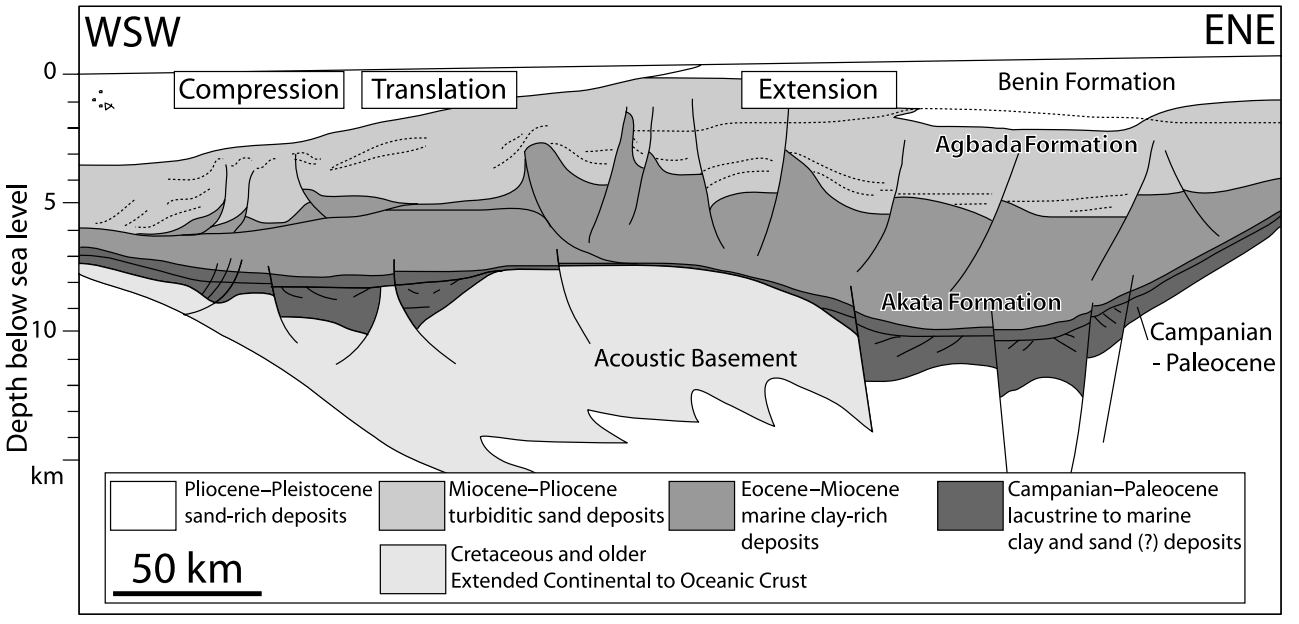

Figure 2. Simplified west-southwest–east-northeast cross section showing the structural features of basement and the sedimentary overburden of the offshore Niger Delta. The structural domains relative to the main structural styles are indicated (modified from Morgan, 2003).

contemporaneously (Figure 1) (Doust, 1990; Damuth, 1994). Deltaic sedimentation began in the Tertiary, and regional seismic lines (Figures 2, 3) show that a 7- to 8-km (4- to 5-mi)-thick sedimentary succession is located above the basement. Immediately above the basement, the Akata Formation is composed of Paleocene to Eocene marine shale. An abnormal decrease of velocity of 1000 m s^{-1} (3000 ft/s) at the top of the Akata has been interpreted as representing overpressured

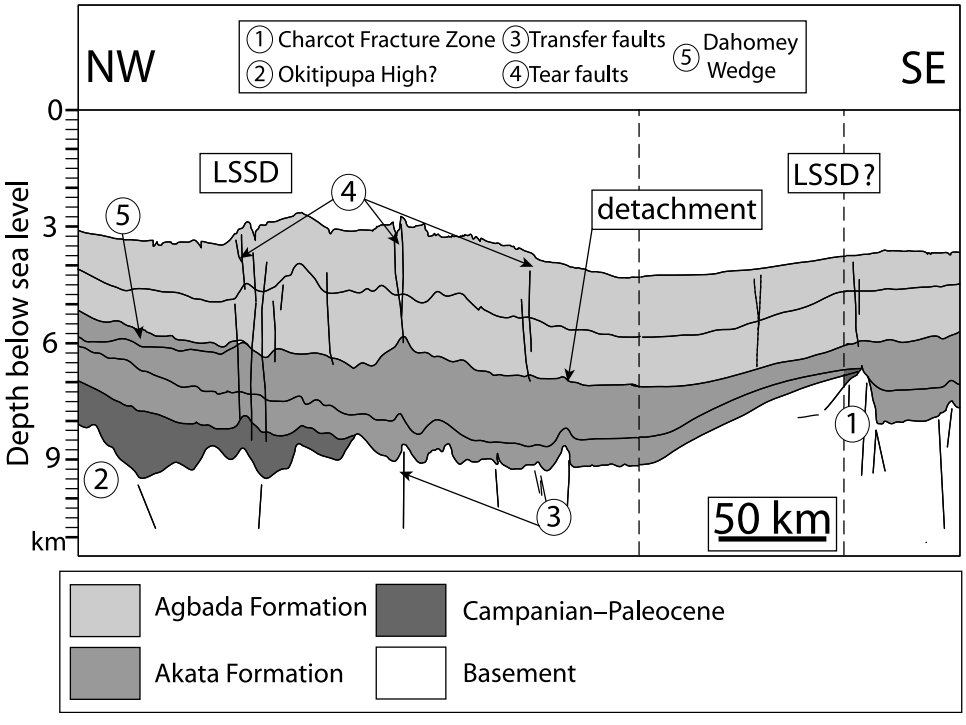

Figure 3. Interpretation of a regional north-northwest–south-southeast two-dimensional seismic section in the western lobe of the Niger Delta. No data between the vertical dotted lines exist; the Charcot fracture zone structure is adapted from Briggs et al. (2009). LSSD = lateral strike-slip domain. The Benin Formation is assumed not seen in this section.

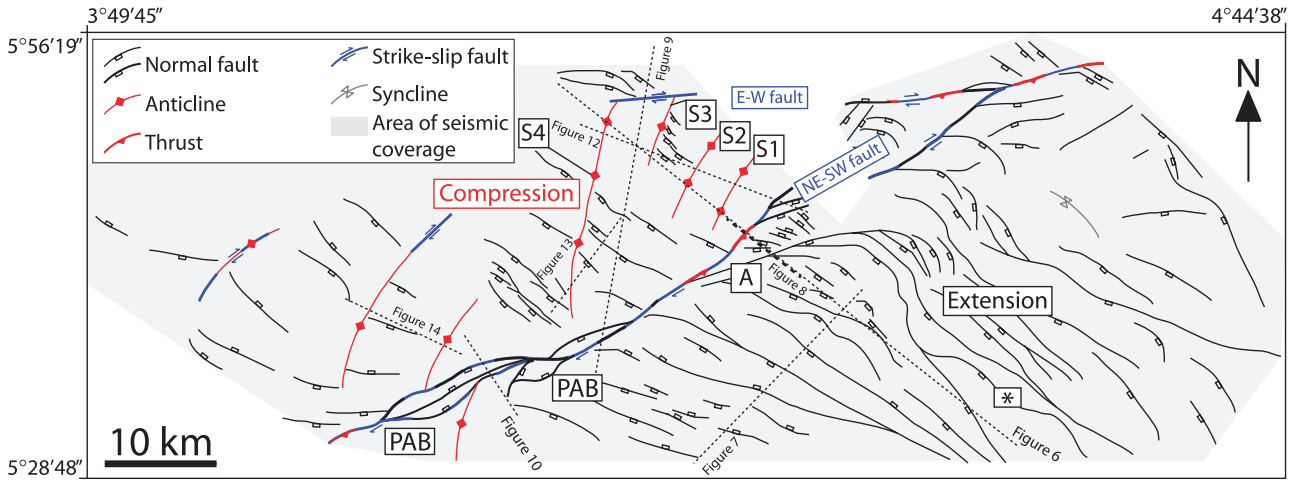

Figure 4. Detailed structural map of the lateral strike-slip domain from horizon interpretations at 3000 to 4000 ms two-way traveltime depth (between interpreted horizons H3 and H4). The positions of Figures 6, 10 and 12–14 are indicated by the dotted straight lines. The extensional zone is located in the southeastern part of the map and the compression zone in the northwest. PAB = pull-apart basin. A = fault trace marked A in Figure 8. The asterisk indicates the normal fault discussed in the section titled Extentional Zone.

conditions (Morgan, 2003). The overpressured interval is roughly coincident with the level at which normal and thrust faults sole out to become bedding-parallel detachments, allowing gravity-driven deformation to occur (Damuth, 1994; Cohen and McClay, 1996; Morley and Guerin, 1996; Briggs et al., 2006). The Akata Formation, which is of Eocene to Pliocene–Pleistocene age, is covered by a succession of turbiditic mass transport and hemipelagic deposits (the Agbada Formation). Over the Agbada Formation, the Benin Formation is sometimes mentioned (Figure 2), which has been defined from seismic facies interpretation in the proximal parts of the delta. Deformation is partitioned into three main structural domains. Both the western and southern lobes are also partitioned by strike-slip faults into several parallel sections sliding at different rates (Morgan, 2004; Cobbold et al., 2009) (Figures 1, 3); these faults are visible on seismic data as subvertical reflection terminations and fault-plane reflections.

We analyze three adjoining 3-D seismic data sets acquired in 2004 that cover most of the area of interest, as outlined on Figure 4. Water depths are between 500 and 2000 m (2000–7000 ft), the seismic surveys cover an area of approximately 4300 km^2 (~1660 mi^2), and bin dimensions are 12.5 × 18.75 m (41.01 × 61.52 ft; see Brown, 2004). At considered depths, frequency bandwidth is estimated to be approximately 30 Hz. Data are zero phased and are displayed in two-way traveltime. Combined use of time-structure maps and seismic attributes (coherency, dip, and amplitude extractions) from high-amplitude continuous reflections allows us to identify faults and folds in the area of interest (Figure 4). At considered horizon reflections, we extracted windowed amplitude maps (+100 and –100 ms) to observe the main structures. Time-thickness maps were computed between given top- and bottom-interpreted horizon reflections. The succession is subdivided into units A, B, and C based on changes in reflection character and the mapping of four reflections (H1–H4; Figure 5). Ages are roughly estimated based on an assumed uniform sedimentation rate of approximately 100 m/m.y. (Davies, 2003). A depth conversion of a key seismic section is presented in Figure 6. The description herein starts with an overview of the regional structures and stratigraphic units. We then focus on structural features identified from both map and seismic cross sections.

OBSERVATIONS

Three structural trends are identified both in map view (Figure 4) and in seismic sections (Figure 6A,

Unit	Horizon	Velocity (m/s)	Minimum–Maximum Depth (m)	Inferred Age	Formation
	sea bed	1480	500–2500	Present Day	
A			1600–2900	Pleistocene	
	H1	2200	1700–3300	Pliocene	Benin/Agbada
	H2	2300	2400–4300	Late Miocene (Messinian)	
B	H3	2700	2600–5000	Miocene	
	H4	2900	3600–6800	Late Oligocene	
C	detachment	2400	5000–9000	Oligocene?	
	basal strong reflection	2500	7500–9000	Eocene?	Akata
			8000–11,000	Paleocene	

Figure 5. Age and depth of stratigraphic units A, B, and C and horizons used in this article, from the seabed to the basal strong reflection. Depths are estimated from the seismic velocity model of Morgan (2003); velocities and depth are estimated from Morgan (2003). Ages are taken from Morgan (2003) and Lawrence (2002). Unit A, defined between the seabed and the interpreted horizon H1 (Pliocene), is composed of high-amplitude reflections within a background of lower amplitude continuous reflections. These reflections are interpreted to be silts and sands deposited within deep-water channels (e.g., Deptuck et al., 2007). Horizon H2 is estimated to be Messinian based on extrapolation from regional sedimentation rates (Davies, 2003). Unit B (situated between horizons H1 and H3) displays parallel reflections that are lower in amplitude than in those in unit A. It displays a sharp erosive contact with the underlying reflection packages. Unit C lies between H3 and the near top Akata reflection (associated with the top of the Akata Formation). Horizon H4 is another prominent reflection within unit C.

B). A major subvertical northeast-southwest–trending fault marks the boundary between two structural zones located to the northwest (compressional zone) and southeast (extensional zone). This distinction is also clear on a vertical section across the northeast-southwest fault (Figure 6A, B). The compressional faults to the northwest of the northeast-southwest fault appear generally much steeper (~60° dips) than the extensional faults to the southeast (~30°). This is only because the section chosen is oblique to the normal faults, whereas it is perpendicular to the shortening structures. Below, we examine each of these trends.

Extensional Zone

Most of the structures in the extensional zone (marked "extension" in Figure 4) are normal faults that strike northwest, dip steeply to the southwest (~60°), and have lengths of as much as 10 to 15 km (6–9 mi; Figures 4, 7). The largest northwest-striking normal fault is in the east of the study area. It can be traced over a distance of 30 km (20 mi) and connects to a northeast-striking normal fault (marked with an asterisk in Figure 4). The northwest-striking normal fault defines the northeast border of a graben of an approximately 10-km (~6-mi) width (Figures 4, 7). A large number of the northwest-striking faults deform H1, H2, H3, H4, and the top Akata reflection. They consist of a series of conjugate normal and growth faults with variable movements and variable length. It is probable that these faults represent several deformation episodes because the related growth sequences appear to have formed during multiple episodes of extension. The main episode of extension is recorded in the upper part of unit C where onlap geometries prograding to the west are found. Other normal faults also exist in the compressional zone, some of which are likely to be the continuation of some northwest-striking normal faults of the extensional zone. They may predate the formation of the strike-slip fault zone. Another hypothesis is to relate these extensional features to a degradation of the fold and thrust belt as they strike perpendicularly to the fold hinges.

Strike-Slip Faults

The northeast-southwest fault zone is composed of a variety of faults with geometries that are kinematically linked (Figure 4). The longest fault

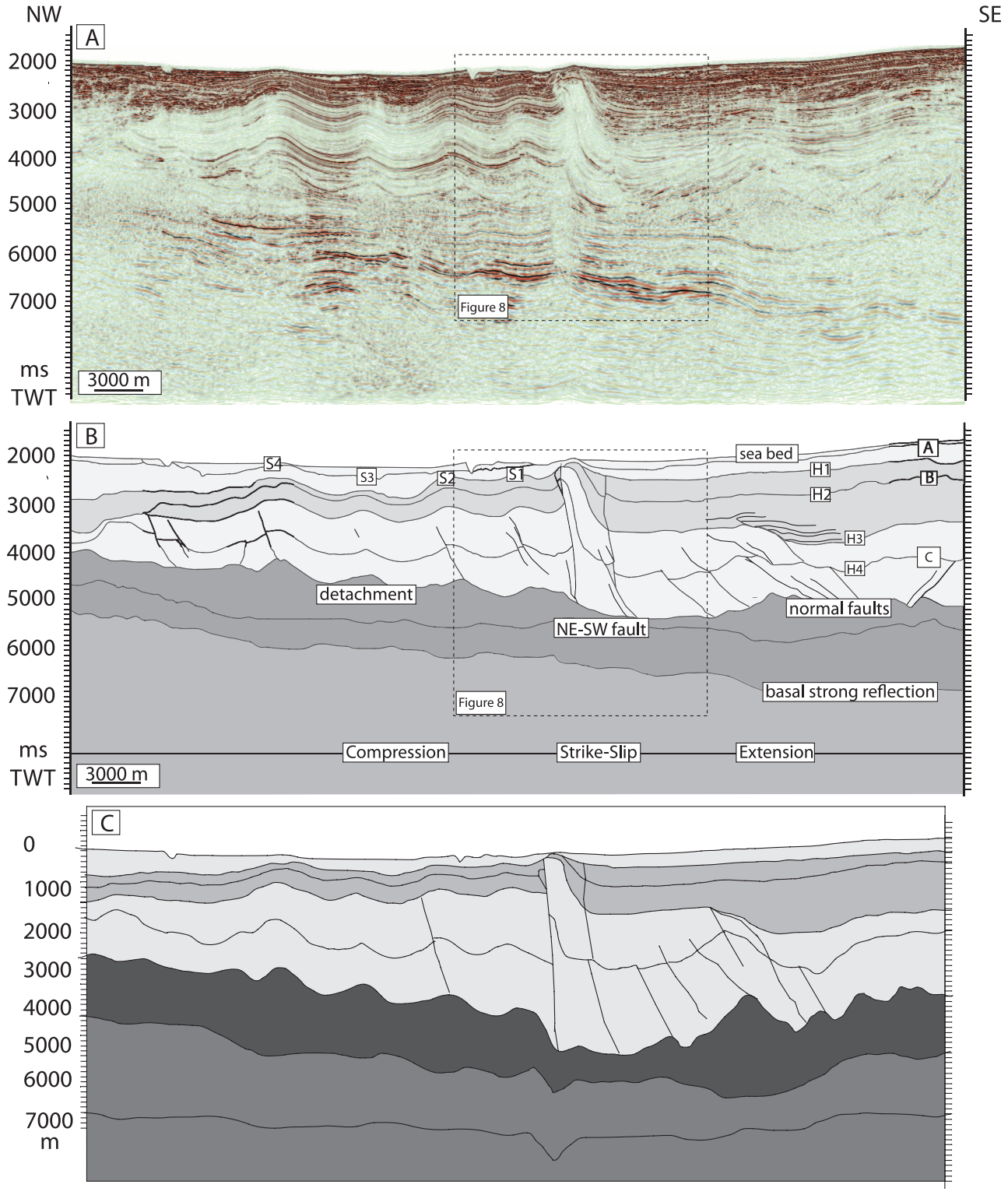

Figure 6. (A, B) Northwest-southeast–oriented interpreted seismic sections selected from a three-dimensional seismic data set crossing the three structural zones of the area of detailed study. Folds are numbered S1 to S4 from the northeast-southwest fault trace to the west. (C) Depth conversion applied to the section displayed in Figure 6A and B. The section is depth converted using interval velocities as shown in Figure 5. This section shows that the geometries and dips of the structures remain comparable on both time- and depth-converted seismic sections. All the following sections are converted. TWT = two-way traveltime.

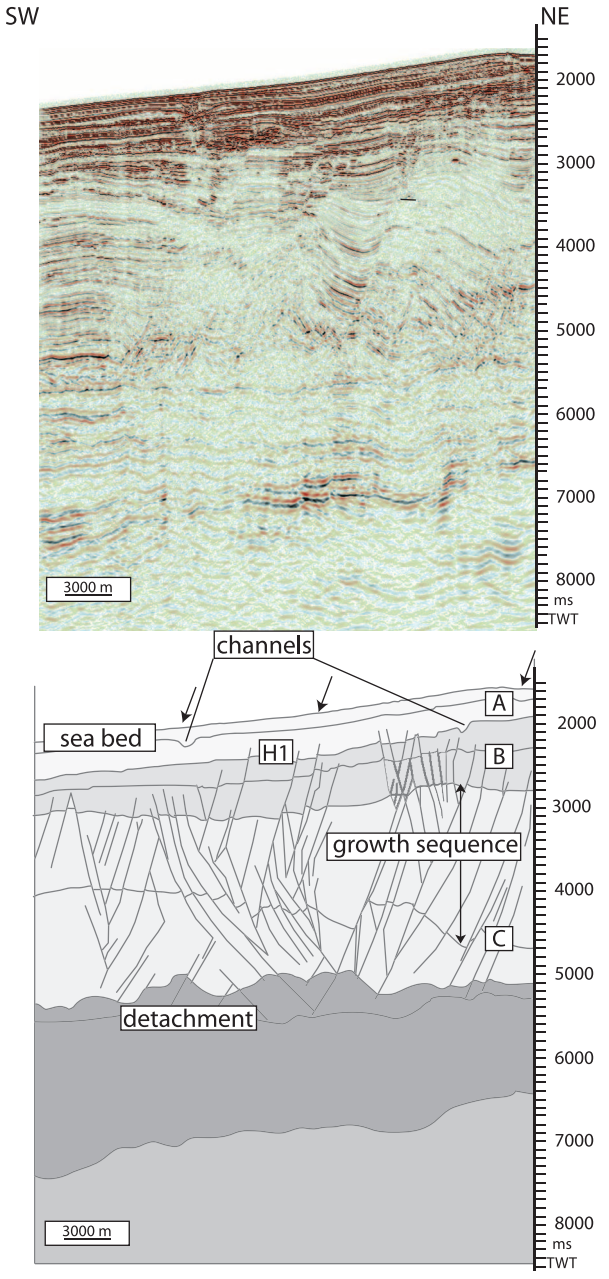

Figure 7. Southwest-northeast–oriented seismic section and interpretation showing a compound graben in the extensional zone. TWT = two-way traveltime.

trace is 75 km (47 mi) long. Because of its complexity, we describe its main geometries from its northeast mapped tip to the southwest along strike (kilometer 0 is at the northernmost mapped point of the fault; kilometer 75 is at the inferred southwest tip). A northern segment (kilometers 0–10) and a central segment (kilometers 33–43) show contraction. On a seismic section, these segments display two subvertical fault traces, both dipping subvertically to the southeast (Figures 6A, B; 8), that extend from the top Akata detachment to the seabed. The southeastern fault trace (Figure 8, marked A) is kinematically linked to the fault trace connecting the northeast-southwest fault to a large normal fault in the extensional zone (Figure 4). The northwestern fault trace is a thrust fault with pronounced folding in the hanging wall that branches into several segments toward the surface. We interpret this fault system as a compressional strike-slip fault system (Harding, 1985).

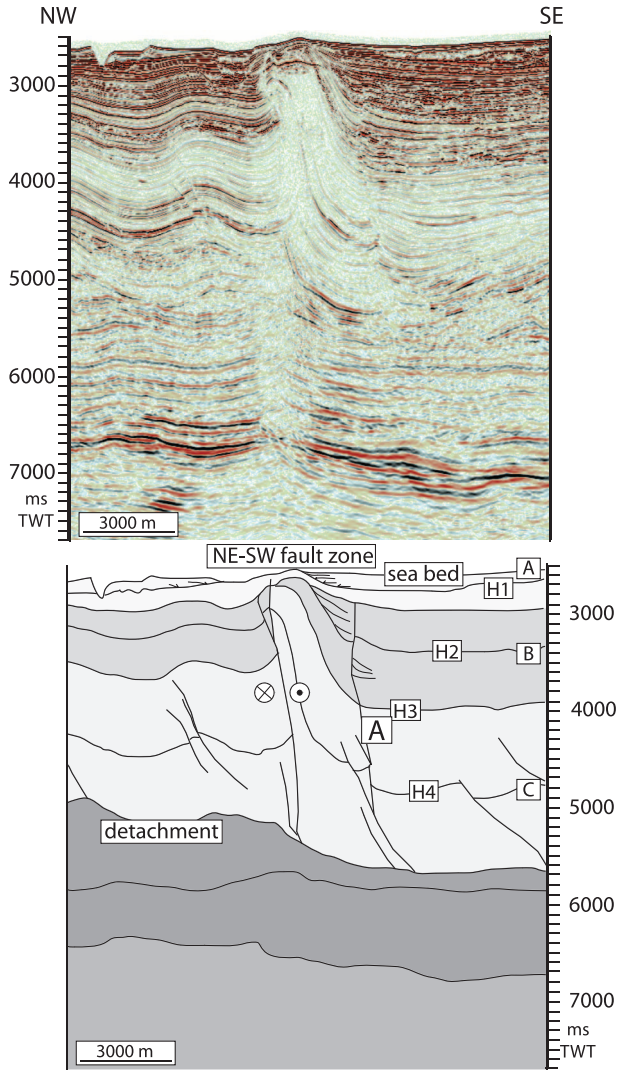

Figure 8. Detailed view of the compressive strike-slip structure shown in the center of Figure 6. The steep fault trace at the northwestern side of the fault zone is bounded by a steep fold. Deformation occurs while sediments are being deposited and eroded. The fault trace marked A represents the southeastern limit of the northeast-southwest fault zone. TWT = two-way traveltime.

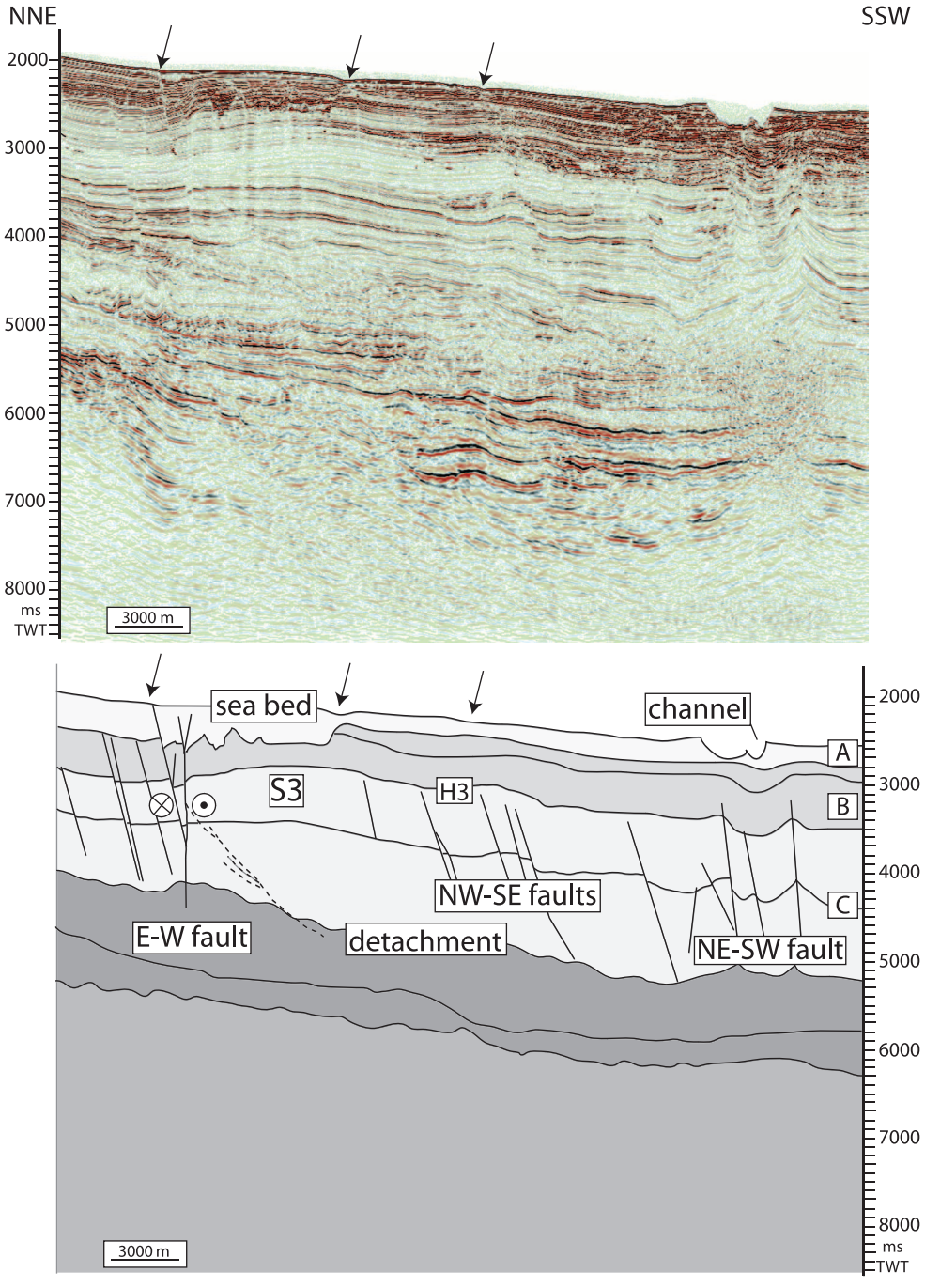

Figure 9. North-northeast–south-southwest–oriented seismic section and interpretation showing the east-west strike-slip fault, normal faults dipping southwest, and the northeast-southwest strike-slip fault system. The thickening of the reflection packages in the northeastern part of the figure is caused by the presence of fold S3, obliquely crosscut by this section. The dashed line shows the position of a thrust fault trace(?) associated with fold S3. The arrows above the seabed reflection indicate the location of apparent subsidence at the seabed, suggesting the present-day activity of the underlying fault traces. TWT = two-way traveltime.

Unconformable contacts are identified at the base of unit A, on H2 and H3. Variations in the thicknesses of these units suggest the occurrence of three episodes of erosion and/or deposition that can be related to possible pulses of activity on the northeast-southwest fault.

Another strike-slip fault, oriented east-west, is located in the north of the study area and connects to the northeast-southwest fault at kilometer 10. Assuming that the fault connects between its eastern and western documented parts, in the area of no seismic coverage, it is approximately 35 km (~22 mi) long (Figure 4). In a vertical section, the east-west fault is expressed as a subvertical fault array that branches and offsets reflections between the seabed and H3 (Figure 9). The east-west fault

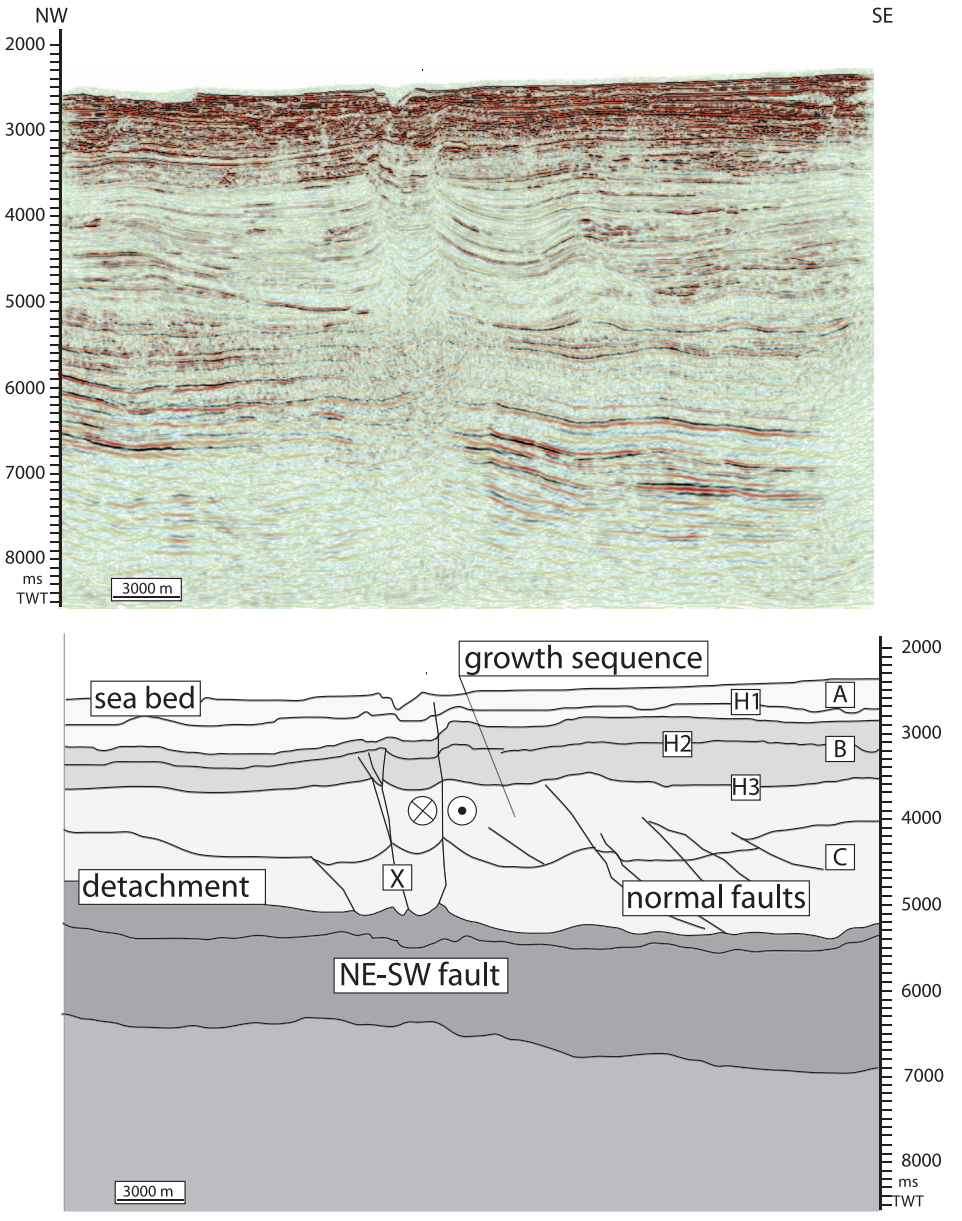

Figure 10. Northwest-southeast–oriented seismic section and interpretation showing a negative flower structure on the northeast-southwest fault. All the fault traces together at the center of the figure are interpreted as a negative flower structure; however, at a smaller scale, the set of fault segments labeled "X" also presents negative flower structure geometries.

displays a negative flower structure (Harding, 1985), with the south-southwestern block downthrown.

From kilometer 43 to its southwestern tip, the northeast-southwest fault splays into a series of normal faults that form small pull-apart basins (Figure 4, marked PAB). These basins are bounded on their northwestern side by the northeast-southwest fault zone and by an east-northeast–west-southwest normal fault dipping northwest on its other side. They are, respectively, from northeast to southwest, 8 km (5 mi) long and 2 km (1 mi) wide, 5 km (3 mi) long and 2.5 km (2 mi) wide, and 14.5 km (9 mi) long and 3 km (2 mi) wide. A typical seismic section along the strike of the northeast-southwest fault in this segment displays a set of high-angle faults that we interpret as a negative flower structure (Harding, 1985) (Figure 10). The northwestern fault trace (Figure 10, marked X) is a steep fault with an apparent downthrow of 200 m (700 ft) to the north on H2 to H3. Offset decreases upsection and goes to zero at the seabed. The other segment branches and cuts reflections between the top Akata reflection and H2. Units B and C are thickening progressively to the southeast, and onlaps suggesting growth sequence are observed in unit C. Extension occurs

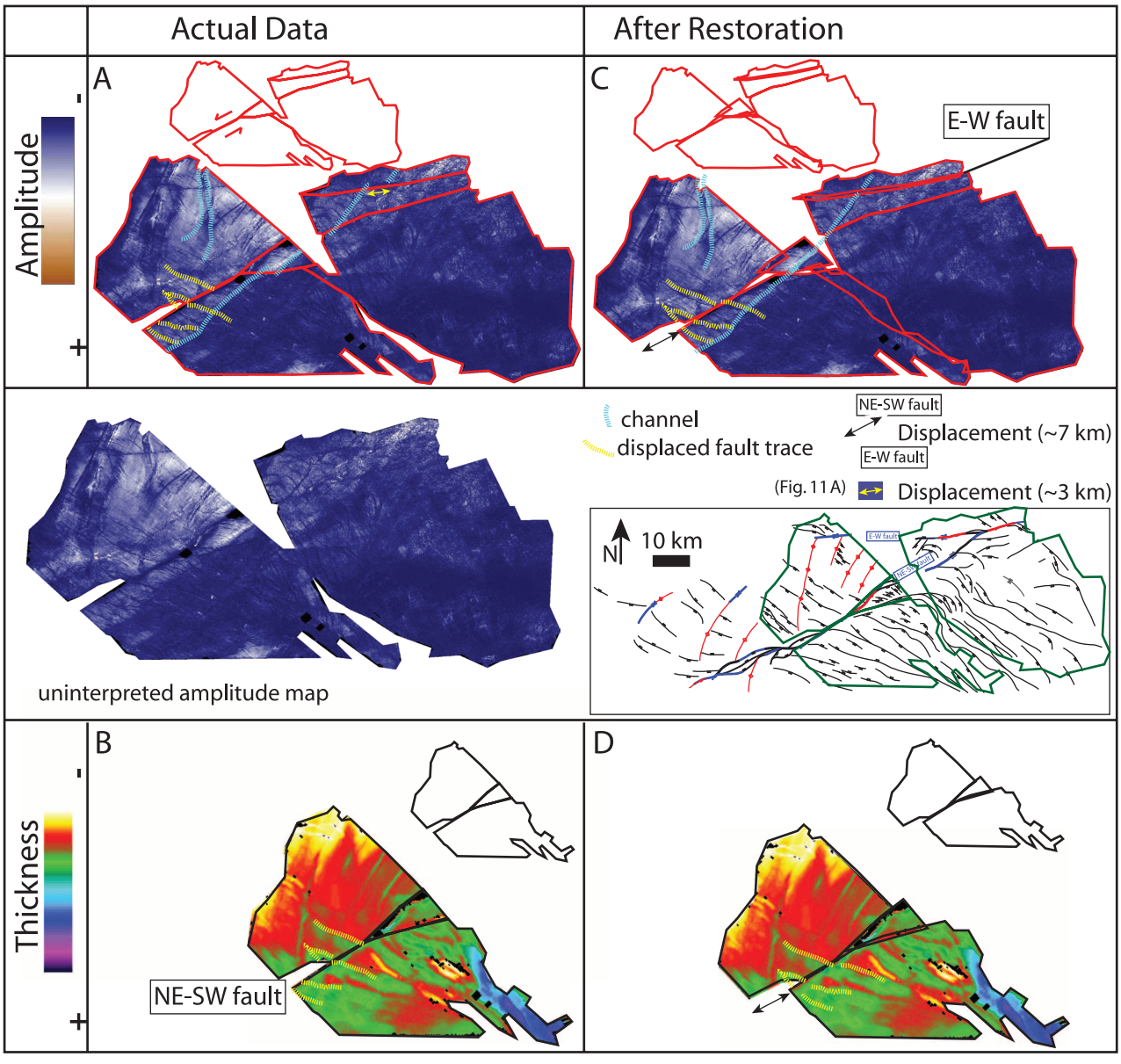

Figure 11. Horizontal displacement on the northeast-southwest and the east-west strike-slip faults. (A, C) Amplitude extractions at H3 (maximum average amplitude, windows 100 ms two-way traveltime (TWT) above and 100 ms TWT below H3, top of the figure) show the horizontal displacement on the east-west fault and the normal fault connecting to the northeast-southwest fault from the offset of the channel marked with the blue line. (B, D) Time isopach map between H3 and H4 showing the displacement of two normal faults bounding a graben by the northeast-southwest fault. The displacement on the east-west fault is indicated by a yellow double arrow (Figure 11A); the black double arrow indicates the displacement on the northeast-southwest fault (Figure 11C).

by the northeast-southwest fault and is likely to occur before and during strike-slip motion. Thus, the same northeast-southwest–striking fault system evolves along strike (on vertical sections) from subvertical fault-propagation fold geometries (Figure 8) to a combination of linked normal faults and pull-apart basins in the southwest (Figures 4, 10). This observation is consistent with a strike-slip fault system interpretation (Harding, 1985).

An amplitude extraction map of H3 and a time-thickness map of unit C show that areas of high amplitude and previous fault traces are offset along the main northeast-southwest fault zone (Figure 11). They can be restored by a lateral translation of matching blocks of the map that show

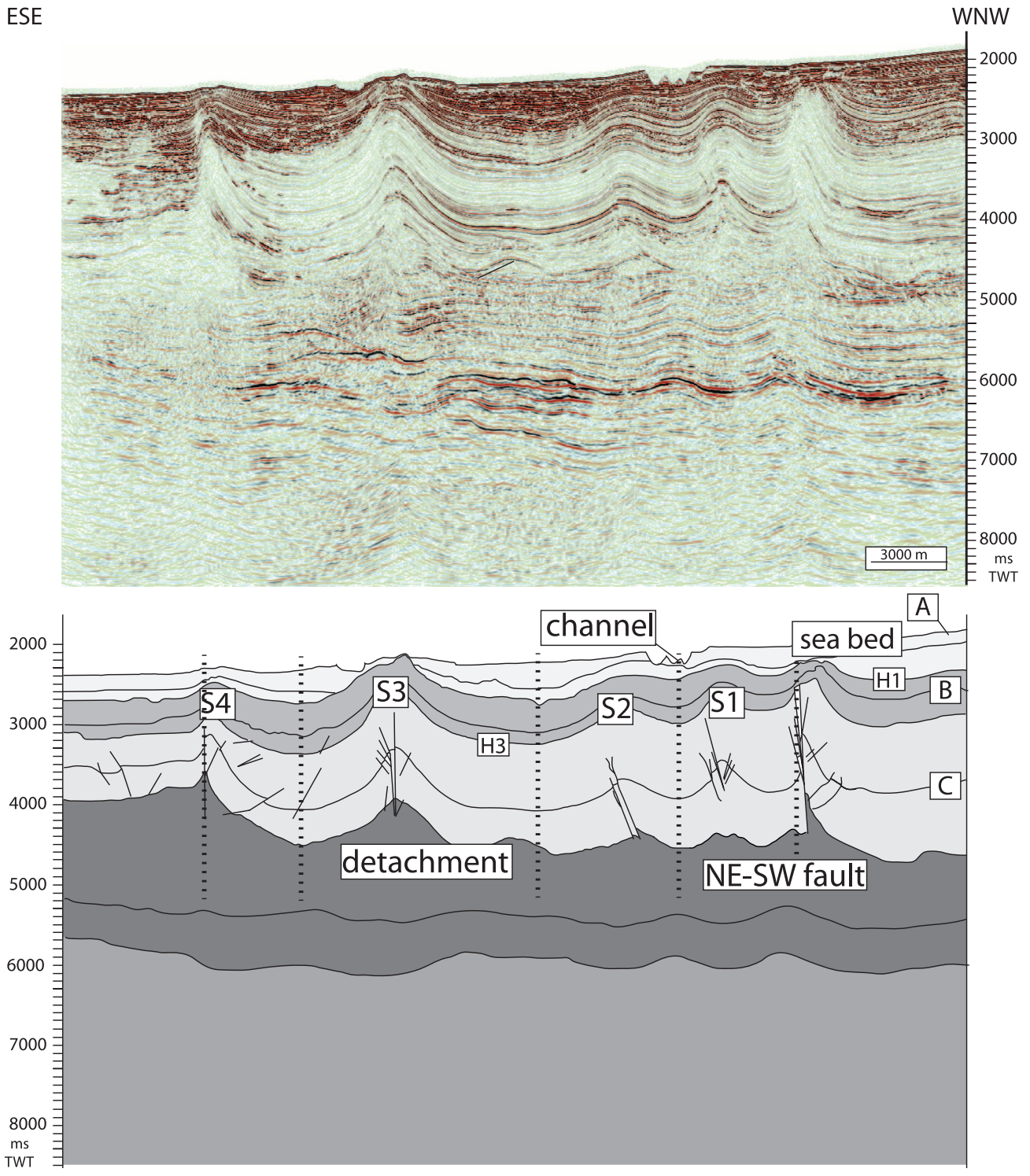

Figure 12. East-west–oriented seismic section and interpretation showing the northeast-southwest fault and the four folds within the area of the restraining bend in the compressional zone. The vertical dashed lines demarcate folds S1 to S4. TWT = two-way traveltime.

the state of the region as it probably was in the late Miocene. These blocks are delineated by the northeast-southwest and the east-west strike faults and by the large northwest-southeast normal faults in the south of the study area. A horizontal displacement of as much as 7 km (4 mi) is found on

the northeast-southwest fault, and 3 km (2 mi) of displacement is observed on the east-west fault.

Compressional Zone

The compressional zone lies from kilometer 10 on the northwest flank of the northeast-southwest fault and to the south of the east-west fault (marked "compression" in Figure 4). This roughly triangular compressional area of approximately 540 km^2 (~210 mi^2) is composed of four arcuate folds numbered S1 to S4. From west to east, the maximum length of their hinge lines is 20, 6.5, 10.4, and 8.5 km (12, 4, 6.5, and 5.3 mi), respectively, at the depth of H1, and the folds have an average wavelength of 5 km (3 mi; Figure 12). Assuming that this was measured on a constant reflection, shortening on each structure is estimated at 2.25, 0.75, 1.5, and 2.2 km (1.40, 0.47, 0.9, and 1.4 mi) for S1 to S4, respectively, yielding a total of 6.7 km (4.2 mi) for the entire system at the depth of H1 (Figure 12). The folds are asymmetric, with a steeper forelimb (near vertical in the case of S4, as displayed on the seismic section). Complex fault traces are visible at the core of the folds, although the fault traces do not extend above H3. Deformation clearly affects the seabed only on folds S3 and S4 (Figure 13), whereas folds 1 and 2 seem to have been buried by the most recent sediment package of unit A. This observation is interpreted as an evidence for a westward propagation of the fold belt, which is perpendicular to the general trend of the continental slope. Folds S3 and S4 gradually die out progressively onto the east-west fault (Figure 4). This suggests that the development of the folds is interrupted by the east-west fault. The folds hinges actually die out onto the east-west fault. In terms of timing relationships, this is interpreted as a contemporaneous development of the strike-slip fault and the shortening features. However, the maximum visible displacement along the east-west fault has been estimated at 3 km (2 mi; Figure 11), which is smaller than the total shortening estimated for the fold and thrust belt. However, the order of magnitude remains similar. It is possible to

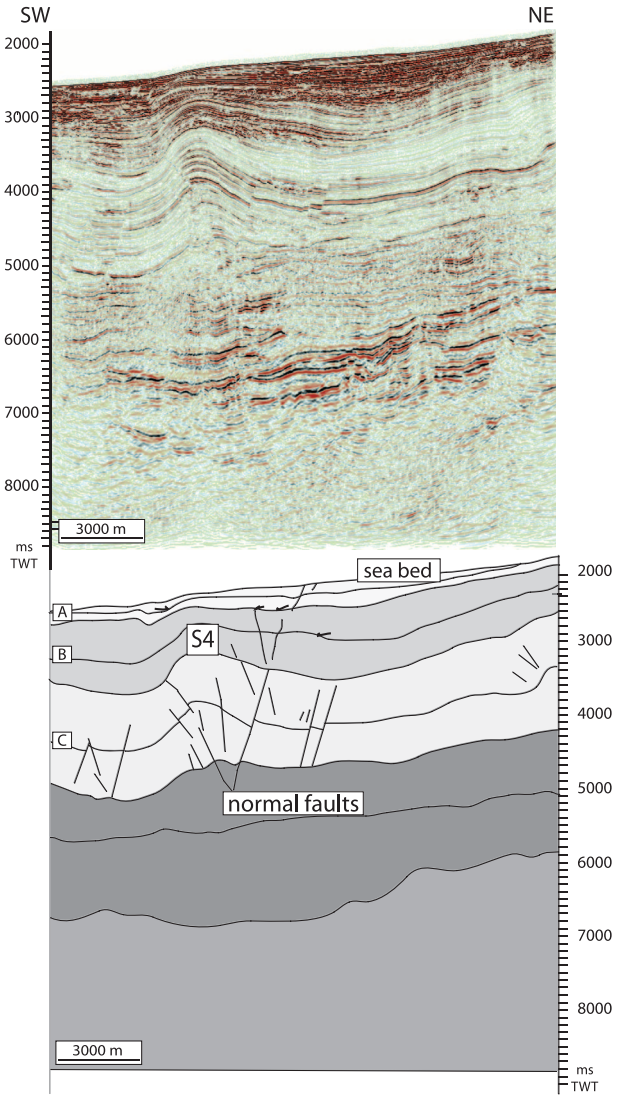

Figure 13. Southwest-northeast–oriented seismic section and interpretation showing rotated normal faults on fold S4. TWT = two-way traveltime.

assess the relative timing of the fold activity by looking at onlap geometries, in particular, around fold S3 (Figure 12). The sediment record is unequal at each fold, suggesting that activity on the folds varies. We suggest that S1 and S2 were active first and that their activity carried on until the present day. Fold S3 is currently buried, which can be interpreted as sedimentation locally overcoming fold growth. Finally, S4 synsedimentary activity occurs the latest because onlaps are only found on the top reflections. A timing relationship can be established as follows: (1) development of the northeast-southwest fault; (2) propagation of the

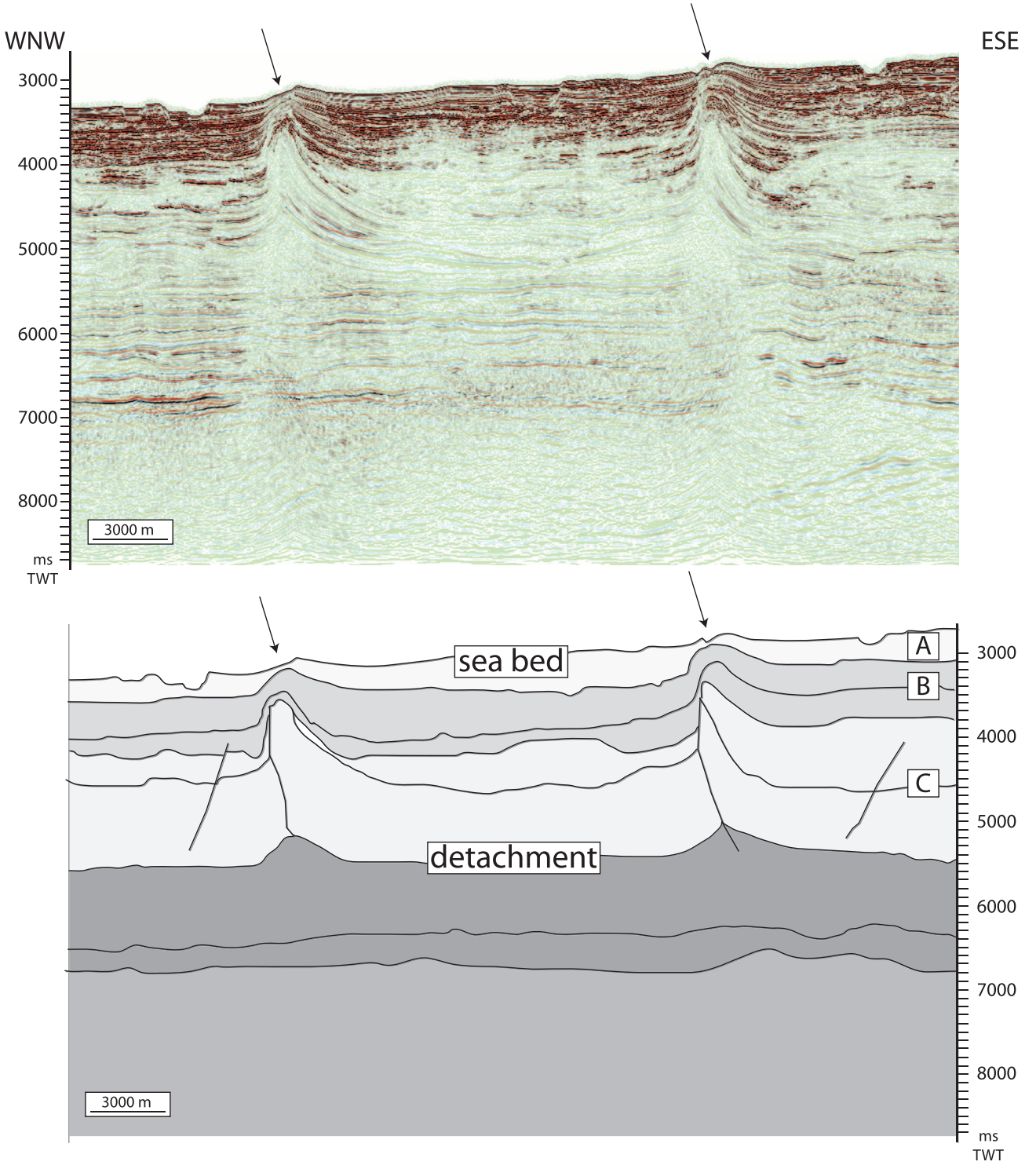

Figure 14. East-west seismic section and interpretation, located west of the lateral strike-slip domain (LSSD), show two present-day developing northeast-southwest–oriented possible strike-slip faults that are just beginning to slip at present; therefore, no offset can yet be observed west of the LSSD. They display very steep (subvertical) fault-propagating fold geometries (presence of a subvertical fault can be inferred at the core of these structures). They could represent similar geometries to what used to be the earliest segments of the northeast-southwest fault geometries in its compressional part. TWT = two-way traveltime.

east-west fault to the west; (3) S1 and S2 growth; and (4) S3? and S4 starting to grow, whereas other structures remain active. Because no biostratigraphic data are available, however, prevents us from proposing any absolute age of deformation events in this article.

Whereas the compressional zone is dominated by folding, a few steep northwest-striking normal faults are also observed, with lengths of 2 to 7 km (1–4 mi; Figures 9, 14). These faults strike almost orthogonally to the folds. Normal faults dipping to the southwest are located on both the forelimb and the backlimb of fold S4. Conjugate normal faults dipping northeast are also located on the forelimb. Horizon H4 is tilted and offset by these faults, but no offset is observed in the younger horizons. Recent subsidence seems to occur over the tip of the fault traces, whereas onlapping is found in unit A; however, it is hard to distinguish what is controlled by the fold growth or by the activity of the northwest-striking faults. These extensional features could either be interpreted as a marker of preexisting extension before the folding or could be resulting from a perpendicular extension contemporaneous to the folding. As evidence of normal fault offset is observed on both sides of the northeast-southwest fault (Figure 11), we suggest that the steep normal faults (Figure 14) are actually incorporated and rotated within fold S4 during the folding event and are therefore older than the fold.

Two other compressional structures are observed in the western end of the studied area (Figures 4, 14). They are steep, listric, west-vergent thrust faults associated with fault-propagation folds. These structures create topography of approximately 300 m (~1000 ft) at the seabed and are responsible for the localized erosion of unit A. Channels are localized at the front of the western structure and over the backlimb of the eastern structure (Figure 14). The faults within the folds are very recent features because no evidence for previous structural control of sedimentation is observed at the periphery of the folds. The folds are parallel with the northeast-southwest trend, and their shape is comparable to the compressional features of the strike-slip fault zone (Figure 8). As a result, we suggest that these structures are associated with a compressional bend within the overall strike-slip domain.

DISCUSSION

Structural Relationships

Christie-Blick and Biddle (1985), Woodcock and Fischer (1986), Woodcock and Schubert (1994), and Cunningham and Mann (2007) provided 3-D models of the various geometries of strike-slip faults. The strike-slip nature of deformation on the northeast-southwest fault system is indicated by the wide range of structural features observed along strike. These features include a horsetail splay at the northeast end of the studied area, linking extensional features to strike-slip features (Figure 4). The angle and the shape of the strike-slip features we described appear to be slightly different to what is found in the literature (Harding, 1985). For instance, the strike-slip compressive structure we present (Figure 8) is comparable to a steep fault-propagation fold, its branching out appearing very asymmetric as the structure tilts westward. These changes in shape could be explained by the fact that sedimentation is syntectonic and will influence the shape of the final structure, as demonstrated in sandbox experiments (Casas et al., 2000), or that braided geometries correspond to an advanced stage of growth.

The northeast-southwest fault and the east-west fault define a major structural boundary at the lateral margin of the sedimentary lobe (Figure 15) (Cobbold et al., 2009), with the east-west fault representing a secondary continuation of the main fault to the west. This fault system is defined as a tear-fault system because it accommodates differential sliding between one sedimentary compartment included in the lobe and another outside the lobe. The dextral sense of slip is compatible with the downdip sliding of the margins of the delta lobe. The northeast-southwest fault thus links and transmits deformation caused by the normal faults in the extensional domain to the outer thrust belt in the compression zone over the detachment surface.

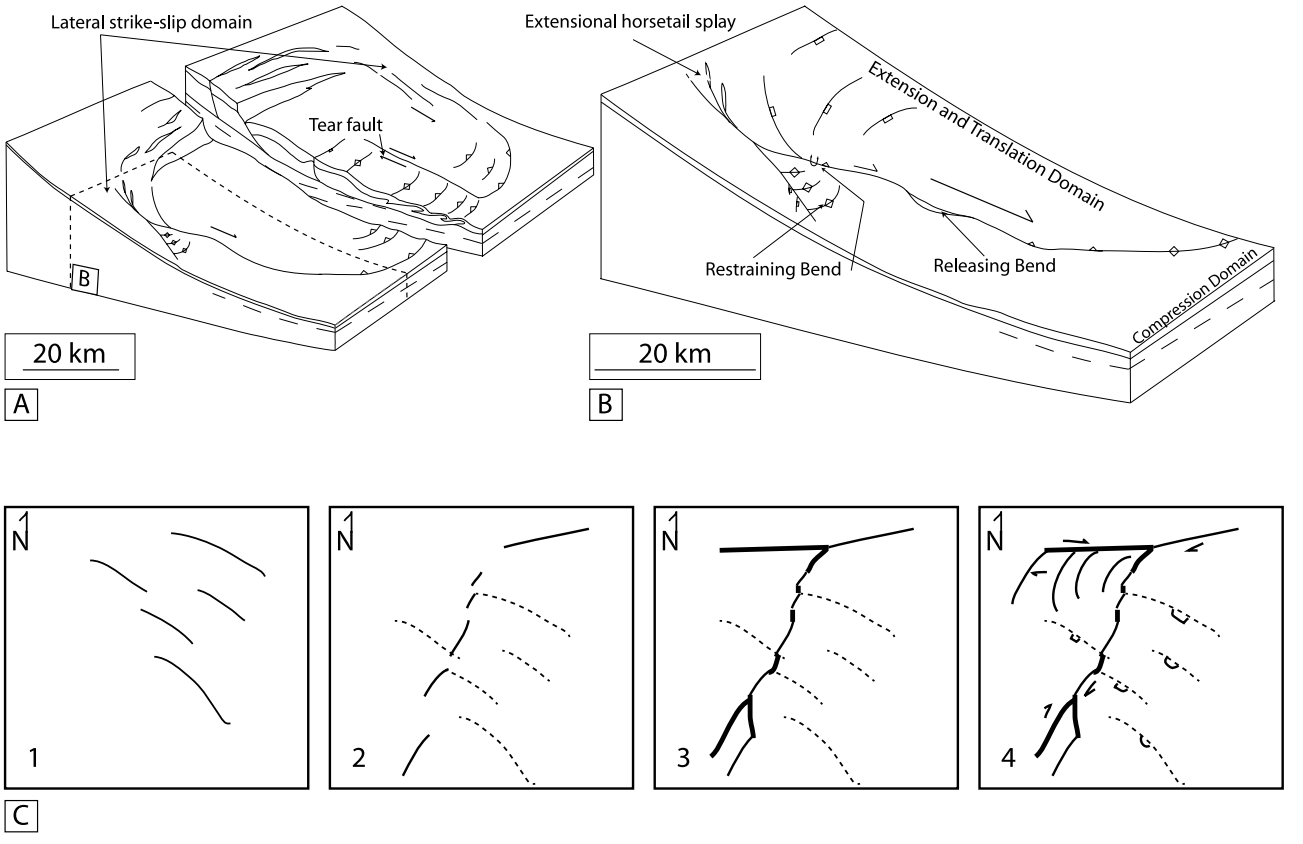

Figure 15. The theoretical model proposed for the lateral strike-slip domain. (A) Three-dimensional block diagram to the scale of the deep-water deltaic lobe showing the geometric interplay between the main structures of each structural domain. (B) Cutaway from A, focusing on the lateral strike-slip domain. (C) Summary of the development of the main structures. 1 = extensional faults; 2 = early stages of strike-slip deformation; 3 = propagation of strike-slip faults; 4 = "restraining bend" area development, including the westward-verging fold and thrust belt as a later stage of regional strike-slip deformation.

The northeast-southwest fault zone was probably used to separate the slide mass from a relatively unfailed material. As it appears at present day, deformation has expanded to the northwest (via the development of the fold belt) so that the active mass has grown in a second more recent episode of deformation.

Relative Timing of Deformation

We can assess the relative timing of activity on the different structures associated with the lateral margin by interpreting crosscutting relationships between the different geometries and sediment growth packages. The complex braided geometries and widespread linkage displayed on the northeast-southwest fault indicate a mature stage in the faulting (Figure 4). The east-west fault shows evidence for only recent stages of deformation in its westernmost segment (onlapping in the youngest packages). We therefore think that the western part of the east-west fault is younger than the northeast-southwest fault. The northeast-southwest fault system is developed as a vertical fault in the east where highly deformed structures similar to inversion structures are sometimes identifiable along strike seismic sections (Figure 6A, B). We suggest that the northeast-southwest fault has therefore locally become a factor both in extension and in compression during strike-slip deformation.

The combined east-west and northeast-southwest tear-fault system shows varying styles of deformation and amount of displacement. Evidence for erosion caused by an uplift of the footwall on the northeast-southwest fault indicates that this fault has been active in the past and is still partly

active at present day as uplifted zones (Figures 6A, B; 9; 12) and subsiding zones (Figures 7, 9, 10) occur on the seabed. The evidence for the deformation of the seabed by the western, but not by the eastern, folds is consistent with a very young age of deformation on the east-west fault. Complementary evidence for this comes from the tilting of units A, B, and C caused by the deformation on the east-west fault (Figure 9), which shows that activity on the western part of the fault occurred very recently. This part of the fault likely developed after deposition of H1 (above which are observed the first growth strata; Figures 9, 12). Furthermore, we do not observe any sedimentary growth packages in the deposits on the footwall of this structure, indicating again very recent deformation. The east-west fault is still propagating westward at the present day.

The fold hinges in the compressional zone are kinematically connected to the east-west fault, whereas no direct geometrical relationship can be established between the fold belt and the northeast-southwest fault. The curved shape of the fold hinges could indicate a decreasing anticlockwise rotation of the deformation front from the east-west fault to the northeast-southwest fault. Shortening in the west occurred at the same time as the east-west fault began to propagate to the west, building up what we interpret as a restraining bend area. We suggest that this area would be controlled by the growth of the east-west fault (Figure 15C). This restraining bend is thought to be formed once the northeast-southwest fault and the east-west fault linked and developed contemporaneously to the propagation of the east-west fault to the west.

The extensional zone consists of numerous extensional fault traces, some of which display growth packages (Figures 4; 6A, B; 7). Growth sequences are visible in the seismic data and are probably associated with successive stages of deformation (Figure 6A, B). We therefore show that this area does not undergo simple compression as it would be thought for a regional deep-water compressional domain (Figure 1). We suggest that the northwest-striking normal faults in the compressional zone (Figures 9, 13) developed contemporaneously to the faults with the same trend in the extensional zone, that is to say before H1. They then probably became inactive and have been reactivated as the fold belt grew in the compressional zone at very recent stages. The deposits over the detachment surface underwent a first phase of extension. During this period, extension was very limited in the compressional zone, and only a few small faults developed. A second phase of extension started after H2 to H3 and has continued to the present day. Strike-slip deformation on both the east-west fault and the northeast-southwest fault probably began before the end of the first phase of extension but became predominant after H2. In fact, most of the structures related to strike-slip deformation seem to control post-H2 sediments. Deformation occurred at different stages along the strike of the strike-slip faults. Numerous smaller normal faults also indicate several ages of faulting. These fault traces are likely to be rotated by later shortening structures, such as the crosscutting fault-propagation fold shown in Figure 13.

Evolution of the Lateral Strike-Slip Domain

A schematic block diagram (Figure 15A, B) including the location of the lateral strike-slip domain in a gravity-driven detachment system shows the geometric interrelations between the extensional, translational, and compressional domains using the analogy of a mass-transport complex. At the scale of 100 m (300 ft) to 10 km (6 mi), lateral margins are mostly documented, and their geometries are comparable to what we observe in the western Niger Delta. Extensional faults evolving to transfer faults and to purely strike-slip deformation have been reported from field examples. For instance, pure strike-slip deformation occurs on slumps of constant width (Martinsen and Bakken, 1990). This evolution in the structures illustrates, in the case of slides, a lateral expansion of the margins, leading to a change in their width.

The compressive structures linked to the lateral strike-slip domain are younging westward, which shows that the structural domain is getting wider with time. Deformation is more likely to propagate laterally over a previously unfailed margin

because it has no constraint to stop its propagation, leading to the development of the lateral strike-slip domain. This increase in width may also indicate that the local overburden cannot effectively slide downslope compared with other areas. This may be because the detachment surface is less conducive to sliding or because the sediment overburden at the lateral margin is relatively thin and less prone to downslope motion. We speculate that a local change in effective stress caused by overpressure development in the lateral variations of sediment thicknesses could cause a control on stress patterns, leading to the expansion of this structural domain. Alternatively, an abrupt increase in the regional sediment input, coupled with spatially nonuniform accumulation, could also trigger the regional partitioning of the slide mass. Therefore, the slope angle would be expected to increase in areas of greater sedimentation and the more central parts of the sedimentary lobes would be more likely to become unstable and begin to slide basinward. The origin and development of tear faults is likely to be common in any gravitational system driven by a high sedimentation (or sediment supply) rate.

Irregularities within the detachment such as a change in the nature or thickness, therefore, rheology of the sediments, such as the Dahomey wedge, a thinner shale unit included in the Akata Formation (Morgan, 2004) (Figure 3), may explain the development of strike-slip stresses in this particular region. Otherwise, Treviño and Vendeville (2008) provided an example of a normal fault in the hanging wall of a major growth-fault complex with a strike line that is perpendicular to the direction of deformation. They suggested that a slight convergence or divergence of the stresses from the center of the structure could lead to the growth of coast-perpendicular structures in the sedimentary cover as coast-parallel convergent stresses occur in the detachment unit. A similar process can be suggested for our strike-slip fault zone because its general strike is perpendicular to coast-parallel extensional features.

Finally, the position of the northeast-southwest strike-slip fault zone could also be controlled by a preexisting basement structure (transfer faults from the rifting event associated with the formation of the underlying oceanic crust). The basement in this area is shallower (~5 km [~3 mi]) than that in the central part of the deep-water delta (up to 10–12 km [6–7 mi]) because the sedimentary overburden is wedging to the northwest and therefore becomes thinner than areas farther to the southeast on the delta lobe. The higher basement could act as a buttress that would confine the slide and control its dimensions.

Tear-fault systems in such a setting may provide probable structural traps for hydrocarbons and localize syndeformation sedimentation in a similar way to continental tear-fault systems. Deep-water sedimentation may be controlled, confined by such structures and migration pathways available through the many various fracture sets generated by structural deformation.

CONCLUSIONS

A complex strike-slip fault zone in the northwestern deep-water Niger Delta is composed of extensional, strike-slip, and reverse faults. The complex forms the northwestern lateral margin of the deep-water western Niger Delta, but comparable structures may occur at the margins of both sedimentary lobes of the Niger Delta, as well as in similar deep-water delta settings on other gravity-driven detachment systems. Situated at the lateral boundary of the translation domain, the lateral strike-slip domain links deformation between the extensional and compressional domains.

This article shows that the lateral margins of a regional-scale gravitational collapse provide clues in understanding the kinematics and timing of deformation between the extensional and compressional parts of such features. Regional lateral margins are structurally complex, but their evolution is predictable. They can also provide interesting structural traps in hydrocarbon exploration. We suggest that the position of the lateral strike-slip domain is either controlled by a modification of the underlying detachment properties and efficiency or that preexisting basement elements still influence the sedimentation and compartmentalization of gravitational collapse.

REFERENCES CITED

Armentrout, J. M., K. M. Kanschat, K. E. Meisling, J. J. Tsakma, L. Antrim, and D. M. McConnell, 2000, Neogene turbidite systems of the Gulf of Guinea continental margin slope, offshore Nigeria: Fine-grained turbidite systems, *in* A. H. Bouma and C. G. Stone, eds., Fine-grained turbidite systems: AAPG Memoir 72/SEPM Special Publication 68, p. 93–108.

Bilotti, F., and J. H. Shaw, 2005, Deep-water Niger Delta fold and thrust belt modeled as a critical-taper wedge: The influence of elevated basal fluid pressure on structural styles: AAPG Bulletin, v. 89, no. 11, p. 1475–1491, doi:10.1306/06130505002.

Blick, N.C., and K. Biddle, 1985, Deformation and basin formation along strike-slip faults: Strike-slip deformation, basin formation and sedimentation: SEPM, v. 37, p. 1–34.

Briggs, S. E., J. Cartwright, R. J. Davies, and R. Morgan, 2006, Multiple detachment levels and their control on fold styles in the compressional domain of the deep-water west Niger Delta: Basin Research, v. 18, p. 435–450, doi:10.1111/j.1365-2117.2006.00300.x.

Briggs, S. E., J. Cartwright, and R. J. Davies, 2009, Crustal structure of the deep-water west Niger Delta passive margin from the interpretation of seismic reflection data: Marine and Petroleum Geology, v. 26, no. 2, p. 404–410.

Brown, A. R., 2004, Interpretation of three-dimensional seismic data, 6th ed.: AAPG Memoir 42, 541 p.

Bull, S., J. Cartwright, and M. Huuse, 2009, A review of kinematic indicators from mass-transport complexes using 3-D seismic data: Marine and Petroleum Geology, v. 26, no. 7, p. 1132–1151.

Butler, R. W. H., and J. P. Turner, 2010, Gravitational collapse at continental margins: Products and processes: An introduction: Journal of the Geological Society (London), v. 167, p. 569–570, doi:10.1144/0016-76492010-003.

Casas, A. M., D. Gapais, T. Nalpas, K. Besnard, and T. Roman-Berdiel, 2000, Analog models of transpressive systems: Journal of Structural Geology, v. 23, p. 733–743.

Clark, I. R., and J. A. Cartwright, 2009, Interactions between submarine channel systems and deformation in deep-water fold belts: Examples from the Levant Basin, eastern Mediterranean Sea: Marine and Petroleum Geology, v. 26, no. 8, p. 1465–1482, doi:10.1016/j.marpetgeo.2009.05.004.

Cobbold, P. R., and P. Szatmari, 1991, Radial gravitational gliding on passive margins: Tectonophysics, v. 188, p. 249–289, doi:10.1016/0040-1951(91)90459-6.

Cobbold, P. R., B. J. Clarke, and H. Løseth, 2009, Structural consequences of fluid overpressure and seepage forces in the outer thrust belt of the Niger Delta: Petroleum Geoscience, v. 15, p. 3–15, doi:10.1144/1354-079309-784.

Cohen, H. A., and K. McClay, 1996, Sedimentation and shale tectonics of the northwestern Niger Delta front: Marine and Petroleum Geology, v. 13, p. 313–328, doi:10.1016/0264-8172(95)00067-4.

Corredor, F., J. H. Shaw, and F. Bilotti, 2005, Structural styles in the deep-water fold and thrust belts of the Niger Delta: AAPG Bulletin, v. 89, p. 753–780, doi:10.1306/02170504074.

Cunningham, W. D., and P. Mann, 2007, Tectonics of strike-slip restraining and releasing bends, *in* W. D. Cunningham and P. Mann, eds., Tectonics of strike-slip restraining and releasing bends: Journal of the Geological Society (London), v. 290, p. 1–12, doi:10.1144/SP290.1.

Damuth, J. E., 1994, Neogene gravity tectonics and depositional processes on the deep Niger Delta continental margin: Marine and Petroleum Geology, v. 11, p. 320–346.

Davies, R. J., 2003, Kilometer-scale fluidization structures formed during early burial of a deep-water slope channel on the Niger Delta: Geology, v. 31, p. 949–952, doi:10.1130/G19835.1.

Davies, R. J., C. J. MacLeod, R. Morgan, and S. E. Briggs, 2005, Termination of a fossil continent-ocean fracture zone imaged with three-dimensional seismic data: The chain fracture zone, eastern equatorial Atlantic: Geology, v. 33, p. 641–644, doi:10.1130/G21530AR.1.

Deptuck, M. E., Z. Sylvester, C. Pirmez, and C. O'Byrne, 2007, Migration-aggradation history and 3-D seismic geomorphology of submarine channels in the Pleistocene Benin-Major Canyon, western Niger Delta slope: Marine and Petroleum Geology, v. 24, p. 406–433, doi:10.1016/j.marpetgeo.2007.01.005.

Doust, H., 1990, Petroleum geology of the Niger Delta, *in* J. Brooks, ed., Classic petroleum provinces: Geological Society (London) Special Publication 50, p. 365.

Frey Martinez, J. F., J. Cartwright, and B. Hall, 2005, 3-D seismic interpretation of slump complexes: Examples from the continental margin of Israel: Basin Research, v. 17, p. 83–108, doi:10.1111/j.1365-2117.2005.00255.x.

Gaullier, V., and B. C. Vendeville, 2005, Salt tectonics driven by sediment progradation: Part II. Radial spreading of sedimentary lobes prograding above salt: AAPG Bulletin, v. 89, p. 1081–1089, doi:10.1306/03310503064.

Gaullier, V., Y. Mart, G. Bellaiche, B. C. Vendeville, T. Zitter, and Second Leg Prismed II Scientific Party, 2000, Salt tectonics in an around the Nile deep-sea fan: Insights from the PRISMED II cruise: Geological Society (London) Special Publication 174, p. 111–129.

Harding, T. P., 1974, Petroleum traps associated with wrench faults: AAPG Bulletin, v. 58, p. 1290–1304.

Harding, T. P., 1985, Seismic characteristics and identification of negative flower structures, positive flower structures, and positive structural inversion: AAPG Bulletin, v. 69, p. 582–600.

Heiniö, P., and R. J. Davies, 2006, Degradation of compressional fold belts: Deep-water Niger Delta: AAPG Bulletin, v. 90, p. 753–770, doi:10.1306/11210505090.

Lawrence, S. R., S. Munday, and R. Bray, 2002, Regional geology and geophysics of the eastern Gulf of Guinea (Niger Delta to Rio Muni): The leading edge, v. 21, p. 1112–1117.

Loncke, L., V. Gaullier, J. Mascle, B. Vendeville, and L. Camera, 2006, The Nile deep-sea fan: An example of interacting sedimentation, salt tectonics, and inherited subsalt paleotopographic features: Marine and Petroleum Geology, v. 23, p. 297–315, doi:10.1016/j.marpetgeo.2006.01.001.

Løseth, H., L. Wensaas, B. Arntsen, N.-M. Hanken, C. Basire and K. Graue, 2010, 1000-m-long gas blowout pipes: Marine and Petroleum Geology, v. 28, no. 5, p. 1047–1060, doi:10.1016/j.marpetgeo.2010.10.001.

Maloney, D., R. Davies, J. Imber, S. Higgins, and S. King, 2010, New insights into deformation mechanisms in the gravitationally driven Niger Delta deep-water fold and thrust belt: AAPG Bulletin, v. 94, p. 1401–1424, doi:10.1306/01051009080.

Martinsen, O. J., and B. Bakken, 1990, Extensional and compressional zones in slumps and slides in the Namurian of County Clare, Ireland: Journal of the Geological Society (London), v. 147, p. 153–164, doi:10.1144/gsjgs.147.1.0153.

Morgan, R., 2003, Prospectivity in ultradeep water: The case for petroleum generation and migration within the outer parts of the Niger Delta apron, *in* T. J. Arthur, D. S. MacGregor, and N. R. Cameron, eds., Petroleum geology of Africa: New themes and developing technologies: Geological Society (London) Special Publication 207, p. 151–164, doi:10.1144/GSL.SP.2003.207.01.08.

Morgan, R., 2004, Structural controls on the positioning of submarine channels on the lower slopes of the Niger Delta, *in* R. J. Davies, J. A. Cartwright, S. A. Stewart, M. Lappin, and J. R. Underhill, eds., 3-D seismic technology: Application to the exploration of sedimentary basins: Geological Society (London) Memoirs 29, p. 45–51, doi:10.1144/GSL.MEM.2004.029.01.05.

Morley, C. K., 2003, Mobile shale-related deformation in large deltas developed on passive and active margins, *in* P. Van Rensbergen, R. R. Hillis, A. J. Maltman, and C. K. Morley, eds., Subsurface sediment mobilization, Geological Society (London) Special Publication 216, p. 335–357, doi:10.1144/GSL.SP.2003.216.01.22.

Morley, C. K., and G. Guerin, 1996, Comparison of gravity-driven deformation styles and behavior associated with mobile shales and salt: Tectonics, v. 15, p. 1154–1170, doi:10.1029/96TC01416.

Peel, F. J., C. J. Travis, and J. R. Hossack, 1995, Genetic structural provinces and salt tectonics of the Cenozoic offshore U.S. Gulf of Mexico: A preliminary analysis: *in* M. P. A. Jackson, D. G. Roberts, and S. Snelson, eds., Salt tectonics: A global perspective: AAPG Memoir 65, p. 153–175.

Rowan, M. G., 2009, Lateral boundaries in deep-water, salt-detached fold and thrust belts: AAPG Hedberg Conference on deep-water fold and thrust belts: Tirrenia, Italy, October 4–9, 2009, http://www.searchanddiscovery.com/abstracts/pdf/2011/2009hedberg-italy/index.htm (accessed October 2011).

Rowan, M. G., F. J. Peel, and B. C. Vendeville, 2004, Gravity-driven fold belts on passive margins, *in* K. R. McClay, ed., Thrust tectonics and hydrocarbon systems: AAPG Memoir 82, p. 157–182.

Stewart, S., 1999, Geometry of thin-skinned tectonic systems in relation to detachment layer thickness in sedimentary basins: Tectonics, v. 18, p. 719–732, doi:10.1029/1999TC900018.

Treviño, R. H., and B. C. Vendeville, 2008, Origin of coast-perpendicular extensional faults, western Gulf of Mexico: The relationship between an early-stage ridge and a late-stage fault: AAPG Bulletin, v. 97, p. 951–964, doi:10.1306/03250807070.

Woodcock, N. H., and M. Fischer, 1986, Strike-slip duplexes: Journal of Structural Geology, v. 8, p. 725–735.

Woodcock, N. H., and C. Schubert, 1994, Continental strike-slip tectonics, *in* P. L. Hancock, ed., Continental deformation: Oxford, Pergamon Press, p. 251–263.

Marine and Petroleum Geology 43 (2013) 423–433

Contents lists available at SciVerse ScienceDirect

Marine and Petroleum Geology

journal homepage: www.elsevier.com/locate/marpetgeo

Fluid flow pipes triggered by lateral pressure transfer in the deepwater western Niger Delta

Amélie M. Leduc [a,*], Richard J. Davies [a], Richard E. Swarbrick [b], Jonathan Imber [a]

[a] CeREES (Centre for Research in Earth Energy Systems), Department of Earth Sciences, Durham University, Science Labs, Durham DH1 3LE, UK
[b] GeoPressure Technology, Rivergreen Centre, Aykley Heads, Durham City DH1 5TS, UK

ARTICLE INFO

Article history:
Received 5 January 2012
Received in revised form
4 December 2012
Accepted 17 December 2012
Available online 26 December 2012

Keywords:
Niger Delta
3D seismic
syn-Sedimentary deformation
Vertical pipes
Overpressure
Lateral pressure transfer

ABSTRACT

Using three-dimensional (3D) seismic data, we establish a simple model for the development of vertical fluid flow pipes in the deepwater western Niger Delta. We analyse two examples of fluid flow pipes that form vertical seismic chimneys that are 400–600 m wide and ~2000–2500 m in height, terminate at the current seabed and have bases located at the crest of rollover anticlines. In both cases we identify buried deepwater channels-complexes located below the pipes that formed prior to the growth of the rollover anticlines. The development of the anticlines caused tilting of these channel complexes and differential loading. We propose the channel complexes represent connected permeable reservoir intervals and that lateral pressure transfer caused the pore pressure at the crest of the structures to reach critical levels, leading to hydraulic fracturing of the overburden. Although hydrocarbons may migrate upwards through the chimney systems, they are not necessarily indicators that the channel complexes were gas or oil charged.

1. Introduction

The occurrence of fluid flow pipes is often linked to the presence of an active petroleum system (Grauls and Baleix, 1994; Ingram and Urai, 1999; Stewart and Davies, 2006; Cartwright et al., 2007) and therefore could be used as a hydrocarbon indicator (Grunau, 1987). Vertical fluid conduits above folds commonly occur in basins with high sedimentation rates (Huuse et al., 2010) on both active margins (Caspian Sea – Stewart and Davies, 2006; Trinidad – Deville et al., 2010; Brunei: Van Rensbergen and Morley, 2003) and passive continental margins, such as the Atlantic Ocean and Gulf of Mexico (Dugan and Flemings, 2000; Seldon and Flemings, 2005; Reilly and Flemings, 2010), the Nile delta (Loncke et al., 2004; Feseker et al., 2010), west Africa (Moss and Cartwright, 2010), and the Niger Delta (Graue, 2000).

Recent research has been focusing on the recognition of fluid flow pipes, mainly from seismic data (Cartwright, 2007; Cartwright et al., 2007; Moss and Cartwright, 2010). Løseth et al. (2010) also compared kilometer-scale fluid flow pipes in the Niger Delta to field examples in Greece. In such environments, it is generally considered that vertical escape pipes result from an escape of buoyant hydrocarbons (Cobbold et al., 2009; Løseth et al., 2010). But vertical conduit systems may be primed and triggered by pressure in reservoir intervals that develops due to the existence of structural relief and connected permeable strata (Bjørkum et al., 1998). The assumption that vertical conduits are the result of hydrocarbons causing seal failure may be erroneous (Bjørkum et al., 1998; Nordgard Bolas and Hermanrud, 2003; Heggland, 2005).

This paper considers the structural and stratigraphic setting of two significant fluid flow pipes in a deepwater environment in order to assess the geological processes leading to critical pressuring and vertical fluid flow. We develop a simple, generally applicable model for a how fine grained deepwater sedimentation, channel development and fold growth, can lead to the establishment of overpressure and catastrophic seal failure without the requirement for a hydrocarbon column.

1.1. Overpressure

High sedimentation rates cause a rapid increase in the vertical stress that is applied onto the stratigraphic column and leads to sediment compaction. In low permeability sediments, pore fluid is prevented from escaping and the lithostatic load is imposed upon

* Corresponding author. Present address: Total S.A., 2, place Jean Millier, La Défense 6, 92078 Courbevoie, France. Tel.: +44 7503188659.
E-mail addresses: amelie.leduc@durham.ac.uk, amelie.leduc@total.com (A.M. Leduc).

0264-8172/$ – see front matter © 2012 Elsevier Ltd. All rights reserved.
http://dx.doi.org/10.1016/j.marpetgeo.2012.12.005

it. This process is known as disequilibrium compaction (Dickinson, 1953) and is the main cause of overpressure in mudstone-rich Cenozoic basins deltas (Swarbrick and Osborne, 1998). Tilting of permeable reservoir intervals can also cause overpressure due to lateral pressure transfer (Yardley and Swarbrick, 2000), otherwise known as the centroid model (Traugott and Heppard, 1994; Finkbeiner et al., 2001). Lateral pressure transfer is characterized by an upward increase in the pressure gradient, in a sealed reservoir at hydrostatic pressure, as a response to the reservoir interval tilt. In this case study, permeable reservoirs are preserved sands from deepwater turbidite channels and structural deformation is a potential source of lateral pressure transfer.

Fluid flow due to lateral pressure transfer in permeable reservoirs can contribute significantly to increasing pore pressure at the crest of the reservoir (Reilly and Flemings, 2010). At a depth termed the centroid depth, pressure is balanced within the reservoir, between the section of the reservoir that is above and below the centroid depth (Traugott and Heppard, 1997). Pressures can reach the pressure required to cause hydraulic fracturing (Fig. 1). Pore pressure and horizontal stress are coupled (Mourgues and Cobbold, 2003) and can be quantified from well data (Mourgues et al., 2011). Well data were not available for publication in this study, we therefore use estimated pressure values based upon well-known and established gradients, such as the hydrostatic gradient, and the shale gradient combined with the minimum stress gradient, estimated from geological analogues (Heppard et al., 1998; Nashaat, 1998; Swarbrick and Osborne, 1998; Tingay et al., 2009).

1.2. Fluid flow pipes

A hydraulic fracture should develop perpendicular to the direction of minimum compressive stress (Secor, 1965; Hubbert and Willis, 1972). Fluid conduits will form if sufficient pressure is present to reach the hydraulic fracture pressure and breach the caprock of a given reservoir interval (Fig. 1). This mechanism has been recognized in previous studies on vertically-focused fluid flows (Hovland and Judd, 1988; Miller, 1995).

Fluid flow pipes can be identified on 3D seismic data as subvertical zones of disturbed reflection or stacked amplitude anomalies (Cartwright, 2007). They can bypass hydrocarbons seals (Cartwright et al., 2007). They were first described in the Niger Delta by Løseth et al. (2010), and literature in the past decade has considered how to recognize fluid flow pipes from 3D seismic data and their morphological, lithological and seismic character (Davies, 2003; Cartwright, 2007; Cartwright et al., 2007 Huuse et al., 2010; Moss and Cartwright, 2010; Løseth et al., 2010).

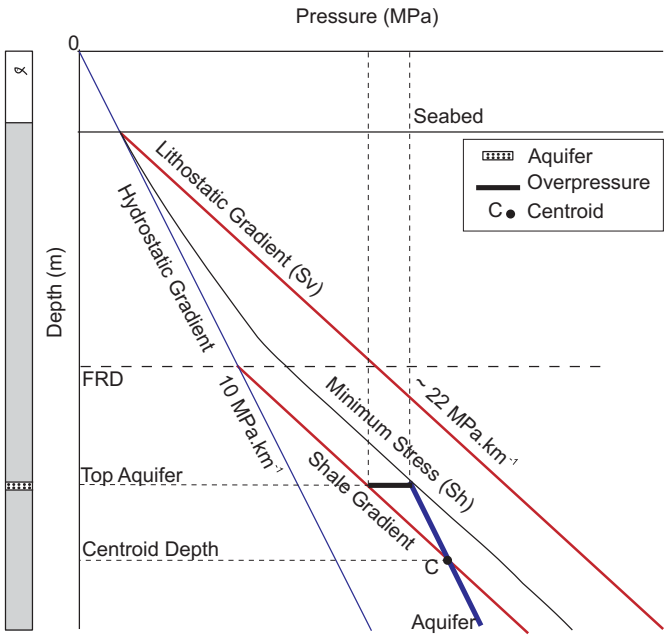

Figure 1. Theoretical pressure–depth plot showing the parameters taken into account to determine overpressure in this case study showing hydrostatic, lithostatic and shale gradient. The shale gradient is drawn from the fluid retention depth (FRD), representing the top of overpressure in the overburden and is function to the local sedimentation rate. The minimum horizontal stress (Sh) is indicated for a structural setting in extension; gradient is obtained from Grauls (1999) and Deville et al. (2010).

1.3. Geological setting

The deepwater western Niger Delta, Gulf of Guinea (Fig. 2A) is a mud-rich Cenozoic prograding sedimentary accumulation, where updip extension expressed by regional-scale growth faults is linked to downdip compression with fold-and-thrust belts (Doust and Omatsola, 1990; Morley and Guerin, 1996). This historically has been considered to occur at the first development of overpressure coincident with detachment faults (e.g. Briggs et al., 2006). The 7–10 km-thick succession was deposited from the middle Miocene to the Holocene (Short and Stauble, 1967). It is part of the Agbada and the Benin Formations. In cross-section, the seismic signature is characterized by mid to high amplitude reflection packages, including, high amplitude parallel to chaotic lenses associated with channel–levees complexes. Deposition of sediments at high rates leads to rapid loading and in low permeability sediment can cause overpressure. Unpublished well data in the study area provide an estimate of about 2000 m in 11.6 Ma (approximately 160 m My^{-1}). Overburden undergoes gravity-driven deformation above deeply buried, overpressured strata (Cobbold et al., 2009). Smaller-scale deformation caused by overpressure and sediment remobilization also occurs, for instance fluid flow pipes and mud volcanoes (Graue, 2000; Heggland et al., 2001; Kopf, 2002) and kilometre-scale fluidization features (Davies, 2003) have been described.

1.4. Structural setting

The area of study is located at the periphery of a major growth fault and a lateral strike-slip fault that developed contemporaneously (Fig. 2B). Here extension, strike-slip deformation and compression are kinematically linked (Leduc et al., 2012). Deformation occurred in several stages as the study area was located within the contractional domain of a regional gravity detachment system in the Miocene. A period of reorganization of the regional system then resulted in the development of strike-slip faulting at the margins of the gravitational detachment lobes, resulting in the growth of E–W to NE–SW oriented elongated structures. Finally, more recent delta progradation and resulting structural evolution triggered regional, coast-parallel normal and growth faulting which structures orientation is approximately WNW–ESE.

2. Data and methodology

We use three seismic volumes located in water depths of between 500 and 2000 m on a southwest-dipping slope and cover an area of 4300 km^2. The surveys were acquired in 1998 with a bin spacing of 12.5 m by 18.75 m. Data are zero-phase migrated and are displayed in two-way travel time (twt), with a vertical resolution of about 10–20 m at the depth of our seismic interpretation. The dominant frequency is ~45–50 Hz. We interpret four regional horizon reflections (named 1, 2, 3 and 4) from the deepest to the shallowest (Fig. 3A and B) mapped around a sub-circular structural high. These horizons delineate five stratigraphic units from

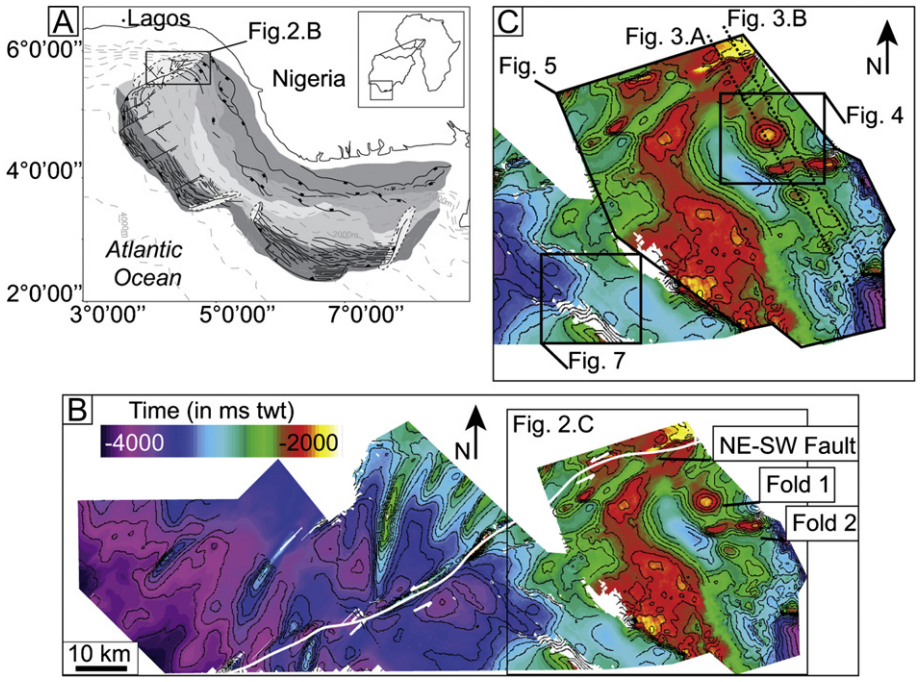

Figure 2. Location maps. A. Location of the study area in the western Niger Delta. B. Time contour map (at depth of horizon 2) showing the structural setting of the area and the location of fold 1 and fold 2. "ms twt" in this and subsequent figures – milliseconds two-way time. C. Location of Figures 3, 4, 5 and 7.

a regional detachment level to the seabed (A, B, C, D and E from the deepest to the shallowest units). Mapping has been carried out by auto-dip tracking of maximum (high amplitude) reflections. A full stack amplitude volume is available for all the seismic surveys. We use interpreted time-structure and time thickness maps (isochron maps) and seismic attributes such as RMS (Root Mean Square) amplitude extractions along the selected horizons with a view to interpret the structural evolution and locating channel migration pathways (Brown, 2011).

To estimate overpressure, we need to know: (1) the lithostatic and hydrostatic gradient; (2) the sedimentation rate, and as a result, the fluid retention depth (FRD), obtained from the empirical relationship established by Swarbrick et al. (2002). This allows one to locate the shale gradient, which represents the pore pressure within the shale, a lithostatic-parallel gradient originating from the FRD (Fig. 1). The numbers used to build the graphical interpretations were obtained by converting the measured depths (in ms twt) into metres using a velocity of 1800 m s^{-1} at the seabed and increasing up to 2100 m s^{-1} at ~1000 ms twt below the seabed reflection, then up to 2500 m s^{-1} at ~1500 ms twt below the seabed reflection, and up to ~3000 m s^{-1} at ~2800 ms twt below the seabed (after Morgan, 2003). In this paper we use the term reservoir to refer to porous and permeable strata where the pore fluid is either gas or water.

3. Observations

3.1. Folds 1 and 2

Fold 1 is a buried sub-circular structure located approximately 12 km southwest of a major listric normal fault and ~10 km south of the lateral boundary of the sedimentary lobe defined by a NE–SW trending strike-slip fault system (Fig. 2A and B). The fold is a symmetrical, positive structure ~5000 m in diameter, with a relief of ~800 m, occurring between 2500 m and the seabed (Figs. 3A and 4). Seismic imaging of the core of the fold is poor below horizon reflection "1"; however we identify fault traces and a thickened package that suggest a structural thickening of the deepest units (Fig. 3A, package A, and Maloney et al., 2010). Onlaps indicating growth of the structure are observed above horizon reflection "3" and the seabed. High amplitude reflections at the crest of the structure suggest the presence of a high amplitude feature at the seabed (Figs. 3A and 4).

A second anticline (fold 2) is located to the south of fold 1 (Fig. 3B) in a comparable structural setting, although its geometries are more elongated in a NE–SW direction. Its hinge is 15 km-long and it is 3 km wide from north to south (Fig. 2C). A low-reflectivity unit disturbed by sub-vertical features is found at the base of fold 2. They are interpreted as either compressive or strike-slip, east–west oriented, fault traces that develop over the detachment (Leduc et al., 2012).

3.2. Channel complexes at folds 1 and 2

Assuming that sedimentation rates are spatially uniform, isochron maps from packages A to E show the evolution of the position of depocentres in the area of folds 1 and 2 (Fig. 5). Contemporaneous with the development of the NE–SW strike-slip fault zone, deposit progressively thin out northwards (Fig. 5, isochron maps A to E). Similarly the development of a syncline to the southwest of folds 1 and 2 is observed at later stages (Fig 3A and B, packages C to E). Areas where the youngest package E is thinner suggest that a bathymetric high prevented sediment deposits from being deposited or preserved above folds 1 and 2 (Fig. 5, unit E).

Five channels are identified to the north and south of fold 1 (Fig. 6). Two different types of sediment pathways developed. At earlier stages all channels are low-sinuosity (Fig. 6, map A). These channels are mud-filled and levee deposits are fine-grained (Fonnesu, 2003). No deflections of the sediment routes are found around fold 1 (Fig. 6, maps A and B). A reorganization of the channels network appears at later stages (Fig. 6, maps C and D) and channels were clearly deflecting around a bathymetric high.

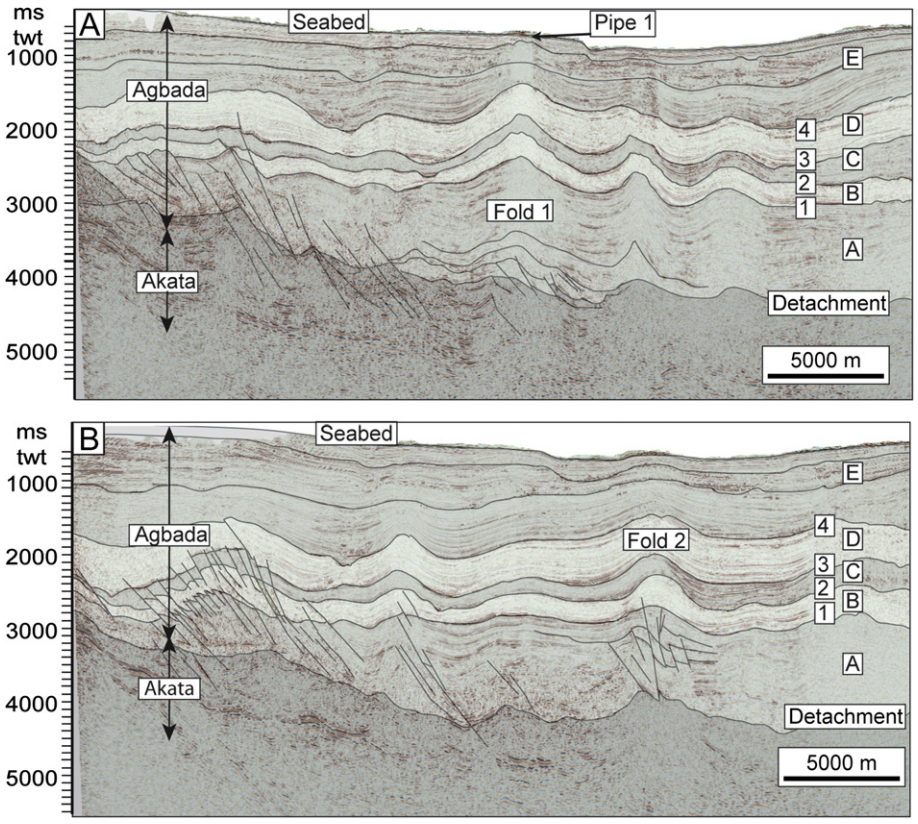

Figure 3. A. Seismic section across fold 1, perpendicular to dip direction. B. Seismic section parallel to A, across fold 2 and perpendicular to dip direction. Both seismic sections show the general structural trends and units A, B, C, D and E which time-thickness (isochron) maps are shown on Figure 6.

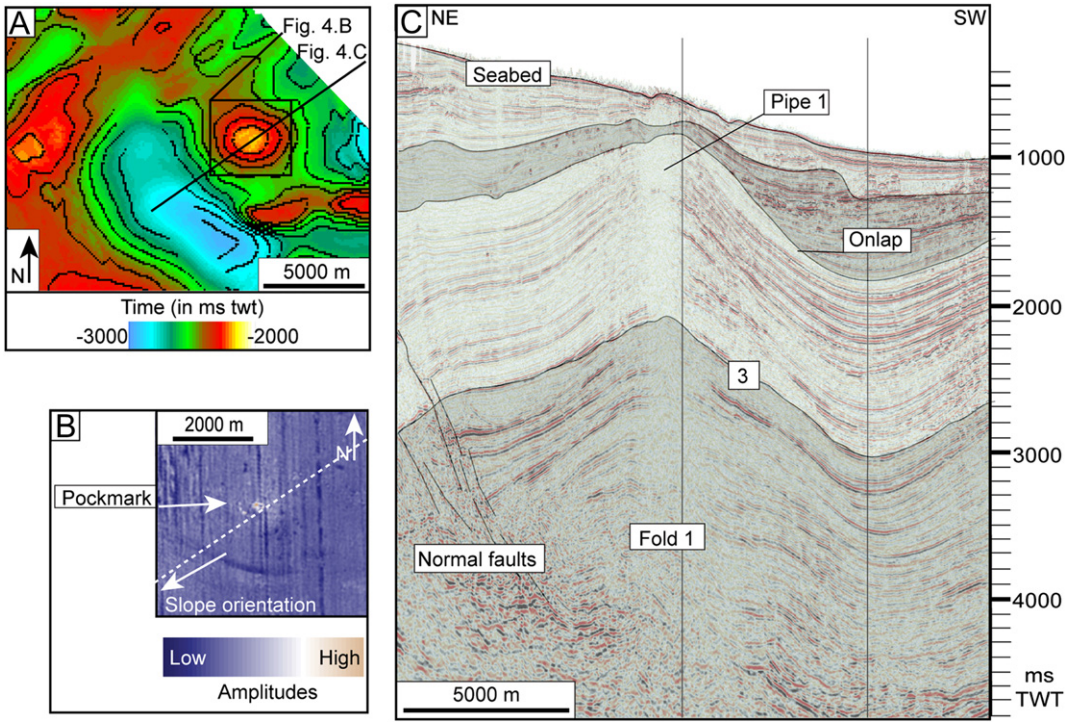

Figure 4. Seismic section showing the fluid flow pipe 1, at the top of fold 1. A seabed amplitude extraction map shows the pockmark at the top of pipe 1 (high amplitude is white to brown; lower amplitudes are shown in blue). "3" refers to the nomenclature presented in Figure 3; this horizon embeds "channel 2" shown on Figure 7. (For interpretation of the references to colour in this figure legend, the reader is referred to the web version of this article.)

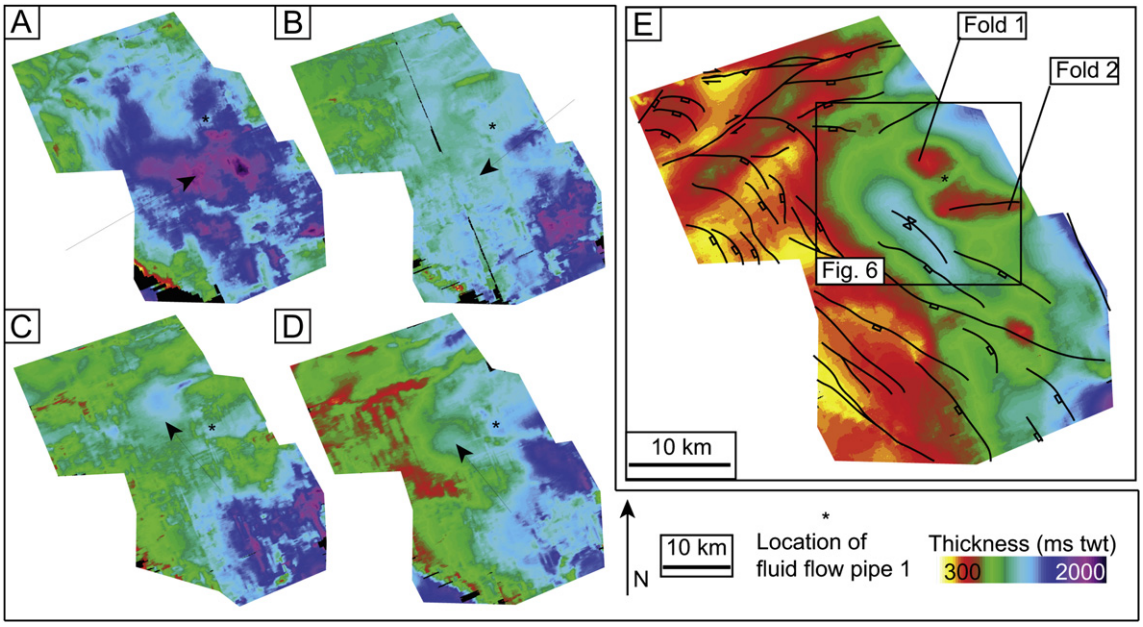

Figure 5. Time thickness maps in the folds 1 and 2 areas for each unit (A, B, C, D and E, over which are represented the main structural trends) defined in Figure 3A and B. Red to yellow indicates thicker areas, blue to purple shows thinner areas. The asterisk shows the location of the fluid flow pipe; the arrows indicate areas where an important change in thickness trend is observed between the previous and the actual map. (For interpretation of the references to colour in this figure legend, the reader is referred to the web version of this article.)

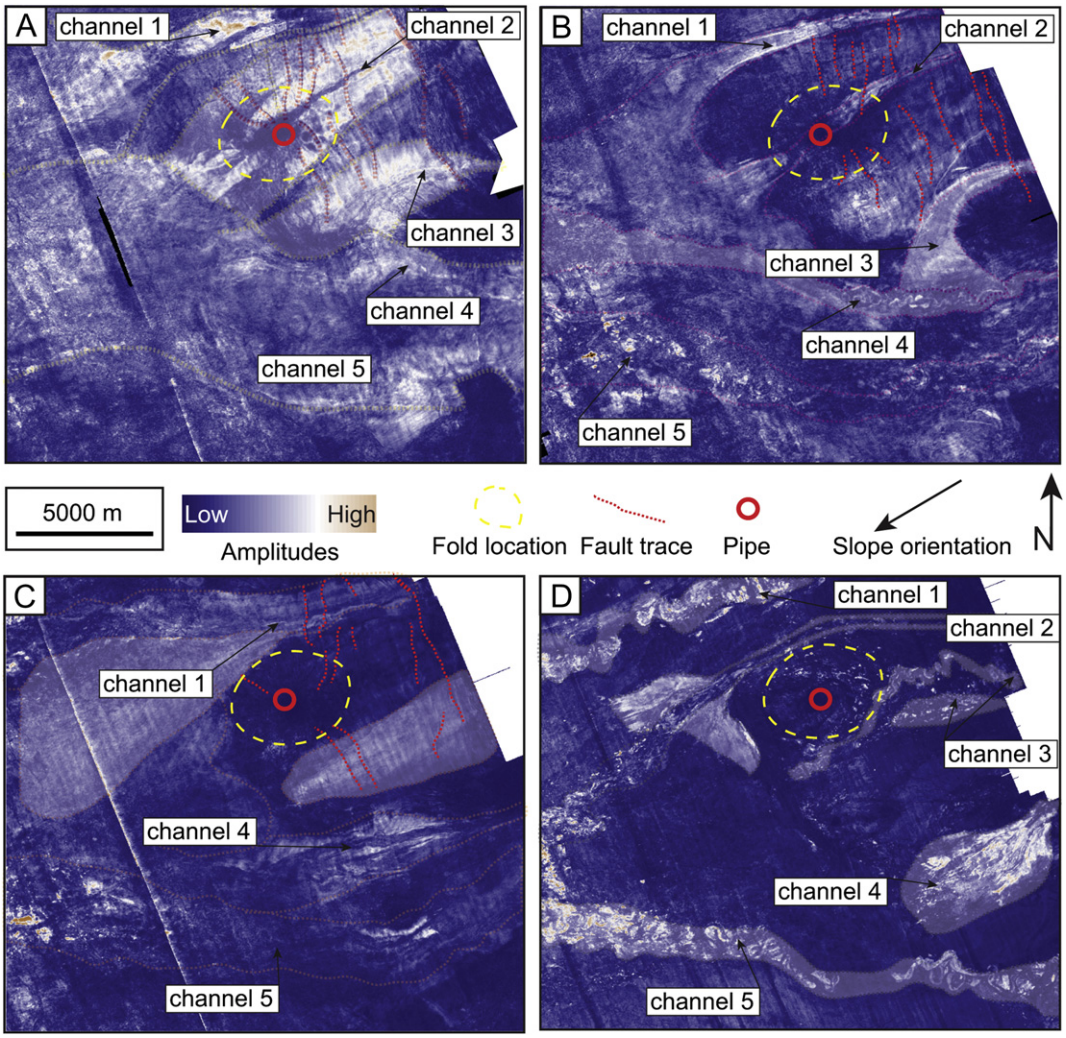

Figure 6. Amplitude extraction maps of horizons A, window: −100+100 ms twt, B, window: −10+80 ms twt, C, window: −10+60 ms twt and D, window: −0+80 ms twt. Red circle indicates the position of the fluid flow pipe 1. Dashed red lines indicate faults and dashed yellow line the position of fold 1. (For interpretation of the references to colour in this figure legend, the reader is referred to the web version of this article.)

3.3. Pipes 1 and 2

A roughly circular high amplitude region of the seabed is apparent at the crest of fold 1 (Figs. 2C and 3). It is underlain by a vertical area of low-reflectivity that extends from the seabed to a depth of 2100 ms twt (approximately 2625 m). A lack of seismic reflectivity is interpreted as an indicator for the presence of gas. Evidence for bottom-simulating reflections and similar amplitude anomalies can be observed at the periphery of the pipe, occurring at depths of approximately 495 m (or 400 ms twt) below the seabed (Fig. 4). It is an approximately cylindrical feature ~650 m in diameter. A similar feature is observed downdip (pipe 2, Fig. 7). Their structural and stratigraphic setting are comparable, as well as their dimensions (~450 m diameter at the seabed; ~1965 m in height). Both are also located above an anticline structure. At pipe 1, the flexure generated a relief of 1340 m between the lowest point (at 3050 ms twt, or 3965 m depth burial) and the highest point (at 2100 ms twt, or 3965 m depth burial) of the channel complex (Fig. 8A). At pipe 2, a relief of ~800 m is measured between the top of the reservoir interval located (2500 ms twt or 3250 m depth burial) and the lowest point (at 3000 ms twt or 4050 m depth burial, Fig. 8B). The channel located below pipe 2 appears as a package of high amplitude, chaotic reflections (Fig. 7). RMS amplitude extraction of the channel shows meandering geometries with low amplitude reflection, indicative of a mud fill in the core of the channel complex and high amplitudes on each side (levee deposits). Both channel complexes can hold potential reservoirs for water and/or hydrocarbon accumulation indicated by very high amplitude reflections (white to brown).

4. Interpretation

4.1. Fluid flow pipes

These observations argue for a fluid escape feature (Cartwright et al., 2007), however there is no evidence for mud flows at the near-surface and no evidence for a buried or active edifice. We herein term the feature a fluid flow pipe (pipes 1 and 2, Figs. 4 and 7) although we recognize that this term does not reflect the likely complexity of the structure (e.g. Morley, 2003). At the seabed a high amplitude reflection may indicate the development of a chemosynthetic community, gas hydrates, or a local seabed diagenetic effect at the summit of the pipe, arguing for gas escape. In both cases a growth package and the presence of normal fault traces support the hypothesis that these structures are rollover anticlines. We propose that there were a series of deformation episodes within this strike-slip domain, and then extension led to the formation of this sub-circular feature. Near-seabed growth packages suggest recent activity of the growth fault (onlapping reflections marked on Figs. 4 and 7, growth strata visible in packages D and E). The vertical pipes then develop in an analogous structural setting and over similar pre-existing depositional features. High amplitude reflection packages, interpreted as channels, are found at the base of the vertical zones of low reflectivity in both cases. In plan view, a low-sinuosity channel located at the base of pipe 1 is identified. Internal low amplitude reflections indicate a mud fill whereas the channel body is interpreted to be fine-grained sand (Fonnesu, 2003). The associated levee deposits display high amplitude reflections (channel 2, Fig. 6).

4.2. Development of fold 1

Fold 1 is sub-circular. Several geological mechanisms can form circular structures, for example diapirs (salt or “mobile shale”), volcanic calderas (magmatic or mud volcanism as a result of overpressure), rollover anticlines, compressive or strike-slip pop-ups (Stewart, 1999). Similar structures have been termed “shale diapirs” (Cohen and McClay, 1996; Kopf, 2002), but with higher-resolution data, it is possible to identify an east–west compressive or strike-slip structure at the core of fold 1. We propose that the slight east–west elongate irregularity may be inherited from early stages of strike-slip deformation as seen in fold 2. It could have

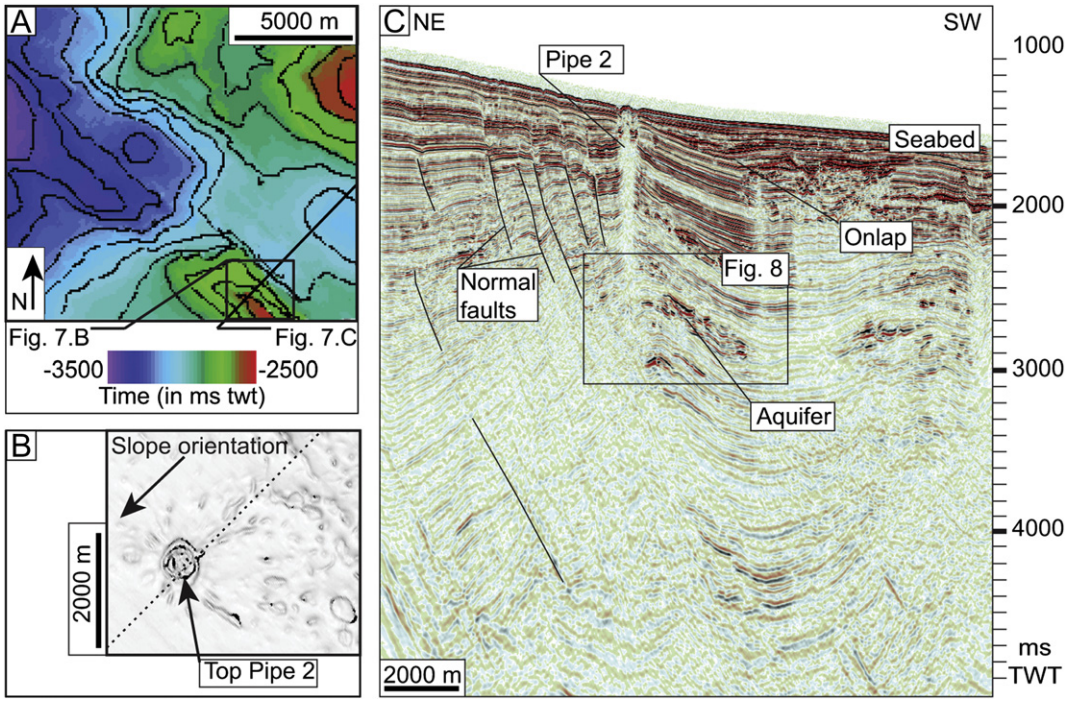

Figure 7. Pipe 2. A. Time contour map (see Fig. 2) locating the following sections. B. Seabed dip map showing the pockmark at the top of pipe 2. C. Seismic section across pipe 2. The potential source of overpressured fluids for this pipe is inferred to be the tilted reservoir interval shown in details in Figure 8.

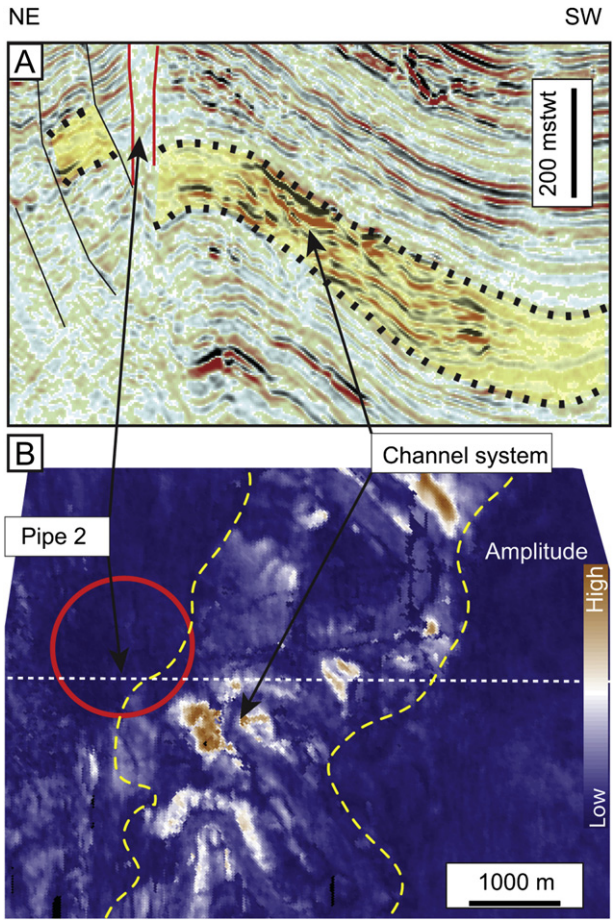

Figure 8. A. Details of the reflections at the level of the reservoir below pipe 2 (area coloured in red; see full section on Fig. 7). B. Amplitude extraction map from a window between the top and the bottom reservoir interval reflections (indicated with dashed lines and highlighted in yellow). High amplitudes are shown in white to brown; lower amplitudes in blue. A meandering channel-levee system can be identified; high amplitudes being located in the potential channel-fill deposits. The fluid flow pipe stands just east of the high amplitude pattern; a discrete fault network possibly links the two. Reverse polarity high amplitudes could suggest the presence of a hydrocarbon-water contact in the reservoir. (For interpretation of the references to colour in this figure legend, the reader is referred to the web version of this article.)

formed as the region underwent the early stages of strike-slip deformation, evidenced by the development of the NE–SW strike-slip fault to the northwest. This deformation event may be followed by a regional extensional event which took place to the northeast of the study area. This later event resulted in the development of growth fault-related rollovers, which may modify the overall geometries of pre-existing structures. Finally, the occurrence of pipe 1 postdates the development of the fold, but is contemporaneous with normal fault growth. It is thought to be contemporaneous to mud volcanism activity, which has been reported in the Pliocene and at present day in other locations of the deepwater delta (Kopf, 2002).

The structural development of fold 1 can be explained in two steps. Evidence for the existence of a growing positive topographic feature is found from seismic reflection amplitude attribute maps (Fig. 6). A channel (marked channel 2, Fig. 6) is identified from a series of time thickness maps calculated between the interpreted horizons. It is deflected around the position of Fold 1 between maps B and C, and that trend is even cleared during the later stages of deposition (Fig. 6, map D). Time thickness maps (Fig. 5) confirm a localized thinning in the area of Fold 1 but only seen on the isochron map for the most recent sedimentation (Fig. 5E). This observation matches the observations from seismic data showing onlap geometries in the overlying sediment package (Fig. 7). However, deposition of sediment packages is not strongly disturbed and the structure is shallow enough for sedimentation to continue at its crest. As a result two episodes of growth are identified, one in the Late Miocene and one between the Pliocene and present day. These observations suggest the following three hypotheses. Either folds 1 and 2 start to grow after the channels deposition, or their rate of uplift is much lower than the rate of burial. It is also possible that another mechanism deforms the upper units (such as differential compaction).

We associate the early stage of fold 1 growth with an earlier stage of the evolution of the gravitational collapse when this area was located in a compression setting. In a second stage, as a result of the delta progradation seaward the structural domains migrate to deeper parts of the basin and the area from then on is in the position of the translational domain, close to the extensional domain. Fold 1 is incorporated at the northern tip end of a large rollover anticline (Fig. 6E) and updip growth strata (Fig. 4) indicate the presence of a large associated normal fault.

4.3. Pore pressure

The porosity of the generally fine-grained sediments is estimated to be 60–70% at the seabed, and is reduced to 40% by compaction at a depth of 800 m (Janik et al., 1998). The density of mud is taken to be 2.1 g cc^{-1} (Janik et al., 1998) and the density of water is 1.03 g cc^{-1}. The hydrostatic gradient is approximately 10 MPa km^{-1}; the lithostatic gradient is estimated to be 22 MPa km^{-1} and the horizontal stress at ~18.2 MPa km^{-1}, as the ratio between the horizontal to the vertical effective stress are estimated to give a fracture gradient of 0.85 which is typical for a basin that is undergoing little extension, similar to Trinidad (Heppard et al., 1998; Deville et al., 2010), the Nile delta (Nashaat, 1998), and Brunei (Tingay et al., 2009). This value is also predicted from the model of Grauls (1999), who proposed that a predictable correlation exists for the maximum fluid pressure value, between the minimum principal stress and depth, for a given tectonic regime, which is, for this study is extensional. Finally, the fluid retention depth (FRD) is expected to be found in a depth interval between 700 and 1400 m below the seabed given the sedimentation rate of approximately 160 m My^{-1} (Swarbrick et al., 2002; Davies, 2003).

Development of fold 1 generated uplift. This uplift, associated to the tilting of the reservoir interval is thought to cause an increase in pore pressure within the reservoir at the base of pipe 1, within channel 2 (Fig. 7, horizon 3; Fig. 6B, marked “channel 2”). Uplift by the tilting of the footwall is a likely cause for lateral pressure transfer (Yardley and Swarbrick, 2000). In addition, no significant evidence for erosion is found at the crest of the anticline, which does not allow arguing for a significant change in reservoir pressures before the pipes formation. For both pipe 1 and pipe 2 systems, it is possible to calculate the amount of overpressure required in each reservoir interval to come sufficiently close to the minimum horizontal stress to generate a fracture (Fig. 9). A graphic construction is proposed in order to define the centroid depth. We present results for pipe 1 (Fig. 10A) and pipe 2 (Fig. 10B). A centroid depth between 3000 m (for a FRD located 700 m below the seabed) and 3850 m (for a deeper FRD, Fig. 10A) is required for Sh min to be reached at the base of pipe 1 escape system, and of at least 3600 m for pipe 2 escape system (Fig. 10B). A difference in overpressure of about 4–13 MPa is required to reach hydraulic fracturing for pipe 1 (Fig. 10A), and 5 MPa of additional overpressure are required for pipe 2 to reach fracturing. In this estimation we do not include the

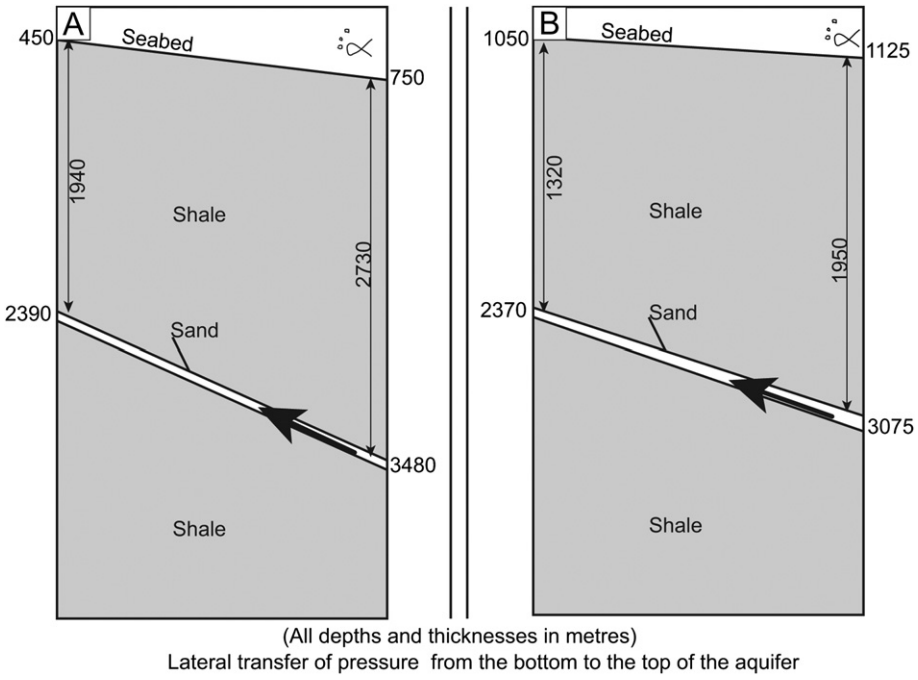

Figure 9. Lateral pressure transfer in a given reservoir. A. Values measured for pipe 1. B. Values measured for pipe 2. In this model, the reservoir is inferred to be a tilted sand body confined in a shale succession. Black arrow denotes lateral pressure transfer. Depths are calculated after Morgan (2003).

role of extensional faults close to the crest of the fold as their role in the release of fluid and lowering of overpressure cannot be estimated from our available data. However, if one assumes these faults could also be used for fluid circulation, the estimated required overpressure for pipe 1 and 2 would be inferior to the above estimated figures. In our case study the lack of relevant data prevents from specifying the role of fault as conduits, which can be estimated in analogue studies, and may help in carrying a full forward model (e.g. Hustoft et al., 2010).

5. Discussion

5.1. Source of overpressured fluids

There are at least two potential sources of overpressured fluids. A deep source of overpressured fluids had been discussed by previous works (Graue, 2000; Cobbold et al., 2004, 2009; Løseth et al., 2010). They suggested that, in the Niger Delta, hydrocarbon cracking at depth would provide a suitable source to generate overpressure in deep reservoir intervals. It is possible that fluids coming from deeper strata migrate to shallower reservoirs in the overburden through a connected detachment fault network (Maloney et al., 2010). However, a combination of disequilibrium compaction and lateral pressure transfer processes could also well explain the presence of shallower overpressure without the need of a large amount of overpressured fluids migrating from deep strata. This shallower source of overpressured fluids would be more likely to generate the studied fluid flow pipes.

5.2. Role of gas

There is evidence for the presence of gas in the pipe and at its periphery. At depth, hydrocarbon accumulation, and specifically gas, is likely to be trapped in sandstone reservoirs which were deposited within deepwater channel deposits. The presence of hydrocarbon accumulations can easily be observed from high amplitude reflections associated with a flat spot on seismic section (Fig. 8). If a vertical failure occurs at the top of these hydrocarbon-filled reservoirs, then this accumulation could escape through a fluid escape pipe. It does however not demonstrate that the hydrocarbon accumulation actually caused the initiation of the failure at the reservoir–caprock interface Hydrocarbon buoyancy, as well as water within a given reservoir modifies the effective stresses by increasing the fluid pressure equidirectionally, but to breach the seal, the failure conditions must be met. An increase in fluid pressure can drive a fluid-filled fracture (e.g. Flemings et al., 2003). Under such conditions grains can separate, allowing seal breaching and fluid escape. Caprock hydraulic fracturing can then occur once the pore fluid pressure exceeds the minimum stress, added to the tensile strength perpendicular to the direction of minimum stress (Hubbert and Willis, 1972; Jolly and Lonergan, 2002; Reilly and Flemings, 2010). Lateral pressure transfer (the centroid model) can help predicting higher pore pressures in a fluid-filled sand body included in a sealing, impermeable shale-rich environment, when structural relief (e.g. caused by tilting) triggers a differential sedimentary loading over the sand body. As a result a hydrostatic pressure gradient parallel to the slope of the hydrostatic gradient develops in the sand body (Traugott and Heppard, 1994; Yardley and Swarbrick, 2000). The lateral transfer of pressure then can locally enhance pore pressures at structural crests (Swarbrick and Osborne, 1998). Mechanically, the lateral transfer of pressure within a tilted reservoir interval can explain the initiation of a vertical failure in this presented case study, with or without the presence of hydrocarbon. The role of hydrocarbon, and gas in particular, in this model, would be limited to the actual propagation of the vertical pipe towards the surface, by escaping of buoyant gas initially present in the reservoir. Rodgers et al. (1999) also suggest that, as an application to Newton's third law of conservation, it can be predicted that hydraulic fracturing is not more likely to occur in gas reservoirs than in water-filled reservoirs. As a result the role of gas is limited to bring the overpressured fluids through the pipe towards the surface. This would explain how the

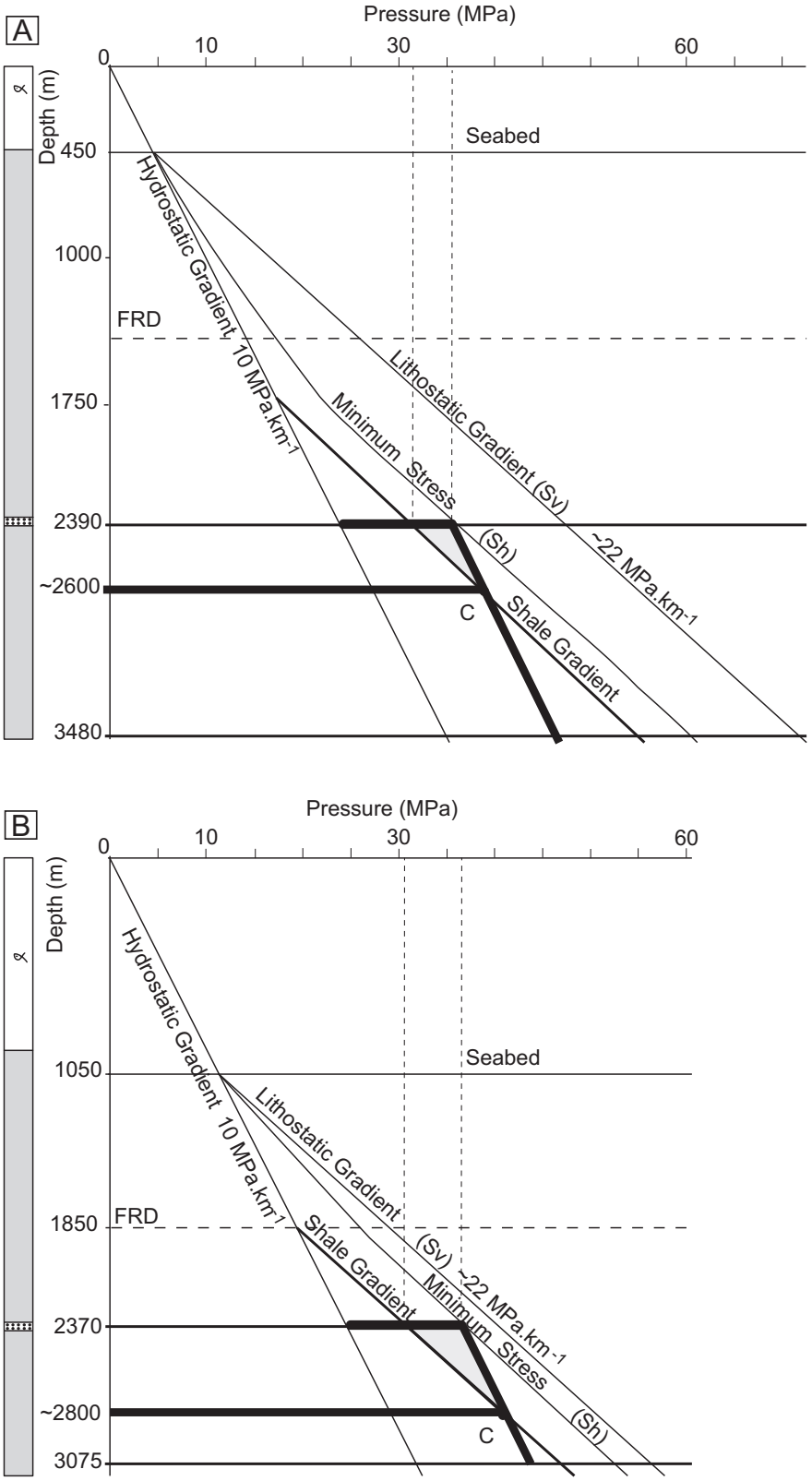

Figure 10. Pressure (MPa) versus depth (m) plot showing the position of the reservoir and the amount of overpressure required to reach the fracture pressure for the case of pipe 1 (A) and pipe 2 (B). FRD (1) – the shallowest estimated fluid retention depth – FRD (2) – the deepest estimated fluid retention depth. The thick, longer horizontal line represents the estimated depth of the centroid (C), located at the intersection between the shale gradient and the hydrostatic-parallel gradient within the reservoir. The thick, shorter horizontal line indicates in case A, the maximum amount of overpressure required to reach seal fracture (~13 MPa), with a FRD located at its deepest, whereas case B shows the opposite situation where a minimum of 4 MPa are required to reach fracture pressure, with the FRD given at its shallowest.

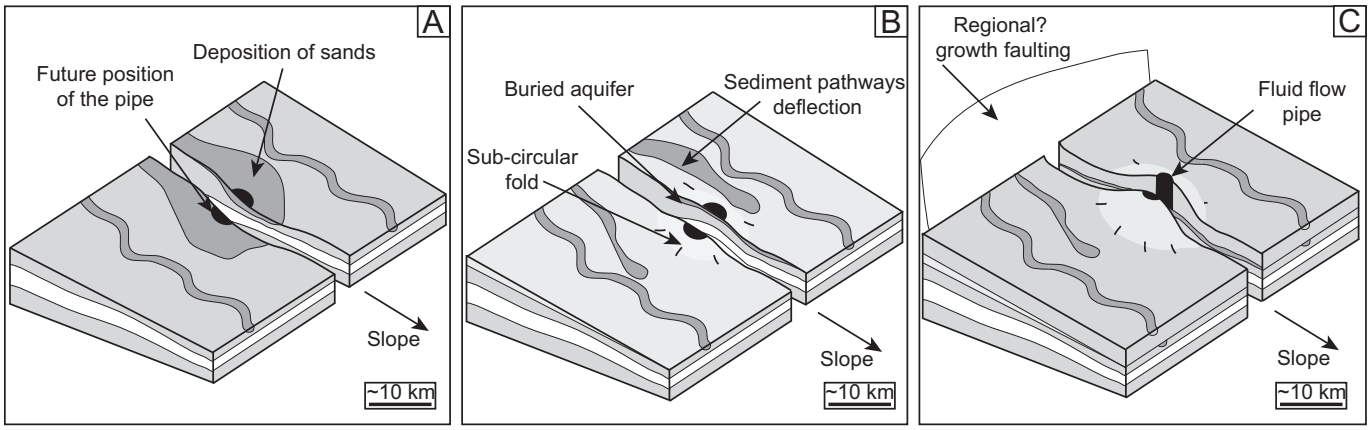

Figure 11. Summary block diagram. A. Deposition of channel complexes downslope. B. Early stage of uplift (i.e. first stage of folding for fold 1; this stage is not observed on the structure of pipe 2). C. Late stage of folding generating enough tilting for the fluid flow pipe to form at the crest of the structure.

pipe propagates vertically to the surface, and why leaking gas may be observed within and at the top of the pipe. This model thus suggests that the effect of hydrocarbon buoyancy needs not be involved to create the pore pressure required for failure (Bjørkum et al., 1998).

Hydrocarbons present in the pores are also buoyant and an increase in volume triggered by their cracking can contribute to an increase in overpressure (Osborne and Swarbrick, 1997; Swarbrick and Osborne, 1998; Grauls, 1999). They are thought to be the main cause of regional overpressure in the deepwater Niger Delta (Cobbold et al., 2009). In this study, however, hydrocarbon accumulation at these depths would not reach a temperature high enough to generate hydrocarbon cracking. We therefore prefer the lateral pressure transfer mechanism for the formation of such large scale fluid flow pipes. Numerous other smaller vertical pipes (less than 1 km long in cross-section) are present; however their formation is not specifically assigned to lateral pressure transfer. Pipes 1 and 2 share two main location characteristics: above a potential reservoir and at the crest of a steep structural high. This has implications in terms of reservoirs integrity as, even though such reservoir intervals may constitute interesting prospects in oil and gas exploration, it is necessary to be careful about the critically pressured state of these objects.

5.3. Model

The chronology of deposition, structural deformation and overpressure development is: (a) first, sedimentation through deepwater clastic-filled channels, including fine sand deposits in a shale-rich succession occurs, and deepwater channels become quickly buried due to rapid loading; (b) overpressure builds up and regional-scale gravitational collapse triggers structural deformation, including rollover anticlines. Local subsidence or uplift causes a local rearrangement of sediment pathways at the periphery of the structure; (c) as structures grow, tilting of the underlying sediments increases and potential overpressured reservoirs – bearing water with or without hydrocarbon accumulation – undergo a redistribution of pressure, a lateral transfer towards the highest point of the reservoir. Structural deformation might also generate a fracture network allowing fluids from deeper reservoir intervals to migrate to a higher position in the stratigraphic succession, which is not seen on the interpreted data. Finally the pressure gradient between the reservoir and the caprock at the highest point of the reservoir becomes high enough to reach hydraulic fracturing, and large, vertical fluid flow pipes develop. A later resulting local deformation and sediment redistribution is likely to occur, and the pipe may remain an active fluid migration pathway as long as overpressure remains in the connected underlying compartments (Fig. 11).

6. Conclusions

We propose that large-scale vertical pipes need not be related to hydrocarbon buoyancy and can form above porous and permeable strata with no hydrocarbon charge. In this study we presented pipes that develop at the crest of anticlines as a result of the following succession of events: (1) rapid sedimentation and loading; (2) uplift; (3) lateral pressure transfer in the reservoir intervals; (4) hydraulic fracturing of the caprock at the shallowest point in the reservoir interval; (5) vertical fluid escape through the overburden to the seabed. Our results suggest that this process, lateral pressure transfer, added to regional-scale disequilibrium compaction is sufficient to generate enough overpressure (~5–10 MPa) to initiate the 2 km-scale fluid flow pipes located right above these water-filled sand bodies. This model could have general applicability to other deepwater settings where vertical fluid pipes are common.

This case study provides complementary information on the nature of low-reflectivity vertical features in a gravity detachment system, which have commonly been interpreted as shale diapirs with lower-resolution data. Appropriate seismic interpretation around each fluid flow pipes allows the mapping the source of fluids escaping through the pipes and the structural setting in which they develop. The results show that kilometer-scale vertical fluid flow pipes can develop as a result of interacting sedimentary, structural and overpressure mechanism and need not be a direct hydrocarbon indicator.

Acknowledgements

We thank CGG Veritas and PGS for making the data available, as well as Dave Stevenson and Gary Wilkinson at Durham University. We also thank ENI S.p.A., Divisione Exploration and Production, Marco Orsi, Franco Fonnesu, and Juan Di Croce for their help and for providing access to their data in San Donato Milanese. The support of this research project by the Landmark Graphics Corporation via the Landmark University Grant program is acknowledged by Durham University. We also thank ENI for funding this Ph.D. project and the Centre for Research into Earth Energy Systems, Durham Energy Institute, Durham University, for hosting the project.

References

Bjørkum, P.A., Walderhaug, O., Nadeau, P.H., 1998. Physical constraints on hydrocarbon leakage and trapping revisited. Petroleum Geoscience 4, 237–239.

Briggs, S.E., Davies, R.J., Cartwright, J.A., Morgan, R., 2006. Multiple detachment levels and their control on fold styles in the compressional domain of the deepwater west Niger Delta. Basin Research 18, 435–450.

Brown, A.R., 2011. Interpretation of Three-dimensional Seismic Data, seventh ed. AAPG Memoir, 42, Tulsa, OK, U.S.A.

Cartwright, J., Huuse, M., Aplin, A., 2007. Seal bypass systems. AAPG Bulletin 91, 1141–1166.

Cartwright, J., 2007. The impact of 3D seismic data on the understanding of compaction, fluid flow and diagenesis in sedimentary basins. Journal of the Geological Society 164, 881–893.

Cobbold, P.R., Mourgues, R., Boyd, K., 2004. Mechanism of thin-skinned detachment in the Amazon Fan: assessing the importance of fluid overpressure and hydrocarbon generation. Marine and Petroleum Geology 21, 1013–1025.

Cobbold, P.R., Clarke, B.J., Løseth, H., 2009. Structural consequences of fluid overpressure and seepage forces in the outer thrust belt of the Niger Delta. Petroleum Geoscience 15, 3–15.

Cohen, H.A., McClay, K., 1996. Sedimentation and shale tectonics of the northwestern Niger Delta front. Marine and Petroleum Geology 13, 313–328.

Davies, R.J., 2003. Kilometer-scale fluidization structures formed during early burial of a deep-water slope channel on the Niger Delta. Geology 31, 949–952.

Deville, É., Guerlais, S.H., Lallemant, S., Scheiner, F., 2010. Fluid dynamics and subsurface sediment mobilization processes: an overview from southeast Caribbean. Basin Research 22, 361–379.

Dickinson, G., 1953. Geological aspects of abnormal reservoir pressures in Gulf Coast Louisiana. AAPG Bulletin 37, 410–432.

Doust, H., Omatsola, E., 1990. Niger Delta. In: Edwards, J.D., Santogrossi, P.A. (Eds.), Divergent/Passive Margin Basins, vol. 48. AAPG Memoir, pp. 201–238.

Dugan, B., Flemings, P.B., 2000. Overpressure and fluid flow in the New Jersey continental slope: implications for slope failure and cold seeps. Science 289, 288–291.

Feseker, T., Brown, K.R., Blanchet, C., Scholz, F., Nuzzo, M., Reitz, A., Schmidt, M., Hensen, C., 2010. Active mud volcanoes on the upper slope of the western Nile deep-sea fan — first results from the P362/2 cruise of R/V Poseidon. Geo-Marine Letters 30, 169–186.

Finkbeiner, T., Zoback, M., Flemings, P., Stump, B., 2001. Stress, pore pressure, and dynamically constrained hydrocarbon columns in the South Eugene Island 330 field, northern Gulf of Mexico. AAPG Bulletin 86 (6), 1007–1031.

Flemings, P.B., Liu, X., Winters, W.J., 2003. Critical pressure and multiphase flow in Blake Ridge gas hydrates. Geology 31 (2), 1057–1060.

Fonnesu, F., 2003. 3D seismic images of a low-sinuosity slope channel and related depositional lobe (west Africa deep-offshore). Marine and Petroleum Geology 20, 615–629.

Graue, K., 2000. Mud volcanoes in deepwater Nigeria. Marine and Petroleum Geology 17, 959–974.

Grauls, D.J., Baleix, J.M., 1994. Role of overpressures and in situ stresses in fault-controlled hydrocarbon migration: a case study. Marine and Petroleum Geology 11, 734–742.

Grauls, D., 1999. Overpressures: causal mechanisms, conventional and hydromechanical approaches. Oil & Gas Science and Technology – Revue d'IFP 54, 667–678.

Grunau, H.R., 1987. A worldwide look at the cap-rock problem. Journal of Petroleum Geology 10, 245–265.

Heggland, R., Hovland, M., Graue, K., Gallagher, J.W., 2001. Mud volcanoes and gas hydrates on the Niger Delta Front. In: Conference Abstract Book: Subsurface Sediment Mobilization. University of Gent, Belgium. Sept, 44.

Heggland, R., 2005. Using gas chimneys in seal integrity analysis: a discussion based on case histories. In: Boult, P., Kaldi, J. (Eds.), Evaluating Fault and Cap Rock Seals. AAPG Hedberg Series, 2, pp. 237–245.

Heppard, P., Cander, H.S., Eggertson, E.B., 1998. Abnormal pressure and the occurrence of hydrocarbons in offshore Eastern Trinidad, West Indies. In: Law, B.E., Ulmishek, G.F., Slavin, V.I. (Eds.), Abnormal Pressures in Hydrocarbon Environments, vol. 70. AAPG Memoir, Tulsa, OK, pp. 215–246.

Hovland, M., Judd, A.G., 1988. Seabed Pockmarks and Seepages: Impact on Geology, Biology and the Marine Environment. Graham and Trotman, London.

Hubbert, M.K., Willis, D.G., 1972. Mechanics of Hydraulic Fracturing, vol. 18. AAPG Memoir, pp. 239–257.

Hustoft, S., Dugan, B., Mienert, J., 2010. Effects of rapid sedimentation on developing the Nyegga pockmark field: constraints from hydrological modeling and 3-D seismic data, offshore mid-Norway. Geochemistry, Geophysics, Geosystems 10 (6), 17.

Huuse, M., Jackson, C.A.L., Van Rensbergen, P., Davies, R.J., Flemings, P.B., Dixon, R.J., 2010. Subsurface sediment remobilization and fluid flow in sedimentary basins: an overview. Basin Research 22, 342–360.

Ingram, G.M., Urai, J.L., 1999. Top-seal leakage through faults and fractures: the role of mudrock properties. In: Aplin, A.C., Fleet, A.J., Macquaker, J.H.S. (Eds.), Muds and Mudstones: Physical and Fluid-flow Properties. Geological Society, Special Publications, London, vol. 158, pp. 125–135.

Janik, A.G., Hood, J.A., Ask, M.V., 1998. Physical properties data at hole 959d: comparison of core and log measurements and a proposed revision of lithologic units. In: Mascle, J., Lohmann, G.P., Moullade, M., et al. (Eds.), Proceedings of the Ocean Drilling Program. Scientific Results, vol. 159. Ocean Drilling Program, College Station, Texas, pp. 241–248.

Jolly, R.J.H., Lonergan, L., 2002. Mechanisms and controls on the formation of sand intrusions. Journal of the Geological Society 159, 605–617.

Kopf, A.J., 2002. Significance of mud volcanism. Review of Geophysics 40, 2.

Leduc, A.M., Davies, R.J., Imber, J., Densmore, A.L., 2012. The lateral strike-slip domain in gravitational detachment delta systems: a case study of the northwest margin of the Niger Delta. AAPG Bulletin 96 (4), 709–728.

Loncke, L., Mascle, FANIL Scientific Parties, 2004. Mud volcanoes, gas chimneys, pockmarks and mounds in the Nile deep-sea fan (Eastern Mediterranean): geophysical evidences. Marine and Petroleum Geology 21, 669–689.

Løseth, H., Wensaas, L., Arntsen, B., Hanken, N.-M., Basire, C., Graue, K., 2010. 1000 m Long gas blow-out pipes. Marine and Petroleum Geology 28 (5), 1047–1060.

Maloney, D.P., Davies, R., Imber, J., Higgins, S., King, S., 2010. New insights into deformation mechanisms in the gravitationally driven Niger Delta deep-water fold and thrust belt. AAPG Bulletin 94, 1401–1424.

Miller, T.W., 1995. New insights on natural hydraulic fractures induced by abnormally high pore pressures. AAPG Bulletin 79, 1005–1018.

Morgan, R., 2003. Prospectivity in ultradeep water: the case for petroleum generation and migration within the outer parts of the Niger Delta apron. In: Arthur, T.J., MacGregor, D.S., Cameron, N.R. (Eds.), Petroleum Geology of Africa: New Themes and Developing Technologies. Geological Society, London, Special Publications, vol. 207, pp. 151–164.

Morley, C.K., Guerin, G., 1996. Comparison of gravity-driven deformation styles and behavior associated with mobile shales and salt. Tectonics 15, 1154–1170.

Morley, C., 2003. Outcrop examples of mudstone intrusions from the Jerudong anticline, Brunei Darussalam and inferences for hydrocarbon reservoirs. In: Van Rensbergen, P., Hillis, R.R., Maltman, A.J., Morley, C.K. (Eds.), Subsurface Sediment Mobilization. Geological Society, London, Special Publication, vol. 216, pp. 381–384.

Moss, J.L., Cartwright, J., 2010. 3d seismic expression of km-scale fluid escape pipes from offshore Namibia. Basin Research 22, 481–501.

Mourgues, R., Cobbold, P.R., 2003. Some tectonic consequences of fluid overpressures and seepage forces as demonstrated by sandbox modelling. Tectonophysics 376, 75–97.

Mourgues, R., Gressier, J.B., Bodet, L., Bureau, D., Gay, A., 2011. "Basin scale" versus "localized" pore pressure/stress coupling – implications for trap integrity evaluation. Marine and Petroleum Geology 28 (5), 1111–1121.

Nashaat, M., 1998. Abnormally high fluid pressure and seals impacts on hydrocarbon accumulations in the Nile Delta and North Sinai Basins, Egypt. In: Law, B.E., Ulmishek, G.F., Slavin, V.I. (Eds.), Abnormal Pressures in Hydrocarbon Environments, vol. 70. AAPG Memoir, Tulsa, OK, pp. 161–180.

Nordgard Bolas, H.M., Hermanrud, C., 2003. Hydrocarbon leakage processes and trap retention capacities offshore Norway. Petroleum Geoscience 9, 321–332.

Osborne, M.J., Swarbrick, R.E., 1997. Mechanisms for generating overpressure in sedimentary basins: a reevaluation. AAPG Bulletin 81, 1023–1041.

Reilly, M.J., Flemings, P.B., 2010. Deep pore pressures and seafloor venting in the Auger Basin, Gulf of Mexico. Basin Research 22, 380–397.

Rodgers, S., Bjørkum, P., Walderhaug, O., Nadeau, P., 1999. Discussion: physical constraints on hydrocarbon leakage and trapping revisited' by P.A. Bjørkum et al. – further aspects. Petroleum Geoscience 5, 421–423.

Secor, D.T., 1965. Role of fluid pressure in jointing. American Journal of Science 263 (8), 633–646.

Seldon, B., Flemings, P.B., 2005. Reservoir pressure and seafloor venting: predicting trap integrity in a Gulf of Mexico deepwater turbidite minibasin. AAPG Bulletin 89, 193–209.

Short, K., Stauble, A., 1967. Outline of geology of Niger Delta. AAPG Bulletin 51, 761–779.

Stewart, S.A., Davies, R.J., 2006. Structure and emplacement of mud volcano systems in the South Caspian Basin. AAPG Bulletin 90, 771–786.

Stewart, S.A., 1999. Seismic interpretation of circular geological structures. Petroleum Geoscience 5, 273–285.

Swarbrick, R.E., Osborne, M.J., 1998. Mechanisms that generate abnormal pressures: an overview. In: Law, B.E., Ulmishek, G.F., Slavin, V.I. (Eds.), Abnormal Pressures in Hydrocarbon Environments, vol. 70. AAPG Memoir, Tulsa, OK, pp. 13–34.

Swarbrick, R.E., Osborne, M.J., Yardley, G.S., 2002. Comparison of overpressure magnitude resulting from the main generating mechanisms. In: Pressure Regimes in Sedimentary Basins and Their Prediction, vol. 76. AAPG Memoir, Tulsa, OK, pp. 1–12.

Tingay, M.R.P., Hillis, R.R., Swarbrick, R.E., Morley, C.K., Damit, A.R., 2009. Origin of overpressure and pore-pressure prediction in the Baram Province, Brunei. AAPG Bulletin 93, 51–74.

Traugott, M.O., Heppard, P.D., 1994. Prediction of pore pressure before and after drilling – taking the risk out of drilling overpressured prospects. In: Law, B.E., Ulmishek, G., Slavin, V.I. (Eds.), AAPG Hedberg Research Conference, Abnormal Pressures in Hydrocarbon Environments: Golden Colorado, June 8–10 (Extended Abstract).

Traugott, M.O., Heppard, P.D., 1997. Pore/fracture pressure determination in deep water. Deep Water Supplement to World Oil.

Van Rensbergen, P., Morley, C.K., 2003. Re-evaluation of mobile shale occurrences on seismic sections of the Champion and Baram Deltas, Offshore Brunei. In: Van Rensbergen, P., Hillis, R.R., Maltman, A.J., Morley, C.K. (Eds.), Subsurface Sediment Mobilization. Geological Society, London, Special Publication, vol. 216, pp. 395–409.

Yardley, G.S., Swarbrick, R.E., 2000. Lateral transfer: a source of additional overpressure? Marine and Petroleum Geology 17, 523–537.

Appendix 04: Dip sections in OPL316 3D datasets located between the extensional structural domain and the translational domain

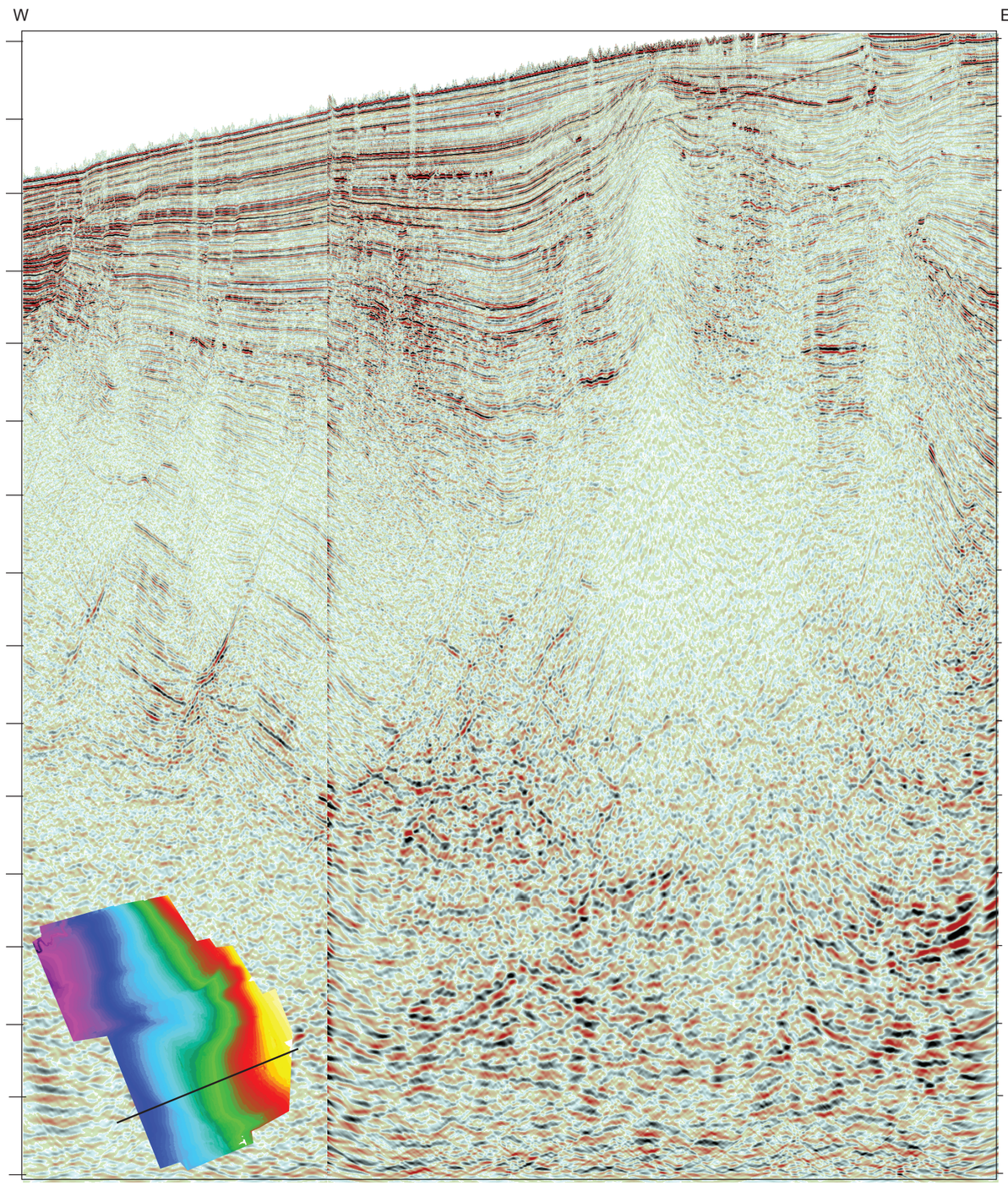

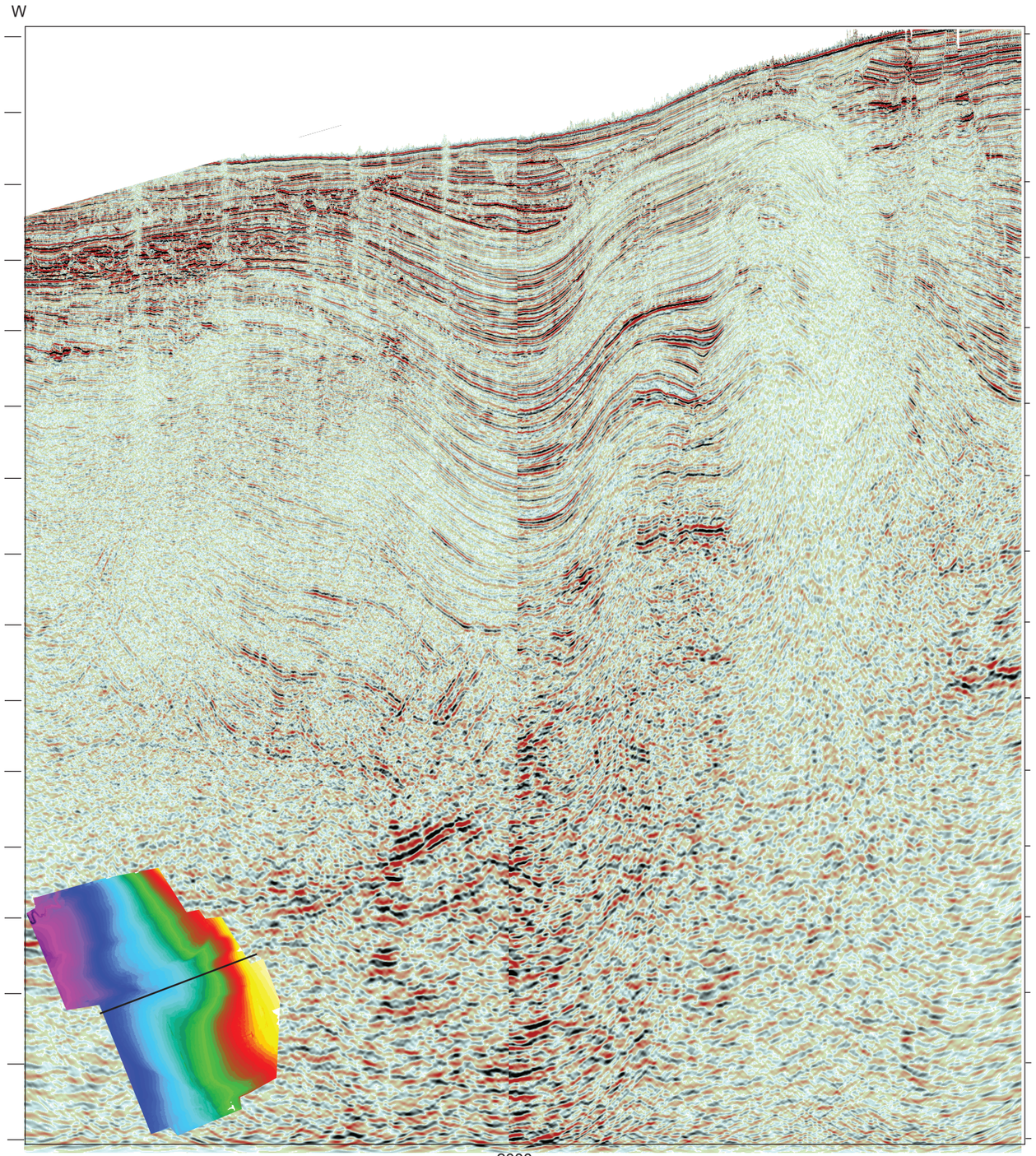

Appendix 05: Random line in OPL316 3D datasets showing a negative flower structure of the lateral strike-slip domain in the north

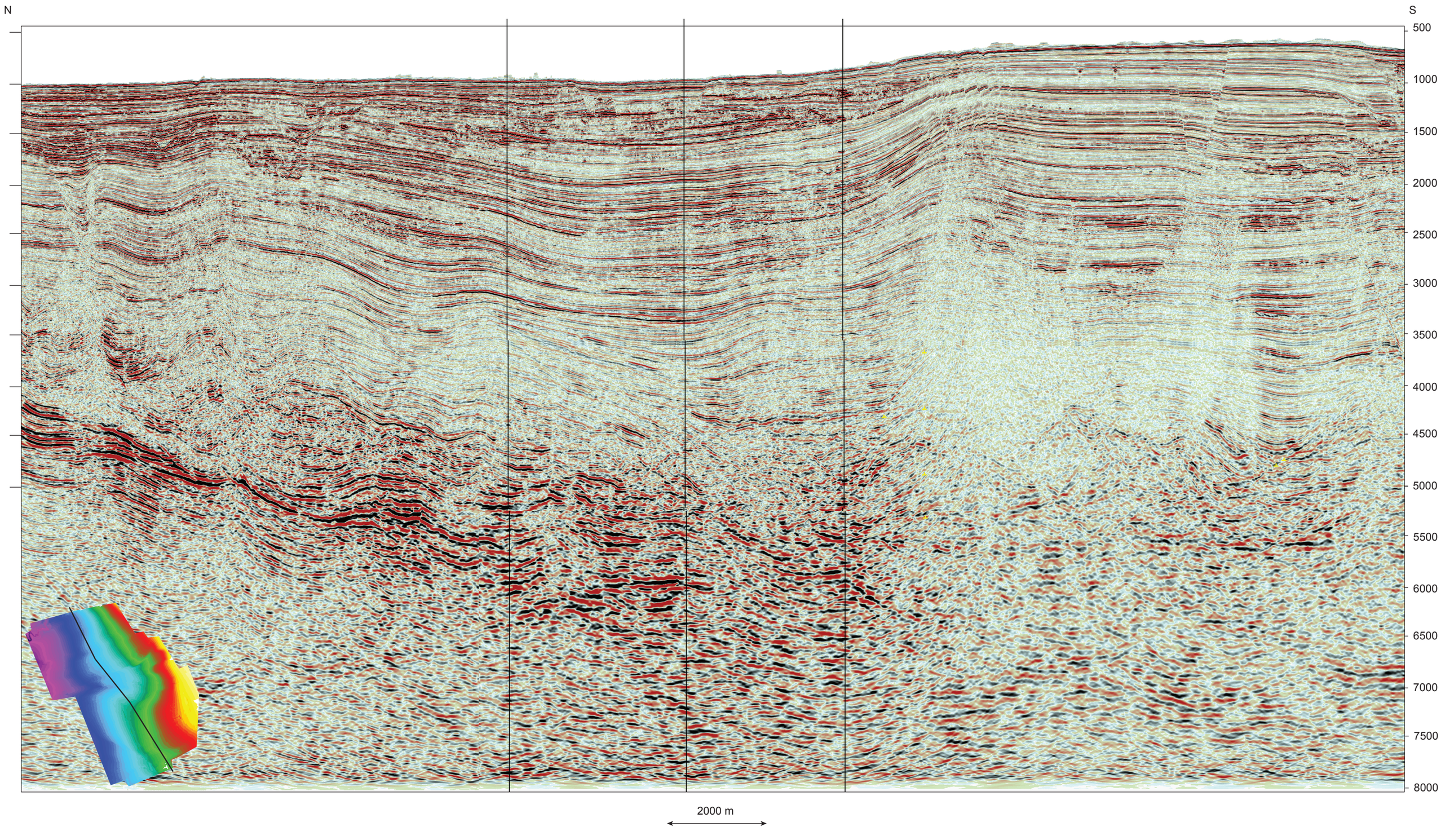

Appendix 06: Strike line in OPL316 3D datasets showing a contractional structure of the lateral strike-slip domain in the north

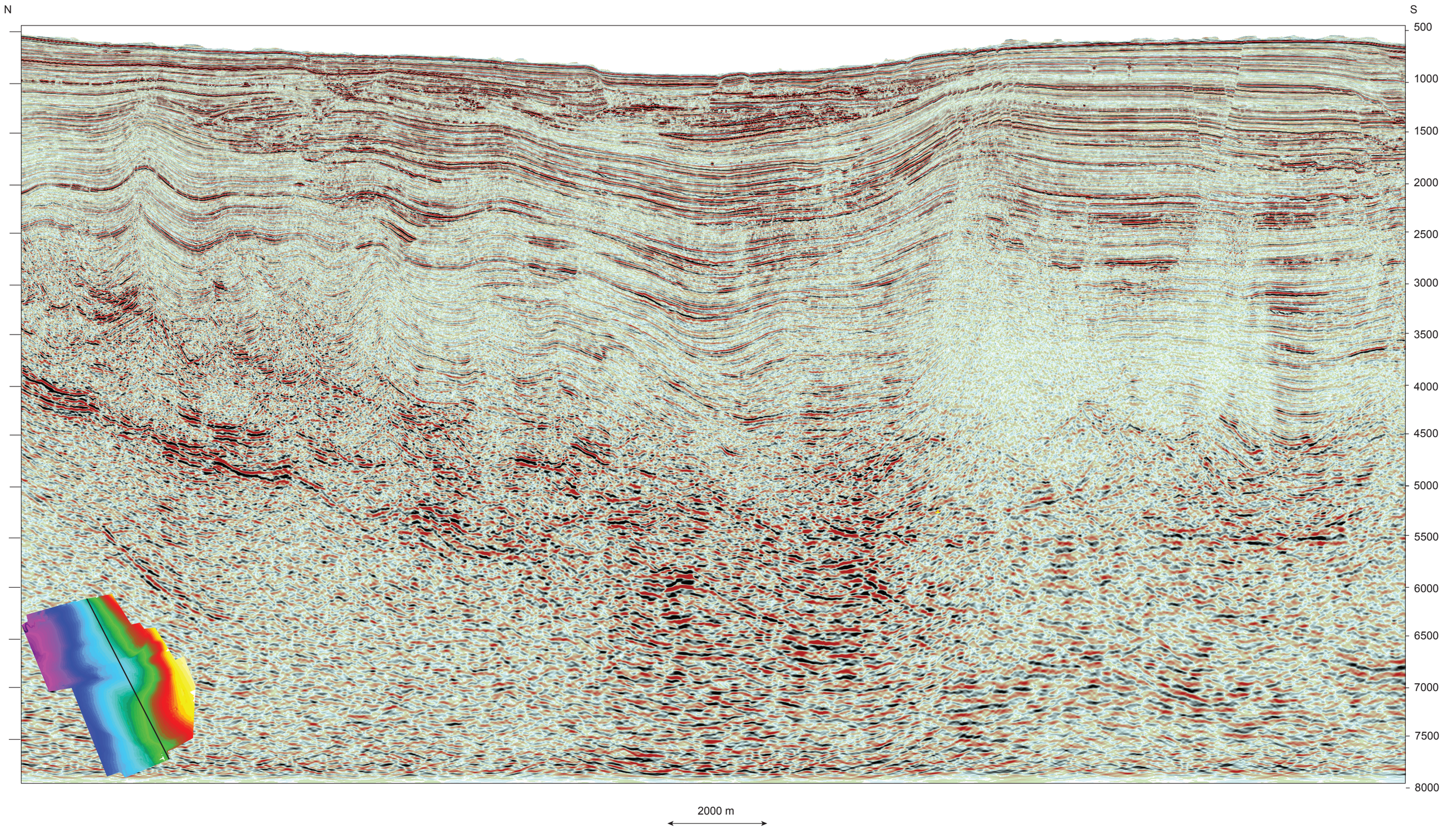

Appendix 07: Isochron maps of the horizons H400 and H300 interpreted in Eni

Isochron H400

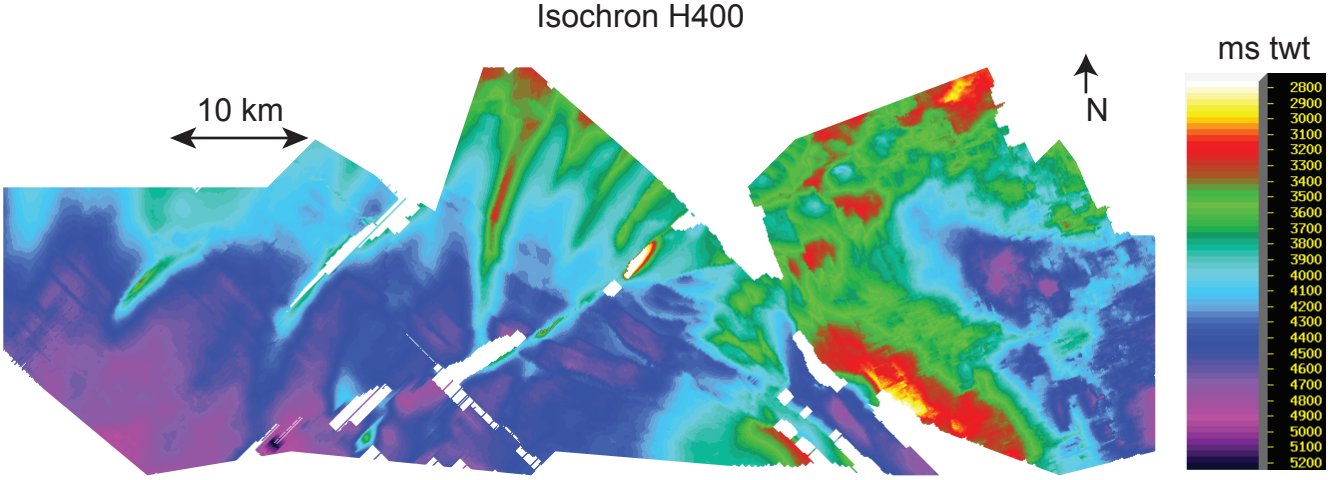

Isochron H300

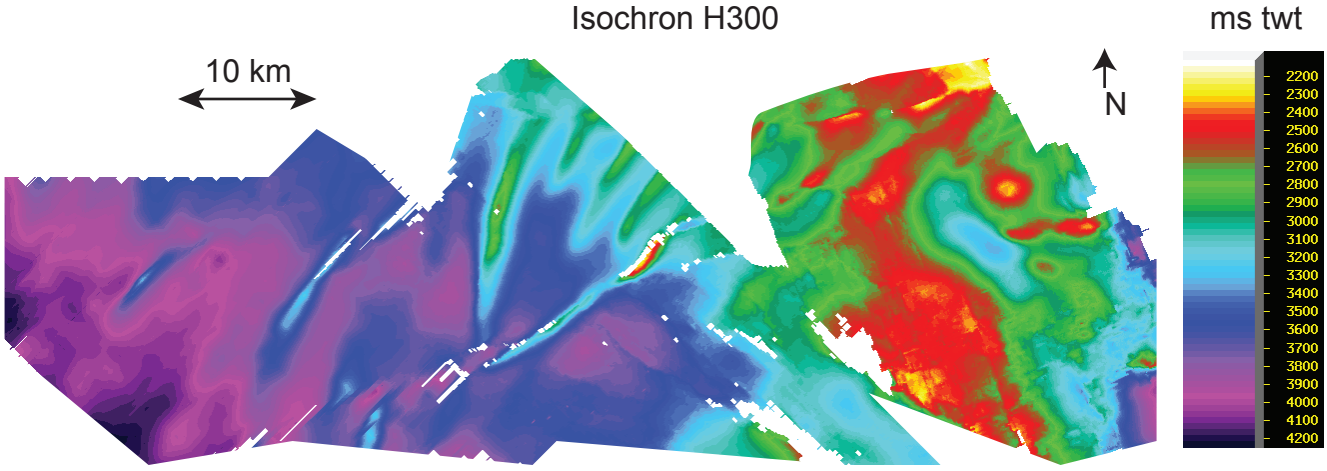

Appendix 08: Isochron maps of the horizon H200 interpreted in Eni (OPL316) and in Durham (OPL314 and 315)

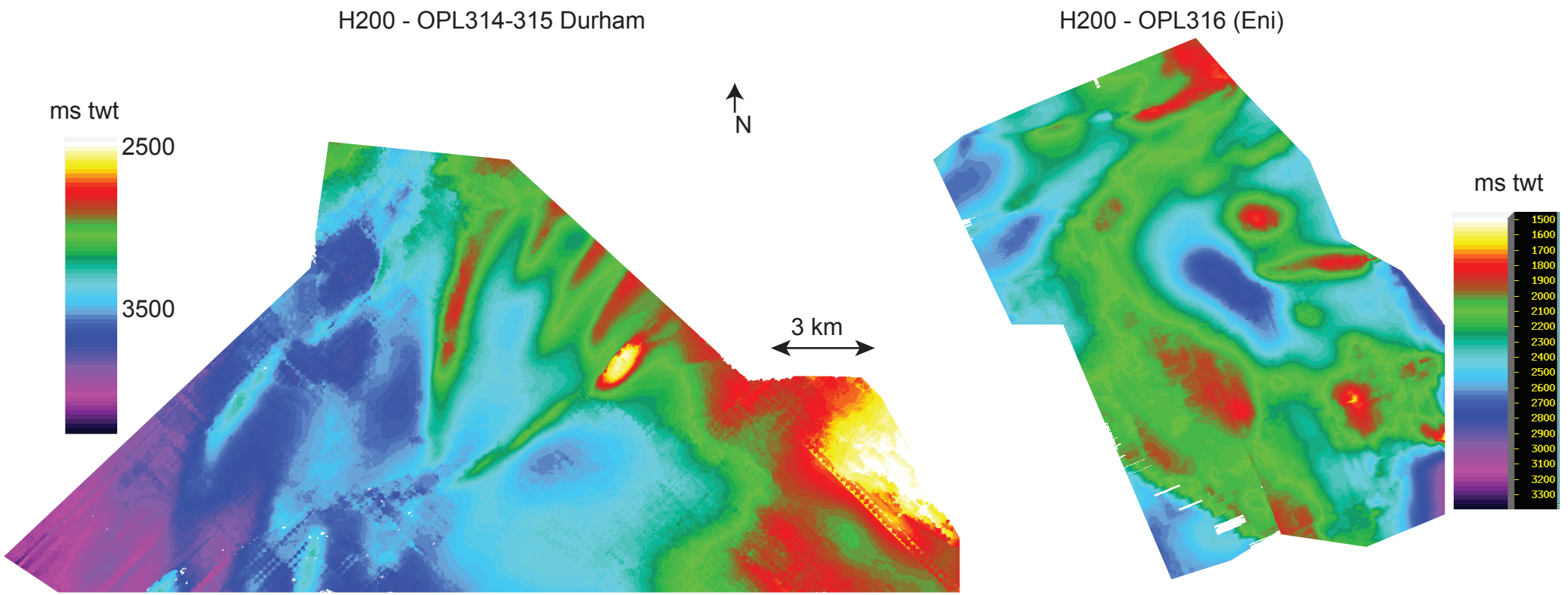

Appendix 09: Isochron maps of the horizons “H250, H150, H100”, and the seabed interpreted in Eni and used for research in chapter 5.

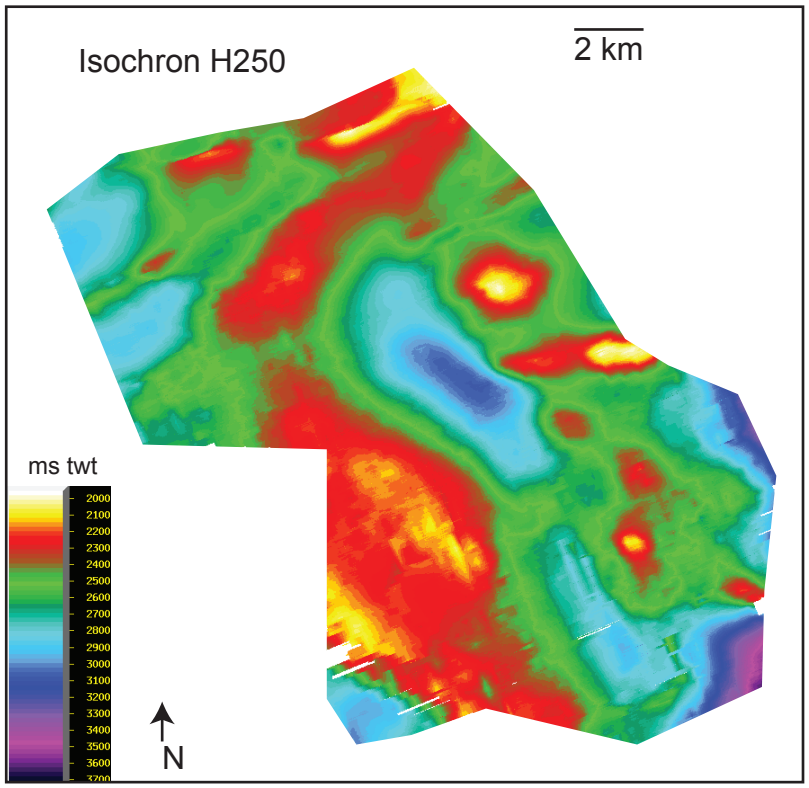

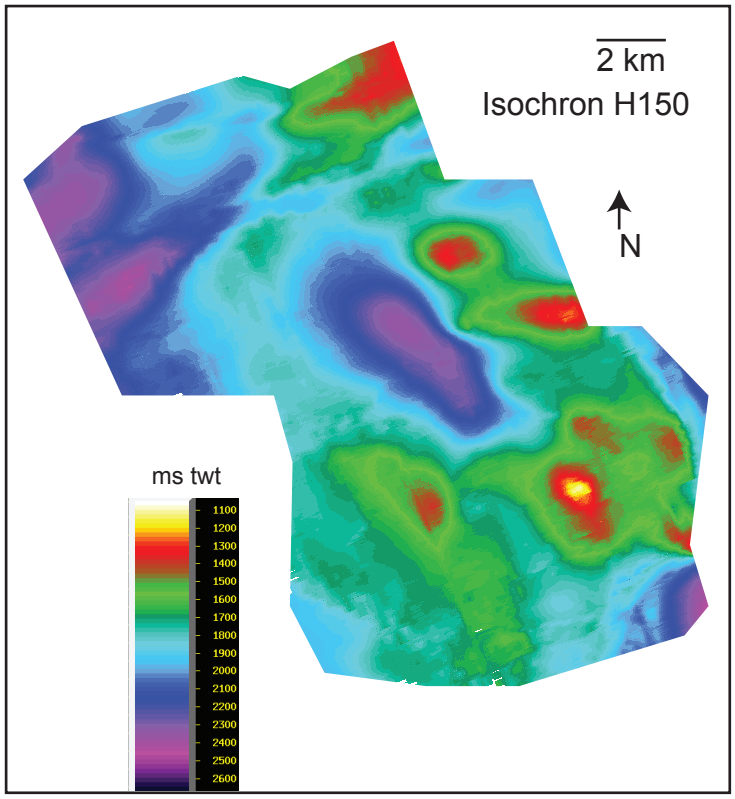

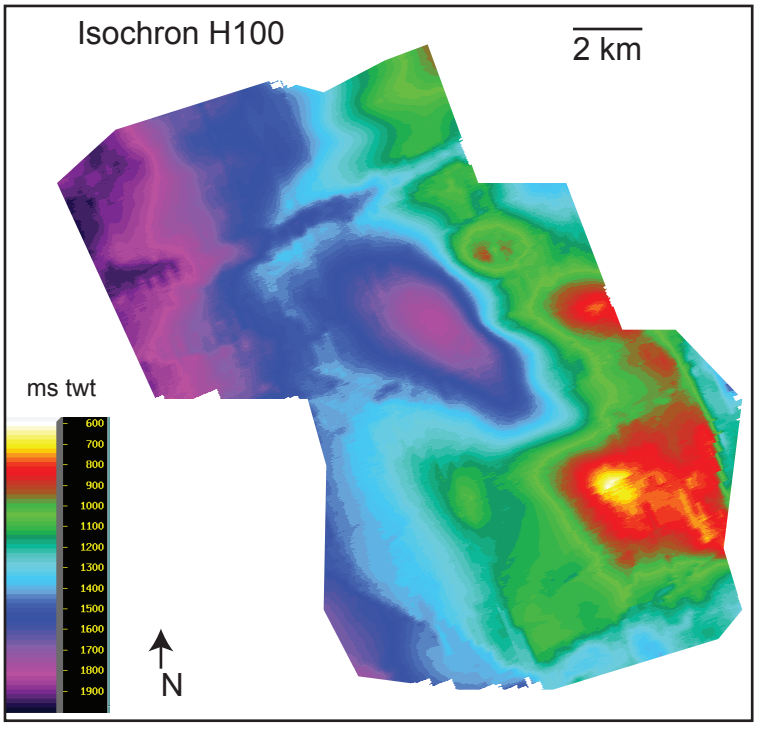

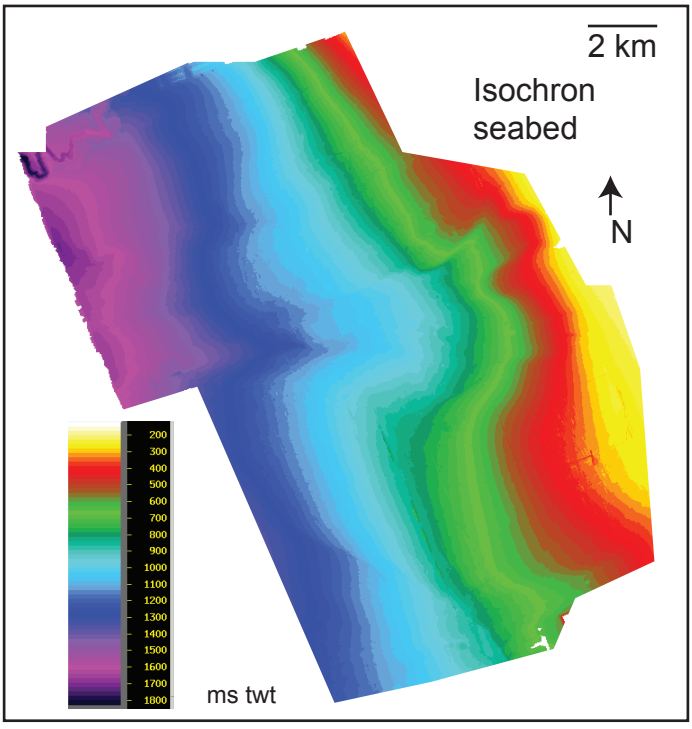

Appendix 10: Parameters used in 2D Move for the depth conversion of Fig.3.6C (chapter 3).

Horizons definition and Velocity parameters

Horizon	Colour	Velocity	k Value	Depth Coefficient	Porosity	Age	Thickness
Seasurface		1480	0.5	0.39	0.56	0	719
seabed		1600	0.5	0.39	0.56	0	452
H1		1700	0.5	0.39	0.56	0	44
H2right		1900	0.5	0.39	0.56	0	298
H2left		1900	0.5	0.39	0.56	0	25
H3left		2200	0.5	0.39	0.56	0	516
H3right		2200	0.5	0.39	0.56	0	405
H4left		2600	0.5	0.39	0.56	0	2
H4right		2600	0.5	0.39	0.56	0	177
H4mid		2600	0.5	0.39	0.56	0	306
H4midright		2600	0.5	0.39	0.56	0	189
detachment		1700	0.5	0.39	0.56	0	607
Basal		3000	0.5	0.39	0.56	0	0

Initial section in time

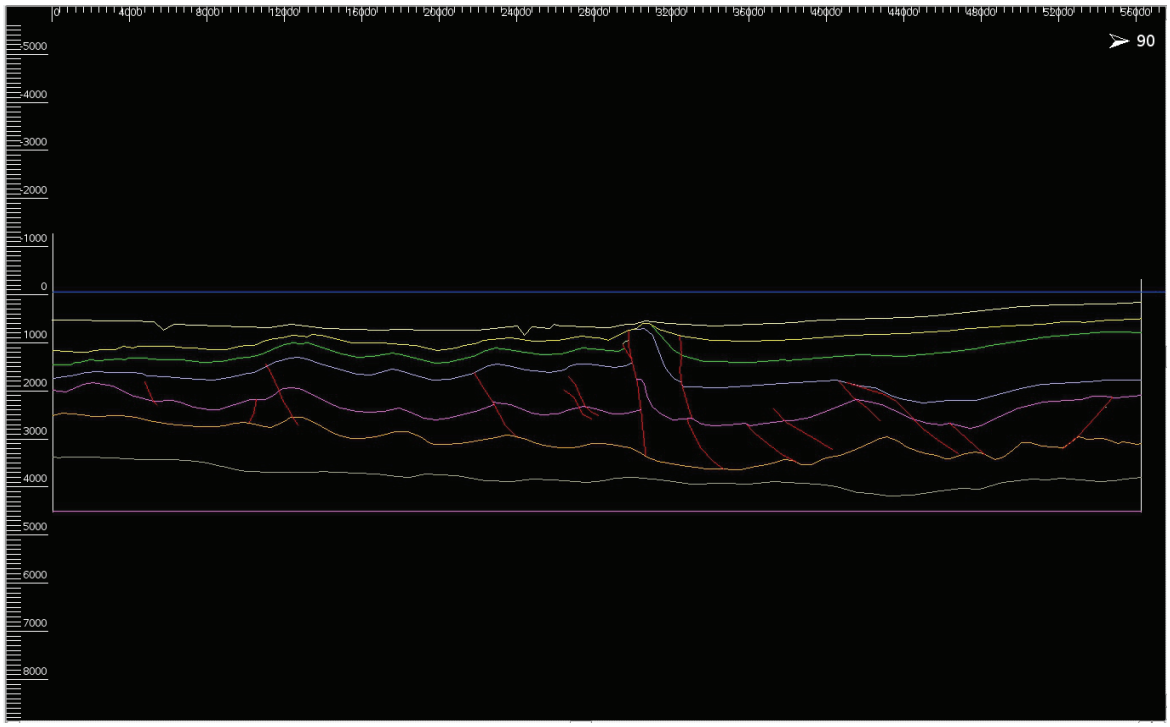

Final section in depth

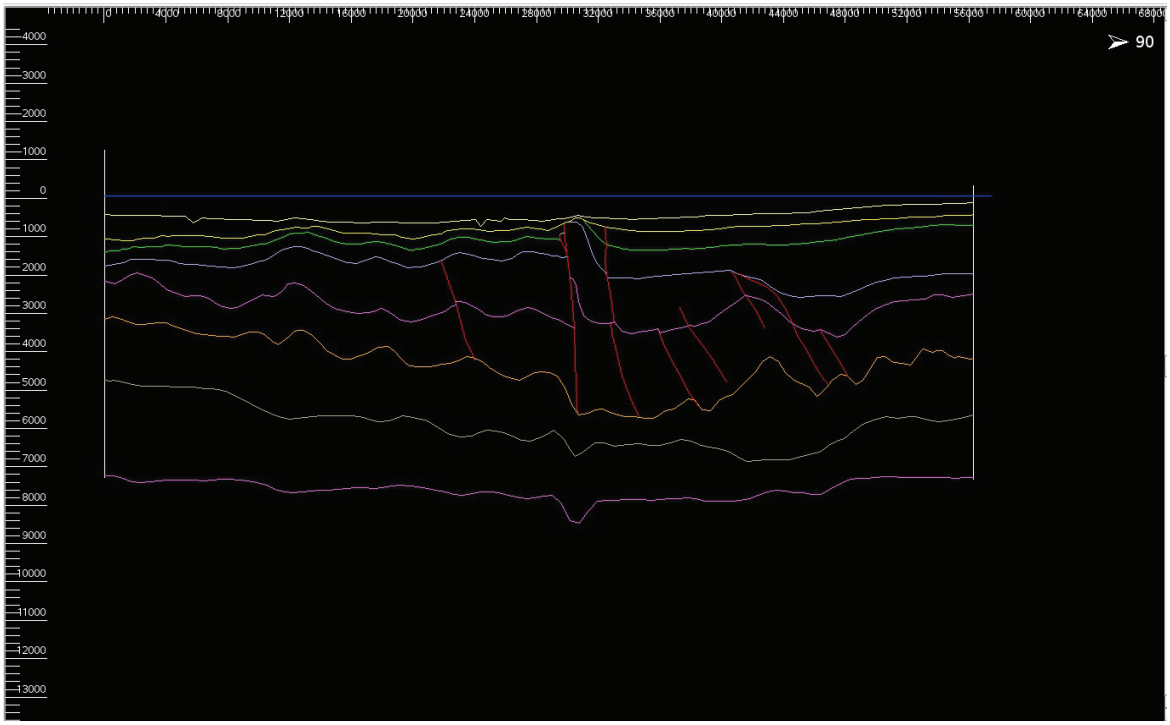

Appendix 11: A seismic section from the 3D dataset OPL324 (CGG Veritas) used in chapter 4 and showing the Ijebu channel and an underlying tear fault.

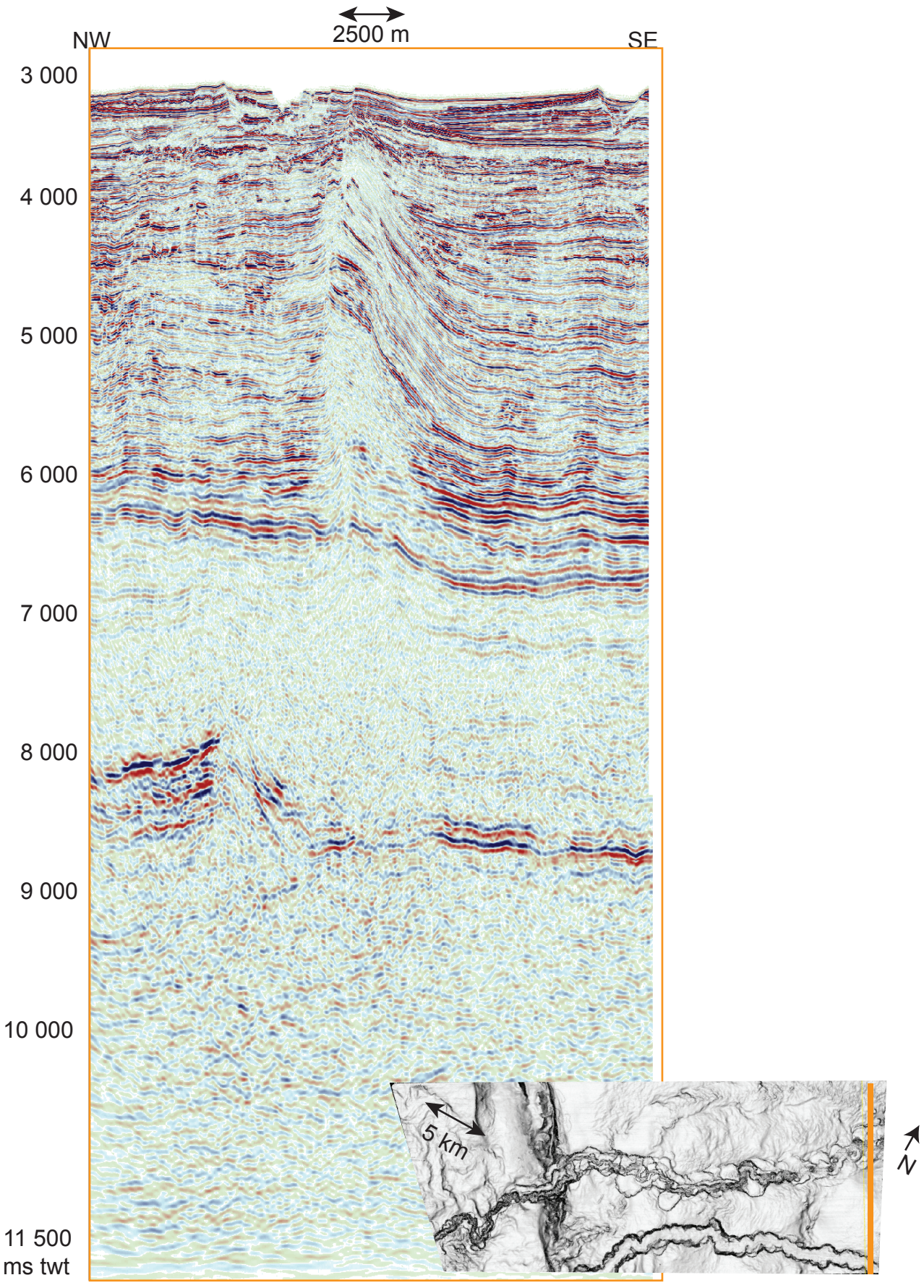

Appendix 12: Seismic sections along the NCS-N and above the “Khop” structure, offshore Mauritania.

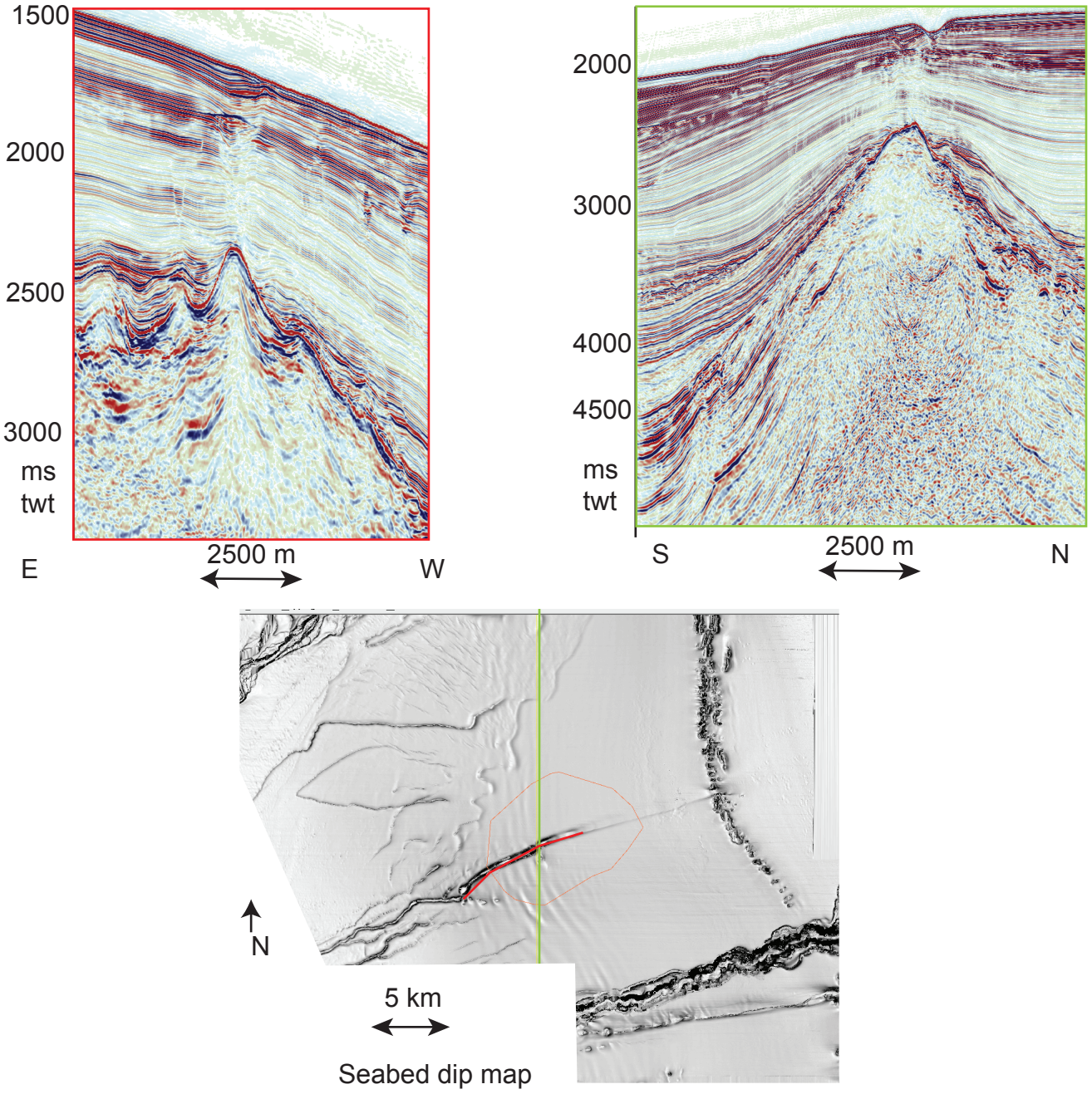

Appendix 13: Glossary

This appendix section provides a series of definition of terms used in this thesis.

2D Two-dimensional.

3D Three-dimensional.

Acoustic impedance Defined by density and seismic velocity. Changes in acoustic impedance are recorded in seismic data (Brown, 2004).

Amplitude extraction Extractions of seismic attribute amplitude from horizons, slices or volumes, which is useful for studying subtle stratigraphic features.

Attribute A derivate of a seismic measurement, such as time, amplitude, frequency and azimuth.

Avulsion Lateral shift of the position of a channel by cut-and-fill process.

Backlimb Shallower limb of a thrust-propagation fold that dips the same direction as the thrust fault.

BSR Bottom simulating reflection.

Canyon Deep, often v-shaped valley incised into continental slope, often fed by a river.

Canyon system A series of stacked canyons that have same source.

Channel Physical confine of flows, normally with negative topography.

Channel-fill Channel-fill elements comprise HARs, passive fill, channel-axis deposits and debris flow and other mass transport deposits that fill channels.

Channel-levee complex A series of stacked channel-levee systems that are fed by the same canyon.

Channel-levee system A single channel-belt that is bordered by outer levees.

Compaction mechanical and chemical processes that change the physical properties of sediments that occur during progressive burial.

Continental margin Area around the continental and oceanic crust boundary including shelf, slope and rise..

Debris flow Viscous sediment-gravity flows that show plastic flow behaviour.

Deepwater water depth of 0.5-1.5 km.

Detachment Describes the apparent depth that brittle deformation ceases separation of brittle-ductile regimes at the point of the faultzone in lithospheric crustal models.

Detachment fault A shallow dipping bedding parallel fault that mechanically links up-dip extension to down-dip contraction and can separate brittle from ductile deformation styles. A detachment fault is identified by the soling of numerous fault planes within the sedimentary overburden where displacement on the faults becomes zero.

Detachment fold Forms at the tip of a propagating bedding parallel thrust fault. Displacement is transferred from the thrust tip into an overlying mechanically weak detachment layer and induces buckling within an overriding mechanical competent layer.

Detachment level Refers to a basal fault (typically bedding parallel) along which numerous fault planes sole and separates brittle deformation styles from undeformed layers at the point of detachment.

Diapir A complex anticlinal feature, usually salt-cored, which internal layers pierce their envelope. Also in terms of “shale diapirs”, a low reflectivity, chaotic discontinuous seismic reflections that on mass appear to rise into overlying laterally continuous reflections.

Dip magnitude map Shows the local dip of the horizon surface.

Disequilibrium compaction Process that causes pore-fluids to become overpressured due to rapid burial of overlying sediments. Pore-fluids are unable to escape with burial and the lithostatic load is imposed onto the pore-fluids generating the overpressure.

Fault-propagation fold Related to a ramp in by a propagating fault plane where displacement at the upper tip line of the propagating fault tip is accommodated by folding.

HARP High-amplitude reflection package.

Hemipelagic sediment Terrigenous sediment transported mainly by wind and surface currents.

Horizon A map produced by interpreting (picking) particular seismic reflection.

Horizontal resolution Defines the area from which a reflection is received called Fresnel zone. Theoretically the Fresnel zone could be reduced to a radius of a quarter of a wavelength.

LAP Lateral Accretion Package.

Mass transport complex General term that includes slumps, slides and debris flows. Recognised on seismic data by contorted, chaotic low-amplitude reflections.

Migration Channel migration is a gradual shift of the channel by systematic erosion on outer bends and deposition on inner bends.

Peak Positive amplitude (SEG normal polarity).

Pelagic sediment Sediment composed of planktonic organisms and related organic matter.

Phase/zero phase Describes the motion of periodic waves. Zero phase means that the wavelet is symmetrical, with the central lobe coinciding with the interface.

Pockmark Depressions formed as a result of catastrophic gas and/or porewater eruption on the seafloor.

Sediment wave Undulating sedimentary structures found on the seafloor and on levees, characterised by steeper lee flanks and shallower or upstream-dipping stoss flanks.

Seismic amplitude Amplitude value of a horizon or a volume of seismic data.

Seismic attribute See 'attribute'.

Seismic velocity The velocity (v), with which seismic waves travel through rocks.

Seismic wave Wave of elastic energy that propagate outwards from a seismic source.

Slide Shear strain with movement along one or several planar surfaces.

Slope Continental slope is the steep (commonly 1-10°) slope below shelf break. Slope is also used to describe inclined surfaces.

Slope failure Any resedimentation process including submarine landslides, slumps, slides, where sediment deposits fail on a slope.

Terrace See 'inner levee'. Terraces can also be formed by erosional processes.

Trough Negative amplitude, decrease in Z (SEG normal polarity).

Tuning Constructional interference that occurs when layer thickness is one quarter of a wavelength. The amplitude can be boosted as the bed thins.

Turbidity current Relatively dilute sediment-suspension-driven sediment-gravity flows that occur in subaqueous environment. Commonly used term even when type of flow cannot be determined.

TWT Two-way travel time of a seismic wave, measured in s or ms.

Ultra-deepwater water depth more than 1.5 km.

Vertical resolution Defines the potential for the seismic data to distinguish individual layers. Measured in terms of wavelength.

Wavelet Record of changes in acoustic impedances including peaks and troughs that represent increase and decrease in acoustic impedance.